

**DOD/ONR/N00014-97-1-0806**

**DISTRIBUTION STATEMENT A**

**Approved for Public Release  
Distribution Unlimited**

# **University Research Initiative Program for Combat Readiness**

**Annual Report**

**for the period**

**June 1, 1998 — June 30, 1999**

**Roger H. Sawyer**

**University of South Carolina  
Columbia, SC 29208**

**May 1999**

**Prepared for**

**THE U.S. DEPARTMENT OF DEFENSE  
OFFICE OF NAVAL RESEARCH  
GRANT NUMBER N00014-97-1-0806**

**19990526 008**

## EXECUTIVE SUMMARY

### ABSTRACT

The *University Research Initiative for Combat Readiness* includes nineteen (19) research and development projects relevant to combat readiness. Projects being supported by this initiative address six major DoD mission areas including: chemical and biological warfare, target acquisition and identification, anti-submarine warfare, combat medicine, biodeterioration, and command, control, and communications. These projects were selected for support based on an existing research capability that could be accelerated to create cost savings to the ONR by bringing results to the field earlier. For the present report period directors of the individual projects report one-hundred and fifty-six (156) publications in progress, in press, or submitted for publication.

### FORWARD

The total amount of this grant is \$9,304,000 for the period of 01 Jun 97 through 29 Jun 00. The award carries a \$27,912,001 non-federal matching commitment. The University of South Carolina provides management costs for the project, and indirect costs are being returned to the project in the form of equipment. For the present report period the project supported seventy (70) faculty/post doctoral associates and sixty-three (63) graduate/undergraduate students. Eleven (11) inventions are reported and emanate from the *"Dynamic Decision Support for Command, Control, and Communication in the Context of Tactical Defense," "Survivable and Reconfigurable Optical/Wireless Tactical Networks,"* and *"Molecular Scale Electronic Arrays for the Design of Ultra-Fast Computational Systems"* component projects. Among the most significant achievements of the present report period is the receipt of a \$2 million award from DARPA to develop a real molecular computer. This award was an outgrowth of the *"Molecular Scale Electronic Arrays for the Design of Ultra-Dense and Ultra-Fast Computational Systems"* component project. Other significant achievements include measurements to determine the feasibility of direct, *in situ* injection of a "bone cement" paste as a delivery system for skeletal repair. This bone cement was a discovery reported in our Year One Annual Report and emanating from the component project *"Tissue-Engineered Cartilage and Advanced Bioadhesives for the Accelerated Healing of Combat and Training Injuries to Bone."*

### DESCRIPTION OF ATTACHMENTS

Attached to this Executive Summary are individual Performance (Technical) Reports for the nineteen (19) component projects and their individual SF-298 Report Documentation Pages.

### REPORT

The University Research Initiative Program for Combat Readiness was prepared in response to BAA 97-006. The purpose of this project is to support on-going research activities in six areas related to combat readiness: chemical and biological warfare, target acquisition and identification, anti-submarine warfare, combat medicine, biodeterioration, and command, control, and communications. Simultaneously, the project is to identify new projects, which offer potential advancement and improvement in combat readiness while offering specific savings in research and other federal expenditures by the accelerated research covered in the initiative.

University Research Initiative Program for Combat Readiness  
Annual Report 06/01/98-05/31/99

---

**Management (\$0, 3 faculty)**

Effective July 14, 1998, and with ONR approval, the Principal Investigator of the University Research Initiative Program for Combat Readiness was changed from Jerome D. Odom to Roger H. Sawyer. Simultaneous with this change in PI were the appointments of Dr. Frank T. Avigione, III and Dr. T. S. Little to Program Director and Manager, respectively. This reorganized management structure is provided on the following page.

With the assistance of Donald E. Polk, the Program Officer representing the United States Government, Management organized and facilitated an on-site review of the program by ONR technical staff in July of 1998. A summary of the review staff is provided below:

Reviewer Name	ONR Division	Component Project Reviewed
Dr. Richard Lau	Mathematical, Computer, and Informational Sciences Division	Wavelet-Based Image Processing For Military Applications  Wavelet-Based Automatic Detection and Recognition  Wavelet-Based Algorithms for Acoustic/Non-Acoustic Antisubmarine Warfare
Mr. Paul Quinn	Mathematical, Computer and Information Sciences Division	Dynamic Decision Support for Command, Control, and Communication in the Context of Tactical Defense  Survivable and Reconfigurable Optical/Wireless Tactical Networks  Massively Parallel Optical Image Compression Using Optical Rank Annihilation
Dr. David Nagel	Superintendent of Condensed Matter and Radiation Physics	Molecular Scale Electronic Arrays for the Design of Ultra-Dense and Ultra-Fast Computational Systems  The Design and Synthesis of Quantum Dot Based Lasers  Real-Time UV Fluorescence for Dissolved Hydrocarbon Tracking  Development of a Field-Portable LIBS System for the Identification of Alloys
Dr. Harold Guard	Biological and Biomedical S&T Division	Accelerated Research in Biofouling Control  Technology Development for Chemical Detection  Small Molecule Transport Through Polymers: Effects of Polymer Inhomogeneity and Dynamics on the Nanometer Length Scale

# UNIVERSITY RESEARCH INITIATIVE PROGRAM FOR COMBAT READINESS UNIVERSITY OF SOUTH CAROLINA

Year 3

DEPARTMENT OF DEFENSE  
Office of Naval Research

PRINCIPAL INVESTIGATOR  
Roger H. Sawyer  
Associate Dean for Research and Graduate Studies  
College of Science and Mathematics

PROJECT DIRECTOR  
Frank T. Avignone III  
Emeritus Professor, Physics & Astronomy

PROGRAM MANAGER  
T. Scott Little  
Research Professor, Chemistry & Biochemistry

Programmatic Issues

Fiscal Issues

## SECTION 1 Target Acquisition and Identification

Automatic Target  
Detection and  
Recognition  
(Jawerth)  
Image Processing for  
Military Applications  
(DeVore)

## SECTION 2 Chemical and Biological Warfare

Identification of Ex-  
plosive Chemicals and  
Chemical Warfare  
Agents (Angel)  
Chemical Detection  
(Myrick)  
Biodection (Fox)  
Small Molecule  
Transport Through  
Polymers (Berg)  
Quantum Dot Based  
Lasers (Adams)  
Biodection of Bac-  
terial Cells (Morgan)

## SECTION 3 Command, Control, and Communications

Decision Support for  
Tactical Defense  
(Rose)  
Optical/Wireless  
Tactical Networks  
(Sengupta)  
Optical Image Com-  
pression (Myrick)  
Molecular Scale Elec-  
tronics in Computa-  
tional Systems  
(Seminario)

## SECTION 4 Combat Medicine

Mosquito Control  
(Vogt)  
Bone Marrow Trans-  
plantation (Henslee-  
Downey)  
Combat/Training  
Bone Injuries (Genge)

## SECTION 5 Anti-Submarine Warfare

Acoustic/Non-  
Acoustic Warfare  
(Jawerth)  
Dissolved Hydro-  
carbon Tracking  
(Myrick)

## SECTION 6 Biodeterioration

Biofouling Control  
(Fletcher)

## SECTION 7 Supporting Research

Field-Portable Element-  
al Analysis (Goode)



University Research Initiative Program for Combat Readiness  
Annual Report 06/01/98-05/31/99

**On-Site Review (continued)**

Reviewer Name	ONR Division	Component Project Reviewed
Dr. Robert Walter	Biological and Biomedical S&T Division	Laboratory for Genetic Diagnosis and Control of Mosquitoes  Insure Access to Allogeneic Bone Marrow Transplantation for Correction of Marrow Failure and Hematologic Malignancies  Tissue-Engineered Cartilage and Advanced Bioadhesives for the Rapid Healing of Combat and Training Injuries to Bone
Dr. Eric Eisenstadt	Biological and Biomedical S&T Division	Line-of-Sight Standoff Identification of Explosive Chemicals and Chemical Warfare Agents  Real-Time Biodetection Using PCR-MS  Rapid Biodetection of Bacterial Cells by Laser

Recently, the Principal Investigator, Roger H. Sawyer, initiated a second review of the program to be complete by August, 1999.

For each component project, within each major DoD mission area, a single project leader has been identified. The project titles, these leaders and the total amount of funding for the total project period (3-years) are provided below:

Title	Project Leader	Budget
The Design and Synthesis of Quantum Dot Based Lasers	Richard D. Adams	\$330,000
Line-of-Sight Standoff Identification of Explosive Chemicals and Chemical Warfare Agents	S. Michael Angel	\$399,901
Small Molecule Transport Through Polymers: Effects of Polymer Inhomogeneity and Dynamics on the Nanometer Length Scale	Mark A. Berg	\$370,000
Wavelet Based Image Processing For Military Applications	Ronald A. DeVore	\$440,001
Insure Access to Allogeneic Bone Marrow Transplantation for Correction of Marrow Failure and Hematologic Malignancies	Jean Henslee-Downey	\$524,001
Accelerated Research in Biofouling Control	Madilyn M. Fletcher	\$383,251
Real-Time Biodetection Using PCR-MS	Karen Fox	\$450,001
Tissue-Engineered Cartilage and Advanced Bioadhesives for the Rapid Healing of Combat and Training Injuries to Bone	Brian Genge	\$900,000
Development of a Field-Portable LIBS System for the Identification of Alloys	Scott R. Goode	\$434,700
Wavelet-Based Automatic Detection and Recognition	Terrence L. Huntsberger	\$510,000
Wavelet-Based Algorithms for Acoustic/Non-Acoustic Antisubmarine Warfare	Bjorn Jawerth	\$525,000
Rapid Biodetection of Bacterial Cells by Laser Pyrolysis/Mass Spectrometry	Stephen L. Morgan	\$434,748
Technology Development for Chemical Detection	M.L. Myrick	\$1,299,999
Real-Time UV Fluorescence for Dissolved Hydrocarbon Tracking	M.L. Myrick	\$290,000
Massively Parallel Optical Image Compression Using Optical Rank Annihilation	M.L. Myrick	\$400,000

***Component Projects (continued)***

Dynamic Decision Support for Command, Control, and Communication in the Context of Tactical Defense	J.R. Rose	\$410,399
Survivable and Reconfigurable Optical/Wireless Tactical Networks	A. Sengupta/B. Beker	\$409,000
Molecular Scale Electronic Arrays for the Design of Ultra-Fast Computational Systems	Jorge M. Seminario	\$293,000
Laboratory for Genetic Diagnosis and Control of Mosquitoes	Richard G. Vogt	\$500,000

**Section 1: Target Acquisition and Identification (\$950,000, 2 component projects, 12 faculty/postdoc, 10 graduate/undergraduate students)**

The first two years of these projects have seen significant advances in the development of the image processing environment by using adaptive basis selection and greedy algorithms, nonlinear algorithms for compression and noise removal derived from functional analytic extremal problems, and customized encoders. Other advances include the development of a method to estimate the signal gradient from noisy images. This method uses probabilistic relaxation and edge-based saliency measurement techniques to achieve a globally consistent gradient configuration. Although investigators from the two component projects report no inventions, more than twenty-five (25) publications/presentations have been submitted, in press, or recently published during the present report period.

**Section 2: Chemical and Biological Warfare (\$3,284,649, 6 component projects, 14 faculty/postdoc, 20 graduate/undergraduate students)**

Preliminary investigations of rapid gas chromatographic techniques and publications describing fast GC techniques have been completed by investigators within the laser pyrolysis/mass spectrometry program. One of the investigators in this section of projects, Richard D. Adams, received the national American Chemical Society Award in Inorganic Chemistry and recently received a Humboldt Senior Scientist Award. The experimental challenges of developing a technique for measuring dynamics on a nanometer scale in polymers have been met for the study of small molecule transport in polymers. There are strong indications that new experimental approaches will provide more direct information on small-molecule diffusion unavailable from standard experiments. Studies of line-of-sight standoff identification of explosive chemicals and chemical defense agents have yielded an improved optical methodology for detecting plumes using chemical imaging based on serpentine fiber-optic image dissection arrays.

**Section 3: Command, Control, and Communications (\$1,512,399, 4 component projects, 15 faculty/postdoc, 9 graduate/undergraduate students)**

Investigators studying the integration of disparate battlefield information, such as voice, video images, and tactical displays, that have varying degrees of reliability, report significant advances in the use of Bayesian networks to solve incomplete and unreliable data entries. Investigators have developed algorithms for mapping agent hierarchy onto the existing network topology, evaluated an agent in a stable environment, and conducted initial evaluations of an agent in a dynamic environment. Investigators studying molecular scale electronic arrays for the design of ultra-dense and ultra-fast computational systems report nine (9) publications submitted, in press, or published delineating nanometer technology in molecular electronics. These investigators also report two inventions, one on the use of electrostatic potentials as signals for atomistic and molecular scale electronic computations and one for Moleware and the Molecular Computer. These investigators also note that funding provided by the Combat Readiness grant resulted in

the development and successful funding of a \$2 million DARPA grant to develop a real molecular computer.

**Section 4: Combat Medicine** (\$1,924,001, 3 component projects, 11 faculty/postdoc, 6 graduate/undergraduate students)

Among the objectives within the component projects of the combat medicine section was the study of tissue engineered cartilage and advanced bio-adhesives for the rapid healing of combat and training injuries to bone. The long-term design goal of this component study is to provide rapid stabilization of bone fractures, even to weight bearing bones, and to aid and accelerate the normal cell-mediated healing process of injured bones. During the first grant period, investigators succeeded in developing formulations of self-hardening bone pastes that may be useful for first-aid to bone injuries. Compression testing of those formulations showed superior strength when compared to other calcium phosphate-based materials reported in the scientific and patent literature. During the present report period, investigators have improved upon the properties of the discovered bone cement and have demonstrated that the cement paste can cure *in vivo* after being surgically injected. Other investigators studying transplant of hematopoietic cells in individuals after they have been exposed to radioactive, chemical, or biological weapons report the exploration of a new methodology for understanding the cellular components and process of hematopoiesis and post-transplant immune function. Investigators report the all primitive hematopoietic stem cells for transplantation can be detected, their "stemness" and numbers can not be maintained without an efficient and reproducible technique. Investigators also report a new method of killing leukemic cells that could provide a new adjunct anti leukemic therapy.

**Section 5: Anti-Submarine Warfare** (\$815,000, 2 component projects, 10 faculty/postdoc, 6 graduate/undergraduate students)

Among the component projects in the anti-submarine warfare section is the design and construction of a 2nd-generation, two-dimensional fluorimeter for rapid detection and speciation of organic compounds in seawater. The purpose of this detection is to recognize the presence of anthropogenic hydrocarbons associated with submarine activity, and to use this hydrocarbon signature for tracking purposes. For the present period investigators report the measurement of the first 2-D Fluorescence spectra with their instrument which is under development. Investigators have also demonstrated the use of 2-D fluorimetry in identifying water sources. Investigators studying wavelet-based algorithms to be used in anti-submarine warfare report seven (7) publications and/or technical reports and one Masters thesis during the present report period. Investigators further report that they have concentrated their efforts on the characterization of acoustic and electromagnetic scattering from surfaces and objects and continue their studies on Lattice Boltzmann models for advanced image processing algorithms.

**Section 6: Biodeterioration** (\$383,251, 1 component project, 6 faculty/postdoc, 8 graduate/undergraduate students)

The formation of biofouling communities on deployment devices, sensors, and on ship and submarine hulls represents a significant limitation to the efficient operation of instrumentation and vessels. Investigators studying biofouling control report the development of several methods to use combinatorial chemistry for depositing novel self-assembled monolayers (SAMs) on glass slides and microtiter plates. Investigators also report the development of methods for

quantifying microbial abundances by using microscopic image analysis. Although investigators have yet to identify a surface chemistry that resists bacterial attachment and colonization, they have demonstrated that different species attach to different surfaces within the first few days of exposure to seawater, and these differences diminish with time as colonization proceeds.

**Section 7: Supporting Research** (\$434,700, 1 component project, 2 faculty/postdoc, 4 graduate/undergraduate students)

Investigators developing a field-portable Laser-Induced-Breakdown-Spectroscopic (LIBS) system for elemental analysis report that fabrication of the instrument is essentially complete. LIBS spectra of alloys including samples of brass, steel, and aluminum have been obtained with the instrument and parametric studies have begun.

REPORT DOCUMENTATION PAGE		Form Approved OMB No. 0704-0188	
Public reporting burden for this collection of information is estimated to average 1 hour per response, including the time for reviewing instructions, searching existing data sources, gathering and maintaining the data needed, and completing and reviewing the collection of information. Send comments regarding this burden estimate or any other aspect of this collection of information, including suggestions for reducing this burden, to Washington Headquarters Services, Directorate for Information Operations and Reports, 1215 Jefferson Davis Highway, Suite 1204, Arlington, VA 22202-4302, and to the Office of Management and Budget, Paperwork Reduction Project (0704-0188), Washington, DC 20503.			
1. AGENCY USE ONLY (Leave blank)	2. REPORT DATE  1 Jun 1999	3. REPORT TYPE AND DATES COVERED  Annual	
4. TITLE AND SUBTITLE  University Research Initiative Program for Combat Readiness		5. FUNDING NUMBERS  Grant: N00014-97-0806 PR: 97PR06312-00	
6. AUTHOR(S)  Roger H. Sawyer			
7. PERFORMING ORGANIZATION NAME(S) AND ADDRESS(ES)  University of South Carolina		8. PERFORMING ORGANIZATION REPORT NUMBER  N00014-97-1-0806-1	
9. SPONSORING / MONITORING AGENCY NAME(S) AND ADDRESS(ES)  ONR		10. SPONSORING / MONITORING AGENCY REPORT NUMBER  ONR	
11. SUPPLEMENTARY NOTES			
12a. DISTRIBUTION / AVAILABILITY STATEMENT  Approved for public release		12b. DISTRIBUTION CODE	
13. ABSTRACT (Maximum 200 words)  The University Research Initiative for Combat Readiness includes nineteen (19) research and development projects relevant to combat readiness. Projects being supported by this initiative address six major DoD mission areas including: chemical and biological warfare, target acquisition and identification, anti-submarine warfare, combat medicine, biodeterioration, and command, control, and communications. These projects were selected for support based on an existing research capability that could be accelerated to create cost savings to the ONR by bringing results to the field earlier. For the present report period directors of the individual projects report one-hundred-fifty-six (156) publications in progress, in press, or submitted for publication.			
14. SUBJECT TERMS  Target Acquisition and Identification Chemical and Biological Defense Command, Control, and Communications Combat Medicine Anti-Submarine Warfare Biodeterioration Supporting Research		15. NUMBER OF PAGES  246	
		16. PRICE CODE	
17. SECURITY CLASSIFICATION OF REPORT  Unclassified	18. SECURITY CLASSIFICATION OF THIS PAGE  Unclassified	19. SECURITY CLASSIFICATION OF ABSTRACT  Unclassified	20. LIMITATION OF ABSTRACT  200 Words

# TABLE OF CONTENTS

## EXECUTIVE SUMMARY

## TABLE OF CONTENTS

<b>I. Target Acquisition and Identification .....</b>	<b>1</b>
1) Wavelet-Based Automatic Target Detection and Recognition.....	2
2) Wavelet-Based Image Processing for Military Applications .....	13
<b>II. Chemical and Biological Warfare.....</b>	<b>22</b>
1) Line-of-Sight Standoff Identification of Explosive Chemicals and Chemical Warfare Agents .....	23
2) Technology Development for Chemical Detection .....	43
3) Real-Time Biodetection Using PCR-MS .....	74
4) Small Molecule Transport Through Polymers: Effects of Polymer Inhomogeneity and Dynamics on the Nanometer Length Scale.....	82
5) The Design and Synthesis of Quantum Dot Based Lasers .....	93
6) Rapid Biodetection of Bacterial Cells by Laser Pyrolysis/Mass Spectrometry and Laser Spectroscopy .....	101
<b>III. Command, Control, and Communications .....</b>	<b>111</b>
1) Dynamic Decision Support for Command, Control, and Communication in the Context of Tactical Defense.....	112
2) Survivable and Reconfigurable Optical/Wireless Tactical Networks .....	124
3) Massively Parallel Optical Image Compression Using Optical Rank Annihilation .....	134
4) Molecular Scale Electronic Arrays for the Design of Ultra-Dense and Ultra-Fast Computational Systems .....	146
<b>IV. Combat Medicine .....</b>	<b>157</b>
1) Laboratory for Genetic Diagnosis and Control of Mosquitoes .....	158
2) Insure Access to Allogeneic Bone Marrow Transplantation for Correction of Marrow Failure and Hematologic Malignancies .....	171
3) Tissue-Engineered Cartilage and Advanced Bioadhesives for the Rapid Healing of Combat and Training Injuries to Bone .....	184
<b>V. Anti-Submarine Warfare.....</b>	<b>195</b>
1) Wavelet-Based Algorithms for Acoustic/Non-Acoustic Antisubmarine Warfare ...	196
2) Real-Time UV Fluorescence for Dissolved Hydrocarbon Tracking .....	203
<b>VI. Biodeterioration .....</b>	<b>215</b>
1) Accelerated Research in Biofouling Control.....	216
<b>VII. Supporting Research .....</b>	<b>233</b>
1) Development of a Field-Portable LIBS System for Elemental Analysis .....	234

**SECTION I: TARGET ACQUISITION AND IDENTIFICATION**

## **Wavelet-Based Algorithms for Automatic Target Detection and Recognition**

**Terry Huntsberger**

Intelligent Systems Laboratory  
Department of Computer Science  
University of South Carolina  
Columbia, SC 29208

Tel: (803)777-2404  
Fax: (803)777-3767  
Email: [terry@cs.sc.edu](mailto:terry@cs.sc.edu)

**Björn Jawerth**

Industrial Mathematics Initiative  
Department of Mathematics  
University of South Carolina  
Columbia, SC 29208

Tel: (803)777-6218  
Fax: (803)777-3783  
Email: [bj@math.sc.edu](mailto:bj@math.sc.edu)



## **Section 1-1: Wavelet-Based Algorithms for Automatic Target Detection and Recognition**

Terry Huntsberger and Björn Jawerth

### **ABSTRACT**

The current down-sizing of DoD manpower has led to the increased reliance on "smart" weapons for effective world-wide tactical response. These systems are based on autonomous and semi-autonomous (man-in-the-loop) techniques for acquisition, identification, targeting, tracking, and damage assessment. During the current contract period we have concentrated on the development of energy minimization methods, FIR/IIR filters, wavelet-based texture features, noise removal, and efficient methods for thermal signature simulation for automatic target detection and recognition.

### **FORWARD**

This project was funded for \$510, 000 for the period 1 Jun 1997 to 30 May 2000. We have decided to use the SKY Computer system with 4 PowerPCs/36 SHARC DSP chips for the implementation of the algorithms. This decision was made after consideration of Navy needs and examination of the algorithms. The system has been ordered and is to be shipped May 1, 1998. The original Year 1 Milestone was the port of our algorithms to the Intel Paragon system, which was postponed due to system downtime.

### **REPORT**

#### ***Statement of the problem***

The problem of decoupling target signatures from background clutter effects lies at the heart of robust ATD/R. Texture measures offer a means of detecting targets in background clutter despite similar spectral characteristics. The "fractal signature" (a feature set based on the fractal surface area function) has previously been shown to be very accurate and robust in multiband texture classification. Extension of this work into a wavelet-based algorithm was recently completed under DARPA funding. In addition, operations such as image enhancement can be performed very efficiently in the wavelet coefficient space.

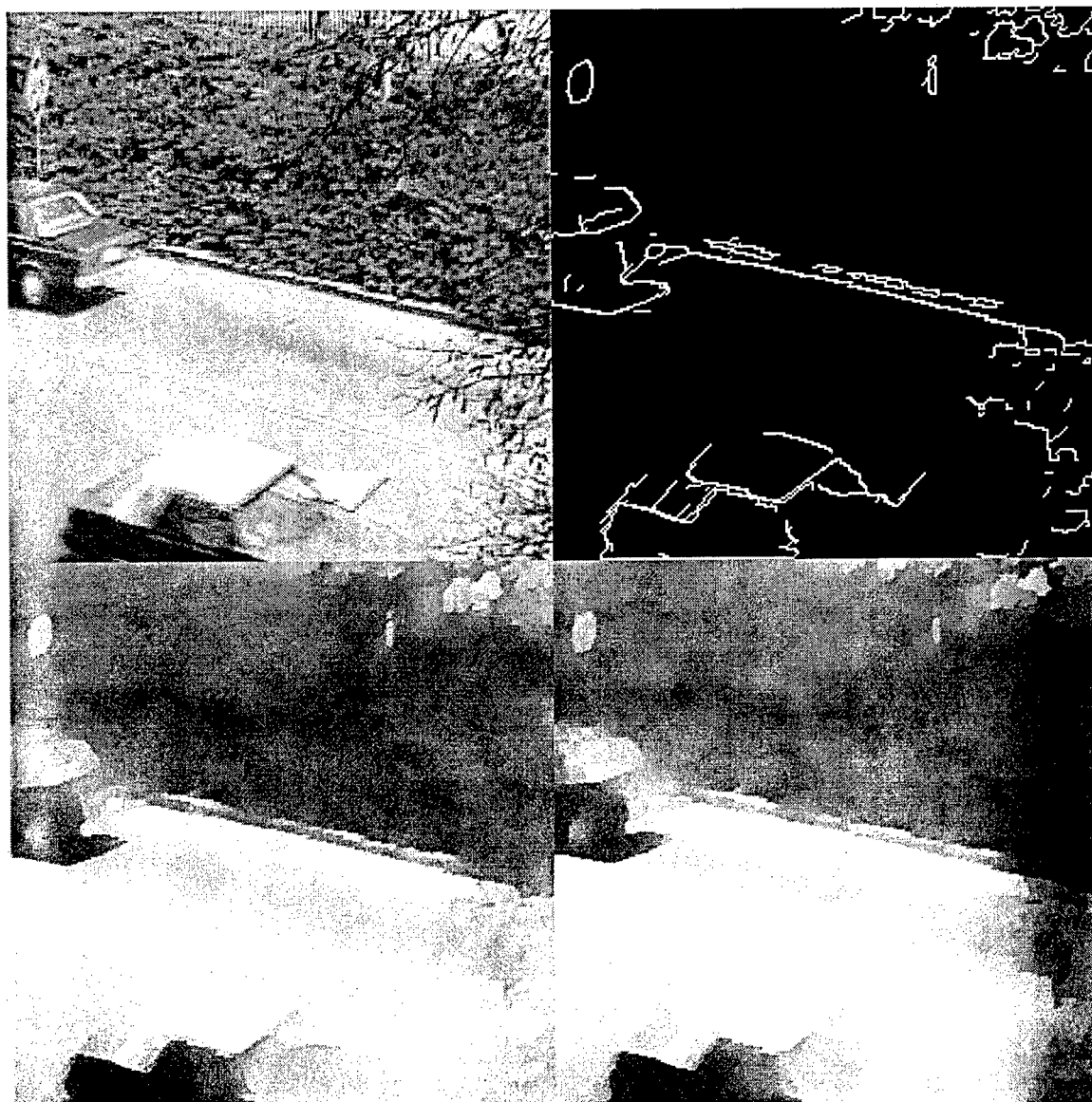
#### ***Summary of the Most Important Results***

##### **Efficient Parallelization of Relaxation Algorithms**

We have studied two parallelization approaches for image processing algorithms which are iterative, localized, and comprised of simple SIMD operations. The approaches are data-partitioning, exploring the spatial parallelism, and iterative pipelining - exploring the temporal parallelism of the algorithms. The former is suitable for either a massively parallel system, where each processor is assigned to a small number of pixels, or a system

with fast communication links, so that the inter-process communication overhead is small relative to the intra-process computation. The latter is suitable for a system with a circular inter-connection topology with fast communication links between two neighbors. This approach is more flexible, scalable, and applicable to any iterative algorithms in general.

The heterogeneous architecture and flexible configuration of its topology make the SKY BoltII system suitable for experimenting two different parallelization techniques. We have implemented two parallel versions of a boundary detection algorithm and the figure below shows the results.



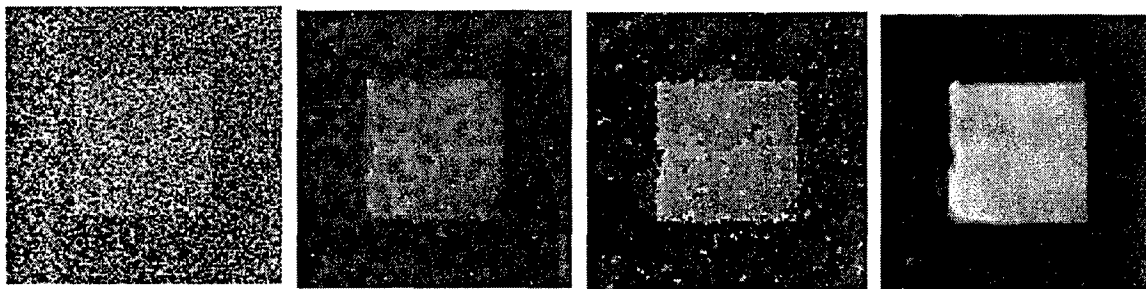
(Top-Left) test image. (Top-right) detected boundaries. (Bottom-left) surface fitting result using iterative pipelining. (Bottom-right) surface fitting result using data partitioning. Diffusion across partitioned regions is ignored.

### Directional Diffusion for Image Restoration

Assume that a 2D signal is corrupted with uncorrelated additive and multiplicative noise sources. It can be shown that given the gradient of the signal, we can remove noise and restore the original signal, within a constant offset and a constant scaling factor, by diffusing the noisy image along the direction perpendicular to the signal's gradient. We propose a method to estimate the signal gradient from the noisy image. It uses probabilistic relaxation and edge-based saliency measurement techniques to achieve a globally consistent gradient configuration.

The main advantages of estimating the gradient of the signal rather than estimating the signal directly are the following: 1) the edge information is often more important than the pixel information. Restoring the gradient is more direct in restoring the edge information; 2) global consistency can be established more easily on the edge information than the pixel information; 3) pixel based image restoration techniques often involves a combinatorial optimization process which is often computationally expensive.

Our study shows that the technique is more robust to noise than the Perona-Malik's non-linear diffusion and the Mumford-Shah boundary detection technique, and achieves an edge preserving stable state.



From left to right: Corrupted image, Perona-Malik's diffusion result, Mumford-Shah smoothing result, and Directional diffusion result.

### Wavelet-Based Object Tracking

Here, we have investigated a real-time target tracking technique in the wavelet domain. The wavelet transform provides a multi-resolution representation of the data which enables a faster block matching process. The technique employs Co-Occurrence Matrices (COM) of the wavelet coefficients to characterize each block and the Full Custom Texture Measurement (FCTM) algorithm for a similarity measure of two blocks.

The algorithm works very well with both high and low-speed motion, and the tracking is accurate whenever the object is distinguishable from the background or other overlapping objects. There is no need for manually changing any parameters when the object changes its speed. The history of the tracking makes it possible to compute the expected new location of the object, and concentrate our efforts in the matching process into a small search area, which speeds up the computations. The frames per second rate for the algorithm is 14 when wavelets and multi-resolution analysis are used, which categorizes it as a real-time object-tracking algorithm.



Results of the Wavelet Based Tracking Algorithm

### **Texture Characterization and Compression Using Wavelets and Auto-Regression**

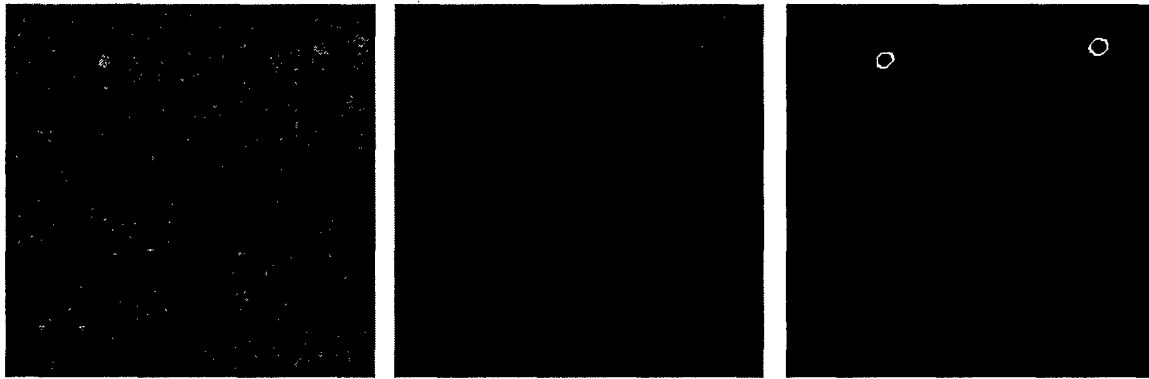
A unique texture oriented wavelet image compression scheme, which uses autoregressive texture segmentation and synthesis, has been studied. It first estimates the information that would be lost at the desired compression ratio. Estimation-minimization multi-resolution segmentation is performed on the residual estimate to identify distinct texture regions and to compute the model parameters necessary for texture synthesis. The model parameters are saved and the lost texture is synthesized and added back to the image during the reconstruction process. We have tested various AR models and found that the causal neighborhood size of 24 gives a good trade-off between the computational cost and the visual quality of a synthesized residual.

### **Pixel-Based Data Fusion for Multi-Spectral Images**

It is of practical importance to fuse data obtained by multiple sensors for improving the performance of computer vision systems. We have investigated a pixel-based data fusion algorithm on the variational framework. An adaptive system fuses data effectively using a process similar to probabilistic relaxation. Previously, we have introduced a technique to fuse gray-scale image and texture extracting features for segmenting an image with both textured and non-textured surfaces. We have extended the study for more general multi-valued data and improved the previous algorithm in terms of the performance and speed.

The main idea is to combine multi-spectra data using a normalized weight and adaptively adjust the weight, based on the energy measure known as the Mumford-Shah Model. A variational method is applied to minimize the energy with respect to the weight to obtain the "optimum" weight adaptively. Parallel to this, adaptive weight adjustment are data diffusion and discontinuity detection processes, whose objectives are also minimizing the same energy model.

Our experiments show that the technique improves noise immunity significantly. The figure below shows a result of the technique applied to a land minefield image of 3 spectra.



Results of pixel-based data fusion for boundary detection technique applied to a minefield image. The left image is the multi-spectra minefield image, the middle image is the result of edge preserving smoothing, and the right image is the result of boundary detection.

### **Land Mine Detection Using a Multi-Resolution Technique**

One of the challenging problems in minefield identification is identifying non-regular mine placement in clutter. In this work, we consider the detection of mines in cluttered background through multi-spectral image data. Our approach involves three steps: 1) estimation of targets through multi-resolution representations at each spectral data; 2) noise removal using the Maximum Noise Fraction transform; and 3) target detection through a majority voting. The multi-resolution image structures are obtained using the Mexican-Hat function at various scales. Our experiments demonstrated effectiveness of the technique in 3-band (thermal, radar, and visual) mine field images.

### **Wavelet-Based Image Matching and Indexing**

We have investigated a wavelet-based image matching and context-based indexing technique. The technique involves edge detection using a bi-orthogonal wavelet transform, edge tracing using a non-maximum suppression technique, and relaxation labeling using the Hopfield network to find the best match in the model database.

Extensive experiments are conducted to evaluate the performance of the algorithm. The wavelet transform achieves a good trade-off between data processing speed due to its compact data size, and relatively effective feature extraction.

### **Study of Reaction-Diffusion Based Image Formation**

This work investigates applicability of reaction-diffusion (RD) processes on various image processing/analysis problems. The RD based systems have been applied for image restoration and shape analysis. However, we believe that their potential has not been fully exploited. We have designed a GUI based image formation system using the Turing's RD equation. A user specifies the parameters of the equation and observes the dynamical development of two chemicals. This tool can be easily extended for more general RD systems to study the fundamental behavior of the systems.

### **Diffusion Based Neural Network Model**

This experimental work study the role of neural processing in the human pre-cortical visual system. We propose a neural network architecture where each cell is sensitive to an edge at a particular orientation within its receptive field. The network is fully connected from each cell to its neighbors of all orientations. Our goal is to design a three dimensional reaction-diffusion system where the diffusion process is anisotropic with its direction determined by the cell's preferred orientation and to achieve perceptual grouping of edges as well as surface diffusion. The system is a competitive process between excitatory chemical and inhibitory chemical. One of the main limitations of existing edge grouping algorithms is that they are either strictly global or have a pre-defined and fixed range of interactions. The RD system only involves local operations, therefore feasible at the pre-cortical level, and does not have a such range limitation.

### **Image Stitching**

In industrial design computer aided geometric design (CAGD) has played a very important role for several decades. Three dimensional objects in CAGD are often represented by a large number of aligned surface patches, forming the surface of the object. Oftentimes these patches are not aligned correctly resulting in small gaps, or errors, between adjacent patches. Our goal is to develop algorithm both for detecting these gaps as well as stitching non-aligned patches together. We have developed a method for measuring the distance between two patches. More specifically we have defined a distance function between two curves corresponding to the boundaries of the patches. We have also been investigating, and intend to further improve, different stitching techniques.

The ability to detect non-aligned patches is applicable to target detection since human designed objects (such as trucks, tanks etc) are often made of flat surfaces at different angles.

### ***Publications and Technical Reports***

1. T. Kubota and T. L. Huntsberger, "Edge dipole and edge field for boundary detection," in *Proc. SPIE Conf. Hybrid Image and Signal Processing VI*, Vol. 3389, Orlando, FL, Apr 1998.
2. F. Espinal and R. Chandran, "Wavelet-based fractal signature for texture classification," in *Proc. SPIE Conf. on Wavelet Applications V*, Vol. 3391, Orlando, FL, Apr 1998.
3. T. Kubota and T. L. Huntsberger, "Adaptive pattern recognition system for scene segmentation," *Optical Engineering, Special Section on Advances in Pattern Recognition*, Vol. 37, No. 3, pp. 829-835, 1998.
4. F. Espinal, T. L. Huntsberger, B. Jawerth, and T. Kubota, "Wavelet-based fractal signature analysis for automatic target recognition," *Optical Engineering, Special Section on Advances in Pattern Recognition*, Vol. 37, No. 1, pp. 166-174, 1998.
5. G. Fernandez and T. L. Huntsberger, "Wavelet-based system for recognition and labeling of polyhedral junctions," *Optical Engineering, Special Section on Advances in Pattern Recognition*, Vol. 37, No. 1, pp. 158-165, 1998.
6. T. Kubota, T. L. Huntsberger and C. O. Alford, "A vision system with real-time feature extractor and relaxation network," to appear in *Int. Journal Pattern Recognition and Artificial Intelligence*, May 1998.
7. T. L. Huntsberger and J. Rose, "Computer Simulation of Bimodal Neurons and Networks: Integrating Infrared and Visual Stimuli," chapter in Computer Simulation of Complex Biological Systems, (Ed. I. S. Iyengar), CRC Press, 1998.
8. T. L. Huntsberger, "Autonomous multirover system for complex planetary retrieval operations," in *Proc. SPIE Symposium on Sensor Fusion and Decentralized Control in Autonomous Robotic Agents*, Vol. 2905, Pittsburgh, PA, Oct 1997, pp. 11-17.
9. B.D. Jawerth, P. Lin, and E.D. Sinzinger, "Lattice Boltzmann methods for anisotropic diffusion of images", *Mathematical Imaging*, in review.
10. K. Debure and T. Kubota, "Autoregressive Texture Segmentation and Synthesis for Wavelet Image On Compression", 10th Image and Multidimensional Digital Signal Processing Workshop, July 1998, Austria.
11. S. Godavarthy and T. L. Huntsberger, "Global illumination using Overlapping Wavelets", *Proc. 8th International Conference on Engineering Computer Graphics and Descriptive Geometry (ICECGDG)*, Aug 1998, Austin, TX.
12. M. Frank, K.O. Vik, "Image Stitching", Master's Thesis, Chalmers University of Technology, Sweden.

### ***Participating Personnel***

Dr. Terry Huntsberger, PI  
Dr Björn Jawerth, co-PI  
Dr. Toshiro Kubota  
Dr. Weimin Zheng  
Dr. Peng Lin  
Fausto Espinal

Srinadh Godavarthy  
Rajesh Chandran  
Ognian Voynikov  
Henrik Storm  
Goran Kronquist

## BIBLIOGRAPHY

- [BEYL95] G. Beylkin "On factored FIR approximation of IIR filters", *Applied and Computational Harmonic Analysis*, Vol. 2, pp 293-298, 1995
- [BOUM91] C. Bouman and B. Liu, "Multiple resolution segmentation of textured images", *IEEE Trans. Pattern Recog. and Machine Intel.*, Vol. 13, pp. 259-302, 1991.
- [BURT89] P. J. Burt, "Multiresolution techniques for image representation analysis, and 'smart' transmission", *Proc. SPIE Conf. on Visual Communication and Image Processing*, pp. 2-15, 1989.
- [CANN86] J. F. Canny, "A computational approach to edge-detection", *IEEE Transaction on Pattern Analysis and Machine Intelligence*, Vol. 8, pp. 679-700, 1986.
- [FREE91] W. T. Freeman and E. H. Adelson, "The design and use of steerable filters", *IEEE Trans. Pattern Analysis and Machine Intel.*, Vol. 13, pp. 401-412, 1991.
- [JAIN77] A. K. Jain, "Partial differential equations and finite difference methods in image processing-Part I: Image representation", *J. Optimiz. Theory and Applications*, Vol. 23, pp. 65-91, 1977.
- [JAIN78] A. K. Jain and J. R. Jain, "Partial differential equations and finite difference methods in image processing-Part II: Image restoration", *IEEE Trans. on Automatic Control*, Vol. 23, pp. 596-613, 1978.
- [LAWS80] K. I. Laws, "Rapid texture identification", *Proceedings of SPIE*, Vol. 238, pp. 376-380, 1980.
- [MARR82] D. Marr, *Vision*, W. H. Freeman and Company, San Francisco, CA. 1982.
- [MUMF89] D. Mumford and J. Shah, "Optimal approximation by piecewise smooth functions and associated variational problems", *Communications on Pure and Applied Mathematics*, pp. 577-685, 1989.
- [PERO90] P. Perona and J. Malik, "Scale-space and edge detection using anisotropic diffusion", *IEEE Trans. Pattern Analysis and Machine Intel.*, Vol. 12, pp. 629-639, 1990.
- [RIOU91] O. Rioul and M. Vetterli, "Wavelets and signal processing", *IEEE Signal Processing Magazine*, pp. 14-38, Oct 1991.
- [SAIT96] N. Saito and R. R. Coifman, "Improved Local Discriminant Bases using empirical probability density estimation, in Proc. Conf. on Statistical Computing, American Statistical Assoc., 1996.
- [SIMO92] E. P. Simoncelli, W. T. Freeman, E. H. Adelson and D. J. Heeger, "Shiftable Multiscale Transforms", *IEEE Trans. on Information Theory*, Vol. 38, pp. 587-607, 1992.



[WATS87] A. B. Watson, "The cortex transforms: rapid computation of simulated neural images", *Computer Vision, Graphics, and Image Processing*, Vol. 39, pp. 311-327, 1987.

[YOUN87] R. A. Young, "The gaussian derivative model for spatial vision: I. Retinal mechanism", *Spatial Vision*, Vol. 2, pp. 273-293, 1987.

University Research Initiative Program for Combat Readiness  
Annual Report 06/01/98-05/31/99

PART 53-FORMS

53.301-298

<b>REPORT DOCUMENTATION PAGE</b>		Form Approved OMB No. 0704-0188	
Public reporting burden for this collection of information is estimated to average 1 hour per response, including the time for reviewing instructions, searching existing data sources, gathering and maintaining the data needed, and completing and reviewing the collection of information. Send comments regarding this burden estimate or any other aspect of this collection of information, including suggestions for reducing this burden, to Washington Headquarters Services, Directorate for Information Operations and Reports, 1215 Jefferson Davis Highway, Suite 1204, Arlington, VA 22202-4302, and to the Office of Management and Budget, Paperwork Reduction Project (0704-0188), Washington, DC 20503.			
1. AGENCY USE ONLY (Leave blank)	2. REPORT DATE June 1, 1999	3. REPORT TYPE AND DATES COVERED Annual	
4. TITLE AND SUBTITLE Wavelet-Based Automatic Target Detection and Recognition		5. FUNDING NUMBERS Grant Number N00014-97-1-0806 PR Number 97PR06312-00 PO Code 353 Disbursing Code N68892 AGO Code N66020 Cage Code 4B489	
6. AUTHOR(S) PI: Björn Jawerth			
7. PERFORMING ORGANIZATION NAME(S) AND ADDRESS(ES) University of South Carolina		8. PERFORMING ORGANIZATION REPORT NUMBER N00014-97-1-0806-1	
9. SPONSORING / MONITORING AGENCY NAME(S) AND ADDRESS(ES) ONR		10. SPONSORING / MONITORING AGENCY REPORT NUMBER ONR	
11. SUPPLEMENTARY NOTES Prepared in coordination with University Research Initiative Program for Combat Readiness			
12a. DISTRIBUTION / AVAILABILITY STATEMENT APPROVED FOR PUBLIC RELEASE		12b. DISTRIBUTION CODE	
13. ABSTRACT (Maximum 200 words) The current down-sizing of DoD manpower has led to the increased reliance on "smart" weapons for effective world-wide tactical response. These systems are based on autonomous and semi-autonomous (man-in-the-loop) techniques for acquisition, identification, targeting, tracking, and damage assessment. During the current contract period we have concentrated on the development of energy minimization methods, FIR/IIR filters, wavelet-based texture features, noise removal, and efficient methods for thermal signature simulation for automatic target detection and recognition.			
14. SUBJECT TERMS Antisubmarine Warfare, Wavelets		15. NUMBER OF PAGES 10 pages	
		16. PRICE CODE	
17. SECURITY CLASSIFICATION OF REPORT  UNCLASSIFIED	18. SECURITY CLASSIFICATION OF THIS PAGE  UNCLASSIFIED	19. SECURITY CLASSIFICATION OF ABSTRACT  UNCLASSIFIED	20. LIMITATION OF ABSTRACT  200 words

NSN 7540-01-280-5500

Standard Form 298 (Rev. 2-89)  
Prescribed by ANSI Std. Z39-18  
298-102

## **Wavelet-Based Image Processing for Military Applications**

Ronald A. DeVore

Department of Mathematics  
University of South Carolina  
Columbia, SC 29208

Tel: (803)777-2632  
Fax: (803)777-6527  
Email: [devore@math.sc.edu](mailto:devore@math.sc.edu)

## **Section 1-2: Wavelet Based Image Processing for Military Applications**

**Ronald A. DeVore**

### **ABSTRACT**

The Principal Investigator, Ronald A. DeVore, and other researchers at USC's Department of Mathematics, are developing wavelet based image processing for automated target recognition and related military applications including autonomous landing of aircraft, registration of images from a database, and identification of cracks in skin of aircraft.

The goal of this research is to substantially reduce imaging times for signal, image, and graphical databases which will enable the real-time processing of images for the purposes of image registration and feature extraction.

An 'end-to-end' image processing environment for these applications is being created by developing fast wavelet based algorithms for the generic problems of image compression, denoising, feature extraction and pattern recognition, image registration and correlation, path tracking and motion detection.

The first two years of this project has seen significant advances in the development of the image processing environment by using adaptive basis selection and greedy algorithms; nonlinear algorithms for compression and noise removal derived from functional analytic extremal problems; and customized encoders.

The third year of the project will proceed with the implementation of adaptive basis techniques including wavelet packets and greedy algorithms. The research will focus on the processing of Digital Terrain Elevation Data (DTED). The DTED maps are important in many military scenarios and provide a robust and challenging environment which can test the newly created image processing environment.

### **FORWARD**

The second year of the project was supported from 1 Jul 1998 through 30 Jun 1999 at a level of \$146,000, with a total three year budget of \$440,001. Basic research on Automatic Target Detection was performed with significant advances made on noise removal and feature extraction. This includes:

- Development of wavelet based methods to solve extremal problems for noise reduction.
- Development of highly nonlinear methods (greedy algorithms) for feature extraction.

- Development of tree encoding algorithms for compression including burning in.
- Rendering of surfaces for DTED maps.

## REPORT

### *Statement of the problem*

The goal of this research is to develop an 'end-to-end' image processing environment to handle in real time the generic tasks encountered in Automated Target Detection (ATD) and related military applications. The research undertaken includes the derivation of complementary theory and algorithms for automated target detection, rapid retargeting, the registration of digitized images, rapid data query and data navigation.

### *Summary of the Most Important Results*

Major advances were made during Years 1 and 2 of this grant through the development of highly nonlinear approximation theoretic techniques which form the foundation of an 'end to end' image processing environment for Automatic Target Detection (ATD). These advances provide direct applications to advanced data compression algorithms, noise removal, feature extraction/registration, greedy algorithms, adaptive pursuit, and neural networks, brief descriptions of which are provided below. This project collaborated with the Naval Air Warfare Center (NAWC) at both PAX River and China Lake through workshops and extended site visits.

### Image Processing

**Entropy encoding and compression.** Compression is a vital component of Automatic Target Recognition (ATR), providing real time communication of images and serving as a preprocessor to other image processing tasks. We have used nonlinear wavelet approximation in our past work to design compression algorithms for images and signals. More recently, we have collaborated with Cohen (Paris VI), Daubechies (Princeton), and Dahmen (RWTH Aachen) [CDDD] to design tree based encoders which have optimal compression properties. The advantage of the tree based algorithm is that more structure results in the encoded file which allows not only high compression but provides a platform for progressive transmission of the image. In other words, a coarse resolution of the image is followed by finer and finer detail. This platform also allows for local refinement ('burning in' to find finer detail in selected localized regions of the image). We have also been successful in describing the performance and potential savings of tree encoding [BDKY]. On another related front, we have developed compression methods [GAS] which can be utilized to compress data in arbitrary dimensions. These techniques find applications in video as well as scientific data query.

**Image processing using statistical characteristics.** Several optimization problems occur in noise removal. One such extremal problem consists of finding minimizers for the K-functional for  $L_2$  and BV (functions of bounded variation). Techniques for finding minimizers for this functional based on variational calculus and

nonlinear partial differential equations have been put forward by several authors (most notably [DMS], [LOR], [MS], [CL]). The main disadvantage of these approaches is that they are numerically intensive. In [CDPX], we prove the surprising result that wavelet thresholding is a minimizer for the K-functional. The proof is deep and depends on a new adaptive algorithm for nonlinear piecewise constant approximation. Our analysis of this extremal problem exposes many interesting properties of Haar decompositions in the space BV. We are now numerically implementing these ideas. We have also applied our results from restricted approximation to analyze [CDKP] noise reduction methods based on thresholding

**Feature extraction and registration.** In [DLY] we previously developed wavelet based methods for extracting microcalcification clusters in mammograms. These techniques utilize image enhancement, very high compression for noise suppression, and pixel enhancement. Using similar ideas, we have developed in [D et al.] wavelet methods for image registration. The method identifies a few hot pixels in the image and registers two images by hot pixels matching. The software implementation currently applies only to images which are affine transformations of one another, but other transformations are being investigated.

### **Nonlinear Approximation**

In our previous work, ideas from nonlinear approximation have provided fundamental insight and advances to several different areas, including image processing, nonlinear PDE's, function spaces, and statistics. Our current interest is focused on highly nonlinear approximation, which includes approximation from libraries (families) of bases and dictionaries (redundant systems).

**Greedy algorithms and adaptive pursuit.** Adaptive pursuit from a dictionary of functions is used frequently in feature extraction. We analyze the theoretical advantages and disadvantages of these highly nonlinear methods. Our main goal is to construct simple and efficient algorithms which provide near best m-term approximation. DeVore and Temlyakov [DT], [DT1], [T], [T1], [T3], [T4], have analyzed the problem in various different settings. Temlyakov [T] proves that greedy type algorithms realize near best m-term approximation in  $L_p$ ,  $1 < p < \infty$ , from the multivariate Haar system and other systems equivalent to the Haar system. In [T3], it is shown, however, that this is not valid for the trigonometric system, nevertheless, the greedy algorithm realizes the best m-term approximation for wide variety of function spaces. In fact, DeVore and Temlyakov [DT] have established a universal estimate for the accuracy of the greedy algorithm. In [T1] a sufficient condition on dictionaries is provided which guarantees that the greedy algorithm gives the order of the best approximation. We have initiated a study of a new set of greedy algorithms which are defined by weaker assumptions and therefore more amenable to practical implementation. We have proved for these algorithms convergence theorems and have given estimates for their rate of approximation. The

convergence and the estimates apply to approximation from an arbitrary dictionary in a Hilbert space.

**Restricted nonlinear approximation.** We have recently considered restricted nonlinear wavelet approximation since it appears naturally in image processing, and in particular noise reduction. Cohen, DeVore, and Hochmuth [CDH] characterize the approximation spaces for restricted nonlinear  $n$ -term wavelet approximation. The results provide the basis to establish theorems about interpolation of Besov spaces which required the development of new techniques for nonlinear wavelet approximation.

**Kolmogorov' widths.** Temlyakov [T3] investigates a generalization of Kolmogorov' width that is suitable for estimating best  $m$ -term approximation. He generalizes Carl's inequality which gives a lower bound estimate for Kolmogorov's widths in terms of the entropy numbers. Some relations between best  $m$ -term approximation and the entropy numbers are also given in [DT].

### Neural Networks

Neural networks are frequently used in statistical decision theory, classification, and feature extraction. Our main goal in this research is to understand their advantages over more traditional numerical methods. In [DOP], we give the first tight theorems on linear approximation by neural networks. An interesting fact was discovered that the feed-forward neural network with one hidden layer of computational nodes given by the unit impulse function has efficiency of approximation  $O(n^{-3/2})$  in two dimensions. Petrushev [P] generalized this result to arbitrary space dimension. New areas and techniques were developed and utilized. These include (a) the Radon transform, (b) orthogonal decomposition of a general function into ridge polynomials, (c) quadrature formulas on the sphere exact for spherical polynomials of degree  $n$ .

Oskolkov [O], [O1] elaborates Radon-Fourier analysis with special emphasis on comparison of free (nonlinear) and equispaced ridge approximation. He established exact duality relations of the problem of ridge approximation and optimization of quadrature formulas. This interpretation enabled him [O], in particular, to obtain lower estimates of free ridge approximation via equispaced one for radial functions. A new and unexpected result was recently proved by Oskolkov [O1] in this direction for harmonic functions. It turns out that freedom in the choice of the wave vectors in unconstrained ridge approximation brings a quite essential gain in the orders of approximation. For each fixed harmonic function, free ridge approximations are 'square times' more efficient than equispaced ones, with the same admissible number of wave vectors along a parallel path, a new effect of collapsed nodes in optimization of quadrature formulas was discovered. The highest harmonic in a band limited signal (trigonometric polynomial) can be recovered with high accuracy even in conditions of an essential deficiency of point values of the signal.

Another important result was established jointly by V. Maiorov, K. Oskolkov and V. Temlyakov [MOT] in qualitative and quantitative theory of greedy algorithms for ridge approximation. (They introduced a new term "gridge approximation" for this circle of problems, where greedy algorithm is applied for approximation of functions of several variables using the dictionary of ridge functions.) Namely, they indicated an effective tool called "Radon compass" which realizes the stepwise optimal choice of both wave vectors and wave profiles. Radon compass is intimately related with Fourier-Chebyshev realization of the Radon inversion operator. Quantitatively, it was discovered that gridge approximation orders are not saturated. More than that, gridge approximation orders are algebraic polynomial ones.

The results of DeVore and Temlyakov [DT1] on greedy algorithms also have strong implications for nonlinear neural networks.

### **Wavelet Bases:**

These bases form the fundamental decompositions used in our image processing algorithms. We are interested in having the most flexible collection of bases in order to have the most robust image processing methods. In this direction, Petrushev [P1] proved the existence of a Schauder basis for  $C[0,1]$  consisting of rational functions of uniformly bounded degrees. This solves an open question of some years concerning the possible existence of such bases. This result follows from a more general construction of bases on  $\mathbb{R}$  and  $[0,1]$ . It is proved that the new bases are unconditional bases for  $L_p$ ,  $1 < p < \infty$ , and Besov spaces. On  $[0,1]$ , they are Schauder bases for  $C[0,1]$  as well. These results are generalized in the  $d$ -dimensional case ( $d > 1$ ) and for other spaces. The new bases are utilized to nonlinear approximation.

### **Publications and Technical Reports**

#### **Papers in Print**

- [DSPKLC] R. DeVore, W. Shao, J. F. Pierce, E. Kaymaz, B. Lerner, and W. J. Campbell, *Using nonlinear wavelet compression to enhance image registration*, SPIE, Vol. 3078, Orlando, FL (1997).
- [DOP] R. DeVore, K. Oskolkov, and P. Petrushev, *Approximation by feed-forward neural networks*, Ann. Numer. Math. 14 (1997), 261-287.
- [DT] R. DeVore and V. Temlyakov, *Nonlinear approximation in finite-dimensional spaces*, J. Complexity 13 (1997), 489-508.
- [O] K. Oskolkov, *Ridge approximation, Chebyshev-Fourier analysis and optimal quadrature formulas*, Proc. Steklov Inst. Math. 219 (1997), 269-285.
- [O1] K. Oskolkov, *Schroedinger equation and oscillatory Hilbert transforms of second degree*, The Journal of Fourier Analysis and Applications, vol. 4, issue 3, 1998, pp. 341-356.



- [P] P. Petrushev, *Approximation by Ridge Functions and Neural Networks*, SIAM J Math. Anal., 30 (1998), 155-189.

#### Papers in Press

- [CDH] A. Cohen, R. DeVore, and R. Hochmuth, *Restricted nonlinear approximation*, Constructive Approximation.
- [CDPX] A. Cohen, R. DeVore, P. Petrushev, and H. Xu, *Nonlinear approximation and the space  $BV(R_2)$* , American Journal of Mathematics.
- [O2] K. Oskolkov, *Non-linearity versus linearity in ridge approximation*, IMI series report 1998:06 (USC), 28 p. to appear (in Russian) in the volume "Contemporary Problems of Function Theory and Harmonic Analysis", dedicated to the 70<sup>th</sup> anniversary of P.L. Ul'yanov, Russian Academy of Sciences.
- [O3] K. Oskolkov, *Ridge Approximation and Kolmogorov-Nikol'skii Problem*, IMI series report 1998:03 (USC), to appear (in Russian) in Russian Mathematics Doklady.
- [T] V. Temlyakov, *The best  $m$ -term approximation and greedy algorithm*, Advances in Comp. Math., to appear.
- [T1] V. Temlyakov, *Nonlinear  $m$ -term approximation with regard to the multivariate Haar system*, East J. on Approximations, to appear.
- [T2] V. Temlyakov, *Nonlinear Kolmogorov's widths*, Math. Notes, to appear.
- [T3] V. Temlyakov, *Greedy algorithm and  $m$ -term trigonometric approximation*, Constructive Approximation, to appear.

#### Papers Submitted

- [CDKP] A. Cohen, R. DeVore, G. Kerkyacharian, D. Picard, *Maximal spaces with given rate of convergence for thresholding*.
- [CDDD] A. Cohen, W. Dahmen, I. Daubechies, and R. DeVore, *Tree approximation with applications to encoding and Kolmogorov entropy*, preprint.
- [O1] K. Oskolkov, *Non-linear versus linearity in ridge approximation*, preprint.
- [GAS] Z. Gao, A. Andreev and R.C. Sharpley, *Data Compression and Elementary Encoding of Wavelet Coefficients*.
- [MOT] V. Maiorov, K. Oskolkov, and V. Temlyakov, *On Gridge Approximation*, preprint.
- [P1] P. Petrushev, *Bases consisting of rational functions of uniformly bounded degrees or more general functions*, preprint.
- [T4] V. Temlyakov, *Greedy algorithms and  $m$ -term approximation with regard to redundant dictionaries*, preprint.
- [T5] V. Temlyakov, *Weak greedy algorithms*, preprint

#### BIBLIOGRAPHY

- [B] A. Barron, *Universal approximation bounds for superposition of sigmoidal functions*, IEEE Transactions on Information Theory 39 (1993), 930-945.
- [CL] A. Chambolle and P.-L. Lions, *Image recovery via total variation minimization and related problems*, Numerische Mathematik 76 (1997), 167-188.
- [DLY] R. DeVore, B. Lucier, and Z. Yang, *Feature extraction in digital mammography*, Wavelets in Biology and Medicine (Akram Aldroubi and Michael Unser, eds.), CRC, Boca Rotan, Florida (1996), 145-161.
- [DMS] G. Dal Maso, J.-M. Morel and S. Solimini, *A variational method in image segmentation: existence and approximation results*, Acta Math. 168 (1992), 89-151.
- [DT1] R. DeVore and V. Temlyakov, *Some remarks on greedy algorithms*, Advances in Computational Math. 5 (1996), 173-187.
- [LOR] P.-L. Lions, S. Osher, and L. Rudin, *Denoising and deblurring using constrained nonlinear partial differential equations*, SIAM J. Numer. Anal., to appear.
- [MS] D. Mumford and J. Shah, *Boundary detection by minimizing functionals*, Proc. of IEEE Conf. on Computer Vision and Pattern Recognition, IEEE, 1985, pp. 22-26.

**University Research Initiative Program for Combat Readiness**  
**Annual Report 06/01/98-05/31/99**

PART 53-FORMS

53.301-298

<b>REPORT DOCUMENTATION PAGE</b>		Form Approved OMB No. 0704-0188	
Public reporting burden for this collection of information is estimated to average 1 hour per response, including the time for reviewing instructions, searching existing data sources, gathering and maintaining the data needed, and completing and reviewing the collection of information. Send comments regarding this burden estimate or any other aspect of this collection of information, including suggestions for reducing this burden, to Washington Headquarters Services, Directorate for Information Operations and Reports, 1215 Jefferson Davis Highway, Suite 1204, Arlington, VA 22202-4302, and to the Office of Management and Budget, Paperwork Reduction Project (0704-0188), Washington, DC 20503.			
1. AGENCY USE ONLY (Leave blank)	2. REPORT DATE June 1, 1999	3. REPORT TYPE AND DATES COVERED Annual	
4. TITLE AND SUBTITLE  Wavelet Based Image Processing for Military Applications		5. FUNDING NUMBERS Grant Number N00014-97-1-0806 PR Number 97PR06312-00 PO Code 353 Disbursing Code N68892 AGO Code N66020 Cage Code 4B489	
6. AUTHOR(S) Ronald A. DeVore			
7. PERFORMING ORGANIZATION NAME(S) AND ADDRESS(ES) University of South Carolina Columbia, South Carolina 29208		8. PERFORMING ORGANIZATION REPORT NUMBER N00014-97-1-0806-2	
9. SPONSORING / MONITORING AGENCY NAME(S) AND ADDRESS(ES) ONR 800 N. Quincy Street Arlington, VA 22217		10. SPONSORING / MONITORING AGENCY REPORT NUMBER ONR	
11. SUPPLEMENTARY NOTES Prepared in coordination with University Research Initiative Program for Combat Readiness			
12a. DISTRIBUTION / AVAILABILITY STATEMENT APPROVED FOR PUBLIC RELEASE		12b. DISTRIBUTION CODE	
13. ABSTRACT (Maximum 200 words) Research was conducted on fundamental problems related to Automated Target Recognition (ATR). Immediate applications include the image processing tasks of compression, noise reduction, feature extraction, image registration, and target identification. Wavelet based multiscale methods were emphasized since they provide a uniform platform for the various tasks. Nonlinear and highly nonlinear methods have been developed for these tasks using recent advances of the researchers at USC in the areas of nonlinear wavelet approximation. This includes greedy algorithms, adaptive basis selection and adaptive pursuit. Emphasis was placed on fast algorithms which can be implemented in real time scenarios.			
14. SUBJECT TERMS Chemical and Biological Warfare, Target Acquisition, Anti-Submarine, Combat Medicine, Biodeterioration, and Command Control and Communication		15. NUMBER OF PAGES 8	
		16. PRICE CODE	
17. SECURITY CLASSIFICATION OF REPORT UNCLASSIFIED	18. SECURITY CLASSIFICATION OF THIS PAGE UNCLASSIFIED	19. SECURITY CLASSIFICATION OF ABSTRACT	20. LIMITATION OF ABSTRACT

NSN 7540-01-280-5500

Standard Form 298 (Rev. 2-89)  
Prescribed by ANSI Std. Z39-18  
298-102

**SECTION II: CHEMICAL AND BIOLOGICAL WARFARE**

**Line-of-Sight Standoff Identification of Explosive Chemicals and  
Chemical Warfare Agents**

S. Michael Angel and Michael L. Myrick

Department of Chemistry and Biochemistry  
University of South Carolina  
Columbia, SC 29208

Tel: (803) 777-2779  
Fax: (803) 777-9521  
Email: angel@psc.sc.edu  
myrick@psc.sc.edu

## **Section 2-1: Line-of-Sight Standoff Identification of Explosive Chemicals and Chemical Warfare Agents**

S. Michael Angel and Michael L. Myrick (Co-Investigators)

### **ABSTRACT**

This work is divided into two main areas. 1) development of the technology for optical detection and identification of chemical agents using absorbance/reflectance spectroscopy in the NIR/MID spectroscopic regions, combined with optical computation pattern recognition. 2) demonstration of a standoff instrument for identification of dangerous chemicals using a small-footprint Raman spectrometer with an LCTF, and demonstrate the use of polymer mirrors for remote Raman. In the first area, we have hired a postdoctoral assistant, who will be arriving from China within the month. We have developed an improved optical methodology for detecting plumes using chemical imaging based on serpentine fiber-optic image dissection arrays. In the second area, the LCTF instrument was purchased and debugged, and the small footprint Raman system was tested for standoff operation at USC and at an Air Force Test Station. Remote Raman measurements were made using this system in collaboration with The University of Hawaii Institute of Geophysics using their mobile LIDAR system and laboratory instruments. A new type of light-wave mirror, made using an epoxy composite, was tested for remote Raman measurements.

### ***Statement of the problem***

The purpose of the first project area is to develop the technology for optical detection and identification of chemical agents using absorbance/reflectance spectroscopy in the NIR/MID spectroscopic regions combined with optical computation pattern recognition. We have also included fiber-array spectroscopic imaging as a viable approach to line-of-sight imaging of chemical plumes. The purpose of the second project area is to develop and test instruments that might be used for standoff identification of explosives and CW agents using laser-induced remote Raman spectroscopy. Specifically, we will build and test a small remote Raman system in terms of sensitivity and range. The unique aspect of the system is the use of an LCTF for spectral discrimination, and fiber-optically coupling the optics and detection system. The NIR study was dropped because of the inability to track stars in the windy conditions at Bellows. Fortunately, we were able to add a new, more relevant task while at Bellows. In this task we made remote Raman measurements using novel light-weight polymer mirrors for stand-off Raman spectroscopy as an alternative to the use of more conventional glass mirrors. The polymer mirror is dramatically lighter and cheaper to make than a comparable glass mirror. However, its

performance for remote spectroscopy is excellent. This has the potential for reducing the cost and size of a remote Raman or fluorescence system dramatically.

### ***Summary of the Most Important Results***

**Area 1** (This work is being performed by Dr. Myrick's research group)

#### **Introduction.**

Multivariate analysis (called "chemometrics" in the chemical literature) is a pattern recognition method.[1-6] We can use an example from music to explain its application. If we consider a symphony as an example, a traditional scientific analysis might attempt to isolate the use of specific notes in the orchestration in order to determine the composer of the symphony. For instance, we might focus on the tone A-flat to determine whether Bach or Beethoven is the composer of the music, clearly a difficult task. On the other hand, these two composers have considerably different musical modalities, obvious to even casual listeners by the patterns in their music. Multivariate analysis permits data analysis to "hear the music" in a complex optical data set, rather than focusing on single wavelengths of light for interpretation.

An illustration of how multiwavelength (multivariate) analysis helps to resolve patterns in a data set is shown in Figure 1 above. On the left is shown a set of hypothetical spectra obtained for two chemical species of interest with an unknown amount of an "interferent" added. If we consider three individual wavelengths from the data set and plot each spectrum in a three-dimensional space as a point with coordinates given by the intensities on those three wavelengths, we obtain the middle picture. There is no clear pattern observed for these samples. However, if we rotate the middle data cube slightly, we can find a special viewing direction that makes our spectroscopy "simple" - i.e., independent of the interference. The right-hand figure shows just such a rotation. In principle we can do this with any data set, although complex data sets will require more than three dimensions (difficult to show on paper, but simple for a computer to process quickly). Once we find the important directions in the data set, we can properly interpret the data.

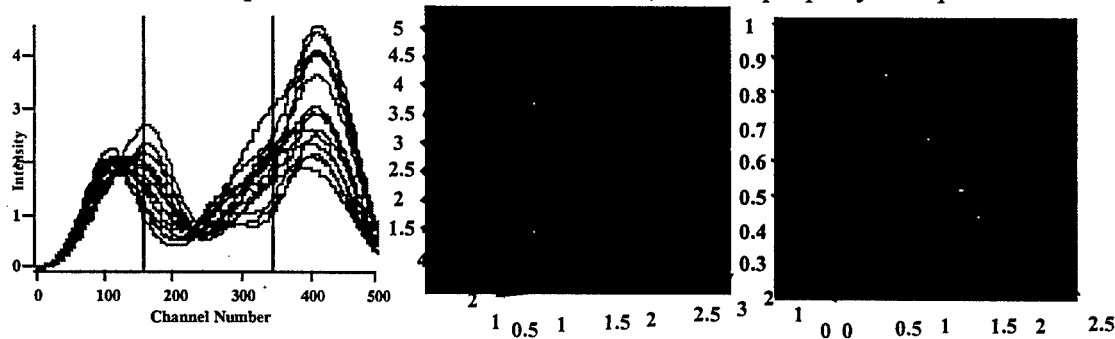


Figure 1 – Example of the way multidimensional representation of spectroscopic data can avoid interferences

In our previous work, we have explored and developed the theme of pattern-recognition-

based imaging using multivariate methods. Among the pattern recognition techniques we have employed are principal components analysis (PCA) and principal components regression (PCR), iterative target transformation factor analysis (ITTFA), etc. We can, for instance, use regression methods to relate spectroscopic patterns to a property of interest (e.g., cancer status) and can produce maps of that property. We can also deconvolve the patterns directly into chemical maps.

Taking PCR as an example, we represent a data set as a two-dimensional matrix,  $A$ , composed of a series of spectra that have been acquired for calibration purposes. PCR then attempts to represent the data matrix as the product of three matrices:

$$A = U S V^T$$

In this equation,  $U$  is a two dimensional matrix consisting of abstract spectra for each pattern recognized in the data set,  $S$  is the magnitude of the patterns in the data set, and  $V$  is the way each sample varies in terms of the patterns it contains.  $T$  in this equation means to "transpose" the matrix, or to invert the matrix about its own diagonal. We use a mathematical procedure called singular value decomposition to decompose our data matrix according to the preceding equation. To determine a spectroscopic pattern that corresponds to a chemical or physical property of interest (e.g., cancer status) we require calibration against a standard technique (e.g., histology). The pattern that corresponds to the property of interest is called a regression vector, symbolized by  $L$ , and is obtained as:

$$L = V S^{-1} U^T C_{\text{std}}$$

where  $C_{\text{std}}$  is the histological result for a series of calibration samples. Once this mathematical procedure is completed,  $L$  is a pattern whose magnitude in every spectrum is equivalent to a "prediction" of the histological result for an unknown specimen.

Chemical (or spectroscopic) imaging combines the power of chemical analysis via spectroscopy with the imaging capabilities associated with, for example, CCD cameras, by recording light intensities as a function of both wavelength and position in the image. The result is a recorded image for each wavelength in the image domain, and a recorded spectrum for each pixel in the spectral domain. Instead of a two-dimensional image, the data that form a single frame of a chemical image is best considered as a cube, as illustrated in Figure 2, in which two of the dimensions are the usual spatial dimensions, but the third is a wavelength space.

The proper spectroscopic interpretation of numerous industrial, medicinal, and environmental samples requires an in-depth knowledge of the spectroscopy at multiple points throughout the sample.



The Myrick group in the Department of Chemistry and Biochemistry at the University of South Carolina has pioneered a new method for chemical imaging [9-15] that permits all the dimensions of the chemical data cube to be collected simultaneously in real time. For the first time, the technology of chemical imaging has reached a level at which it can be productively applied to the quantitative imaging of gas plumes.

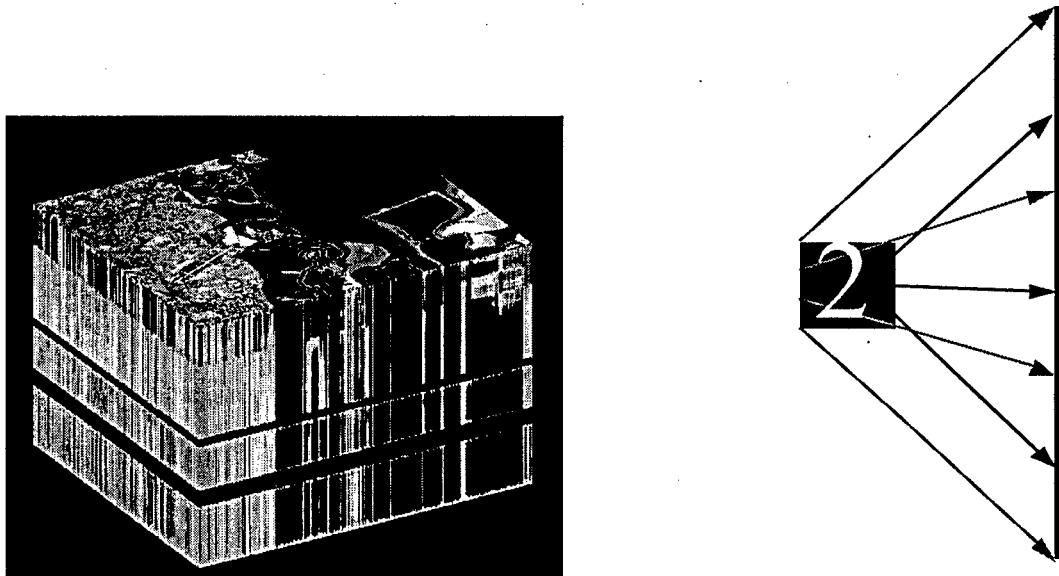


Figure 2. - (left) A data cube from the Jet Propulsion Laboratory used for remote geological imaging.  
Figure 3. - (right) Schematic illustration of the "serpentine dissection" performed by our arrays.

The heart of the new technology developed at USC is a specially-manufactured serpentine fiber-optic array. Most fiber-optic arrays used in imaging are "coherent", meaning that an image that enters on end of the array appears unchanged on the other end. The arrays we have developed perform a "serpentine dissection" of the image. Figure 3 illustrates this concept. In our arrays, an image is directed at a two-dimensional fiber array. The rows of the fiber array are then stretched apart in a serpentine pattern to form a stacked line of fibers. In Figure 3, the arrows indicate the ends of each row and where they shift in going from the two-dimensional side to the one-dimensional side. The purpose behind this dissection is to make sure that each fiber in the one-dimensional side is directly beside a fiber that it adjoins on the two-dimensional side. After this dissection, the light emerging from the one-dimensional side is injected in parallel to a spectrograph, and recorded by a CCD array. This provides a spectrum for each point in the original image. These data, approximately 1 Mbyte per image, are then processed by sophisticated multivariate algorithms to extract their spectroscopic pattern content, which is then automatically displayed in the form of reconstructed chemical images. The spectroscopic pattern content can be directly related to properties of the sample, or to chemical concentrations in the sample.

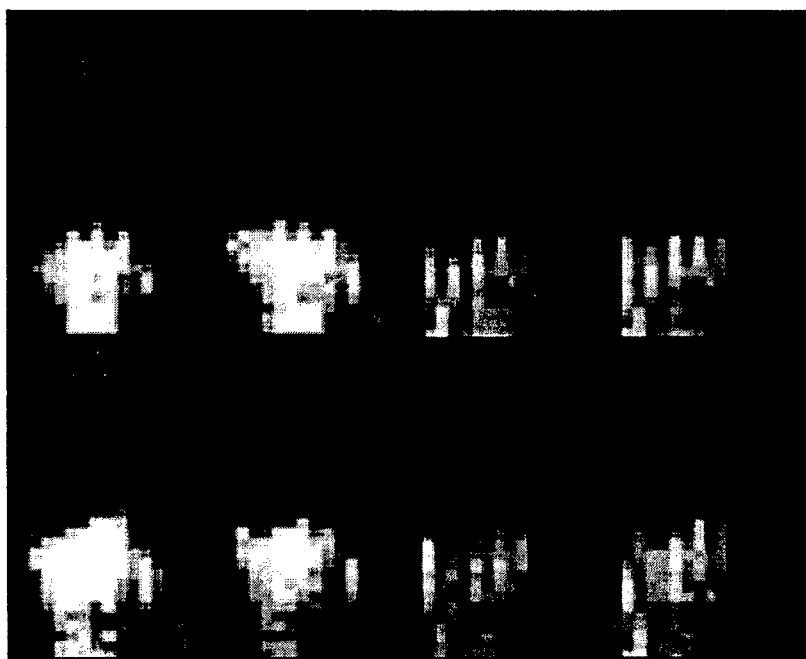


Figure 4: left – four intensity images of laser plumes. right – four chemical maps of laser plumes. Green = N, Violet = Pb.

The previous work by the Myrick group in this area has been directed at technique development, with imaging of the chemistry of laser-induced sparks as a test case. Laser sparks were chosen because they were an easy sample for us to generate, and because they occur so rapidly that they can only be studied effectively using our technique. Figure 4 shows a comparison of regular "white light" pictures of laser plumes to chemical images that show the way different chemical species vary inside the plume. The same technology used for this laser-plume study is directly applicable to measurement of speciation in biomedical samples, provided a multivariate data analysis approach is used for interpretation of the spectroscopy.

**Area 2:** (This work is being performed by Dr. Angel's research group)

The goal of the part of the research is to build a portable remote Raman system using a liquid crystal tunable filter (LCTF) and a CCD with fiber-optic optical coupling. And, to test this system in terms of measurement range and sensitivity. The LCTF used for this work was delivered late in the project and only became fully operational late in 1998, and is still showing some problems. The experiments are not yet complete, and will continue through the summer. This report is a list of accomplishments to date.

The specific accomplishments of this project include: 1) an LCTF-based remote Raman spectrometer was built and tested using two different mirror systems; 2) the remote Raman system was taken to Bellows Air Force Base on Oahu and tested under field conditions; 3) remote Raman spectra were acquired of solids and liquids at distances up

to 80 m (266 ft) using collection optics ranging from ~0.5-in to 11-in diameter; 4) remote Raman imaging was demonstrated using a 1-mm image guide coupled to the remote Raman system; 5) a novel polymer collection mirror, many times lighter and cheaper than glass mirrors, was demonstrated to be useful for remote Raman measurements; 6) important collaborations/partnerships were established at Beals Air Force Base, and at The University of Hawaii that will likely lead to future research and funding opportunities.

(1) The portable LCTF imaging Raman spectrometer, was completed in December and is shown in Figure 5 (LCTF detection system) and Figure 6 (fiber-coupled collection optic). The telescope shown in Figure 6 is coupled to the remote Raman detection system by a small-diameter, 1-mm, flexible image guide. This greatly improves the flexibility of the system, allowing easy use of a variety of different collection systems. The LCTF-based remote Raman detection system, shown in Figure 5, is comprised of (from left to right) the optical fiber image guide and holder, an infinity corrected 10 x microscope objective for collimating light from the fiber, the LCTF, and a charge-coupled device (CCD) detector with an attached 50 mm Nikon lens. The system footprint is 2 x 1 ft and it is easily transportable. In addition, an AOTF-based imaging Raman spectrometer using the identical small-footprint of the LCTF-based system was constructed for similar testing for comparison.

Preliminary experiments show that the resolution of the device is sufficient, ~0.35 nm, to acquire high-quality Raman spectra (see Figure 7). This corresponds to a Raman band pass of about  $12 \text{ cm}^{-1}$  at the wavelength used for these measurements, less than a typical Raman band width and comparable to a medium-resolution Raman spectrometer.

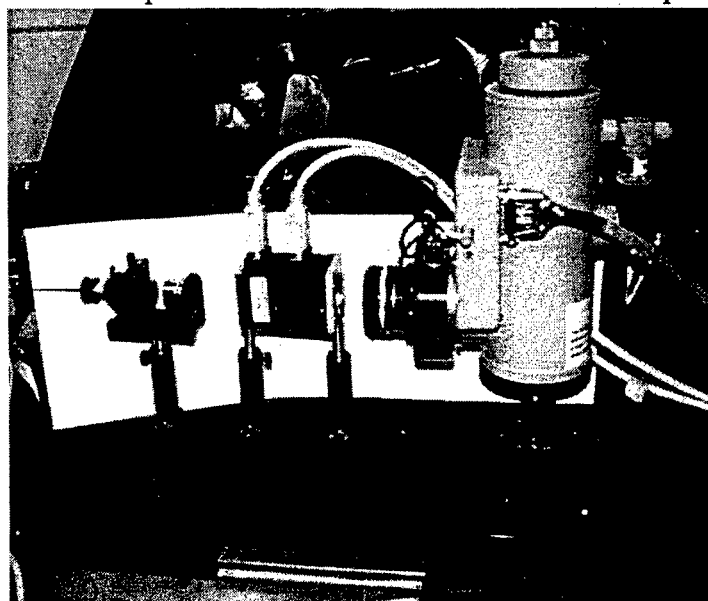


Figure 5. The portable LCTF Raman imaging spectrometer coupled to a collection optic (not shown) via an image guide.

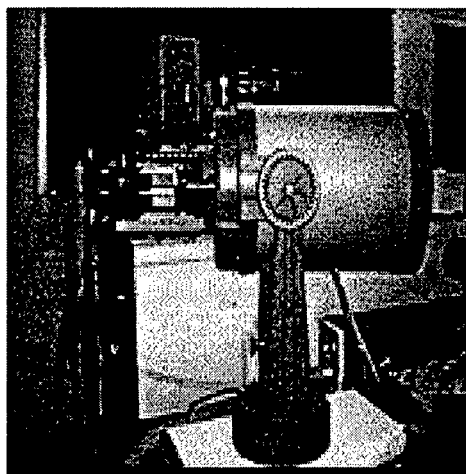


Figure 6. Telescope adapted for optical fibers and image guide use. An optical fiber image guide is visible in the photo exiting the rear of the telescope.

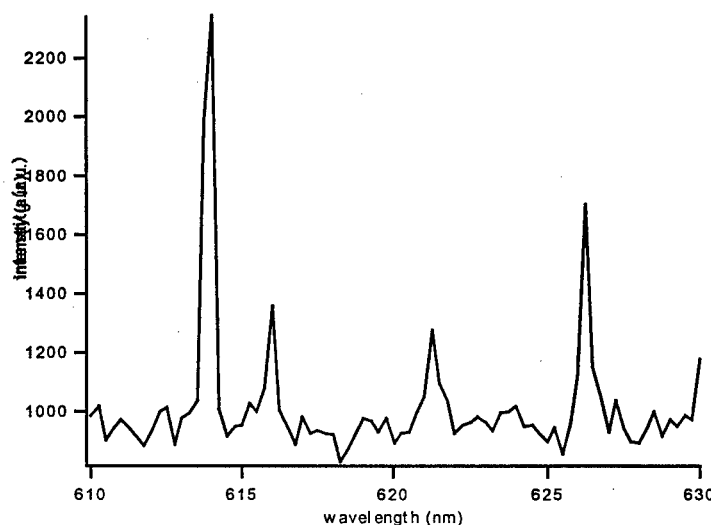


Figure 7: Low-pressure neon lamp emission spectrum measured by scanning the LCTF in 0.35 nm increments. This corresponds to a Raman band pass of about  $12 \text{ cm}^{-1}$  at the wavelength used for these measurements.

(2) The remote Raman system was taken to Bellows Air Force Base and tested under field conditions;

Two graduate students are currently working half time on this project and another has worked part time. The two half-time students participated in field tests at Bellows Air Force Base with Professor Shiv Sharma of the Institute of Geophysics at the University of Hawaii (UH). The University of Hawaii has several mobile Lidar systems on the island of Oahu. One of these is currently stationed at Bellows Air Force Base. The USC portable remote Raman instrument was taken to this site for tests of range and sensitivity and for comparisons with the existing mobile system. The USC system was easily

integrated into the UH system because of the use of the image guide-coupled detection optics. At Bellows, this allowed the use of the UH 11-inch telescope as the collection optic, and the UH lasers for excitation.

Figure 8 shows the Bellows mobile laboratory with 60 ft measurement tower. Figure 9 shows the main collection system for the Bellows mobile laboratory system. This consists of an 11-inch telescope and mirror scanning system. What cannot be seen in this picture is that the system sits on a beach where the winds and surf are very rough. The high winds prevented us from carrying out the NIR measurements because of problems tracking the stars. The Bellows mirror scanner was not capable of tracking stars with any precision. The telescope mount from USC was not useful for tracking in the high winds. These conditions also contributed to the other problems with the UH instruments. A substitute experiment, testing polymer mirrors for remote Raman measurements, is described below.

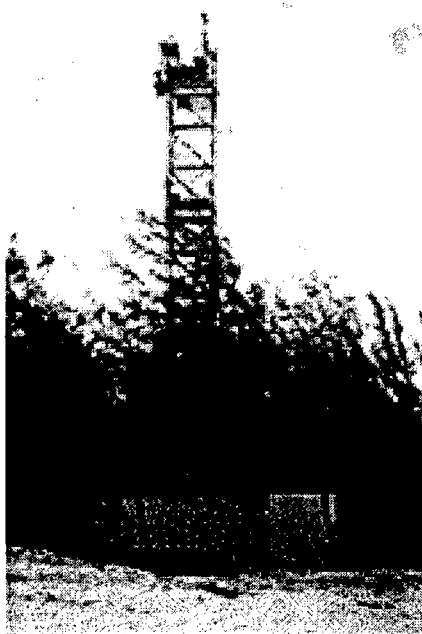


Figure 8. The mobile spectroscopy laboratory (trailer in foreground) located at Bellows Air Force Station.

Unfortunately, because of problems with the UH laser and detection system at Bellows, the results obtained there were not satisfactory, and were not as good as results obtained at USC or in Prof. Sharma's facilities at UH. Thus, most of the successful measurements were acquired at these two places. However, some useful information was obtained using the Bellows system. For example, we obtained Raman spectra at the longest range for either of the groups, USC or UH. Figure 10 shows the Raman spectrum of toluene. In this experiment the toluene sample was placed 80-m from the mobile laboratory. The spectrum is a 30-s exposure using only ~50 mW of laser power. Although the conditions were not nearly optimal for this measurement, based on the S/N ratio of the spectrum we obtained, we can predict a detection range of at least twice this distance. This range

could be extended considerably using even a modest laser power. Furthermore, the telescope and laser optics used for this measurement were severely damaged prior to our arrival at Bellows. With a good quality telescope mirror and beam directing optics this range would increase still further. A more precise estimate of detection range will be determined during the remainder of the project.

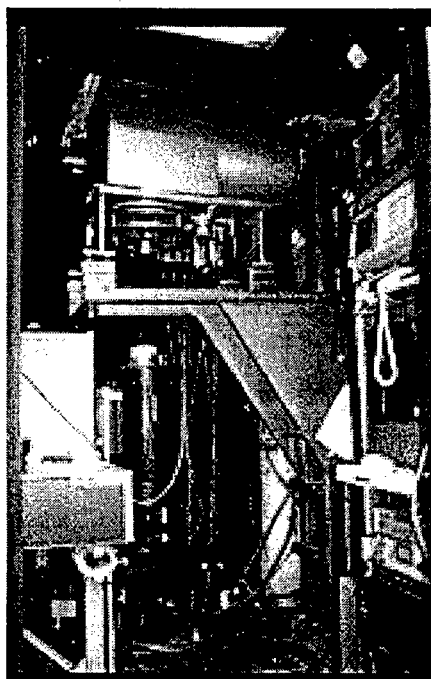


Figure 9. The custom scanner (top) can be raised and lowered from within the lab to target excitation radiation using the control center (right) shown.

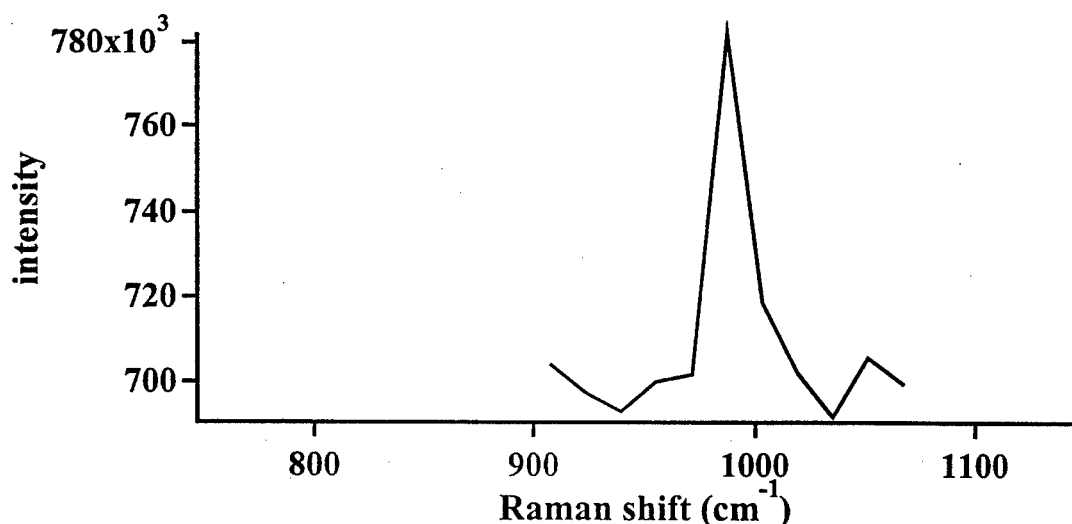


Figure 10. Raman spectrum of a single peak from a toluene sample at a distance of 80 m (266 ft) using ~50 mW of 532-nm excitation and a telescope with an 11 in-diameter collection optic. The telescope was directly coupled to an LCTF. This spectrum was

acquired by scanning the LCTF in 0.5 nm increments with a 30 s exposure time per image.

(3) Remote Raman spectra were acquired of solids and liquids at distances up to 266 feet using collection optics ranging from ~0.5-in to 8-in diameter. Even before the tests at Bellows, we were routinely measuring Raman spectra at >100 feet using a fiber-optic coupled Raman spectrometer. The system used for most of these tests consisted of a holographic grating f/1.8 Raman spectrometer (Kaiser Holospec) with an attached holographic Raman probe and CCD detector, and a diode-pumped 300-mW Nd:YAG laser. This system has a footprint similar to the LCTF system. Figure 11 shows two spectra measured using this system at distances of 1 (top) and 60 feet (lower).

Another example is shown in Figure 12. In this case Raman spectra were obtained simultaneously of both a  $\text{TiO}_2$  sample and a marble sample at a distance of 12 m (39.5 ft) using ~700 mW of 488-nm excitation and a telescope with an 8 in-diameter collection optic. The telescope was coupled to an imaging spectrograph via a 350  $\mu\text{m}$  optical fiber, where the total field of view included both samples. A photograph of the samples is shown in Figure 13. The scatter image in Figure 14 shows the field of view of the measurement. The calcite sample is on the right—brighter region. The marble sample sits in front of a large  $\text{TiO}_2$  target. Marble contains mostly calcite, and it is the calcite Raman band that is shown in the following spectra. This spectrum was measured in 60 s using a 120- $\mu\text{m}$  slit with a 1200 gr/mm grating.

Next, the simple optical fiber used to acquire the spectra shown in Figure 12 was replaced with the 1-mm diameter image guide so that remote Raman images could be acquired. For the following measurements, an acousto-optic tunable filter (AOTF) was used in place of the LCTF, because of problems with the operation of the LCTF.

(4) Raman imaging was demonstrated using a 1-mm diameter image guide coupled to the remote Raman system.

All successful Raman imaging experiments, both with and without the image guide, were carried out at the UH campus facilities or at USC. Again, Figures 13 and 14 show a photograph of the samples and the field of view versus the Raman system, respectively. Both of the test substances,  $\text{TiO}_2$  and calcite, produce unique Raman spectra which can be used as a reference for future measurements. Figures 15 and 16 show Raman spectra generated by obtaining Raman images, then binning pixels in the  $\text{TiO}_2$  and calcite regions, respectively. These two spectra, along with the image in Figure 14, demonstrate the power of Raman imaging. Raman spectra can be generated anywhere in the field of view by examining the appropriate region of the images, taken over a range of different Raman shifts, and binning only pixels in that region.

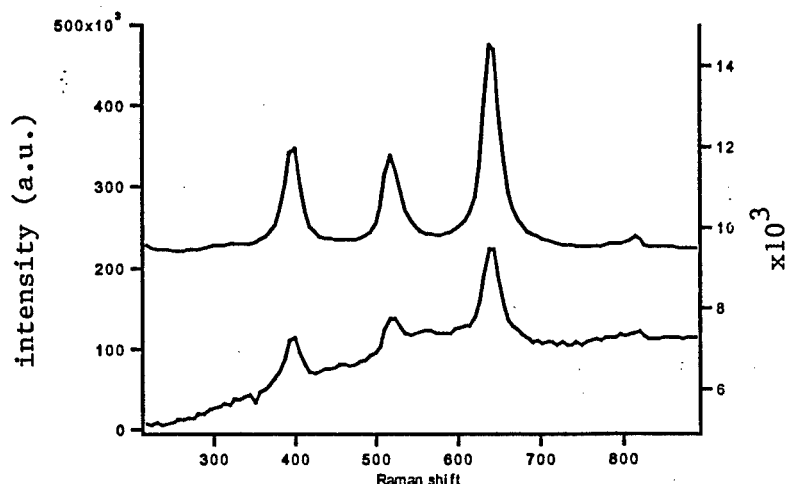


Figure 11. Raman spectrum of  $\text{TiO}_2$  measured at 60 ft (bottom) versus 1 ft (top) using the holographic grating f/1.8 Raman spectrometer with a  $\sim 0.5$  in diameter collection optic and a collimated laser beam from a fiber-optic probe.

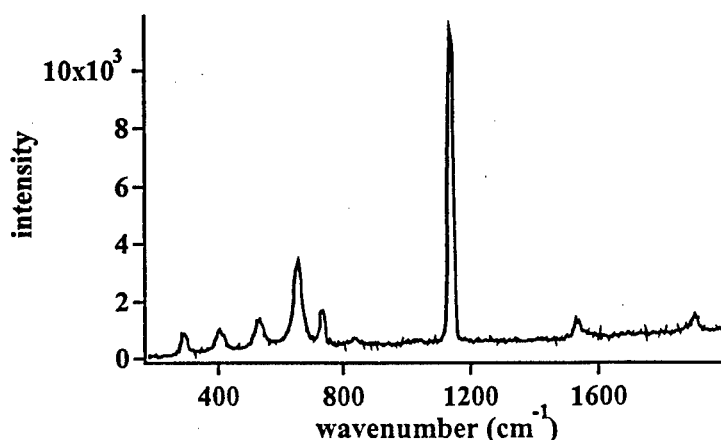


Figure 12. Raman spectrum of a  $\text{TiO}_2$  sample and a marble sample containing calcite measured simultaneously at a distance of 12 m (39.5 ft) using  $\sim 700$  mW of 488-nm excitation and a telescope with an 8 in-diameter collection optic. The telescope was coupled to an imaging spectrograph via a  $350\text{ }\mu\text{m}$  optical fiber. This spectrum was measured in 60 s using a  $120\text{-}\mu\text{m}$  slit with a  $1200\text{ gr/mm}$  grating. The spectrum was acquired prior to replacing the optical fiber with a 1 mm image guide and imaging with the portable AOTF Raman spectrometer.





Figure 13. The marble containing calcite crystals is shown on the right side of the photo setting on a black stand. A  $\text{TiO}_2$  target is seen in the background of the photo. The field of view FOV for imaging included half marble and half  $\text{TiO}_2$ .

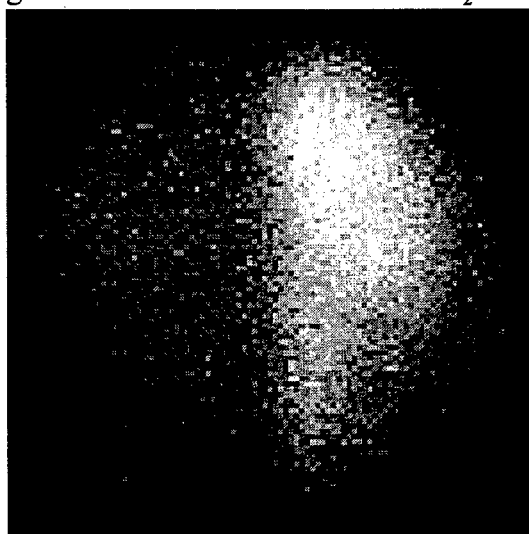


Figure 14. This is a scatter image, obtained by setting the AOTF to a wavelength (500 nm) corresponding to a position close to a Raman band of calcite, showing the field of view of the measurements. This image also shows the boundary region between  $\text{TiO}_2$  (left) and calcite (right)

(5) A novel polymer collection mirror, many times lighter and cheaper than glass mirrors, was demonstrated to be useful for remote Raman measurements. Although not originally planned in this proposal, we felt this study was appropriate for two reasons. 1) the NIR studies using a star as a light source were put off because of the inability to track stars at Bellows, and 2) this study is highly relevant to the goal of demonstrating a portable and fieldable system.

Polymer mirrors were supplied by Dr. Wally Scrivens. These mirrors are made using a proprietary technique developed by Scrivens. The mirror material is a special epoxy

composite. For remote Raman spectroscopy the mirrors have several major advantages including

- light weight (5-10 times less than comparable glass mirrors)
- inexpensive (~\$5 for materials for an 11-inch diameter mirror)
- extremely low  $f/\#$ , high light gathering power ( $f/2$  for an 11-inch mirror!)
- made by a process that inherently produces a parabolic curvature (for higher focused power) compared to a spherical curvature for many mirrors used in spectroscopy.

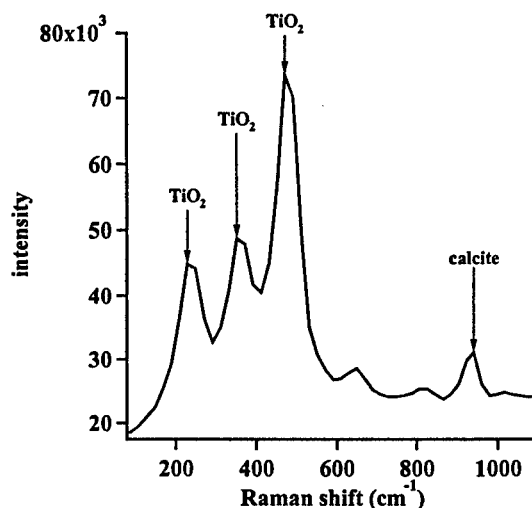


Figure 15. Raman spectrum of a  $\text{TiO}_2$  sample and a marble sample containing calcite measured at a distance of 12 m (39.5 ft) using ~700 mW of 488-nm excitation and a telescope with an 8 in-diameter collection optic. This scan was obtained by binning CCD pixels region of the image corresponding to the  $\text{TiO}_2$  sample. The telescope was coupled to an AOTF via a 1 mm image guide. This spectrum was acquired by scanning in 0.5 nm increments with a 30 s exposure time per image. Inset: This Raman images (4 x 4 binning) was acquired at 500 nm and corresponds to the most intense peak shown in the toluene spectrum.

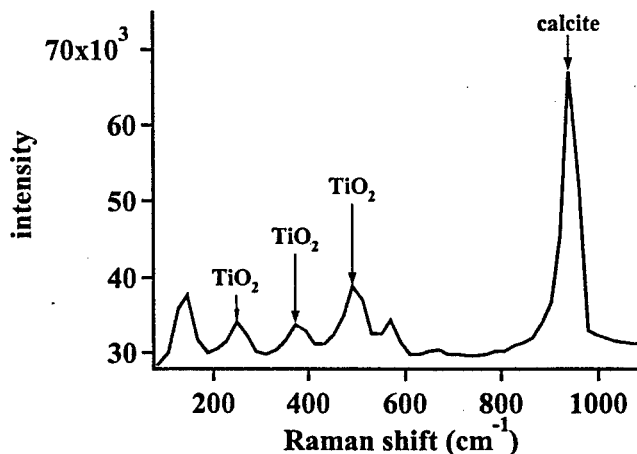


Figure 16. Raman spectrum of a  $\text{TiO}_2$  sample and a marble sample containing calcite measured at a distance of 12 m (39.5 ft) using ~700 mW of 488-nm excitation and a

telescope with an 8 in-diameter collection optic. This scan was obtained by binning CCD pixels region of the image corresponding to the marble containing calcite sample. The telescope was coupled to an AOTF via a 1 mm image guide. This spectrum was acquired by scanning in 0.5 nm increments with a 30 s exposure time per image. Inset: This Raman images (4 x 4 binning) was acquired at 500 nm and corresponds to the most intense peak shown in the calcite spectrum.

Figure 17. shows a photograph of an f/2 11-inch diameter mirror. The total weight of the mirror, including a metal mount, is 3 pounds. A comparable glass mirror would weigh anywhere from 15 to 30 pounds depending on its thickness, without the mount! This weight reduction is even more important when you consider the mounts that have to be included to use the mirror in a detection device.

At UH, we tested an f/4, 4.25-inch polymer mirror for remote Raman measurements and found that it worked as well as a comparable glass mirror. The imaging quality isn't as good as a commercial telescope mirror, but for remote Raman measurements image quality isn't as important as for astronomical imaging. Figure 18 shows the Raman spectrum of toluene measured at a distance of 5m (16.5 ft) using ~300 mW of 532 nm excitation and the f/4, 4.25-inch polymer mirror. The collection optic and the LCTF were directly coupled. This spectrum was measured by scanning the LCTF from 553 to 572 nm at 0.2 nm increments and an exposure time of 10 sec/image. This spectrum is as good as would be obtained using a commercial f/10 4.25 glass mirror. However, the polymer mirror weighed only 190 g as opposed to 353 g for the glass mirror. And, the polymer mirror was twice as thick and produced a small focus spot (f/4 versus f/10).

(6) Important collaborations/partnerships were established at Bellows Air Force Base, and at The University of Hawaii that will likely lead to future research and funding opportunities.

Perhaps the most important thing to come out of this project are the collaborations at Bellows Air Force base, with Prof. Shiv Sharma and with Dr. Wally Scrivens. These collaborations will certainly lead to new research and funding opportunities in the future. Prof. Sharma and the group at USC plan to continue the current studies until the end of this project. We will also seek additional DOD funding to extend these studies. Dr. Wally Scrivens is already planning to submit an SBIR proposal with the USC group.



Figure 17. F/2, 11-inch diameter polymer mirror supplied by Dr. Wally Scrivens for this project.

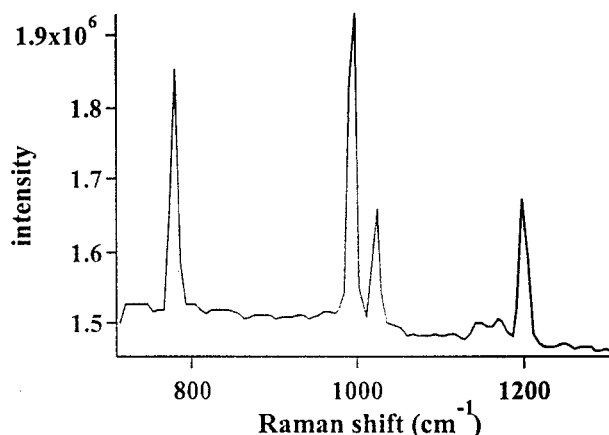


Figure 18. Raman spectrum of toluene measured at a distance of 5m (16.5 ft) using ~300 mW of 532 -nm excitation and a novel polymer mirror with a 4.25 in-diameter collection optic (f/4). The collection optic and the LCTF were directly coupled. This spectrum was measured by scanning the LCTF from 553 to 572 nm at 0.2 nm increments and an exposure time of 10 sec/image.

***Publications and Technical Reports***

**Design of Thin Film Filters for the Monitoring of Chemical Reactions"**

J.A. Dobrowolski, P.G. Verly, J.F. Aust, M.P. Nelson and M.L. Myrick  
in Proceedings of the SPIE Annual Meeting on Optical Science and Engineering,  
San Diego, California, July, 1997 (in press, 1998).

Single-Shot Multiwavelength Imaging of Laser Plumes M.P. Nelson, W.C. Bell, M.L.  
McLester, and M.L. Myrick Appl. Spectrosc. **52**(1998), 179-89.

**Fabrication and Evaluation of a Dimension-Reduction Fiber-Optic System for Chemical  
Imaging Applications**

M.P. Nelson and M.L. Myrick Rev. Sci. Instrum. (in press, 1999).

**Time-Dependent Multivariate Single-Frame Chemical Imaging Spectroscopy of Laser  
Plumes Using an Improved Dimension Reduction Fiber-Optic Array**

M.P. Nelson and M.L. Myrick Anal. Chem. (in press, 1999).

**Single-Frame Chemical Imaging: Dimension Reduction Fiber-Optic Array  
Improvements and Application to Laser-Induced Breakdown Spectroscopy**

M.P. Nelson and M.L. Myrick Appl. Spectrosc. (submitted, 1999)

**Single-Frame Chemical Imaging: Chemometric Analysis and Interpretation**

M.P. Nelson and M.L. Myrick Anal. Chim. Acta (submitted, 1999).

**Single-Shot Multiwavelength Imaging of Laser Plumes**

M.P. Nelson, W.C. Bell, M.L. McLester and M.L. Myrick SPIE **3261**(1998), 289-  
98.

**Time-dependent multivariate single-frame chemical imaging spectroscopy of laser  
plumes using a dimension reduction fiber optic array**

M. P. Nelson, M. L. Myrick, SPIE **3649**(1999) (in press)

**Multivariate Optical Computation for Predictive Spectroscopy**

M.P. Nelson and M.L. Myrick  
Anal. Chem. **70**(1998), 73.

**Single-Shot Multiwavelength Imaging of Laser Plumes**

M.P. Nelson, W.C. Bell, M.L. McLester, and M.L. Myrick  
presented at Pittsburgh Conference, New Orleans, LA, Mar 1-6, 1998.

**Multivariate Optical Computation for Predictive Spectroscopy**

M.L. Myrick, M.P. Nelson, J.F. Aust, J.A. Dobrowolski, and P.G. Verly  
presented at Pittsburgh Conference, New Orleans, LA, Mar 1-6, 1998.

**Remote Raman Using Polymer Mirrors**

J. Chance Carter, Dimitra N. Stratis, S. K. Sharma, Wally A. Scrivens,  
and S. Michael Angel, accepted for Proceedings of The Annual SPIE Conference,  
Boston, Massachusetts, September, 1999.

**Feasibility of Remote Raman Imaging Using Tunable Filters**

J. Chance Carter, Dimitra N. Stratis, S. K. Sharma, and S. Michael Angel,  
accepted for Proceedings of The Annual SPIE Conference  
Boston, Massachusetts, September, 1999.

**Imaging Spectroscopy using Optical Fibers**

S. Michael Angel, H. Trey Skinner, and Brian J. Marquardt  
presented at ANACHEM Award Symposium at 24th Annual Conference of the Federation  
of Analytical Chemistry and Spectroscopy Societies (FACSS), Providence, RI,  
invited paper October 27-31, 1997.

**Imaging Spectroscopy using Fiber Optics**

S. Michael Angel, H. Trey Skinner, and Brian J. Marquardt, ", " presented at Microscopy  
and MicroAnalysis '97, Cleveland, Ohio, invited paper August 13, 1997.

**Remote Sensing Using Fiber-optics**

S. Michael Angel  
presented at University Alaska, Fairbanks, June 26, 1997.

***Participating Personnel***

Area 1: Personnel

Dr. Xiong Gong (beginning 4/99)

Matthew P. Nelson, graduate assistant (12 months)

Dr. Pramod Khulbe, post-doctoral associate ( 1/2 time, 3 months)

Area 2: Personnel

Chance Carter, graduate assistant (half time)

Dimitra Stratis (half time)

Brian Marquardt (10% time)

Area 1: *No inventions or attachments*

Area 2: *No inventions or attachments*

**BIBLIOGRAPHY**

1. E. R. Malinowski, Factor Analysis in Chemistry, 2nd ed. (John Wiley & Sons, New York, 1991), p 1.
2. M. A. Sharaf, D. L. Illman, and B. R. Kowalski, Chemometrics (John Wiley & Sons, New York, 1986).
3. D. L. Massart, B. G. M. Vandeginste, S. N. Deming, Y. Michotte, and L. Kaufman, Chemometrics: a Textbook (Elsevier, Amsterdam, 1988).

4. I. T. Jolliffe, *Principal Component Analysis* (Springer-Verlag, New York, 1986).
5. "Resolution of Mixture Components by Target Transformation Factor Analysis and Determinant Analysis for the Selection of Targets" X. Liang, J. Andrews, and J. A. Haseeth, Anal. Chem. **68**(1996), 378-85.
6. "Target Transformation Factor Analysis with Linear Inequality Constraints Applied to Spectroscopic-Chromatographic Data" P. J. Gemperline, Anal. Chem. **58**(1986), 2656-63.
7. "Multivariate Raman Imaging of Simulated and "Real World" Glass-Reinforced Composites" C. M. Stellman, K. S. Booksh, and M. L. Myrick, Appl. Spectrosc. **50**(1996), 552-60.
8. "Multivariate Fluorescence Imaging of Gel on Nylon 66 Production Pack Screens" C. M. Stellman, K. S. Booksh, and M. L. Myrick, Appl. Spectrosc. **49**(1995), 1545-52.
9. "Single-Shot Multiwavelength Imaging of Laser Plumes" M.P. Nelson, W.C. Bell, M.L. McLester, and M.L. Myrick Appl. Spectrosc. **52**(1998), 179-89.
10. "Fabrication and Evaluation of a Dimension-Reduction Fiber-Optic System for Chemical Imaging Applications" M.P. Nelson and M.L. Myrick Rev. Sci. Instrum. (in press, 1999).
11. "Time-Dependent Multivariate Single-Frame Chemical Imaging Spectroscopy of Laser Plumes Using an Improved Dimension Reduction Fiber-Optic Array" M.P. Nelson and M.L. Myrick Anal. Chem. (in press, 1999).
12. "Single-Frame Chemical Imaging: Dimension Reduction Fiber-Optic Array Improvements and Application to Laser-Induced Breakdown Spectroscopy." M.P. Nelson and M.L. Myrick Appl. Spectrosc. (submitted, 1999)
13. "Single-Frame Chemical Imaging: Chemometric Analysis and Interpretation" M.P. Nelson and M.L. Myrick Anal. Chim. Acta (submitted, 1999).
14. "Single-Shot Multiwavelength Imaging of Laser Plumes" M.P. Nelson, W.C. Bell, M.L. McLester and M.L. Myrick SPIE **3261**(1998), 289-98.
15. "Time-dependent multivariate single-frame chemical imaging spectroscopy of laser plumes using a dimension reduction fiber optic array", M. P. Nelson, M. L. Myrick, SPIE **3649**(1999) (in press)

**University Research Initiative Program for Combat Readiness**  
**Annual Report 06/01/98-05/31/99**

PART 53-FORMS

53.301-298

<b>REPORT DOCUMENTATION PAGE</b>		Form Approved OMB No. 0704-0188	
Public reporting burden for this collection of information is estimated to average 1 hour per response, including the time for reviewing instructions, searching existing data sources, gathering and maintaining the data needed, and completing and reviewing the collection of information. Send comments regarding this burden estimate or any other aspect of this collection of information, including suggestions for reducing this burden, to Washington Headquarters Services, Directorate for Information Operations and Reports, 1215 Jefferson Davis Highway, Suite 1204, Arlington, VA 22202-4302, and to the Office of Management and Budget, Paperwork Reduction Project (0704-0188), Washington, DC 20503.			
1. AGENCY USE ONLY (Leave blank)	2. REPORT DATE June 1, 1998	3. REPORT TYPE AND DATES COVERED Annual	
4. TITLE AND SUBTITLE <b>Line-of-Sight Standoff Identification of Explosive Chemicals and Chemical Warfare Agents</b>		5. FUNDING NUMBERS Grant Number N00014-97-1-0806 PR Number 97PR06312-00 PO Code 353 Disbursing Code N68892 AGO Code N66020 Cage Code 4B489	
6. AUTHOR(S) S. Michael Angel & Michael L. Myrick			
7. PERFORMING ORGANIZATION NAME(S) AND ADDRESS(ES) University of South Carolina		8. PERFORMING ORGANIZATION REPORT NUMBER N00014-97-1-0806-1	
9. SPONSORING / MONITORING AGENCY NAME(S) AND ADDRESS(ES) ONR		10. SPONSORING / MONITORING AGENCY REPORT NUMBER ONR	
11. SUPPLEMENTARY NOTES Prepared in coordination with University Research Initiative Program for Combat Readiness			
12a. DISTRIBUTION / AVAILABILITY STATEMENT APPROVED FOR PUBLIC RELEASE		12b. DISTRIBUTION CODE	
13. ABSTRACT (Maximum 200 words) This work is divided into two main areas. 1) development of the technology for optical detection and identification of chemical agents using absorbance/reflectance spectroscopy in the NIR/MID spectroscopic regions, combined with optical computation pattern recognition. 2) demonstration of a standoff instrument for identification of dangerous chemicals using a small-footprint Raman spectrometer with an LCTF, and demonstrate the use of polymer mirrors for remote Raman. In the first area, we have hired a postdoctoral assistant, who will be arriving from China within the month. We have developed an improved optical methodology for detecting plumes using chemical imaging based on serpentine fiber-optic image dissection arrays. In the second area, the LCTF instrument was purchased and debugged, and the small footprint Raman system was tested for standoff operation at USC and at an Air Force Test Station. Remote Raman measurements were made using this system in collaboration with The University of Hawaii Institute of Geophysics using their mobile LIDAR system and laboratory instruments. A new type of light-wave mirror, made using an epoxy composite, was tested for remote Raman measurements.			
14. SUBJECT TERMS Chemical and Biological Warfare, Target Acquisition, Anti-Submarine, Combat Medicine, Biodeterioration, and Command Control and Communication		15. NUMBER OF PAGES 20	
		16. PRICE CODE	
17. SECURITY CLASSIFICATION OF REPORT UNCLASSIFIED	18. SECURITY CLASSIFICATION OF THIS PAGE UNCLASSIFIED	19. SECURITY CLASSIFICATION OF ABSTRACT UNCLASSIFIED	20. LIMITATION OF ABSTRACT 200 words

NSN 7540-01-280-5500

Standard Form 298 (Rev. 2-89)  
Prescribed by ANSI Std. Z39-18  
298-102



## **Technology Development for Chemical Detection**

M.L. Myrick

Department of Chemistry and Biochemistry  
University of South Carolina  
Columbia, SC 29208

Tel: (803) 777-6018  
Fax: (803) 777-9521  
Email: myrick@psc.sc.edu

## Section 2-2: Technology Development for Chemical Detection

M.L. Myrick

### ABSTRACT

Our research has focussed on two major sensor types. The first is based on selective hydrolysis of fluorine-containing chemical agents such as simulate Sarin and Soman using diisopropyl fluorophosphate (DFP) as a simulant. The basis of the method is that in neutral solutions, the hydrolysis rate of fluorophosphate nerve agents is dramatically increased by the presence of a metal chelate compound, and results in the release of fluoride ion. The released fluoride ion can then be detected by a fluoride-ion-selective electrode. The technique is highly selective for these agents because only fluoride ions can be detected, and because only fluoride-containing compounds whose hydrolysis is catalyzed by the metal chelates will release fluoride. We believe this methodology will result in a reusable, continuous monitoring system for these agents. Our second focus area is in optical sensing. We are developing sensor molecules which form covalent adducts with organophosphonates. These sensors are based on molecular cleft scaffold chemistry, and incorporate both an oxime and fluorescent transducer group made with bipyridyl units to be connected to environmentally-sensitive metal chelate complexes. Detection is not based on the identification of specific nerve gas hydrolysis by-products (e.g., HF) but rather on the spectroscopic differences caused by the nerve gas-sensor oxime phosphate ester adducts on the sensitive spectroscopy of the metal chelate.

### FORWARD

This project was initially funded in June, 1997 at the level of \$1.3 M over three years. Our key results thus far are:

- Development of a novel electrochemical method for sensing fluorophosphate nerve agent simulants that is amenable to continuous monitoring with simple instrumentation.
- Synthesis of sensor molecules using molecular-cleft scaffold chemistry that rely of highly selective oxime chemistry to produce measurable effects on electrochemical and optical phenomena.
- Development of optical computation interference filters to simplify spectroscopic detection of analytes by increasing discrimination between desired and undesired chemical reactivity.

### REPORT

#### *Statement of the problem*

The objective of this proposal by the research team of Myrick, Popov, Salvatore, Bryson and zur Loye is to develop remote sensors for chemical agents based on optical and electrochemical effects, using methodologies applicable to all classes of CW agents. The specific objective of this

proposal is to develop new and novel input transducers that will be responsive to the concentrations of nerve agents using optical or electrochemical signal transduction. These sensors are of importance to US military preparedness in determining the avoidance and decontamination strategy in the case of use of chemical agents.

### **Background**

In the Hague Declaration of 1899, most world powers pledged not to use "projectiles the sole object of which is the diffusion of asphyxiating or deleterious gases." Nevertheless, Germany began using poisoned gas weapons less than two decades later during World War I when the opposing French and British forces were far less sophisticated in chemical operations than the Germans themselves. German use of chemicals in WWI only ceased when the opposition reached a level of skill comparable to themselves.<sup>1</sup>

The Geneva Protocol of 1925 also sought to eliminate the use of poisoned or toxic weaponry in war, yet the Japanese used chemical weapons (CW) in China during the 1930s, and both sides during WWII possessed offensive capabilities for waging war in a chemical environment. The US military alone kept reserves of gas weaponry sufficient to completely bridge the Italian peninsula with a toxic barrier.<sup>2</sup> Why were these weapons not used by either side (including the Japanese) during WWII? German military archives indicate that one major reason is that the Germans and Japanese felt the Allies had a superior defensive and offensive capability to themselves. History seems to bear out that chemical weapons are most likely to be used when the enemy is perceived as relatively vulnerable.<sup>3</sup> General Omar Bradley stated that, had the Germans used even a small amount of poisoned gas on Omaha Beach, the action would have been decisive and would have resulted in the failure of the Invasion of Normandy in June 1944.<sup>2</sup> Thus, sophistication and technical progress in the area of chemical weaponry, including detection capabilities, can have a profound impact on survivability during chemical attack — but perhaps an even greater impact as a deterrent.

A number of government studies have indicated that US military forces are currently vulnerable to chemical attack. The DoD's assessment has been that most US forces would survive an initial chemical attack, with the possible exception of Navy shore establishments. The General Accounting Office, however, notes that the primary means of detecting chemical agents all have serious flaws and reports an Army assertion that the major difficulty in the development of new detection methods is the lack of technological breakthroughs upon which those detection methods would be based.<sup>4</sup>

The problems of achieving an effective detection capability have grown through the years as the number of chemical agents and their modes of operation have increased. Agents that a military unit could encounter today range from persistent (weeks of activity) to non-persistent (minutes to hours of activity). They include acetylcholinesterase inhibitors (nerve gases such as sarin, tabun, soman and VX), compounds that block oxygen transport (blood agents such as HCN and cyanogen chloride), compounds that cause choking (e.g., phosgene and diphosgene), agents that cause severe blistering (e.g., sulfur mustard, nitrogen mustard and lewisite), and plant toxins such

as the trichothecene family of toxins (e.g., Diacetoxyscirpenol, T-2, verricanol, zearalenone, DON and nivalenol, all produced by *Fusarium*, which attack the major organs.

According to the Army, the nuclear, biological and chemical (NBC) threat has developed into one of the world's most troubling concerns,<sup>5</sup> with as many as 25 nations producing and stockpiling chemical weapons of all types. Current research on new CW agents is being conducted on materials that will be more difficult to detect, decontaminate, and treat, and may penetrate standard charcoal filters in protective equipment such as the Army's M-40 series masks.

The detection technologies for chemical weapons (CW) can be divided into two general categories; point and standoff.<sup>6-8</sup> Point detectors sample the air for presence of CW agents in the immediate vicinity of the detector using techniques such as ion mobility spectrometry, flame photometry, mass spectrometry, photoacoustic, infrared spectroscopy, detection kits and electrochemistry. Standoff detectors use infrared remote sensing techniques to detect the presence of CW agents in a range of one to five kilometers.

Most of the point CW agent detectors in use by military forces worldwide utilize ion mobility spectrometry (IMS) and reagent-based detection kits and tickets. IMS operates by drawing an air sample directly into a reaction region where all constituents in the air are ionized. The sample is then injected through a shutter and into a drift tube where the ions move under the influence of a weak electric field gradient to a detector plate. As the ions collide with the detector plate, the dependence of the signal (either charge or current) on drift time is registered as is done for a vacuum time-of-flight instrument. The generated graph of current vs. time is the ion mobility spectrum. This method is simple and sensitive, but is affected adversely by environmental factors such as changing humidity, temperature, and the composition of the air sample, all of which may influence the detector response.

Detection kits and tickets use chemical reactions that occur when CW agents interact with the various solutions and substrates. The most common indicator is a color change. This technology is even simpler and more sensitive, but it can not be used for continuous monitoring. Also oxidizing agents such as  $\text{Cl}_2$ ,  $\text{Br}_2$  and  $\text{NO}_2$  or acidic species  $\text{CO}_2$ ,  $\text{SO}_2$ , and  $\text{NO}_2$  cause a false response.<sup>6</sup>

Other detection technologies are not commonly used because of their practical limitations. Flame photometry and mass spectrometry are only used extensively as laboratory analytical techniques. Flame photometry suffers from interference from other compounds containing the same elements, while mass spectrometry is too complex and expensive. IMS is, in fact, the only version of mass spectrometry (albeit of lower selectivity) that has found any significant usage for *in situ* chemical agent detection.

Photoacoustic IR spectroscopy is a relatively recent CW detection technology. This technique is easily affected by humidity and other environmental factors<sup>6</sup>, and is exactly equivalent to standard infrared spectroscopy except that absorbance is detected by the heating of a sample instead of a photoelectric effect. Given the additional factors that complicate this detection scheme, its applicability is probably less than that of standard IR spectroscopy.

Several CW agent detectors operate on the electrochemical principles. A common type of electrochemical cell for nerve gas detection monitors the hydrolytic activity of cholinesterase by interaction with butylthiocholine followed by an electrochemical determination of the hydrolysis product, thiocholine, using a graphite working electrode. This type of sensor can utilize a continuous supply of butylthiocholine to provide long-term continuous detection. Electrochemical sensors based on conductivity also can be used for continuous monitoring. However conductivity meters suffer from interference from acidic gases, which dissociate into ions in aqueous solution.

Much of the hoped-for future technology may require revolutionary breakthroughs (e.g., new materials, new chemistries, new detection concepts, new integrations of technologies) in detection capability, rather than evolutionary progress down the same paths already trod repeatedly.

#### ***Summary of the Most Important Results***

The project can be divided into the following tasks:

Task 1. Design and Synthesize Sensing Chemistries. Changes in the redox potential or absorption/fluorescence of small transducer molecules, or changes in the conductivity of the sensor support media are all viable bases for detection.

Task 2. Design Supports for the Chemistries. To effectively allow the nerve gas analyte to be detected, it will be necessary to react it with the sensing chemistries or indicator. This can best be achieved if the indicator is dispersed on an inert high surface area support. Candidates for such supports range from insulating high surface area silica, alumina, and titania to framework-type materials, such as zeolites, to conducting supports, such as high surface area carbon.

Task 3. Develop Wide-Band Optical Detection Methods. We can capitalize on existing and new optical-detection reagent chemistries (colorimetric, fluorescimetric, etc.) by using the selectivity of multivariate data analytic methods, provided a sensitive and cost-effective means of implementing them can be developed. Our approach to this problem is through multivariate optical computation.

Task 4. Develop Remote Sensors Based on Electrochemical Effects. Potentiometric and microgalvanic transducers and transduction mechanisms are the basis for making small electrochemical sensors. We will develop such microtransducers to serve as efficient and selective ion and molecule detectors using ion-selective membranes and selective redox cycles for dissolved and airborne nerve gas species.

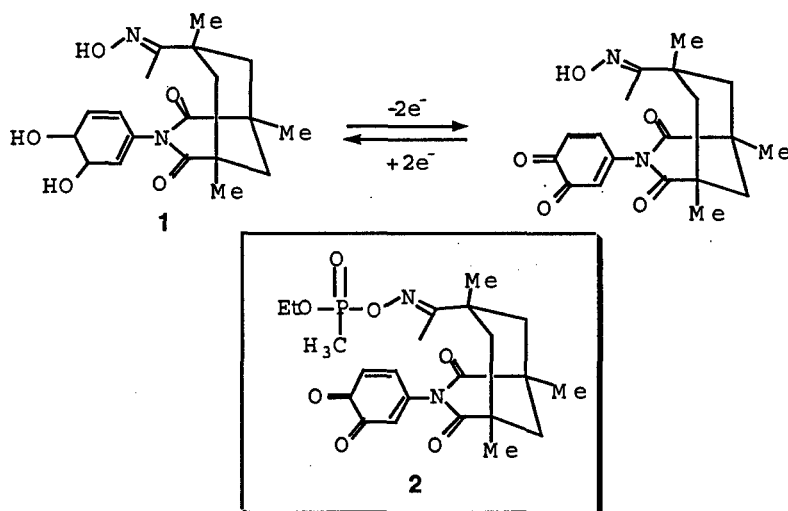
Our progress in each of the task areas is summarized below.

#### *Task 1*

##### **Introduction**

Nerve gases are generally low molecular weight, neutral organophosphonate esters which are very potent inhibitors of acetylcholinesterase. We are developing small transducer molecules which could form the basis for new chemical sensors that are capable of remotely detecting phosphorus-based nerve gas molecules in the atmosphere. We seek to employ either electrochemistry or fluorescence spectroscopy to detect changes in these transducer moieties upon covalent binding with organophosphonates. Due to the high reactivity of organophosphonate nerve gasses with oximes, we have incorporated this functionality into our synthetic targets. These molecules contain both an oxime, and either a fluorescence- or redox-active group, within a molecular cleft scaffold. We aim to demonstrate that such molecular transducers are capable of detecting covalently-bound organophosphonates nerve gasses. For example, our proposed electrochemical sensor (1) incorporates a catechol subunit which can be subjected to a sweeping alternating electrical potential (e.g.,  $\pm 0.5$  V). Based on prior electrochemical studies on molecular cleft scaffolds,<sup>9</sup> we predict that binding of a nerve gas in the molecular cleft will produce a measurable change in the redox potential and the current/voltage relationship of the catechol transducer moiety (Figure 1).

Figure 1



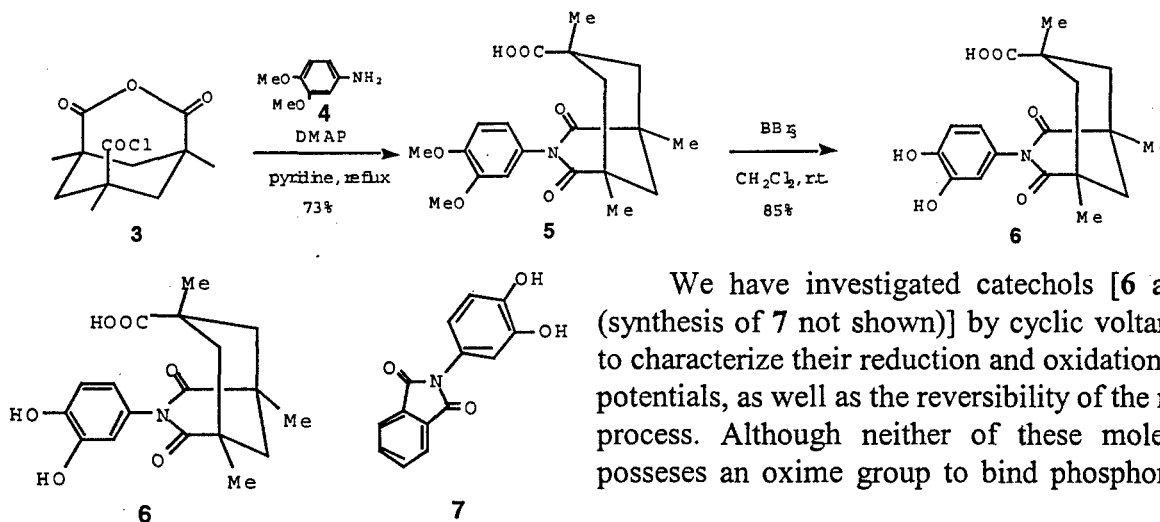
bound VX phosphonate species

(detected by linear sweep voltammetry)

### Synthesis of Electrochemically-Based Nerve Gas Sensors

Our syntheses of all the proposed transducer molecules begins with the known acid chloride anhydride (3), which can be prepared in three steps from Kemp's triacid.<sup>10</sup> For the electrochemical sensors, this acid chloride is condensed with a protected catechol moiety [4-aminoveratrole (4)] in hot pyridine, with a catalytic amount of 4-(dimethylamino)-pyridine (DMAP),<sup>11</sup> to furnish imide (5). The two methyl protecting groups in 5 can be removed with boron tribromide,<sup>12</sup> to provide catechol (6) in excellent yield.

Scheme 1



We have investigated catechols [6 and 7 (synthesis of 7 not shown)] by cyclic voltammetry to characterize their reduction and oxidation peak potentials, as well as the reversibility of the redox process. Although neither of these molecules possesses an oxime group to bind phosphonates,

both compounds did show stable cyclable electrochemical behavior, although **6** did not display the reversible behavior observed with **7**.

### Attempted Synthesis of Oxime (**9**)

Scheme 2 illustrates our attempted synthesis of oxime (**9**). Methyl ketone (**8**) was prepared from carboxylic acid (**5**) in good yield by using excess methyl lithium, followed by treatment with trimethylsilyl chloride, which protects the ketone during the workup.<sup>13</sup> The structure of this ketone was confirmed by <sup>1</sup>H and <sup>13</sup>C NMR, as well as FAB mass spectrometry. Our attempts at preparing oxime (**9**) from ketone (**8**) are summarized in Table 1. Unfortunately, none of the desired oxime was ever obtained. We believe that the methyl group in **8** is both sterically and electronically shielded. Evidence for electronic shielding by the  $\pi$ -system of the aromatic ring was seen in the proton NMR spectrum of **8**, where the methyl protons were shifted upfield substantially (0.6 ppm) from where they would normally be found.

Scheme 2

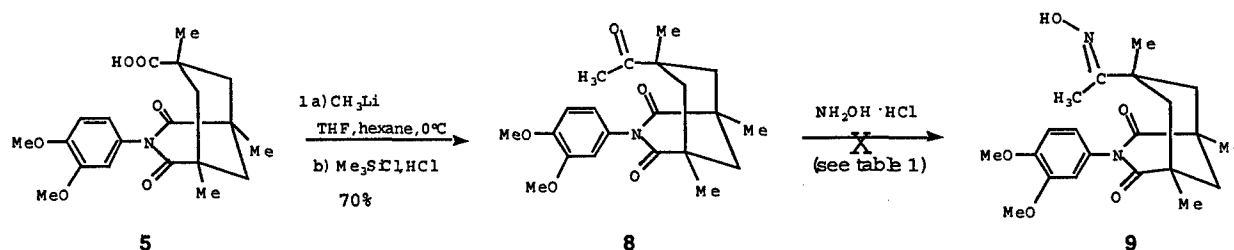


Table 1

#	Base	Solvent	Temperature	Duration	Results
1	NaOAc	ethanol	rt. $\rightarrow$ reflux	overnight	no reaction
2	none	ethanol/pyridine	rt. $\rightarrow$ reflux	overnight	no reaction
3	none	pyridine	rt. $\rightarrow$ reflux	48 hr.	no reaction
4	NaOAc	ethanol	microwave various power levels	5-30 min.	no reaction
5	none	ethanol/pyridine	microwave various power levels	5-30 min.	no reaction at low power decomp. at high power
6	none	pyridine	microwave various power levels	5-30 min.	no reaction at low power decomp. at high power
7	KOAc	pyridine	microwave various power levels	5-30 min.	no reaction at low power decomp. at high power

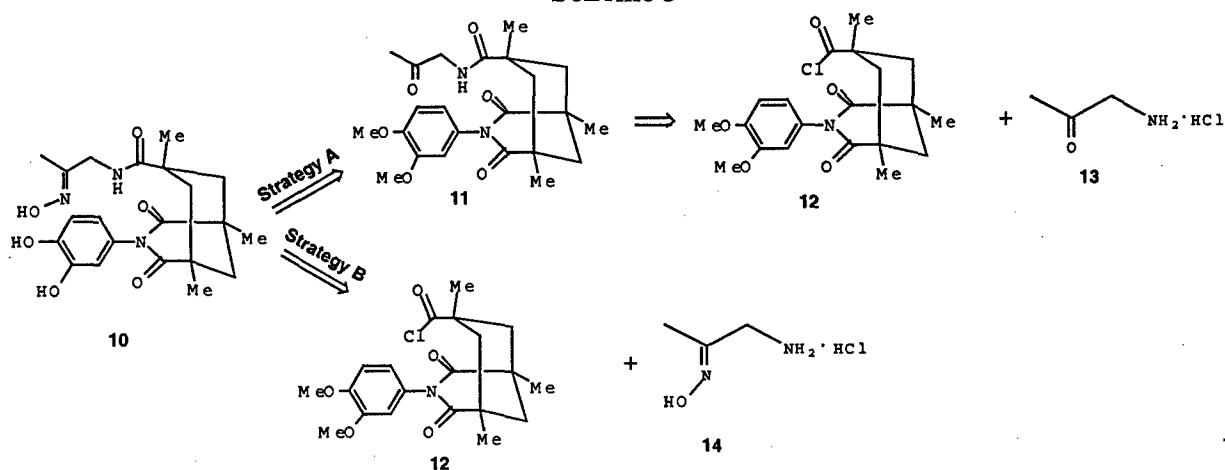
### Synthesis of Modified Electrochemical Sensor Target (**10**)

Due to the difficulties we encountered in the preparation of oxime (**9**) from ketone (**8**), we modified our initial target to oxime (**10**), which is shown in Scheme 3. By comparison with the



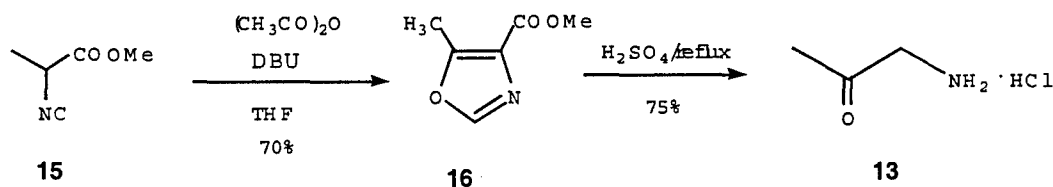
original oxime target (9), oxime (10) contains three additional atoms (a methylene carbon, an amide nitrogen, and a carbonyl carbon) between the oxime and the bicyclic scaffold. This results in a greater degree of conformational flexibility around the ketone. Moreover, the oxime group in 10 is not located as deep within the cleft as had been the case with 9. These differences should improve the ease of oxime formation. Scheme 3 shows two possible retrosynthetic strategies toward oxime (10). Results from recent investigations of "Strategy A" are described here. This approach involves formation of oxime (10) from ketone 11, which, itself, is prepared from acid chloride (12) and amino acetone hydrochloride (13). An alternative approach ("Strategy B") involves acylation of a pre-formed amino oxime (14) with 12. This alternative strategy has not yet been explored, although it represents a more convergent synthetic approach to 10 than "Strategy A".

Scheme 3



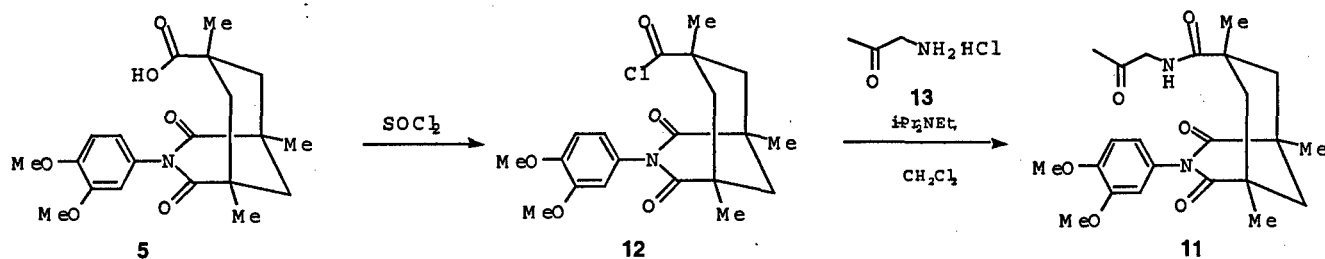
Scheme 4 illustrates the synthesis of the known glycine methyl ketone hydrochloride (13). The requisite oxazole (16) was easily obtained by the reaction of  $\alpha$ -isocyanoacetate analog (15) with acetic anhydride in the presence of an organic base such as DBU (1,8-diazabicyclo-[5.4.0]-undec-7-ene).<sup>14</sup> Acid hydrolysis of this oxazole gave  $\alpha$ -amino ketone (13).

Scheme 4



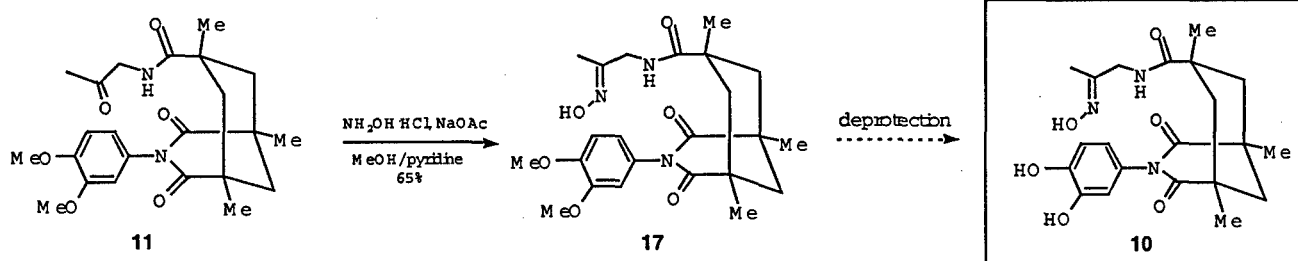
Scheme 5 illustrates the use of amino ketone (13) in the synthesis of ketone (11). Acid (5) was first treated with thionyl chloride, and the resulting acid chloride (12) reacted with 13 to provide the desired ketone (11).

### Scheme 5



Oxime **17** was then prepared by the reaction between ketone **11** and hydroxylamine hydrochloride (Scheme 6). Preliminary proton NMR spectral evidence confirms that we have successfully synthesized oxime **17**. Currently, Dr. Popov's group is assisting us in the deprotection of the catechol moiety in **17**, via electrochemical means, to achieve our targeted sensor (**10**).

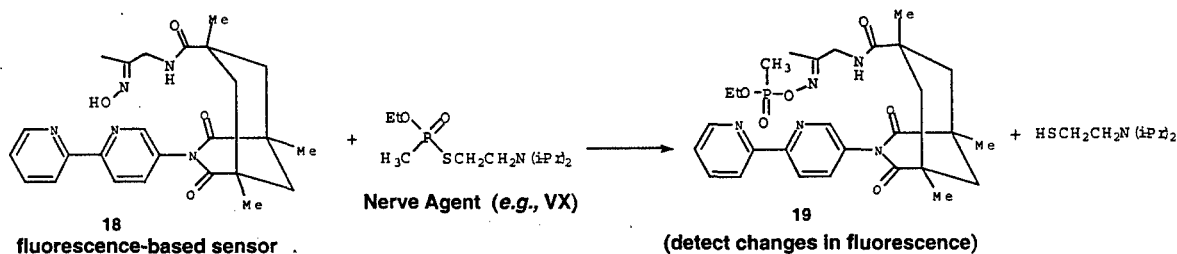
### Scheme 6



### Fluorescence-based Nerve Gas Sensor

Recently, we have also initiated work on a fluorescence-based nerve gas sensor (**18**, Scheme 7). This sensor incorporates a cleft-bound oxime, along with a solvatochromic bipyridyl moiety. Upon reaction with an organophosphonate nerve gas, the resulting oxime phosphonate ester will be positioned

### Scheme 7

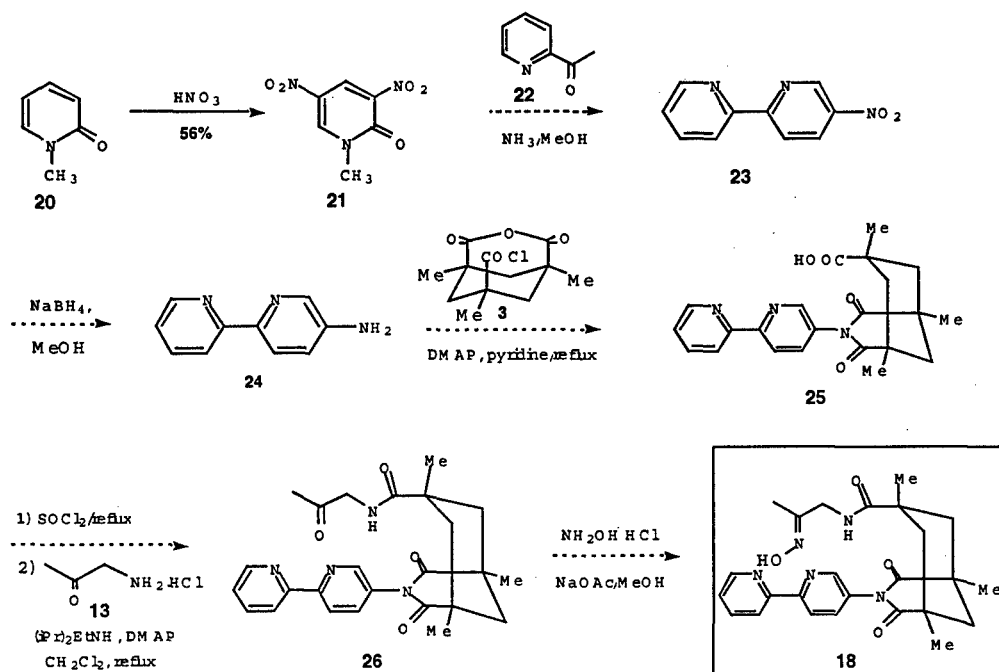


directly above the bipyridyl chromophore. We expect to see marked changes in the fluorescence frequency and/or intensity of the chromophore upon phosphonate ester formation (**19** compared to **18**).

### Proposed Synthesis for Fluorescence-Based Sensor (18)

Scheme 8 illustrates our proposed synthesis of the fluorescence-based sensor (18). Nitration of 1-methyl-2-pyridone (20) provided the known 3,5-dinitro-2-pyridone (21).<sup>15</sup> Treatment of 21 with 2-acetyl pyridine (22) in the presence of ammonia will provide the 5-nitro-2,2'-bipyridine (23).<sup>16</sup> Nitro group reduction with sodium borohydride in methanol will furnish the known amino bipyridine (24).<sup>17</sup> Reaction of this amine and acid chloride/anhydride (3) will give carboxylic acid (25). Treatment of 25 with thionyl chloride and acylation of amine (13) with the resulting acid chloride will provide ketone (26). Oxime formation from this ketone will then furnish the targeted optically-based sensor (18). Note that this approach to 18 is comparable to "Strategy A" described for the synthesis of 10 in Scheme 3.

Scheme 8

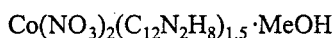
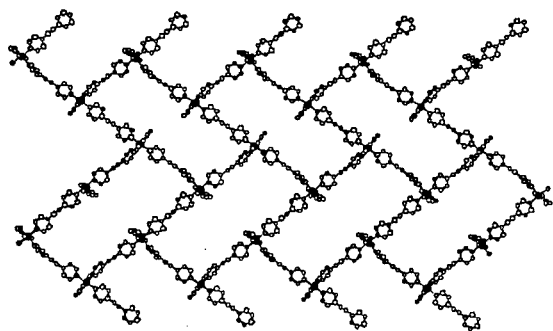


### Task 2

To effectively allow the nerve gas analyte to be detected, it will be necessary to react it with the sensing chemistries or indicator. This can best be achieved if the indicator is dispersed on an inert high surface area support. Candidates for such supports range from insulating high surface area silica, alumina, and titania to framework-type materials, such as zeolites, to conducting supports, such as high surface area carbon. The surface chemistry of the support must be chemically compatible - that is, there must not be any detrimental interactions - with the indicator as well as the analyte, and in addition, the support must not interfere with the electrochemical characterization of the indicator-analyte complex. Therefore, we will identify a suitable high surface area support. Once one or two suitable supports have been identified, the procedures necessary to disperse the diverse indicators on the support must be established.

We have investigated the preparation of porous framework solids onto which to disperse the analyte. To achieve this goal, we have reacted bidentate, non-chelating ligands with transition metal ions to generate new families of porous organic/inorganic coordination polymers. The synthetic approach has concentrated on solution and solvothermal syntheses. In both cases, high quality single crystals of new materials have been obtained and structurally characterized by single crystal X-ray diffraction. Several of these new framework solids have porous structures and their thermal stability has been determined by thermogravimetric analysis. Below, the structures of several of these new materials are shown and described. At the end of the report, copies of papers that have been submitted and that acknowledge the DOD grant are attached.

Compound 1 adopts a novel infinite interpenetrating molecular parquet motif, in which each parquet tile in the pattern consists of six 1,2-bis(4-pyridyl)ethyne ligands and six cobalt atoms. In fact, it is a 66-member ring structure. The two-dimensional parquet layers are not perfectly flat, but undulate due to the distorted T-joint ligand coordination geometry around the cobalt atoms. This parquet pattern is distinctly different from the brick wall pattern reported previously for  $\text{Cd}[\text{1,4-methylenepyridyl}]\text{2,3,5,6-tetrafluorobenzene)}_{1.5}]_n (\text{NO}_3)_2$ , in which the rectangular units are joined together in parallel. In compound 1, two sets of tiles are joined together nearly perpendicularly to each other. Each tile is offset by half a "step" along each axis. During the X-ray analysis, significant electron density was found within the cavities of the parquet framework. This is consistent with a disordered methanol solvent molecule, a common phenomenon in coordination polymer chemistry. It was refined with the methanolic carbon position fully occupied, and two oxygen sites each half-occupied. This disorder model reasonably accounted for all significant residual electron density found in the Fourier analysis.



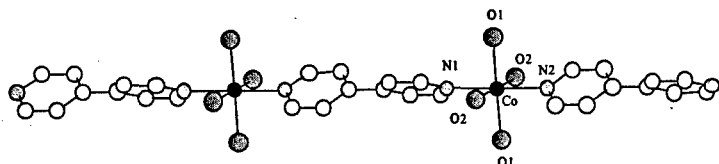
Compound 2

Compound 2 has an infinite 1D structure with interpenetrating molecular ladders, which involves a 44 member square structure. The square structure consists of four 1,2-bis(4-pyridyl)ethyne ligands and four cobalt atoms. The ladder pattern is generated via the 1,2-bis(4-pyridyl)ethyne ligands with each bridging two Co(II) centers. A disordered solvent molecule is present, which was modeled as a methanol in a similar fashion as in compound 1. Compound 2 may be termed a flat ladder with all linking ligands coplanar, of which there are few known examples,  $[\text{Co}(\text{NO}_3)_2(1,2\text{-bis}(4\text{-pyridyl)ethane})_{1.5}]_n$ ,  $\text{Co}(\text{NO}_3)_2(4,4'\text{-bpy})_{1.5}]_n$ , and

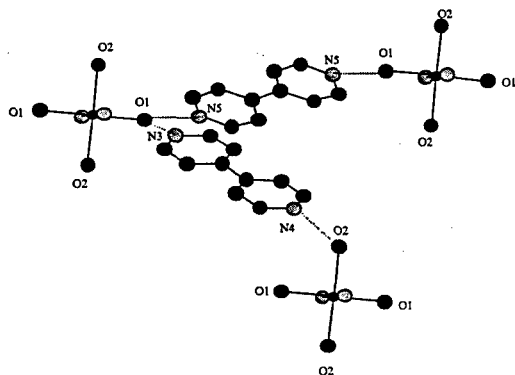
$[\text{Cd}(\text{NO}_3)_2(1,4\text{-bis}(4\text{-methylenepyridyl)benzene})_{1.5}]_n$ . It is, however, quite different from the ladder generated from the reaction of  $[\text{Cu}(\text{MeCN})_4]\text{PF}_6$  with 1,4-bis(4-pyridyl)-butadiyne, the structure of which contains an undulating ladder that results from the tetrahedral Cu(I) centers.

As shown in the figure, the structure of compound 3 features hexacoordinate  $\text{Co}^{2+}$  centers assembled into linear chains through intervening bipy ligands. The coordination environment of each cobalt atom consists of two pyridyl nitrogen donors from two bipy ligands and four aquo oxygen donors. The pseudo-octahedral coordination geometry may be described as a basal plane associated with O(1) and O(2) from the four water molecules ( $\text{O}(1)\text{-Co-N}(1) = 90.44^\circ(9)$ ,  $\text{O}(1)\text{-}$

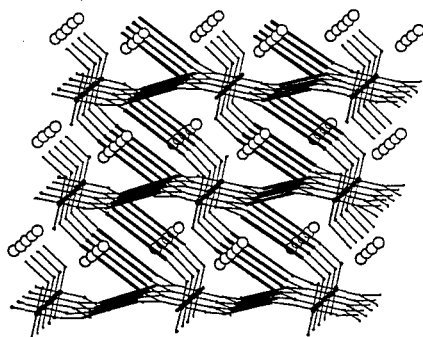
Co-N(2) = 89.56°(9), O(2)-Co-N(1) = 88.97°(8) and O(2)-Co-N(2) = 91.03°(8)), having Co-O bond lengths of 2.054(3) Å and 2.144(3) Å, respectively, with axial positions occupied by *trans* nitrogen donors N(1) and N(2), having Co-N distances of 2.150(5) Å and 2.170(5) Å, respectively.



The one-dimensional  $[\text{Co}(\text{H}_2\text{O})_4(\text{bipy})_2]$  chain in compound 3. Hydrogen atoms omitted for clarity.



$\text{Co}-\text{H}_2\text{O} \cdots (\text{bipy})_2 \cdots (\text{H}_2\text{O}-\text{Co})_2$  hydrogen bonding linkage in compound 3.



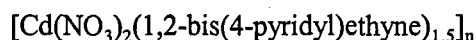
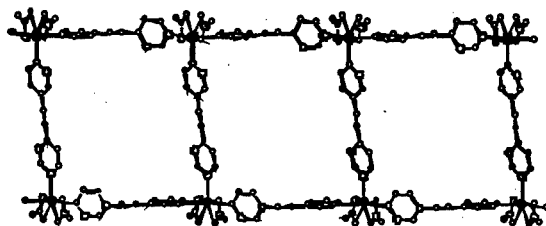
Crystal packing pattern of  $[\text{Co}(\text{H}_2\text{O})_4(\text{bipy})_2][\text{PF}_6]_2 \cdot 2\text{bipy}$ , compound 3, viewed down the *b* axis (parallel to the  $[\text{Co}(\text{H}_2\text{O})_4(\text{bipy})_2]$  polymer chains) showing the extended 3-D network formed by  $\text{Co}-\text{H}_2\text{O} \cdots (\text{bipy})_2 \cdots (\text{H}_2\text{O}-\text{Co})_2$  hydrogen bonding linkages. Cobalt centers are shown as larger black circles, coordinated aquo oxygen atoms as smaller black circles and interpolymer bipy ligands as heavy black lines. The  $\text{PF}_6^-$  anions are represented as large open circles; all H atoms are omitted for clarity.

The crystal packing observed in compound 3 reveals that the main structural feature is the presence of linear -Co-bipy-Co-bipy- chains oriented parallel to the crystallographic *b* axis. The two pyridyl groups of the bipy molecules within

these chains are rotated by ca. 60° with respect to one another. The chains themselves connect to each other through hydrogen bonds,  $\text{OH} \cdots \text{N}$ , ( $\text{O} \cdots \text{N}$  range 2.72 - 2.84 Å), involving coordinated water and uncoordinated bipy molecules. In contrast to the coordinated bipy molecules, the pyridyl groups of the uncoordinated bipy molecules are strictly coplanar.

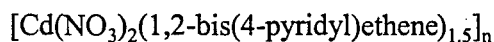
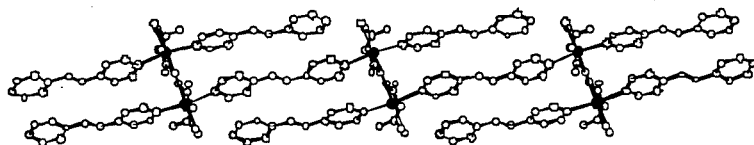
There are two types of coordinated water molecules in compound 3, as shown in the figure, due to  $\text{H}_2\text{O}(1)$  forming hydrogen bonds with two uncoordinated bipy molecules ( $\text{H}_2\text{O}(1) \cdots (\text{bipy})_2$ ,  $d(\text{O} \cdots \text{N}) = 2.832(7)$  Å) and due to  $\text{H}_2\text{O}(2)$  forming a hydrogen bond with only one uncoordinated bipy molecule ( $\text{H}_2\text{O}(2) \cdots (\text{bipy})$ ,  $d(\text{O} \cdots \text{N}) = 2.722(7)$  Å). One of two  $\text{H}_2\text{O}(1) \cdots \text{bipy}$  linkages binds the cobalt centers into zigzag chains along the crystallographic *c* axis, while the other  $\text{H}_2\text{O}(1) \cdots \text{bipy}$  and  $\text{H}_2\text{O}(2) \cdots \text{bipy}$  linkages involve the same cobalt centers to give hexahedrons connected to each other *via* cobalt joints extending in the crystallographic *ac* plane. The positive charge of this metallo-ligand lattice is balanced by  $\text{PF}_6^-$  counterions located in the large

cavities formed by  $\text{Co-H}_2\text{O}\cdots\text{bipy}\cdots\text{H}_2\text{O}$  linkages. The lengths of the hydrogen-bonded interchain  $\text{Co-H}_2\text{O}(1)\cdots\text{bipy}\cdots\text{H}_2\text{O}(1)\text{-Co}$  and  $\text{Co-H}_2\text{O}(1)\cdots\text{bipy}\cdots\text{H}_2\text{O}(2)\text{-Co}$  segments are 17.011(7) Å and 16.887(6) Å, respectively, significantly longer than the intrachain  $\text{Co}\cdots\text{Co}$  distance (11.397(6) Å) linked *via* coordination bonds through bipy ligands.



Compound 4

The X-ray structural analysis of compound 4 revealed that the Cd(II) centers assume a heptacoordinate environment. The three 1,2-bis(4-pyridyl)ethyne ligands form a "T-joint" at the Cd(II) atoms ( $\text{Cd}(1)\text{-N}(3) = 2.312(6)$  Å,  $\text{Cd}(1)\text{-N}(4) = 2.314(6)$  Å,  $\text{Cd}(1)\text{-N}(5) = 2.354(6)$  Å), which is slightly distorted:  $\text{N}(3)\text{-Cd-N}(4) = 173.8(2)^\circ$ ,  $\text{N}(3)\text{-Cd-N}(5) = 88.7(2)^\circ$ ,  $\text{N}(4)\text{-Cd-N}(5) = 96.8(2)^\circ$ . The remaining four coordination sites are occupied by the two bidentate nitrate anions. The bond distances (Å) between the Cd(II) atom and the four oxygen atoms in the two incorporated nitrate anions are:  $\text{Cd-O}(1) = 2.419(6)$ ,  $\text{Cd-O}(2) = 2.419(2)$ ,  $\text{Cd-O}(4) = 2.456(6)$ ,  $\text{Cd-O}(5) = 2.435(6)$ . The T-shaped building blocks in compound 4 are connected to each other to form an infinite 1D structure with interpenetrating molecular ladders which involve 44-member square rings. Each large square ring has dimensions of 14.249(4) Å x 14.315(4) Å and is enclosed by four 1,2-bis(4-pyridyl)ethyne ligands and four Cd(II) atoms.



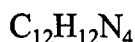
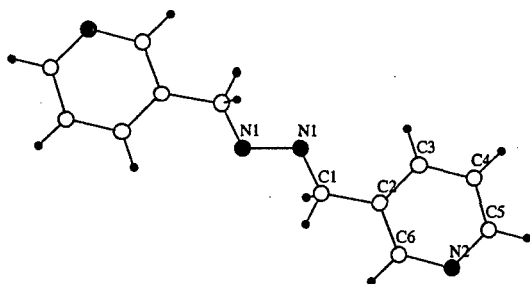
Compound 5

$[\text{Co}(\text{NO}_3)_2(1,2\text{-bis}(4\text{-pyridyl})\text{ethane})_{1.5}]_n$  and  $[\text{Co}(\text{NO}_3)_2(4,4'\text{-bipyridine})_{1.5}]_n$ . All of the metal centers mentioned above adopt a pseudo-octahedral or octahedral coordination geometry from which a flat ladder pattern with all coplanar ligands is generated. It is, however, distinctly different from the ladder pattern generated from the reaction of  $[\text{Cu}(\text{MeCN})_4]\text{PF}_6$  with 1,4-bis(4-

The coordination geometry of the metal center plays an important role in the packing arrangement of the polymer. The coordination geometry around the Cd(II) center in compound 4 is similar to that around the Cd(II) atom in  $[\text{Cd}(\text{NO}_3)_2(1,4\text{-methylenepyridyl})\text{benzene}]_{1.5}]_n$ .

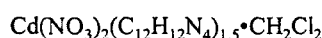
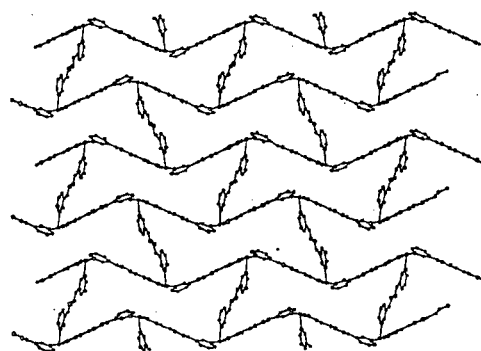
Such heptacoordinate environments have also been found in cobalt analogues:

pyridyl)butadiyne, the structure of which contains an undulating ladder resulting from the tetrahedral Cu(I) centers.



Compound 6

= 2.303(4) Å), and three oxygen donors from two nitrate anions. Two of three oxygen atoms of the nitrate anions are shared by two Cd(II) centers to form a Cd-O-Cd-O four-member ring, with Cd-O distances of 2.567(4) Å and 2.460(4) Å, respectively. It is worth noticing that there are two types of 1,2-bis(4-pyridyl)ethene ligands in compound 5. One type forms a bridge between two Cd(II) centers using two terminal pyridine groups. However, the other type of ligand only uses one terminal pyridine group to coordinate to the Cd(II) atoms, while the other terminal pyridine group is uncoordinated. Two types of *trans*-1,2-bis(4-pyridyl)ethene ligands and Cd(II) centers form a *trans*-1,2-bis(4-pyridyl)ethene-Cd-*trans*-1,2-bis(4-pyridyl)ethene-Cd-*trans*-1,2-bis(4-pyridyl)ethene linear structural unit. These units are linked by two oxygen atoms from the nitrate anions through the cadmium atoms to form a novel infinite non-interpenetrating zigzag molecular chain, which is unlike the one-dimensional double chain patterns found in [Cu(NO<sub>3</sub>)<sub>2</sub>(1,2-bis(4-pyridyl)ethyne)]0.5EtOH and [Co(4,4'-bipyridine)(CH<sub>3</sub>COO)<sub>2</sub>] polymers. Double chain structures consist of two one-dimensional linear chains which extend in parallel

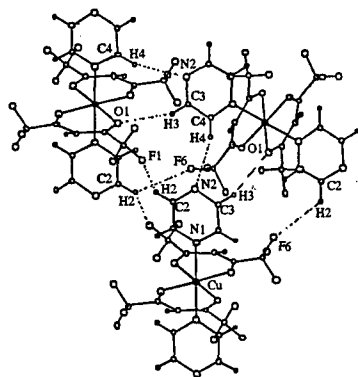


Compound 7

It is worth pointing out that two of the three ligands in this T-shaped building block in compound 4 have the terminal pyridine groups rotated by 90° with respect to one another, while the pyridine groups in the third coordinating ligand are strictly coplanar.

The situation for compound 5 is quite different from that of compound 4, both in the coordination geometry of the Cd(II) centers and in the structure. In 5, the Cd(II) atoms adopt an octahedral geometry. The coordination sphere is defined by two pyridyl nitrogen donors from two *trans*-1,2-bis(4-pyridyl)ethene ligands (Cd-N(3) = 2.295(4) Å, Cd-N(4) = 2.246(4) Å), one oxygen donor from the water molecule (Cd-O(7)

= 2.303(4) Å), and three oxygen donors from two nitrate anions. Two of three oxygen atoms of the nitrate anions are shared by two Cd(II) centers to form a Cd-O-Cd-O four-member ring, with Cd-O distances of 2.567(4) Å and 2.460(4) Å, respectively. It is worth noticing that there are two types of 1,2-bis(4-pyridyl)ethene ligands in compound 5. One type forms a bridge between two Cd(II) centers using two terminal pyridine groups. However, the other type of ligand only uses one terminal pyridine group to coordinate to the Cd(II) atoms, while the other terminal pyridine group is uncoordinated. Two types of *trans*-1,2-bis(4-pyridyl)ethene ligands and Cd(II) centers form a *trans*-1,2-bis(4-pyridyl)ethene-Cd-*trans*-1,2-bis(4-pyridyl)ethene-Cd-*trans*-1,2-bis(4-pyridyl)ethene linear structural unit. These units are linked by two oxygen atoms from the nitrate anions through the cadmium atoms to form a novel infinite non-interpenetrating zigzag molecular chain, which is unlike the one-dimensional double chain patterns found in [Cu(NO<sub>3</sub>)<sub>2</sub>(1,2-bis(4-pyridyl)ethyne)]0.5EtOH and [Co(4,4'-bipyridine)(CH<sub>3</sub>COO)<sub>2</sub>] polymers. Double chain structures consist of two one-dimensional linear chains which extend in parallel pairs joined by bridging incorporated anions in a ladder fashion. The structural motif of compound 5, however, is made up of only one stair-like chain, although the metal centers are all in octahedral environments. This kind of unique motif results from the different coordination of the two types of 1,2-bis(4-pyridyl)ethene ligands in 5. Zigzag chains containing other metals, such as Cu, Ag, and Mn, have been reported previously. Compound 5 is the first example of a zigzag chain containing cadmium atoms. It is worth noting that the direction of the chain is almost perpendicular to the Cd<sub>2</sub>O<sub>2</sub> plane (for O(1)-Cd-



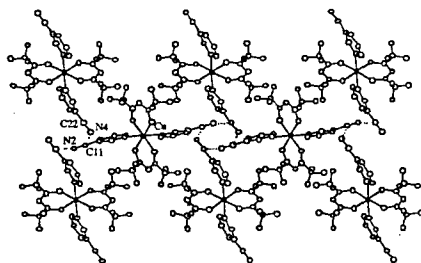
$\text{Cu}(\text{hfacac})_2(\text{pyrazine})_2$

Crystal packing of compound 8. The intermolecular hydrogen bonds are shown as dotted lines.

bidentate nitrate anions (Cd-O distances are 2.397(4), 2.414(5), 2.518(3) and 2.391(4) Å).

Compound 7 adopts a novel infinite molecular polyhexane molif, in which each "hexane" in the pattern consists of six ligands and six Cd(II) atoms. In fact, it is a 78-member ring structures. This polyhexane motif is distinctly from the brick wall and parquet pattern reported before.

As shown in the figure the structure of compound 8 is constructed from six coordinate copper sites, exhibiting 4 + 2 octahedral geometry and linked into linear chains through two *trans* pyrazine ligands. This geometry is quite different from the geometry found in  $\text{Cu}(\text{hfacac})_2(\text{pyridine})_2$ , which forms a complex made up of a *cis* bis(pyridine) adduct to  $\text{Cu}(\text{hfacac})_2$ . The coordination sphere of 8 is defined by two nitrogen donors from two pyrazine ligands, and four oxygen donors from two (hfacac) chelate ligands. The Cu-N bond in 8 is 2.055(5) Å, which is very close to the Cu-N bond length (2.043(4) Å) found in  $\text{Cu}(\text{hfacac})_2(\text{mpydz})_2$ , but is significantly shorter than the Cu-N bond in  $\text{Cu}(\text{hfacac})_2(\text{pyrazine})$  (Cu-N, 2.529(4) Å) and  $\text{Cu}(\text{hfacac})(\text{ted})$  (Cu-N, 2.566(7) Å). The Cu-O bond lengths in 8 are 2.225(4) and 1.995(7) Å, respectively, which are slightly longer than the Cu-O distances (2.004(7) and 1.924(7) Å) in  $\text{Cu}(\text{hfacac})_2(\text{pyrazine})$ . They are very similar to the values of 2.228(4) and 2.009(3) Å which were found in  $\text{Cu}(\text{hfacac})_2(\text{mpydz})_2$ . The two pyrazine rings in 8 are strictly coplanar, which are perpendicular to the plane consisting of the Cu(II) center and two (hfacac) chelate ligands. In the solid state, the molecules are interconnected to each other to give a three dimensional network through the weak hydrogen bonding systems involving



$\text{Cu}(\text{hfacac})_2(3\text{-cyanopyrazine})_2$

The crystal packing of 9 as projected on the *ab* plane. Hydrogen atoms are omitted for clarity.

$\text{N}(3) = 87.7(1)^\circ$ ,  $\text{O}(1)\text{-Cd-N}(3) = 85.8(1)^\circ$ .

Compound 6 is the bidentate ligand which has a linkage of  $\text{-HC=N-N=CH-}$  as a bridge. It is composed of zig-zag chains.

In compound 7, Cd(II) centers lie in a heptacoordinate environment. The three ligands form a distorted "T-joint" at Cd(II) atoms ( $\text{N}(8)\text{-Cd-N}(11) = 83.72(4)^\circ$ ,  $\text{N}(3)\text{-Cd-N}(11) = 92.41(3)^\circ$ . Cd-N distances are 2.353(5), 2.328(5) and 2.391(3) sites are occupied by two

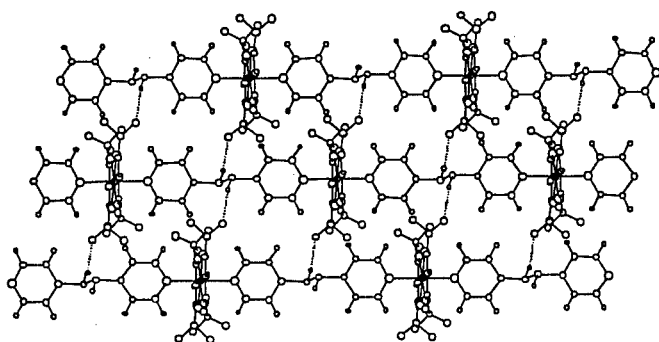


the F(1), N(2), F(6), and O(1) atoms and the H(2), H(3) and H(4) atoms on the pyrazine ligands of neighbor molecule. The F(1)···H(2), F(6)···H(2), N(2)···H(4) and O(1)···H(3) distances are 2.835(5), 2.983(6), 2.630(6) and 2.708(6) Å, respectively. The corresponding F(1)···C(2), F(6)···C(2), N(2)···C(4) and O(1)···C(3) distances are 3.412(5), 3.653(4), 3.541(5) and 3.574(4) Å, respectively, and the corresponding F(1)···H(2)-C(2), F(6)···H(2)-C(2), N(2)···H(4)-C(4) and O(1)···H(3)-C(3) angles are 120.48(5)°, 129.10(4)°, 159.97(3)° and 155.20(4)°, respectively. The similar hydrogen bonding systems were observed in the (C<sub>14</sub>H<sub>12</sub>N<sub>2</sub>)[Cu(opba)]·3H<sub>2</sub>O and Na<sub>2</sub>(C<sub>12</sub>H<sub>12</sub>N<sub>2</sub>)[Cu(opba)]<sub>2</sub>·4H<sub>2</sub>O (opba = *o*-phenylenebis(oxamate)). On the other hand, intramolecular hydrogen bonds also exist in 8 between the oxygen atom of (hfacac) ligand and hydrogen atom of pyrazine ligand. The O2···H4 distances is 2.686(5) Å. The corresponding O(2)···C(4) distance is 3.063(5) Å.

In compound 9, there are two different types Cu(hfacac)<sub>2</sub>(3-cyanopyridine)<sub>2</sub> molecules in the unit cell. The structures of both A and B are basically same. Their coordination environments around the Cu(II) centers consist of two pyridine nitrogen atoms from two 3-cyanopyridine and four oxygen atoms from two (hfacac) chelate ligands in a slightly octahedral configuration in molecule A with O(1)-Cu(1)-O(2) = 91.1(1)°, O(1)-Cu(1)-N(1) = 90.5(2)° and O(2)-Cu(1)-N(1) = 90.3(1)°, and a distorted octahedral geometry in molecule B with O(3)-Cu(2)-O(4) = 88.3(2)°, O(3)-Cu(2)-N(3) = 89.6(2)° and O(4)-Cu(2)-N(3) = 93.0(2)°. The Cu(II) centers

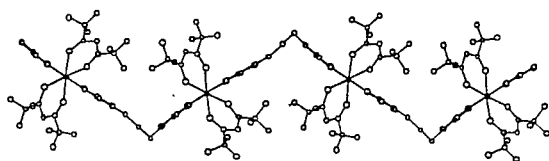
of A and B are linked to two 3-cyanopyridine ligands through pyridine nitrogen atoms to form a chain in a zigzag fashion running parallel to the *b* axis (molecule A) and *a* axis (molecule B), respectively. It is worth pointing out that the nitrogen donors in the 3-cyanopyridine ligands have a different bond length with the copper center in A and B. In molecule B, a long Cu-N (2.389(5) Å) bond resulting from Jahn-Teller distortions was found which is significantly longer than the Cu-N bond (2.097(4) Å) in molecule A, but it is very close to the Cu-N bond (2.381(5)

Å) which was found in Cu(hfacac)<sub>2</sub>(bipy), while the Cu-O distances (Cu(2)-O(3) = 1.970(4), and Cu(2)-O(4) = 1.994(4) Å) are slightly shorter than those of in molecule A (Cu(1)-O(1) = 1.991(4) and Cu(1)-O(2) = 2.184(4) Å). As shown in the crystal structure, ligating molecules of A and B have neighboring molecules B and A at short distances of 3.448(6) Å [N(2)···C(22)≡N(4)] and 3.403(6) Å [N(4)···C(11)≡N(2)], respectively, suggesting that the uncoordinated



Cu(hfacac)<sub>2</sub>(1,2-bis(4-pyridyl)ethane)

The crystal packing of compound 10 as projected on the *ac* plane.  
The inter-polymer hydrogen bonds are shown as dotted lines.

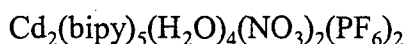
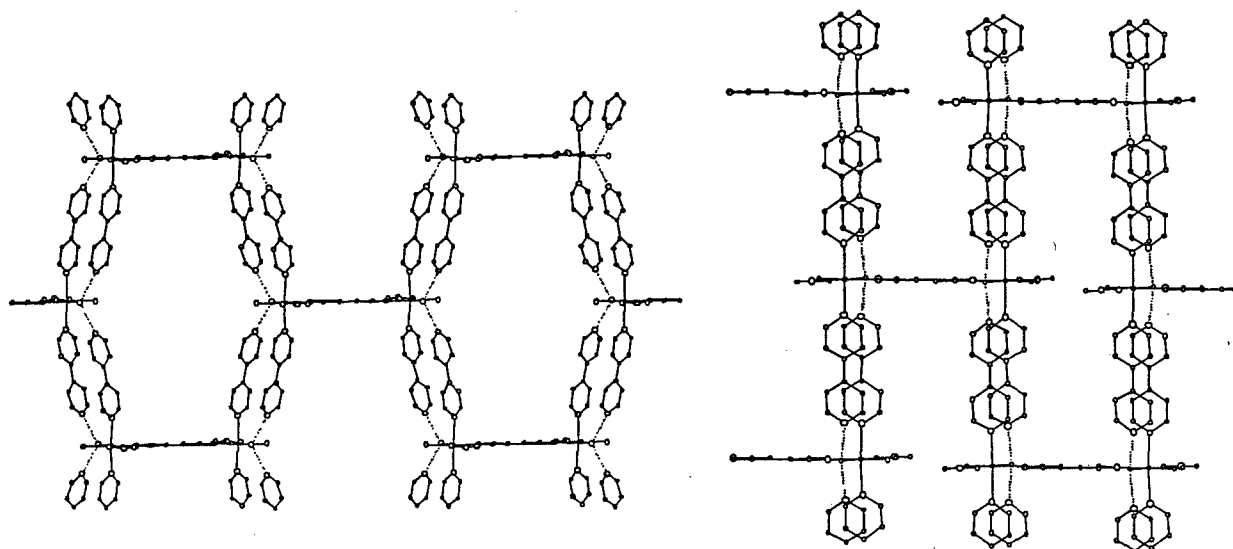


Cu(hfacac)<sub>2</sub>(4,4'-trimethylenebipyridine)

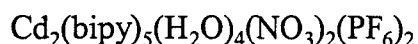
The one-dimensional sinusoidal chain of 11 (down *a* axis).  
The hydrogen atoms are omitted for clarity.

nitrile groups would interact with each other intermolecularly.

X-ray analyses of compounds **10** and **11** show that they have polymeric structures based on networks of octahedrally coordinated Cu(II) centers linked by 1,2-bis(4-pyridyl)ethane and 4,4'-trimethylenebipyridine, respectively. The local geometry of Cu(II) in compound **10** is similar to the geometry of the copper center in compound **8**. The octahedral Cu(II) sphere consists of two nitrogen donors from two *anti* 1,2-bis(4-pyridyl)ethane ligands and four coordinated oxygen atoms from two (hfacac) chelate ligands. The Cu-N = 2.014(6) and Cu-O = 2.129(8) Å are very close to the Cu-N and Cu-O bond lengths that were found in compound **8**. The Cu(II) centers are linked to each other by *anti* 1,2-bis(4-pyridyl)ethane through the pyridyl nitrogen atoms into a one-dimensional zigzag chain along the [-101] direction. Intra-polymer Cu...Cu contact is 13.296(6) Å. Inter-polymer Cu...Cu contacts are 7.922(6) and 10.163(6) Å. In addition, hydrogen bonding interactions were observed in **10**. Intramolecular bifurcated hydrogen bonds were found between two oxygen atoms of (hfacac) ligands and two hydrogen atoms on the pyridine rings, and also fluorine between hydrogen atoms in the (hfacac) ligand.

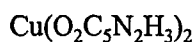
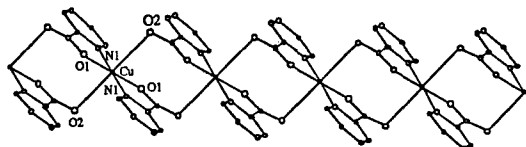


Compound **12**



Compound **12**

All these values are in agreement with the reported geometries for bifurcated hydrogen bonded systems. Ligating polymers of **10** have neighboring polymers at a short distance resulting from interpolymer hydrogen bonding interaction. The hydrogen bonding system involving F(4) of the (hfacac) ligand and H(4) on the 1,2-bis(4-pyridyl)ethane ligand of the neighboring polymer chain. The F(4)...H(4) contact is 2.562(5) Å which is shorter than the sum of the van der Waals radii of hydrogen and fluorine (2.67 Å). The F(4)...C(4) distance and F(4)...H(4)-C(4) angle are 3.481(6) Å and 170.64(5)°, respectively. The interpolymer hydrogen bonding interaction give rise to a 2-D arrangement of 1-D polymers parallel to the *ac* plane. As for **11**, the Cu(II) center lies in a 4 + 2 Jahn-Teller distorted octahedral environment (O(1)-Cu-O(2) = 86.9(6)°, O(1)-Cu-O(3) = 176.9(3)°, O(2)-Cu-O(4) = 175.9(3)°, O(2)-Cu-O(3) = 96.2(3)°, O(1)-Cu-N(1) = 88.9(3)°, O(1)-Cu-N(2) = 88.9(3)°, O(2)-Cu-N(1) = 88.9(3)°, O(2)-Cu-N(2) = 88.9(3)°).



Compound 13

conformation. It is worth pointing out that the GG' conformation of 4,4'-trimethylenepyridine in **11** is different from the TT conformation found in the 1-D polymer  $\text{Ag}(4,4'\text{-trimethylenepyridine})(\text{CF}_3\text{SO}_3)\cdot\text{EtOH}$ , although they all adopt a sinusoidal chain fashion, which results in two sets of  $\text{Cu}(\text{hfacac})_2$  planes in **11** with a dihedral angle  $\sim 60^\circ$ . The  $\text{Cu}(\text{hfacac})_2$  planes in each set are parallel to each other. In **11**, intramolecular bifurcated hydrogen bonds were found between two fluorine atoms and one hydrogen atom in the (hfacac) ligand with  $\text{F}(4)\cdots\text{H}(16) = 2.377(6) \text{ \AA}$  and  $\text{F}(2)\cdots\text{H}(16) = 2.353(6) \text{ \AA}$ . The contacts of  $\text{F}(4)\cdots\text{C}(16)$  and  $\text{F}(2)\cdots\text{C}(16)$  are  $2.727(4)$  and  $2.739(4) \text{ \AA}$ , respectively. However, no interpolymer hydrogen bonding interaction was found in **11**, which is quite different from **10**.

The formula of compound **12** is  $\text{Cd}_2(\text{bipy})_5(\text{H}_2\text{O})_4(\text{NO}_3)_2(\text{PF}_6)_2$ . The Cd(II) center lies in an octahedral geometry. The coordination sphere is defined by three nitrogen donors from three bipy ligands ( $\text{Cu-N} = 2.294(4) \text{ \AA}$ ), and two oxygen donors from coordination water molecules ( $\text{Cu-O} = 2.332(4) \text{ \AA}$ ), and one oxygen donor from nitrate counter ion ( $\text{Cu-O} = 2.400(4) \text{ \AA}$ ). In addition, each Cd(II) contains one uncoordinated  $\text{PF}_6^-$  counter ion. The five bipy ligands and two Cd(II) centers form a "H" shaped molecule. Two uncoordinated  $\text{PF}_6^-$  ions lie in the space surrounded by five bipy ligands.

There are two types of bipy ligands in the complex, one type forms a bridge between two Cd(II) centers using two terminal pyridine groups, the other type of ligand only use one terminal pyridine group to coordinate to the Cd(II) centers, while the other terminal pyridine is uncoordinated. However, they form the bifurcated intermolecular hydrogen bonds with the aquo ligand in the neighbor molecule ( $\text{N}\cdots\text{O}$  distance is  $2.831(4) \text{ \AA}$ ), which results in a novel 2-D pattern.

In compound **13**, the Cu center adopts  $\{\text{CuO}_4\text{N}_2\}$  coordination geometry, defined by four oxygen donors and two nitrogen donors from four 2-pyrazinecarboxylate ligands. The six coordination is best described as  $4 + 2$  distorted octahedral geometry. The equatorial plane is defined by two nitrogen donors with Cu-N distance of  $1.983(4) \text{ \AA}$  and two Cu-carboxylate oxygen donors at  $1.937(4) \text{ \AA}$ . The axial position are occupied by another two carboxylate oxygen donors with a long distance of  $2.740(3) \text{ \AA}$ . The structure of **13** consists of parallel one-dimensional chains along the *a* axis. The Cu $\cdots$ Cu contact in the chain is  $5.051(4) \text{ \AA}$ .

### Task 3.

Before the fluorescence sensors being prepared in Task 1 are ready, we have endeavored to demonstrate our techniques with other sensors. A major goal for the past year for us has been fine-tuning our processes so that we can effect solutions as soon as the spectroscopy of the sensors is known.

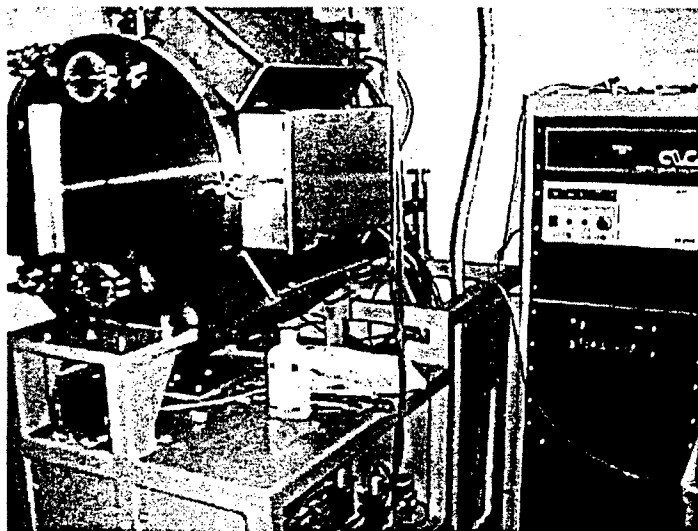


Figure 2 – Reactive Magnetron Sputtering system.

and is shown in Figure 2. This deposition system gives us unparalleled ability to produce interference devices that reproduce nearly exactly the theoretical curves derived by our computer modeling. We use  $\text{SiO}_2$  and  $\text{Nb}_2\text{O}_5$  as the thin-film materials for our filter construction.

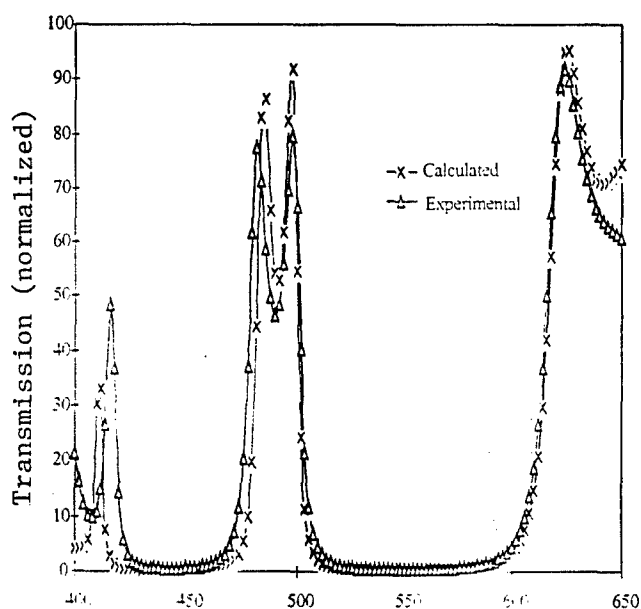


Figure 3 – Theory and Experimental comparison for one of 5 interference devices constructed for a vapor detection system.

We joined with a team from Tufts University (Dr. David Walt) preparing fluorescence-based sensors for detection of explosives vapors that are operationally similar to those being made for the present project. During the fall of 1998 and spring of 1999, we have successfully made optical interference filters for their sensor system using targeted filter design and a magnetron sputtering vacuum system (Model CVC 5.1) for manufacturing. The magnetron deposition system was installed by Corona Vacuum Coater, Inc., in the basement of the Physical Science Building during late summer of 1998,

The Tufts University instrument for detecting explosives via artificial nose sensing utilizes high-powered blue and green LED light sources, optical sensors that emit at two different wavelengths, and five precisely designed optical filters. Operationally it is almost identical to the optical systems we have proposed for chemical agent detection (actually, it is somewhat more complex), and it provides an excellent test case for us to design an optical train. Due to the complex combination of optical spectrum of the excitation source and the excitation and emission spectra of the sensor dyes, five specially design filters were produced to achieve the goal.

Our first steps in making interference devices was to design the structure of the films to obtain an optimized performance. This was done with an iterative computer algorithm. The filters were designed using commercial TFCalc<sup>ref</sup> software based on target excitation and emission profiles provided by researchers at MIT and Tufts, who had synthesized the sensing molecules. This software provides the physical thickness as well as the optical thickness of each layer of a multilayer thin-film structure.

We successfully completed our design and construction test. Filters were designed and fabricated with acceptable accuracy. Figure 3 shows theoretical and experimental spectra for one of the five filters for the Tufts fluorescence sensors. The Tufts explosives vapor detection system was field tested over a mock military mine field at Ft. Leonard Wood in Missouri during September, 1998 with optics designed and constructed in our laboratory. The optics performed as designed, although the sensors themselves had not been as thoroughly debugged as we might have liked.

During the process of preparing our filters, we encountered a number of unforeseen problems and dealt with each of them successfully. One of these problems was intermixing of materials ( $\text{SiO}_2$  and  $\text{Nb}_2\text{O}_5$ ) during deposition. This was solved by appropriate masking, and the instrument manufacturer is now using our masking solution on other instruments.

Another problem we identified was operator fatigue – in other words, the exacting precision required for deposition runs that take more than 24 hours of continuous deposition is more than a typical operator can maintain. The instrument software was rewritten to run a deposition fully automatically, and this has largely solved the fatigue problem.

Another problem we identified is the need for extreme accuracy in the optical constants of the thin-film materials. Without knowledge of the refractive indices and dispersion coefficients for the materials to within 0.0001 units, it is very difficult to design and accurately produce highly precise interference structures. This is not usually a problem in normal optical filter construction because the accuracy achievable in normal processing is so much less that minor errors in refractive indices can be neglected. We are still working to refine our knowledge of the optical constants from our system. However, even without what we would consider an optimal set of optical constants, we were able to design and fabricate a device for Stanford University that demonstrated a state-of-the-art capability. We fabricated a Gaussian-shaped bandpass device with  $20 \text{ cm}^{-1}$  FWHM (design was  $15 \text{ cm}^{-1}$ ), and center wavelength of 797.0 nm (within  $2 \text{ cm}^{-1}$  of design). Our less than perfect knowledge of the optical constants for our films is best shown in the peak transmittance of the bandpass – we designed for 90% and achieved 50%. This represents an ability to design and fabricate optical devices with accuracy of 1 part in about  $10^4$ . Although this value is nearly an order of magnitude better than conventional processing, we would like to be at least one order of magnitude better. Such extreme accuracy is necessary for this technique to be useful in vibrational spectroscopy, although it is not so important to this project focussed on fluorescence sensing.

#### Task 4

##### Introduction

The detection technologies such as ion mobility spectrometry (IMS) and the detection kits and tickets are widely used by military forces.<sup>18</sup> However, the "matrix effects" such as humidity, temperature, and the composition of the air sample can easily influence IMS detector response. Also, oxidizing agents or acidic species may cause a false response to the detection kits and tickets.

Since nerve gases are very difficult to be oxidized or reduced, electrochemical sensor doesn't exist for direct detection. The two common types of indirect electrochemical sensors are based on conductivity and enzymatic reaction. These sensors are selective but not sensitive with a detection limit of approximately  $1 \times 10^{-5}$  M. Recently we developed a novel electrochemical detection technique for nerve gases<sup>19</sup>. This method is more sensitive than the sensors based on conductivity and enzymatic reaction and has a detection limit of  $2 \times 10^{-6}$  M. However, it can only be used for Tabun detection.

Since both Sarin and Soman contain fluorine bonded to the phosphorus atom, one may develop a method for their detection by substituting and then releasing fluorine from the nerve gas molecule and thus detecting the presence of fluoride ion. This method may also be applied for detection of Tabun and VX. Also, oximes can react with nerve gases to produce  $\text{HF}$ <sup>20,21</sup>. However, because of the slow kinetics, this reaction is not fast enough for the detection of nerve gases at low concentration, even in case when the concentration of oximes is quite high. In 1960s, there were a few reports describing the hydrolysis of Sarin and its simulant. An attempt was made in these studies to accelerate the reaction using a wide variety of metal chelate compounds<sup>22,23</sup>. The kinetics was studied by the time-dependent release of acid, which was titrated at constant pH by an automatic titrator. However, there has been no report to use this catalyzed hydrolysis reaction for analytical purposes.

The objective of this work is to develop a simple and convenient but reliable detection method for Sarin and Soman based on their catalyzed hydrolysis and potentiometric detection. An attempt was made to use the recorded potential-time curve for kinetic analysis.

##### Experimental

The following chemicals were used as received: diisopropyl fluorophosphate (DFP) (Sigma, >95%), diethyl cyanophosphonate (DECP) (Sigma, >95%), sodium fluoride (Sigma, 99%), 2,2'-bipyridyl (Aldrich, >99%), copper chloride dihydrate (Aldrich, >99%), dimethyl methylphosphonate (Aldrich, 97%), dimethyl phosphinic acid (Aldrich, 97%), trimethyl phosphate (Aldrich, 97%), methyl phosphonic acid (Aldrich, 98%), diethyl chlorophosphate (Aldrich, 97%),  $\text{NaH}_2\text{PO}_4$ ,  $\text{Na}_2\text{HPO}_4$  (Fisher, >99%),  $\text{NaHCO}_3$  (Aldrich, >99%),  $\text{HCl}$  (Aldrich, 37%).

The solutions were prepared by using deionized water (Bornstead). Since 2,2'-dipyridyl is only slightly soluble in water, a mixture of water and ethanol (50/50, v/v) was used to prepare a 50 mM stock solution. The solution of nerve gas simulant was freshly prepared before experiments. All experiments were carried out at room temperature and in air.

The experimental setup contains a two-electrode cell and a Model 273 potentiostat (EG&G PARC). The potentiostat was used to measure the open-circuit potential and its variation with time. A fluoride ion-selective electrode (ISE) (Orion, Model 94-09) was used as the indicator electrode while a single junction reference electrode (Orion, Model 90-01) was used as reference electrode.

## Results and discussion

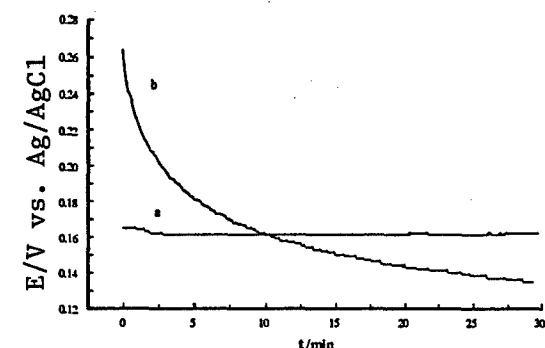
### 1. Hydrolysis of DFP Catalyzed by Metal Chelate Compounds

In the absence of DFP, after 30 min stabilization in the blank solution at pH=6.8, the fluoride ISE has a very stable potential value of about 0.16 V. The stabilized potential depends

on pH of the blank solution<sup>24,25</sup>. After adding  $4 \times 10^{-5}$  M DFP, the electrode potential decreases slightly at the beginning and then remains constant for a long period of time indicating that the hydrolysis of DFP is very slow. Its half-life time is longer than 100 hours. As shown in Fig. 4 "a" very small amount of fluoride ion were produced from hydrolysis.

However, the situation changes when a small amount of metal chelate is added in the solution. If the solution contains metal chelate, 5 mM Cu(II)-bipy, the electrode potential shows a more positive stable value of about 0.26 V. As shown in Fig. 4, curve "b", after addition of  $4 \times 10^{-5}$  M DFP, the potential decreases rapidly with time. At  $t=0$ , DFP is introduced into the solution. The

Fig.4 The potential-time responses of fluoride ISE to  $4 \times 10^{-5}$  M DFP in the absence (dotted curve) and the presence (solid curve) of 5 mM Cu(II)-bipy. 10 mM bicarbonate- $\text{CO}_2$  buffer (pH 6.8).



decrease of the electrode potential indicates the production of fluoride ion. Comparing the two curves in Fig. 4, it is apparent that the decomposition of DFP is accelerated in the presence of Cu(II)-bipy.

Also, several other metal chelate compounds were tested. Copper chelate compounds were found to be more effective. Among tested copper chelate compounds, the compounds of copper with 2,2'-bipyridyl, 4,4'-dimethyl-2,2'-bipyridyl, and N,N,N',N'-tetramethylethylenediamine are the most effective. In this study, we used copper-2,2'-bipyridyl compound as the catalyst. Copper with 4,4'-dimethyl-2,2'-bipyridyl and N,N,N',N'-tetramethylethylenediamine perform even better, however, there are problems with their solubility and stability. Further experiments are in progress.

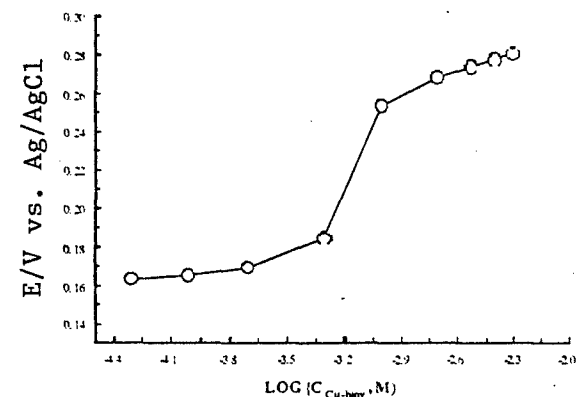


Fig.5 The dependence of the stabilized electrode potential on the concentration of Cu(II)-bipy. 10 mM bicarbonate- $\text{CO}_2$  buffer (pH 6.8).

## 2. The Behavior of Fluoride ISE in the Presence of Metal Chelate Compounds

In the presence of metal chelates in the supporting electrolyte (in absence of DFP), the initial potentials of the fluoride are more positive than that in the absence of metal chelates. This is probably due to their adsorption on the electrode surface. The metal ion-bipy chelates are positively charged, which causes the electrode potential to become more positive. As expected, the adsorption is not strong, since the electrode potential goes back to 0.16 V after the electrode is rinsed and moved to a solution containing no metal chelates.

Fig. 5 shows the dependence of the electrode potentials on the concentration of Cu(II)-bipy. At lower or higher concentration of Cu(II)-bipy, the electrode potential slightly increases with increasing the concentration. When the concentration is between 0.5 to 1.0 mM, the electrode potential increases rapidly. The curve resembles to an adsorption isotherm, which indicates that the positive shift of the electrode potential is due to the adsorption of the metal chelate on the electrode. Only a slight pH change was measured in presence of different concentrations of Cu(II)-bipy in the supporting electrolyte.

It should be pointed out that the adsorption of Cu(II)-bipy has no influence on the potential responses of the electrode to fluoride ion. Actually, there is a very good linear relationship between the electrode potential and the logarithm of the concentration of fluoride ion, even the concentration is as low as  $1 \times 10^{-6}$  M. On the other hand, the more positive initial potential of the electrode is beneficial for setting a discriminating potential for detection of nerve gases at low concentrations. In the absence of Cu(II)-bipy, the initial electrode potential is about 0.16 V at pH 6.8. A concentration of  $2 \times 10^{-6}$  M  $F^-$  causes almost no change to the electrode potential, thus the detection of  $F^-$  and DFP is impossible in absence of catalyst. The stabilized electrode potential in the presence of Cu(II)-bipy is about 0.26 V. After adding  $2 \times 10^{-6}$  M  $F^-$ , the electrode potential drops to below 0.20 V. The observed potential change is large enough to be used as an indicator for detection of  $F^-$  or DFP.

## 3. Influences of Buffer Solution

At pH range of 6.5 to 7.5, the potential-time curves for the hydrolysis of DFP are almost the same indicating that the hydrolysis has the same rate. At pH lower than 6.0 and at pH 8.0 or higher, the electrode potential decreases more slowly and has more positive values indicating that less HF is produced in more acidic or more alkali solution. We choose pH 6.8 for the further experiments.

The experiments carried out using the same concentration of phosphate buffer instead of bicarbonate- $CO_2$  buffer give more positive electrode potentials for the same hydrolysis time indicating that carbonate buffer is more effective for the hydrolysis of DFP catalyzed by Cu(II)-bipy chelate.

The buffer concentration has some influence on the catalyzed hydrolysis of DFP. Increasing the buffer concentration, the initial electrode potential decreases, but when DFP is introduced into the solution, the potential decreases more slowly. When the buffer concentration is lower than 10 mM, the differences are smaller than 2 mV. Generally, we used 10 mM bicarbonate- $CO_2$  buffer to carry out the experiments.

The influence of the buffer concentration can not be explained as the influence of ion-strength. For the same buffer solution, the addition of  $KClO_4$  has no influence on the hydrolysis rate of DFP. According to ref.(P6), the presence of two aquo groups on the metal ion and the



presence of maximum positive charge on the metal chelate are main factors which increase the maximum catalytic activity of Cu(II) catalysts. At higher concentration of bicarbonate-CO<sub>2</sub> buffer, the negatively charged bicarbonate ion has more chances to replace the aquo groups on the metal ion. In such a case, the metal chelate has less positive charge which explains why the buffer concentration influences the catalytic activity of Cu(II) chelate.

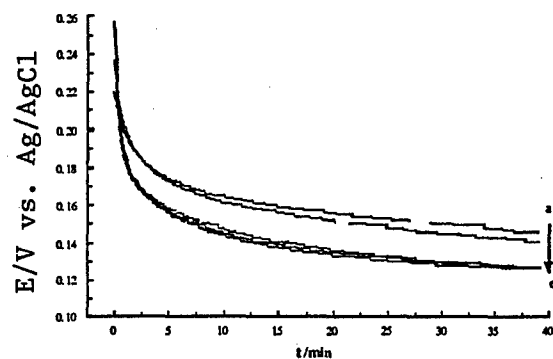


Fig. 6 The potential-time responses of fluoride ion-selective electrode to  $4 \times 10^{-5}$  M DFP at different concentrations of Cu(II)-bipy. 10 mM bicarbonate-CO<sub>2</sub> buffer (pH 6.8), Cu(II)-bipy (mM): a 0.5; b 1.0; c 2.0; d 5.0; e 10.

On the other hand, the initial electrode potential decreases with increasing the concentration ratio of 2,2'-bipyridyl to CuCl<sub>2</sub>, which is also not good for lowering the detection limit. Thus, we used 1:1 Cu(II):bipy chelate ratio as the hydrolytic catalyst of DFP.

### 5 Kinetics Studies

As shown in Fig. 5, increasing the concentration of Cu(II)-bipy chelate increases the initial

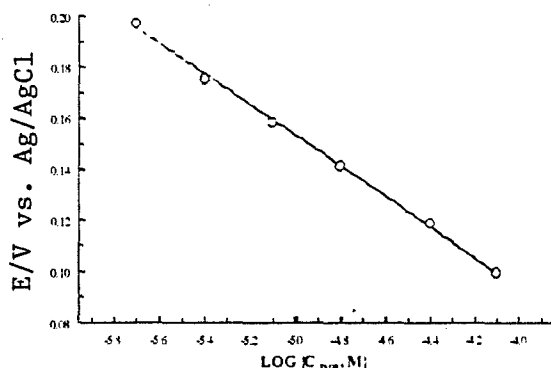


Fig. 7 Plot of  $\log\{C_i - C_F\}$  against  $t$ . 20 mM bicarbonate-CO<sub>2</sub> buffer (pH 6.8), 5 mM Cu(II)-bipy,  $4 \times 10^{-5}$  M DFP.

### 4. Effect of 2,2'-Bipyridyl Concentration

Cu(II)-bipy chelate was prepared by mixing solutions of CuCl<sub>2</sub> and 2,2'-bipyridyl. If the concentration of 2,2'-bipyridyl is lower than that of CuCl<sub>2</sub>, a fraction of copper ion precipitates immediately in the neutral solution as copper hydroxide or copper oxide. When the amounts of CuCl<sub>2</sub> and 2,2'-bipyridyl are equal, a 1:1 Cu(II)-bipy chelate is formed, which has the incomplete coordination on metal ion and is very effective hydrolytic catalyst [5,6]. If the concentration of 2,2'-bipyridyl is higher than that of CuCl<sub>2</sub>, the solution contains a mixture of 1:1 and 1:2 Cu(II)-bipy chelates. The 1:2 Cu(II)-bipy chelate has less catalytic activity for the hydrolysis of DFP [5], so that the electrode potential drops more slowly. On

the other hand, the initial electrode potential decreases with increasing the concentration ratio of 2,2'-bipyridyl to CuCl<sub>2</sub>, which is also not good for lowering the detection limit. Thus, we used 1:1 Cu(II):bipy chelate ratio as the hydrolytic catalyst of DFP.

The potential-time dependence can be used for the kinetic study<sup>26,27</sup>. Usually, the DFP hydrolysis rate constant is determined by measuring the amount of acid produced (HF and phosphorous acid) at a constant pH through

titration. However, the amount of acids released during hydrolysis depends on pH of the solution<sup>22</sup>. For example, the hydrolysis of 1 mM DFP may produce 2 mM acids at one pH and 1.5 mM acids at another pH which complicates the determination. On the other hand, the addition of NaOH may cause the local high pH before NaOH is homogeneously distributed which may influence the hydrolysis rate. By using the fluoride ISE, only the by-product,  $F^-$ , is measured, which is directly related to the rate of hydrolysis. The experiment showed that the electrode has very rapid response to the fluoride ion and it takes several minutes for the electrode to reach a stable potential even for  $2 \times 10^{-6} M F^-$ . However, the electrode potential stabilizes much more slowly in the case of DFP because of the rate-limited hydrolysis. So the inherent response time of the electrode will have no apparent influence on the kinetics of the hydrolysis.

The DFP hydrolysis rate was found experimentally to be of the first-order with respect to the total concentration of unreacted DFP<sup>22,23,26,27</sup>. This can be expressed as:

$$-\frac{d[DFP]}{dt} = k_{obsd}[DFP] \quad (1)$$

If  $C_i$  is the initial concentration of DFP and  $C_F$  is the concentration of free fluoride ion produced by hydrolysis, integration of Eq. 1 results in

$$\ln\{C_i - C_F\} = \ln C_i - k_{obsd}t \quad (2)$$

where  $t$  is the hydrolysis time. In order to measure  $C_F$  at time  $t$ , a working curve of free fluoride ion instead of DFP is necessary in the presence of Cu(II)-bipy. During the hydrolysis, the concentration of the released fluoride ion can be measured by measuring the electrode potential, and then the kinetic parameter can be obtained by plotting Eq(2). Fig. 7 shows the plot of  $\log\{C_i - C_F\}$  vs  $t$ . The apparent rate constant,  $k_{obsd}$ , can be obtained from the slope of the straight line in Fig. 7.

The rate constant is expected to depend on the concentration of Cu(II)-bipy chelate. The experiments show that the observed rate constant increases linearly with increasing the concentration of Cu(II)-bipy chelate (at lower concentrations) and almost approaches a constant value when the concentration of Cu(II)-bipy is 2 mM or higher.

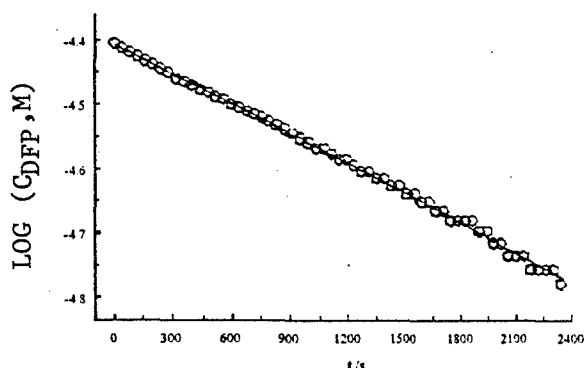


Fig.8 The working curve for the determination of DFP. 10 mM bicarbonate- $CO_2$  buffer (pH 6.8), 5 mM Cu(II)-bipy.

#### 6. Working Curve and Detection Limit for DFP and Long Term Stability

In the presence of Cu(II)-bipy, the hydrolysis of DFP is accelerated and the released fluoride ion can be measured, thus that the concentration of DFP can be determined indirectly. Since the hydrolysis is kinetically controlled, the electrode potential is measured 30 min after DFP is added into the solution. In Fig. 8, the working curve for DFP, which shows a very good linear relationship between the potential and the logarithm of the concentration of Cu(II)-bipy chelate. Note that this straight line is slightly different from the one obtained by

using a solution of free  $F^-$  since not all DFP molecules are decomposed into  $F^-$  in 30 min.

The fluoride ISE shows an extraordinary stability in the test solution. A very little change of the electrode potential was observed in the same solution after using it for five months. The solid curve in Fig. 9 shows a variation of the electrode potential with time after the electrode has been introduced into the test solution. The initial electrode potential is about 0.24 V and increases gradually and then finally becomes quite stable at 0.26 V. In this figure, the stability is shown only for 55 hours. Note that the electrode potential in the same test solution has less influence on the potential after adding DFP. In the other words, the initial electrode potential before adding DFP has no influence on the working curve for DFP or  $F^-$ . However, it does influence the detection limit. If the electrode potential is about 0.26 V before adding DFP and is stable, a higher discriminating value of the electrode potential could be used and the detection

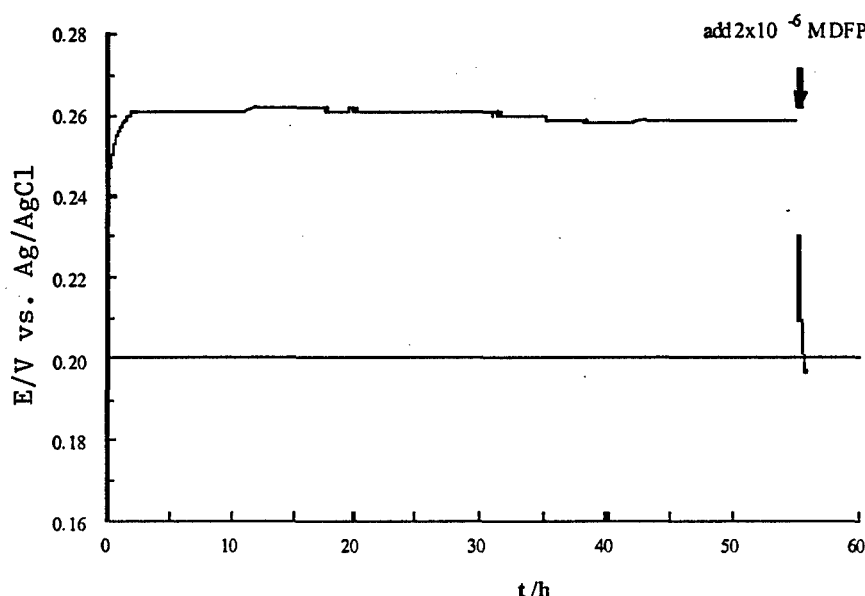


Fig.9 Long term potential-time response of fluoride ion-selective electrode in the absence and the presence of  $2 \times 10^{-6}$  M DFP. 10 mM bicarbonate- $CO_2$  buffer

limit could be lower. In this work, a discriminating potential is set to be 0.20 V as indicated by the parallel line, which is much lower than the potential of the fluoride ISE in this test solution. It can be seen that the addition of  $2 \times 10^{-6}$  M DFP causes a big potential drop of about 60 mV, which can be easily detected. This method is more sensitive than the other electrochemical methods<sup>18,20</sup>.

### 7. Interferences

This method is more selective than any other methods such as IMS and the detection kits or tickets. We have tested the following similar compounds: dimethyl methylphosphonate, dimethyl phosphinic acid, trimethyl phosphate, methyl phosphonic acid, diethyl chlorophosphate. None of them causes any potential drop at concentration up to 5 mm. Also, acidic gases do not have any response on the electrode.

### ***Publications and Technical Reports***

"Multivariate Optical Computation for Predictive Spectroscopy" M.P. Nelson, J.F. Aust, J.A. Dobrowolski, P.G. Verly, and M.L. Myrick *Proceedings of the SPIE Symposium on Three-Dimensional and Multidimensional Microscopy, Image Acquisition and Processing V*, 232-243, San Jose, California, January 27-29, 1998.

"Design of Thin Film Filters for the Monitoring of Chemical Reactions" J.A. Dobrowolski, P.G. Verly, J.F. Aust, M.P. Nelson and M.L. Myrick in *Proceedings of the SPIE Annual Meeting on Optical Science and Engineering*, San Diego, California, July, 1997, 232..

"Time-dependent multivariate single-frame chemical imaging spectroscopy of laser plumes using a dimension reduction fiber optic array" M. P. Nelson, M. L. Myrick *SPIE* 3649(1999) (in press)

"Single-Shot Multiwavelength Imaging of Laser Plumes" M.P. Nelson, W.C. Bell, M.L. McLester, and M.L. Myrick *Appl. Spectrosc.* 52(1998), 179.

"Multivariate Optical Computation for Predictive Spectroscopy" M.P. Nelson and M.L. Myrick *Anal. Chem.* 70(1998), 73.

"Single-Shot Multiwavelength Imaging of Laser Plumes" M.P. Nelson, W.C. Bell, M.L. McLester, and M.L. Myrick presented at Pittsburgh Conference, New Orleans, LA, Mar 1-6, 1998.

"Multivariate Optical Computation for Predictive Spectroscopy" M.L. Myrick, M.P. Nelson, J.F. Aust, J.A. Dobrowolski, and P.G. Verly presented at Pittsburgh Conference, New Orleans, LA, Mar 1-6, 1998.

"Molecular Transducers for Detecting Organophosphonate Nerve Gas Simulants" Mehrnaz Kamal and Brian A. Salvatore (to be presented at the 217th American Chemical Society National Meeting (Organic Chemistry Division), August 17-23, 1998, Boston, MA.)

"A Novel Electrochemical Detection Technology for Nerve Gases" Yuanwu Xie, Branko N. Popov and Ralph E. White, Extended Abstract, Annual AIChE meeting, 1998, 11, Miami, Florida.

"A Novel Electrochemical Detection Technology for Nerve Gases" Yuanwu Xie, and Branko N. Popov (in preparation to be submitted in *Journal of Electrochem. Soc.*)

### ***Participating Personnel***

In addition to the principal investigators (M. Myrick, B. Salvatore, H. zur Loye, B. Popov and T. Bryson), the following personnel are involved in this research project:

Dr. Jeevananda P

Delia Ciurtin - graduate student with H. zur Loye

John Claridge - postdoctoral associate with H. zur Loye

Chris Dyke - graduate student with T. Bryson

Jeanne Jennings - graduate student with T. Bryson (partial support)

Bill Kemnitzer - graduate student with T. Bryson (partial support)

Wendy Bell - graduate student with M. Myrick (partial support)

Matthew Nelson - graduate student with M. Myrick (partial support)

Dr. Mehrnaz Kamal - postdoctoral associate with B. Salvatore

We anticipate the addition of a post-doctoral associate to the Bryson group in the near term, as the position has been offered to a candidate. The Myrick group will add Raju Prajesh, currently a graduate student in Physics at Louisiana State University with expertise in probe microscopy and oxide film preparation, Baton Rouge, LA, in May, 1998. Mr. Prajesh will work on optical computational devices during summer, 1998 as a research associate, and will finish his Ph.D. during early fall, 1998. After that time he will be converted to a post-doctoral associate.

## BIBLIOGRAPHY

1. Hearing before the Committee on Armed Services. United States Senate, Ninety-Ninth Congress, May 1, 1985. Chemical Warfare Review Commission, S. Hrg. 99-255.
2. Brooks E. Kleber and Dale Birdsell, *The Chemical Warfare Service: Chemicals in Combat*. U.S. Government Printing Office, 1966.
3. Other examples include: (a) Vietnam, suspected of chemical operations against Kampuchea but not against the US during the Vietnam War, and (b) Iraq, known to have conducted chemical operations against the Kurdish population of Iraq and against Iran during the Iran-Iraq War, but not against the Allies during Desert Storm.
4. For example: (a) *Chemical Warfare Progress and Problems in Defensive Capability*. General Accounting Office, PEMD-86-11, July 31, 1986; (b) *Chemical Warfare. Soldiers Inadequately Equipped and Trained to Conduct Chemical Operations*. General Accounting Office, NSIAD-91-197, May 29, 1991.
5. *The 1996 United States Army Modernization Plan*, Department of the Army, 1996.
6. N. R. Brletich, M. J. Waters, G. W. Bowen and M. F. Tracy, *Worldwide Chemical Detection Equipment Handbook*, Chemical and Biological Defense Information Analysis Center, 1995.
7. J. Emsley, *The Chemistry of Phosphorus*, John Wiley & Sons, N.Y., 1976, p 494.
8. A. J. Bard and H. Lund, Eds, *Encyclopedia of the Electrochemistry of the Elements*, vol.3, Marcel Dekker, N.Y., 19XX.
9. E.C. Breinlinger, C.J. Keenan, and V.M. Rotello, *J. Am. Chem. Soc.*, 1998, **120**, 8606.
10. D.S. Kemp and K.S. Petrakis, *J. Org. Chem.*, 1981, **46**, 5140.
11. J. Rebek Jr., L. Marshall, R. Wolak, K. Parris, M. Killoran, B. Askew, D. Nemeth, and N. Islam, *J. Am. Chem. Soc.*, 1985, **107**, 7476.
12. A.M. Felix, *J. Org. Chem.*, 1974, **39**, 1427.

13. G.M. Rubottom and C. W. Kim, *J. Org. Chem.*, 1983, **48**, 1550.
14. M. Suzuki, T. Iwasaki, M. Miyoshi, K. Okumura and K. Matsumoto, *J. Org. Chem.*, 1973, **38**, 3571.
15. E. Matsumura, M. Ariga, and Y. Tohda, *Bull. Chem. Soc. Jpn.*, 1979, **52**, 2413.
16. Y. Tohda, M. Eiraku, T. Nakagawa, Y. Usami, M. Ariga, T. Kawashima, K. Tani., H. Watanabe, and Y. Mori, *Bull. Chem. Soc. Jpn.*, 1990, **63**, 2820.
17. M. Sprecher, R. Breslow, O. Uziel, and T.M. Link, *OPPI Briefs*, 1994, **26**, 696.
18. N. R. Brletich, M. J. Waters, G. W. Bowen and M. F. Tracy, Worldwide Chemical Detection Equipment handbook, Chemical and Biological Defense Information Analysis Center, Maryland, 1995.
19. Y. Xie, B. N. Popov and R. E. White, *J. Electroanal. Chem.*, in press.
20. J. Emsley, The Chemistry of Phosphorus, John Wiley & Sons, New York, 1976.
21. M. Somani, Chemical Warfare Agents, Academic Press, California, 1992.
22. T. Wagner-Jauregg, B. E. Hackley, Jr., T. A. Lies, O. O. Owens and R. Proper, *J. Am. Chem. Soc.*, 77(1955)922.
23. R. C. Courtney, R. L. Gustafson, S. J. Westerback, H. Hyytiainen, S. C. Chaberek, Jr., and A. E. Martell, *J. Am. Chem. Soc.*, 79(1957)3030.
24. J. Koryta, Ion Selective Electrodes, Cambridge University Press, Cambridge, 1975.
25. H. Freiser, Ion-Selective Electrodes in Analytical Chemistry, vol. 1, Plenum Press, New York, 1978.
26. R. L. Gustafson, S. Chaberek, Jr. and A. E. Martell, *J. Am. Chem. Soc.*, 85(1963)598.
27. Y. Murakami and A. E. Martell, *J. Am. Chem. Soc.*, 86(1964)2119.

University Research Initiative Program for Combat Readiness  
Annual Report 06/01/98-05/31/99

PART 53-FORMS

53.301-298

<b>REPORT DOCUMENTATION PAGE</b>		Form Approved OMB No. 0704-0188	
Public reporting burden for this collection of information is estimated to average 1 hour per response, including the time for reviewing instructions, searching existing data sources, gathering and maintaining the data needed, and completing and reviewing the collection of information. Send comments regarding this burden estimate or any other aspect of this collection of information, including suggestions for reducing this burden, to Washington Headquarters Services, Directorate for Information Operations and Reports, 1215 Jefferson Davis Highway, Suite 1204, Arlington, VA 22202-4302, and to the Office of Management and Budget, Paperwork Reduction Project (0704-0188), Washington, DC 20503.			
1. AGENCY USE ONLY (Leave blank)	2. REPORT DATE June 1, 1999	3. REPORT TYPE AND DATES COVERED Annual	
4. TITLE AND SUBTITLE Technology Development for Chemical Detection		5. FUNDING NUMBERS Grant Number N00014-97-1-0806 PR Number 97PR06312-00	
6. AUTHOR(S) M.L. Myrick, B. Salvatore, H. zur Loye, T. Bryson, and B. Popov		PO Code 353 Disbursing Code N68892 AGO Code N66020 Cage Code 4B489	
7. PERFORMING ORGANIZATION NAME(S) AND ADDRESS(ES)  University of South Carolina		8. PERFORMING ORGANIZATION REPORT NUMBER  N00014-97-0806-1	
9. SPONSORING / MONITORING AGENCY NAME(S) AND ADDRESS(ES)  ONR		10. SPONSORING / MONITORING AGENCY REPORT NUMBER  ONR	
11. SUPPLEMENTARY NOTES Prepared in coordination with University Research Initiative Program for Combat Readiness			
12a. DISTRIBUTION / AVAILABILITY STATEMENT  APPROVED FOR PUBLIC RELEASE		12b. DISTRIBUTION CODE	
13. ABSTRACT (Maximum 200 words) Our research has focussed on two major sensor types. The first is based on selective hydrolysis of fluorine-containing chemical agents such as simulate Sarin and Soman using diisopropyl fluorophosphate (DFP) as a simulant. The basis of the method is that in neutral solutions, the hydrolysis rate of fluorophosphate nerve agents is dramatically increased by the presence of a metal chelate compound, and results in the release of fluoride ion. The released fluoride ion can then be detected by a fluoride-ion-selective electrode. The technique is highly selective for these agents because only fluoride ions can be detected, and because only fluoride-containing compounds whose hydrolysis is catalyzed by the metal chelates will release fluoride. We believe this methodology will result in a reusable, continuous monitoring system for these agents. Our second focus area is in optical sensing. We are developing sensor molecules which form covalent adducts with organophosphonates. These sensors are based on molecular cleft scaffold chemistry, and incorporate both an oxime and fluorescent transducer group made with bipyridyl units to be connected to environmentally-sensitive metal chelate complexes. Detection is not based on the identification of specific nerve gas hydrolysis by-products (e.g., HF) but rather on the spectroscopic differences caused by the nerve gas-sensor oxime phosphate ester adducts on the sensitive spectroscopy of the metal chelate.			
14. SUBJECT TERMS Chemical and Biological Warfare, Target Acquisition, Snti-Submarine, Combat Medicine, Biodeterioration, Command Control and Communication		15. NUMBER OF PAGES 13	
		16. PRICE CODE	
17. SECURITY CLASSIFICATION OF REPORT  UNCLASSIFIED	18. SECURITY CLASSIFICATION OF THIS PAGE  UNCLASSIFIED	19. SECURITY CLASSIFICATION OF ABSTRACT  UNCLASSIFIED	20. LIMITATION OF ABSTRACT  200 WDS

NSN 7540-01-280-5500

Standard Form 298 (Rev. 2-89)

Prescribed by ANSI Std. Z39-18  
298-102

## **Real-Time Biodetection Using PCR-MS**

Alvin Fox and Karen Fox

Department of Microbiology and Immunology  
School of Medicine  
University of South Carolina  
Columbia, SC 29208

Tel: (803)733-3288  
Fax: (803)733-3192  
Email: afox@med.sc.edu  
kfox@med.sc.edu



## Section 2-3: Real Time Biodetection Using PCR-MS

Alvin Fox and Karen Fox

### ABSTRACT

There is a real need for an approach for the rapid detection/identification of potential biological warfare (BW) agents during in airborne attack. Ideally, such a method should be fast (<~15 min), highly specific, sensitive and flexible for use against new threats. Conventional microbiological and molecular biology based techniques are far too slow to meet the needs of biodetection. The first technology for real-time detection/identification of pathogenic microbes (based upon the combination of polymerase chain reaction [PCR] and electrospray ionization ([ESI] mass spectrometry) was originally developed by the P.I. and his collaborators. The power of the approach is the use of mass spectrometric analysis that provides rapid detection/identification (<1 min), a speed that greatly exceeds that of conventional electrophoresis approaches. This work involved the use of a state-of-the-art electrospray ionization Fourier transform ion cyclotron resonance mass spectrometer (FTICR-MS). This approach could be extended to integrate the various steps of PCR amplification, clean-up and mass spectrometry into one procedure/instrument for field use. This will include the use of simpler, MS instrumentation amenable to routine use. Further evaluation of the use of PCR-MS for trace detection of appropriate genetic regions in environmental matrices is needed. The major accomplishments of last year include: Successful routine analysis of PCR products using an ESI quadrupole MS instrument for the first time in our, or indeed any other, laboratory. Analysis of PCR products (interspace region between 16S and 23S rRNA) using both conventional techniques including electrophoresis and Sanger sequencing and/or PCR -MS for *B. atrophaeus* (*B. subtilis* var. *niger*, used as a BW simulant) and *Brucella melitensis* (a BW agent). Information, relevant to biodetection and combating biological terrorism, continues to be expanded.

### FORWARD

The total award was \$309,000 (direct costs) for the period 9/1/98 to 9/2001. The original goals of this project encompassed the following:

1. Develop high speed isolation of DNA from bacterial cells present in a dust matrix collected from aerosols in a form suitable for PCR-MS analysis.
2. Incorporation of an approach for rapid fully automated on-line continuous PCR-MS, incorporating the various steps of capillary based PCR amplification, clean-up and mass spectrometry into one integrated procedure.
3. Determination of the relative sensitivity/specificity obtainable by ESI-FTICR vs triple quadrupole and ion trap MS instrumentation for the characterization of PCR products.

Although the resolution and accuracy of triple quadrupole and quadrupole ion trap instruments are lower (compared to FTICR), these instruments are less expensive and have already been adapted for field use.

4. Evaluation and extension of PCR-MS to trace analysis of appropriate chemical markers (including virulence genes and the ribosomal RNA operon) in environmental matrices. Additional development in sample preparation and/or instrumental analysis are anticipated as we extend analysis from PCR of isolated bacterial cells to more complex environmental matrices.

## REPORT

### *Statement of the problem*

There is great interest in an approach for the rapid detection of potential biological warfare (BW) agents during in potential threat. Ideally, such a biodetection method should be fast (<~15 min), highly specific, sensitive and flexible for use against new threats. Fortunately, there are only a limited number of organisms that are likely BW agents and the number one threat is considered by many to be *Bacillus anthracis* (the causative agent of anthrax). This organism has the following characteristics: high virulence for man, ease of production, infection by the respiratory route and ability to survive under adverse environmental conditions. However, a biodetection approach should be sufficiently flexible to be adaptable to identification of multiple and previously unknown threats. *Brucella melitensis* (brucellosis) for example is also among the lead contenders for possible use as a BW agent.

The use of modern instrumental analytical chemical approaches (including electrospray and/or matrix assisted laser desorption mass spectrometry) is essential. Biodetection is based on detecting markers; structures present in specific target microbes and absent in other related bacterial species. The organisms that are key agents for biodetection (including *B. anthracis* and *B. melitensis*) are not widely studied and chemotaxonomic differentiation schemes have required further development in our laboratory.

### ***Summary of the Most Important Results***

ESI FTICR mass spectrometry (MS) is the only technique previously used for accurate MW analysis of PCR products above 100 bp in size. This is important in demonstrating the potential for MS in making a major contributions in biodetection (as well the molecular biology and genomics areas). In the near future, it is more likely that less expensive, more user friendly MS techniques will be used for high throughput analyses (including MALDI-TOF [matrix-assisted laser desorption ionization-time of flight] and ESI-[electrospray ionization] quadrupole). There have been numerous reports on the use of MALDI-TOF.

The current report is to the first to evaluate the use of ESI-quadrupole analysis of PCR products. Synthetic oligonucleotides (30 and 89 mers) and polymerase chain reaction products of varying MW (62, 88, 89, and 114 base pairs [bp]) were analyzed by ESI using a quadrupole MS. The mass accuracy for nucleic acids in the 30-62 bp range was shown to allow determination of nucleotide substitutions and additions/deletions. For higher MW PCR products (88-114 bp) the mass accuracy of ESI-MS distinguishes single or multiple nucleotide insertions/deletions. In addition, ESI-quadrupole MS allows determination of MW of both strands of higher MW ds PCR products and can distinguish nucleotide modifications (e.g. with biotin). In conclusion, it is demonstrated that ESI-MS occupies an intermediate position (as compared to MALDI-TOF and ESI-FTICR) with regard to mass accuracy and resolution in analysis of nucleic acids.

As noted above, our initial studies were performed with a state-of-the-art mass spectrometer (a Fourier transform ion cyclotron resonance instrument). This instrument can not be fielded on battlefield. It is vital to demonstrate that analysis of PCR products can be achieved using an instrument more suited for routine analysis (quadrupole) instrument. Our instrument was purchased with a megafLOW source which was not configured for high sensitivity analysis. Since funds were not available to buy a commercial source (approximately \$50,000) or a new instrument (approximately \$200,000 for an MS/MS ion trap) we converted the megafLOW source of our instrument to microflow; The ESI source used was modified by removing the standard pepper-pot used for megafLOW on-line liquid chromatography MS analysis. The standard skimmer cone lens was replaced with a spherical cone lens (Scientific Instrument Services, Ringoes, NJ). The Micromass "pepper pot" counter electrode contains 4 orifices which disperse most of the nebulized sample away from skimmer lens entrance. Thus only a small fraction (approximately 5%) of the sample reaches the analyzer entrance for detection. The Quattro 11 with modified source was shown to provide excellent sensitivity, mass accuracy and resolution for routine analysis of PCR products.

We continue to focus on the interspace region in the 16S- 23S RNA operon since it is present universally in all bacterial pathogens. However since there is limited selection pressure on the interspace region, there is great diversity on the sequence and nucleotide length of this genomic region. However, the genes on either side of the spacer region (16S and 23S rRNA respectively) contain several conserved regions. Accordingly using primers against two conserved regions (in the 16S and 23S rRNA), different lengths/sequences of 16S-23S rRNA interspace region are

generated for each characteristic BW agent. Experience gained with one group of BW agents is readily applied to other groups.

Strains W23 and 168 represent two distinct genetic clusters within the species *Bacillus subtilis*. *B. atrophaeus* (*B. subtilis* strain var. *niger*) was selected as a member of a group of species closely related to *B. subtilis*. Furthermore, *B. atrophaeus* is commonly used as a simulant for the number one BW agent (*B. anthracis*). Comparison of the 10 rDNA operons, available from genbank, for *B. subtilis* 168 shows 3 distinct types of interspace (ISR) regions. Two of the ten 16S-23S ISRs contain the sequences for isoleucine and alanine tRNA and are identical in sequence. The remaining 8 ISRs lack tRNA sequences and have 2 distinct sizes. Variability among non-tRNA operons ranged from 97-100%. Counting the tRNA insert as one change, variability between tRNA and non-tRNA containing sequences ranged from 95.3-97%. The sequences of equivalent 16S-23S ribosomal operon interspace regions (ISRs) are highly conserved between W23 and 168 (99.9-100%). Thus the sequence differences between strains 168 and W23 are less than between multiple operons within 168. However, the sequence of an ISR from *B. atrophaeus* var. *niger* is quite distinct from any of the ISRs found in *B. subtilis* (range 88.2-91.6%). These observations are consistent with the previous suggestion that *B. atrophaeus* is a separate but closely related species to *B. subtilis*. This is the first study to make sequence comparisons at the level of operon, strain and species for the rRNA interspace region. Considerations of this type will be important in using ISRs to differentiate other closely related bacterial species. It is worthy to note that *B. subtilis* and *B. atrophaeus* are both quite distinct from *B. anthracis*.

Molecular and chemical characteristics often provide complementary information in differentiation of closely related organisms. The genus *Brucella* is a highly conserved group of organisms. Identification of the 4 species pathogenic for man (*B. melitensis*, *B. abortus*, *B. suis* and *B. canis*) is problematic for many clinical laboratories depending primarily on serology and phenotypic characteristics. *B. melitensis* is one of a small group of bacterial pathogens suitable for use as a BW agent. PCR amplification of the 16S/23S rDNA interspace region was evaluated for species-specific polymorphism. *B. abortus*, *B. melitensis*, *B. suis* and *B. canis* produced identical PCR interspace profiles. However, these PCR products were unique to brucellae allowing them to be readily distinguished from other gram-negative bacteria (including *Bartonella* and *Agrobacterium*). Carbohydrate profiles differentiated *B. canis* from the other 3 *Brucella* species due to the absence of the rare aminosugar quinovosamine. PCR of the rRNA interspace region is useful in identification of the genus *Brucella* whilst carbohydrate profiling is capable of differentiating *B. canis* from the other *Brucella* species.

#### ***Publications and Technical Reports***

Y. Johnson, M. Krahmer, P. Ross, K. and A. Fox. Rapid and simple preparation of single stranded PCR products for ESI quadrupole MS analysis. American Society for Mass Spectrometry (ASMS), Annual Meeting, May, 1998.

M., Nagpal, A. Fox and K. Fox. Discrimination of *Bacillus subtilis* and *Bacillus atrophaeus*: Inter and intra-species comparison of the 16S-23S intragenic spacer region. Amer. Society for Microbiology. Annual Meeting. May, 1998

Krahmer M. T., Johnson Y., Walters M., Fox K. F. and Nagpal M. Electrospray quadrupole mass spectrometry analysis of model oligonucleotides and polymerase chain reaction products: determination of base substitutions, nucleotide additions/deletions and chemical modifications. Analy. Chem. (Submitted, 1999).

A. Fox. Preparedness research in SC: anthrax. AAAS Research Competitive Program. Research in Domestic Preparedness, Stillwater, Oklahoma, Mar 1999.

A. Fox. Y. Johnson, Krahmer M., Walters J. and Fox, K. Analysis of structurally similar PCR products of the 16S-23S rRNA interspace region of bacilli by electrospray quadrupole . Applications in microbiology symposium. American Society for Mass Spectrometry. 1999. June 1999.

Nagpal M., Fox K. and Fox A. Utility of 16S-23S rRNA spacer region methodology: how similar are interspace regions within a genome and between strains for closely related organisms. J. Microbiol. Meth. 33: 211-219. 1998

Fox K., Fox A., Nagpal M., Steinberg P. and Heroux K. Identification of *Brucella* by ribosomal spacer region PCR and differentiation of *B. canis* from other *Brucella* pathogenic for man by carbohydrate profiles. J. Clin. Microbiol. 36: 3217-3222. 1998.

#### **Participating Personnel**

K. Fox (Research Associate Professor) and A. Fox. (Professor) - Co-P.I.s

M. Nagpal (Research Associate Professor)

M. Krahmer (post-doctoral fellow)

Y. Johnson, M. Kozar W., Walters (Graduate students)

P. Steinberg (Technician)

#### **BIBLIOGRAPHY**

1. Wunschel, D., Fox, K., Black, G. and Fox, A. Discrimination among the *B.cereus* group, in comparison to *B. subtilis*, by structural carbohydrate profiles and ribosomal RNA spacer region PCR. System. Appl. Microbiol. 17: 625-635. 1994

2. Wunschel D., Fox K., Fox A., Bruce J., Muddiman D. and Smith R. Analysis of double stranded polymerase chain amplification products from the *B.cereus* group by electrospray ionization fourier transform ion cyclotron resonance mass spectrometry. Rapid Commun. Mass Spectrom. 10: 29-35. 1996.

3. Muddiman D.C., Wunschel D. , Liu C., Pasa-Tolic L., Fox K., Fox A. and Smith R. Characterization of PCR products from bacilli using electrospray ionization FTICR mass spectrometry. Analyt Chem. 68:3705-3712. 1996.

4. Wunschel D., Fox K., Fox A., Nagpal M., Kim K. and Stewart G. Quantitative analysis of neutral and acidic sugars in whole bacterial cell hydrolysates using high performance anion exchange liquid chromatography electrospray ionization tandem mass spectrometry. J. Chromatogr. 776: 205-219. 1997.

5. Fox K., Wunschel D., Fox A. and Stewart G. Complementarity of GC-MS and LC-MS analyses for determination of carbohydrate profiles of vegetative cells and spores of bacilli. J. Microbiol. Meth. 33: 1-12. 1998
6. Wunschel D., Muddiman D., Fox K., Fox A. and Smith R.D. Heterogeneity in *B. cereus* PCR products detected by ESI-FTICR mass spectrometry. Analyt. Chem. 70: 1203-1207.1998.

University Research Initiative Program for Combat Readiness  
Annual Report 06/01/98-05/31/99

PART 53-FORMS

53.301-298

<b>REPORT DOCUMENTATION PAGE</b>		Form Approved OMB No. 0704-0188	
Public reporting burden for this collection of information is estimated to average 1 hour per response, including the time for reviewing instructions, searching existing data sources, gathering and maintaining the data needed, and completing and reviewing the collection of information. Send comments regarding this burden estimate or any other aspect of this collection of information, including suggestions for reducing this burden, to Washington Headquarters Services, Directorate for Information Operations and Reports, 1215 Jefferson Davis Highway, Suite 1204, Arlington, VA 22202-4302, and to the Office of Management and Budget, Paperwork Reduction Project (0704-0188), Washington, DC 20503.			
1. AGENCY USE ONLY (Leave blank)	2. REPORT DATE June 1, 1999	3. REPORT TYPE AND DATES COVERED Annual	
4. TITLE AND SUBTITLE Real Time Biodetection Using PCR-MS		5. FUNDING NUMBERS Grant Number N00014-97-1-0806; PR Number 97PR06312-00; PO Code 353; Disbursing Code N68892; AGO Code N66020; Cage Code 4B489	
6. AUTHOR(S) Karen Fox, Ph.D.			
7. PERFORMING ORGANIZATION NAME(S) AND ADDRESS(ES) University of South Carolina Columbia, South Carolina 29208		8. PERFORMING ORGANIZATION REPORT NUMBER  N00014-97-1-0806-2	
9. SPONSORING / MONITORING AGENCY NAME(S) AND ADDRESS(ES) Office of Navy Research 800 North Quinley Street Arlington, VA 22217-5660		10. SPONSORING / MONITORING AGENCY REPORT NUMBER  ONR	
11. SUPPLEMENTARY NOTES Prepared in coordination with University Research Initiative Program for Combat Readiness			
12a. DISTRIBUTION / AVAILABILITY STATEMENT APPROVED FOR PUBLIC RELEASE		12b. DISTRIBUTION CODE	
13. ABSTRACT (Maximum 200 words) An approach for rapid detection of biological warfare (BW) agents during an airborne attack must be developed. This method, unlike microbiological and molecular biology approaches, should be extremely fast. The first technology for real-time detection of pathogenic microbes (based upon the combination of polymerase chain reaction [PCR] and electrospray ionization [ESI] mass spectrometry) was originally developed by the P.I. and his collaborators. This work involved the use of a state-of-the-art electrospray ionization Fourier transform ion cyclotron resonance mass spectrometer (FTICR-MS). This approach could be extended to integrate the various steps of PCR amplification, clean-up and mass spectrometry into one procedure/instrument for field use. This will include the use of simpler, MS instrumentation amenable to routine use. The major accomplishments of last year include: Successful routine analysis of PCR products using an ESI quadrupole MS instrument for the first time in our, or indeed any other, laboratory. PCR products (interspace region between 16S and 23S rRNA) were analyzed by electrophoresis, Sanger sequencing and PCR-MS for <i>B. atrophaeus</i> ( <i>B. subtilis</i> var. <i>niger</i> , used as a BW simulant) and <i>Brucella melitensis</i> (a BW agent). Information, relevant to biodetection and combating biological terrorism, continues to be expanded.			
14. SUBJECT TERMS Chemical and Biological Defense, Target Acquisition, Anti-Submarine, Combat Medicine, Biodeterioration, and Command Control and Communication		15. NUMBER OF PAGES 6	
		16. PRICE CODE	
17. SECURITY CLASSIFICATION OF REPORT UNCLASSIFIED	18. SECURITY CLASSIFICATION OF THIS PAGE UNCLASSIFIED	19. SECURITY CLASSIFICATION OF ABSTRACT UNCLASSIFIED	20. LIMITATION OF ABSTRACT  200

NSN 7540-01-280-5500

Standard Form 298 (Rev. 2-89)

Prescribed by ANSI Std. Z39-18  
298-102

**Small Molecule Transport Through Polymers:  
Effects of Polymer Inhomogeneity and Dynamics on the Nanometer Length  
Scale**

Mark A. Berg

Department of Chemistry and Biochemistry  
University of South Carolina  
Columbia, SC 29208

Tel: (803) 777-1514  
Fax: (803) 777-9521  
Email: [berg@psc.sc.edu](mailto:berg@psc.sc.edu)



## **Section 2-4: Small Molecule Transport Through Polymers: Effects of Polymer Inhomogeneity and Dynamics on the Nanometer Length Scale**

Mark A. Berg

### **ABSTRACT**

This project seeks to elucidate the mechanism of small-molecule diffusion through polymers by examining the polymer's dynamics on a nanometer length scale. The methodology for measuring nanoviscosity was developed in the first year of the project and now has been applied to polyisobutylene. By varying the chain length of the polymer, we have shown that the unique features of polymer dynamics begin at very short chain lengths. This result will allow the properties of high-polymers to be predicted using the more powerful theoretical and modeling techniques that can be applied to short chains. The rotation of our probe molecule develops a multiexponential form in polymers, whereas a single exponential form occurs in small-molecule solvents. This result suggests that polymers form nanostructures, i.e., "cavities" or "channels", around a small penetrant molecule. Lastly, measurements have been started on polydimethylsiloxane, an elastomer that is structurally similar to PIB, but supports much more rapid diffusion. The nanoviscosity in PDMS is dramatically lower than in PIB, even under conditions where the bulk viscosities are the same. This finding supports the central hypothesis of this project - diffusion of small molecules is determined by polymer properties on the nanometer scale, not by bulk properties.

### **FORWARD**

This project entails total costs of \$370,000 over a period of three years. Its goal is to generate a better understanding of penetrant diffusion through polymers by using ultrafast spectroscopy to examine polymer dynamics at the nanometer length scale. The diffusion of small organic penetrants is important for both chemical warfare defense and general military and civilian applications of polymers. Control of penetrant diffusion is essential to improving barrier materials for control of chemical agents and for the design of catalytic or selectively permeable polymers for use in sensors for chemical agents. Penetrant diffusion also plays a critical role in other applications of polymers including chemical coating and processing, adhesion, curing behavior, degradation processes, advanced ultrafiltration and separations, and long-term drug delivery.

Both theory and macroscopic experiments suggest that the mechanism of penetrant diffusion in polymers is different than in small-molecule solvents. For example, diffusion in polymers slows below the glass transition, but does not cease, as it does in small-molecule solvents. Computer simulations have suggested that the entanglement of the polymer chains favors the formation of nanometer-sized cavities in the polymer and that the penetrant occupies these cavities.[1, 2] In the so-called "Red-Sea" mechanism, transport occurs when a channel opens between these cavities, and the penetrant hops to a new cavity, before the channel closes.[1, 2] In transition-state theories of polymer diffusion, it is hypothesized that the channel open and closing is governed by simple elastic movement of the polymer chains and does not require structural relaxation.[1-3]

As these models illustrate, small-molecule diffusion is determined by the structure and mechanical properties of polymers at a nanometer length scale, i.e., lengths shorter than the polymer chains. However, most experiments on polymers measure long length scale, macroscopic properties. For example, macroscopic viscosity measurements are determined by chain entanglement and flow over large distances, whereas small-molecule diffusion is determined by flexing and distortion of small cavities and channels. As a result, there is almost no experimental evidence to either support or refute existing theoretical models of polymer nanostructure. The purpose of this project is to directly examine the mechanical properties and structure of polymers at nanometer length scales. The long range goal is to explain the origin of differing diffusivities in different polymers and thereby improve our ability to design, model and control diffusivity in new materials.

In the first year of this project, the methodology for measuring nanoviscosity was developed. Ultrafast polarization spectroscopy was used to measure rotation times of anthracene, which serves as a nanometer sized viscosity sensor. This sensor was calibrated in small-molecule liquids and a hydrodynamic model was developed to relate rotation times to the local viscosity of the anthracene molecule.

In the current period, these methods have been applied to polyisobutylene (PIB), and to a lesser extent, to polydimethylsiloxane (PDMS). The primary accomplishments of this period are:

**Located the Cross Over from Small-Molecule Behavior to Polymer Behavior.** Although the transport in high polymers and small-molecules liquids is known to be fundamentally different, it has not been known how long the polymer must be to develop its unique properties. Our results show that polymer-like dynamics are well developed even in short polymers. As a result, powerful simulation and modeling techniques, which are only practical for short polymers, may be extrapolated to design realistic high polymer systems.

**Found Indications of Nano-Structure Formation in Polymers.** In small-molecule liquids, anthracene rotation is single exponential. However in polymers, we have found that the rotation is multiexponential. The most straightforward interpretation is that the polymers have nanostructure, i.e., cavities, which allow more rapid rotation about one axis than about another. Although such nanostructures are commonly hypothesized, previously there has not been an experimental method to directly verify their existence or to probe their properties.

**Nanoviscosity Correlates with Macroscopic Diffusivity.** The central hypothesis of this project is that measurement of nanometer mechanical properties will give greater insight into diffusion than bulk measurement. Initial measurement on PDMS support this idea. PDMS is structurally very similar to PIB, but has dramatically higher diffusion rates. Our measurements show that PDMS also has dramatically lower nanoviscosity than PIB, even under conditions where the macroscopic viscosity is the same.

The initial delays in building the equipment for measuring time-resolved fluorescence anisotropy lifetimes have been overcome. As a result, our measurements now extend over a much greater range of times and polymer lengths. The Kerr-Effect with Resonant Detection experiment reported last time as a method for making nanoelasticity measurements is contaminated with an unexplained solvent signal. As a result, efforts have focussed on the more productive

nanoviscosity measurements. The discrepancy between bulk and nanoviscosity in PDMS has been unexpectedly large. As a result, new sample handling methods are being developed to measure materials with high bulk viscosity in our ultrafast dichroism experiment.

## REPORT

**Nanoviscosity Measurements.** In small-molecule liquids, the relationship between viscosity  $\eta$  and diffusion constant  $D$  is well established in the Stokes-Einstein law

$$D = \frac{kT}{6\pi r\eta}, \quad (1)$$

where  $T$  is the temperature and  $r$  is the molecular radius. The viscosity is also related to the rotation time of a molecule

$$\tau_{rot} = \kappa \frac{\lambda V \eta}{kT} + \tau_0, \quad (2)$$

where  $V$  is the molecular volume,  $\lambda$  is a factor for the shape of the effective ellipsoid representing the rotating molecule and  $\kappa$  is a correction for nonhydrodynamic effects. When the solvent molecules are smaller than the rotating molecule, there is no need to distinguish bulk viscosity from nanoviscosity.

In polymers, these relationships between diffusion, bulk viscosity and rotation time break down. However, Eq. 2 can be used to define a nanoviscosity based on the rotation time of a nanometer sized molecule. The nanoviscosity specifically reflects the flexibility and mobility of the "cavity" containing the solute. Thus, it is hypothesized that the nanoviscosity will be directly related to small molecule diffusion in a way that the bulk viscosity is not.

In the last grant period, we developed the specific methodology needed to measure rotation times of a probe molecule and to convert these times to nanoviscosities. Anthracene was chosen as an optimized probe molecule, and the constants in Eq. 2 were calibrated in small-molecule liquids (Fig. 1).

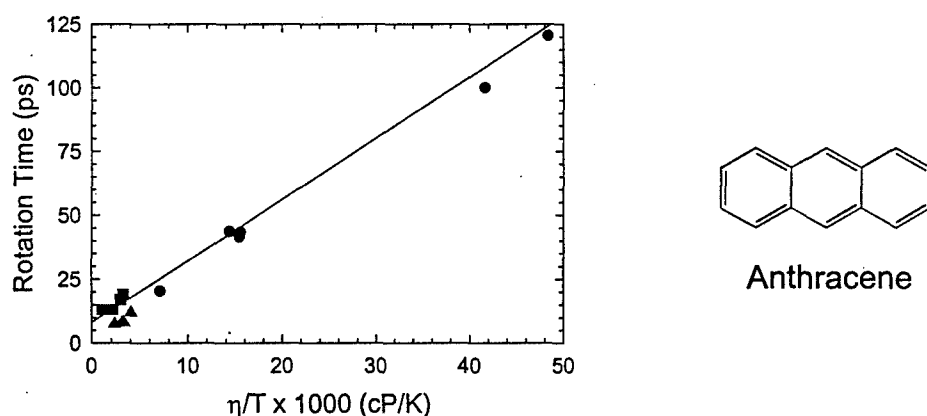


Figure 1. A calibration curve relating anthracene rotation times to its local viscosity. These measurements in small-molecule liquids are related to the bulk viscosity by Eq. 2. The parameters from this calibration are used to extract polymers nanoviscosities from measurements of rotation times. (●) This project, (▲) Ref. 4, (■) Ref. 5.

In general, a molecule with anthracene's symmetry can have two rotation times, reflecting rotation of the transition dipole about two different axes. However, anthracene's specific shape causes these two times to be nearly identical. Its rotational decay in small-molecule liquids was found to be purely single exponential. This feature makes anthracene very sensitive to formation of anisotropic structures in polymers, which favor rotation about one axis over the other.

**Nanoviscosity in Polyisobutylene - Development of Polymer Behavior.** Polyisobutylene (PIB) is a commonly used elastomer - it is the basis of "butyl rubbers." We have measured the rotation time of anthracene in PIB as a function of the chain length. In Fig. 2, these times are plotted against the bulk viscosity. For comparison, the small-molecule relationship from Fig. 1 is shown as the dashed line. The rotation times are converted to nanoviscosities and compared to the bulk viscosity in Fig. 3.

Prior to these measurement, it was known that small solutes in polymers have mobilities which are unexpectedly large based on the bulk viscosity. However, it was not known how large a solvent molecule needed to be to show the unique features of a polymer. Figures 2 and 3 show that polymer-like behavior begins for short chains only slightly longer than the solute molecule. In particular, it occur for chains shorter than the entanglement length of the polymer. Thus entanglement phenomena cannot be invoked as an essential feature in describing the diffusion properties of polymers. These results are a major step in completing the project objective of quantifying the relationship between nanometer scale dynamics and macroscopic transport properties.

This result opens up important methods for the design and modeling of diffusion in polymers. Many powerful theoretical techniques, for example computer modeling, cannot be applied to polymers of realistic length. However, these results suggest that the qualitative differences between polymers can be identified in short chains for which these techniques are practical. Further work on this project will allow quantitative extrapolation of short-chain models to long-chain materials.

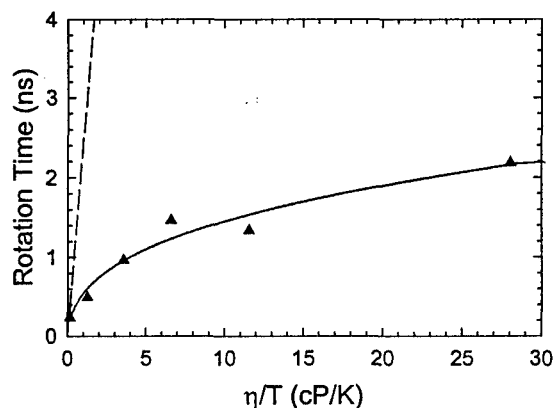


Figure 2. The average rotation times of anthracene in PIB with varying chain lengths. The relationship between rotation time and viscosity found in small-molecule solvents is shown as the dashed line. These measurements show a dramatically increased mobility for a small solute in a polymer relative to a small-molecule solvent.

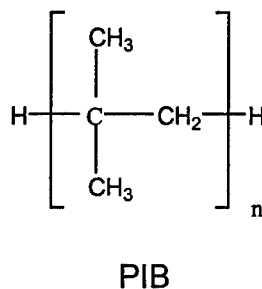
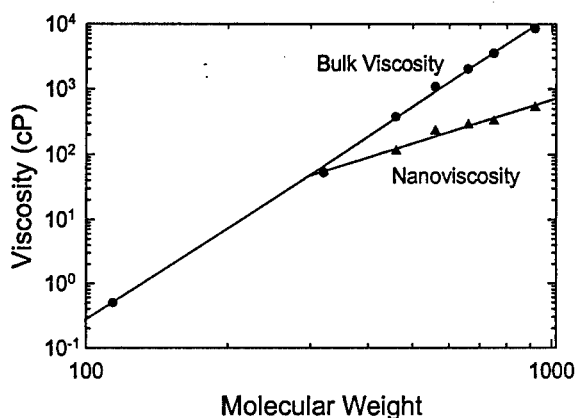


Figure 3. The nanoviscosity of PIB ( $\blacktriangle$ ) vs. molecular weight of the chain on a log-log plot. The bulk viscosity ( $\bullet$ ) is shown for comparison. The distinction between bulk and nanoviscosity begins with polymer chains only twice as large as the solute molecule (MW 154).

**Nonexponential Decay Shapes - Evidence for Nanostructure in Polymers.** In small-molecule solvents, the decay of the fluorescence anisotropy of anthracene is single exponential. We have found that in polymers, it is not. Figure 4 shows anisotropy decays scaled by the average decay time to emphasize the shape of the decays. A straight line representing a single exponential decay is shown for comparison. The decays are distinctly nonexponential for all the polymers and appear to be approaching an asymptotic shape at high molecular weight.

The most straightforward explanation for this phenomenon is that we are observing the formation of the often hypothesized "cavities" which contain solutes in polymers. These nanostructures impose different restrictions on rotation about the different axes of the anthracene molecule. Because a preexisting void the size of an anthracene is not possible, this cavity must form in response to the solute and is not characteristic of the unperturbed polymer. Thus, we have found the experimental evidence of inhomogeneity in polymer structure and dynamics that was an objective of this project. Further work will provide the first specific experimental information on the properties of these nanocavities.

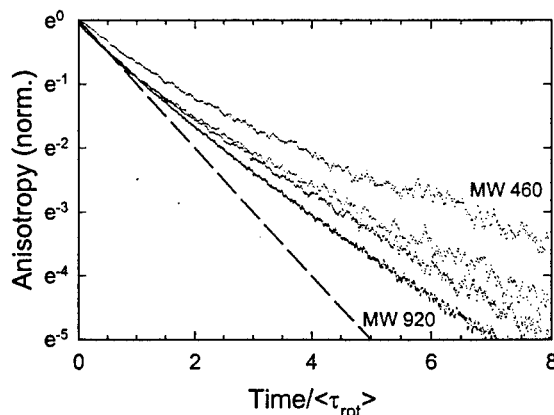


Figure 4. Anisotropy decays of in PIB on a normalized time axis to emphasis the decay shape. Top to bottom: MW 460, 560, 660, 920. A single exponential decay (dashed line) is shown for comparison. The polymer decays are nonexponential and approach an asymptotic shape for long chains.

**Polyisobutylene vs Polydimethylsiloxane - Correlation of Nanoviscosity with Diffusivity.** Polydimethylsiloxane (PDMS) is another common elastomer with a molecular shape very similar to PIB (Figs. 3 and 6). Despite this similarity, PIB has a very low diffusivity, whereas PDMS has a very high diffusivity.[6, 7] If our nanoviscosity measurements are closely related to diffusivity, as we hypothesized, the differences in these materials should show up in nanoviscosity measurements, even when the bulk dynamics are similar.

Figure 5 shows anisotropy decay measurements in PIB and PDMS samples with very similar bulk viscosities. The PIB shows a very slow decay and a long rotation time. The PDMS has decay so fast, it cannot be resolved from our instrument response function.

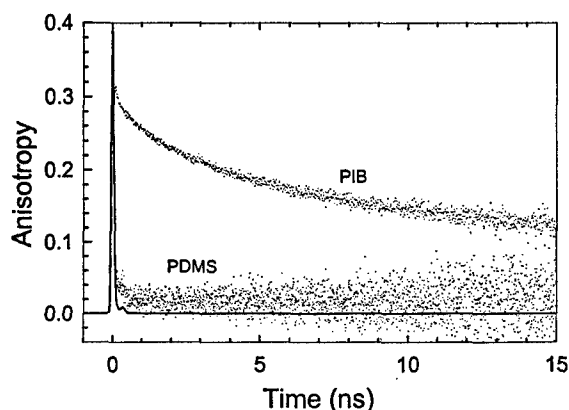


Figure 5. Anisotropy decays in PIB and PDMS samples with similar bulk viscosities (PIB  $\eta = 85$  P; PDMS  $\eta = 100$  P). The decay times, which are directly related to the nanoviscosity, differ by several orders-of-magnitude. The PDMS decay cannot be resolved from the instrument response function (solid curve).

Results expressed as nanoviscosities vs molecular weight are shown in Fig. and can be compared to the PIB results in Fig. 3. In the case of PDMS, the nanoviscosity is so low that the current measurements have only established upper bounds.

In both Fig. 5 and Fig. 6, it is apparent that our measurements are showing a dramatically increased mobility of the solute in PDMS compared to PIB. It is very likely that the low nanoviscosity of PDMS is due to the same factors that cause its high diffusivity. Thus, these results support the premise of the project that small-molecule diffusion in polymers is governed by nanoscale properties which can be determined with ultrafast measurements of suitable probe molecules.

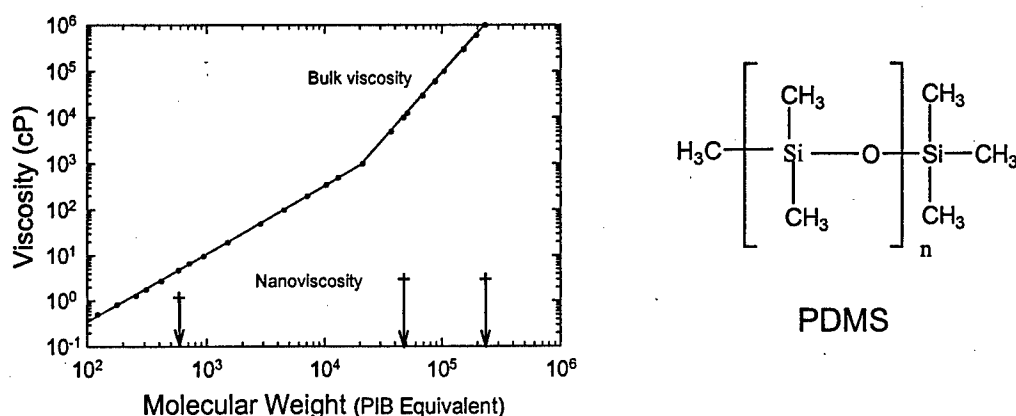


Figure 6. The nanoviscosity of PDMS (+) vs. molecular weight of the chain on a log-log plot. Only upper bounds on the nanoviscosity have been determined. The bulk viscosity (•) is shown for comparison (cf. Fig. 3).

**Equipment Development.** A major complication of this project is the broad range of rotation times and viscosities involved, which in turn, requires multiple techniques for measurement. Time-resolved dichroism spectroscopy is suitable for rotation times in the range of 100 fs to 200 ps. Fluorescence depolarization measurements are useful from 30 ps to 30 ns. In the first report on this project, we reported delays in completing the apparatus for the depolarization measurements. This apparatus is now functioning and produced the majority of the new results reported here.

The rotation times in PDMS are so dramatically fast, despite the high bulk viscosity, that the depolarization measurements only give upper bounds to the nanoviscosity. However, the faster dichroism technique requires a flowing sample. We are just finishing a new sample handling system to allow us to flow samples with very high viscosity through our dichroism spectrometer.

**Future Work.** In the first two years of this project, the major objectives of the project have been achieved at a qualitative level. The experimental challenges of developing a technique for measuring dynamics on a nanometer scale in polymers have been met. The basic phenomenology has been outlined in the target polymers and there are strong indications that our approach will provide more direct information on small-molecule diffusion unavailable from standard experiments.

Now that the major experimental and conceptual difficulties have been overcome, the final year of the project will be devoted to quantifying the phenomena we have found and expanding the data sets. Because of the novelty of our approach, there is no specific preexisting theoretical context within which to quantitatively analyze our data. Thus it is important to produce high quality data sets to simulate theoretical analysis of our results.

We can anticipate that at the end of the project, a new experimental approach to studying diffusion in polymers will be well established in standard polymer systems. The method will then be available to study specific materials of interest to particular problems.

#### **Publications and Technical Reports**

Y. Zhang and M. Berg, "Nonpolar Solvation and Inertial Dynamics by Ultrafast Dichroism Spectroscopy: Measurements on Anthracene in Benzyl Alcohol", in preparation.

***Participating Scientific Personnel***

Mark A. Berg (PI)

Mark Somoza (PhD in progress)

Xiaotian Zhang

Tianshu Lai

Yunhan Zhang (PhD in progress)



## BIBLIOGRAPHY

1. *Diffusion in Polymers*, edited by P. Neogi (Marcel Dekker, New York, 1996).
2. "Dynamics of Small Molecules in Bulk Polymers," A. A. Gusev, F. Müller-Plathe, W. F. van Gunsteren and U. W. Suter, *Adv. Poly. Sci.* **116**, 207 (1994).
3. "Transition-State Theory Model for the Diffusion Coefficients of Small Penetrants in Glassy Polymers," A. A. Gray-Weale, R. H. Henchman, R. G. Gilbert, M. L. Greenfield and D. N. Theodorou, *Macromolecules* **30**, 7296 (1997).
4. "Influence of Temperature and Viscosity on Anthracene Rotational Diffusion in Organic Solvents: Molecular Dynamics Simulations and Fluorescence Anisotropy Study," G. S. Jas, Y. Wang, S. W. Pauls, C. K. Johnson and K. Kuczera, *J. Chem. Phys.* **107**, 8800 (1997).
5. "Orientational Motion of Anthracene in Liquid Solution Studied by IR/UV Double-Resonance Spectroscopy," M. Lettenberger, F. Emmerling, N. H. Gottfried, A. Laubereau, *Chem. Phys. Lett.* **240**, 324 (1995).
6. *Polymer Permiability*, edited by J. Comyn (Elsevier Applied Science, London, 1985). 1969).

University Research Initiative Program for Combat Readiness  
Annual Report 06/01/98-05/31/99

PART 53-FORMS

53.301-298

<b>REPORT DOCUMENTATION PAGE</b>		Form Approved OMB No. 0704-0188	
Public reporting burden for this collection of information is estimated to average 1 hour per response, including the time for reviewing instructions, searching existing data sources, gathering and maintaining the data needed, and completing and reviewing the collection of information. Send comments regarding this burden estimate or any other aspect of this collection of information, including suggestions for reducing this burden, to Washington Headquarters Services, Directorate for Information Operations and Reports, 1215 Jefferson Davis Highway, Suite 1204, Arlington, VA 22202-4302, and to the Office of Management and Budget, Paperwork Reduction Project (0704-0188), Washington, DC 20503.			
1. AGENCY USE ONLY (Leave blank)	2. REPORT DATE June 1, 1999	3. REPORT TYPE AND DATES COVERED Annual	
4. TITLE AND SUBTITLE Small Molecule Transport Through Polymers: Effects of Polymer Inhomogeneity and Dynamics on the Nanometer Length Scale		5. FUNDING NUMBERS Grant Number N00014-97-1-0806 PR Number 97PR06312-00 Disbursing Code N68892 AGO Code N66020 Cage Code 4B489	
6. AUTHOR(S) Mark A. Berg			
7. PERFORMING ORGANIZATION NAME(S) AND ADDRESS(ES) University of South Carolina		8. PERFORMING ORGANIZATION REPORT NUMBER  N00014-97-1-0806	
9. SPONSORING / MONITORING AGENCY NAME(S) AND ADDRESS(ES)  ONR		10. SPONSORING / MONITORING AGENCY REPORT NUMBER  ONR	
11. SUPPLEMENTARY NOTES Prepared in coordination with University Research Initiative Program for Combat Readiness			
12a. DISTRIBUTION / AVAILABILITY STATEMENT APPROVED FOR PUBLIC RELEASE		12b. DISTRIBUTION CODE	
13. ABSTRACT (Maximum 200 words)  This project seeks to elucidate the mechanism of small-molecule diffusion through polymers by examining the polymer's dynamics on a nanometer length scale. The methodology for measuring nanoviscosity was developed in the first year of the project and now has been applied to polyisobutylene. By varying the chain length of the polymer, we have shown that the unique features of polymer dynamics begin at very short chain lengths. This result will allow the properties of high-polymers to be predicted using the more powerful theoretical and modeling techniques that can be applied to short chains. The rotation of our probe molecule develops a multiexponential form in polymers, whereas a single exponential form occurs in small-molecule solvents. This result suggests that polymers form nanostructures, i.e., "cavities" or "channels", around a small penetrant molecule. Lastly, measurements have been started on polydimethylsiloxane, an elastomer that is structurally similar to PIB, but supports much more rapid diffusion. The nanoviscosity in PDMS is dramatically lower than in PIB, even under conditions where the bulk viscosities are the same. This finding supports the central hypothesis of this project - diffusion of small molecules is determined by polymer properties on the nanometer scale, not by bulk properties.			
14. SUBJECT TERMS Chemical and Biological Defense, Target Acquisition, Anti-Submarine, Combat Medicine, Biodeterioration, Command Control and Communication		15. NUMBER OF PAGES 8	
		16. PRICE CODE	
17. SECURITY CLASSIFICATION OF REPORT  UNCLASSIFIED	18. SECURITY CLASSIFICATION OF THIS PAGE  UNCLASSIFIED	19. SECURITY CLASSIFICATION OF ABSTRACT  UNCLASSIFIED	20. LIMITATION OF ABSTRACT  200 words

NSN 7540-01-280-5500

Standard Form 298 (Rev. 2-89)

Prescribed by ANSI Std. Z39-18  
298-102

## **The Design and Synthesis of Quantum Dot Based Lasers**

Richard D. Adams

Department of Chemistry and Biochemistry  
University of South Carolina  
Columbia, SC 29208

Tel: (803)777-7187  
Fax: (803)777-6781  
Email: [adams@psc.sc.edu](mailto:adams@psc.sc.edu)

## Section 2-5: The Design and Synthesis of Quantum Dot Based Lasers

Richard Adams

### ABSTRACT

In Year 2 we have continued our investigations of the photoemission properties of thiolate containing cadmium sulfide  $\text{Cd}_{10}\text{S}_4$  cluster complexes. We have examined the photoemission of single crystals and performed measurements of the lifetimes of the excited states. In new directions we have turned our attention to investigation of the less toxic zinc homologs. We have prepared some new zinc thiolate cluster compounds (e.g.  $[\text{NEt}_3\text{H}]_2[\text{Zn}_4(\text{S-p-C}_6\text{H}_4\text{CH}_3)_{10}]$ ) and have investigated their structural and photoluminescence properties. These compounds exhibit photoluminescence at 77K.

### FORWARD

Amount: \$330,000. Period: July 1, 1997 - June 30, 2000.

We have prepared and crystallographically characterized the new zinc thiolate cluster complex  $[\text{NEt}_3\text{H}]_2[\text{Zn}_4(\text{Sp-C}_6\text{H}_4\text{CH}_3)_{10}]$  and measured photoluminescence spectra at low temperature. This complex exhibits longer excited state lifetimes and has significant shifts of its photoemission to lower energy compared to similar complexes reported previously.

### REPORT

#### *Statement of the problem*

Semiconductor quantum dots are a new class of nanoscale particles that exhibit size-dependent properties.<sup>1</sup> One of these properties of particular interest is known as photoluminescence, which arises from the radiative recombination of a photogenerated electron-hole pair. The wavelength maximum and intensity of the photoluminescence are strongly influenced by the nature of the particle surface. In this work we are examining atomically well-defined nanoclusters and are exploring the effect of ligands on the emission properties.

#### *Summary of the Most Important Results.*

1) The optical properties of the  $[\text{Cd}_{10}\text{S}_4\text{X}_4(\text{SR})_{12}]^{2-}$ , X = Br, I; R =  $\text{C}_6\text{H}_5$  or  $\text{p-C}_6\text{H}_4\text{CH}_3$ , clusters have been examined in the solid state. We find that the photoluminescence and excitation spectra essentially overlap for samples in solution compared to single crystal materials (Figure 1) This is of practical importance for device-making; solids are much easier to fabricate into well-defined layers than solutions.

We have sent a single-crystalline sample to the University of Maryland's Center for Fluorescence Spectroscopy to obtain time-resolved luminescence lifetime data. For  $[\text{Cd}_4\text{L}_4(\text{S-p-C}_6\text{H}_4\text{CH}_3)_{12}]^{2-}$ , the best-fit model to the data is a complicated tri-exponential decay with components of 5.0 ns

(92%), 58.9 ns (4.7%) and 151.5 ns (3.3%). Attempts to model the data with a bi-exponential yielded 6.2 ns (41%) and 117.2 ns (59%) components, but the fits were not as good as the tri-exponential case. For a pure molecule with a single emitting state, a single exponential decay is expected. To account for the complicated luminescence decays we observe, either (i) the sample is impure, or has decomposed to yield an emitting product (unlikely), or (ii) the sample is pure and has multiple emitting states. If the emission arises from charge-transfer transitions, and metal-halide and metal-thiolate states are both involved, then the latter explanation is plausible.

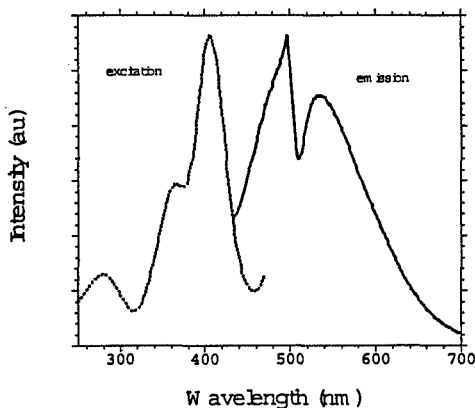


Figure 1. Excitation and emission spectra of a single crystal of  $[\text{Cd}_{10}\text{S}_4\text{Br}_4(\text{p-SC}_6\text{H}_4\text{CH}_3)_{12}][\text{NEt}_4]_2$ . The sample was excited at 408 nm for acquisition of the emission spectrum, and excitation data were gathered at an emission wavelength of 495 nm.

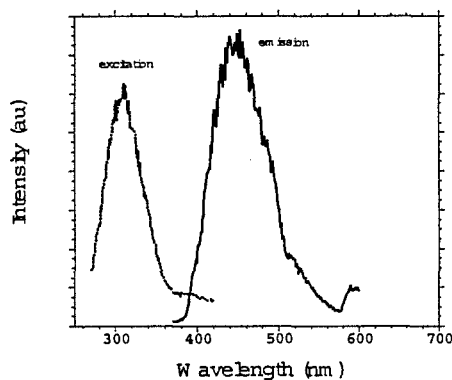


Figure 2

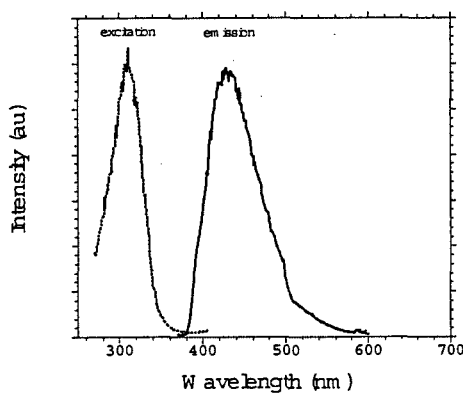


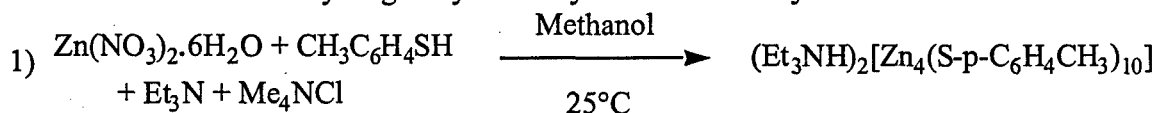
Figure 3

Figure 2. Excitation and emission spectra of  $[\text{NEt}_4]_2[\text{Zn}_{10}\text{S}_4(\text{p-SC}_6\text{H}_4\text{CH}_3)_{16}]$  in DMSO/methanol glass at 77 K.

Figure 3. Excitation and emission spectra of single crystalline  $[\text{NEt}_4]_2[\text{Zn}_{10}\text{S}_4(\text{p-SC}_6\text{H}_4\text{CH}_3)_{16}]$  at 77 K.

2) ZnS in the bulk is a semiconductor that has a larger bandgap than CdS; nanoparticles of  $\sim 50$  Å ZnS emit in the blue.<sup>2</sup> The optical properties of well-defined ZnS cluster molecules have not been explored nearly as much as the CdS analogs; Zn also has the advantage of lower toxicity compared to Cd. Accordingly, we have pursued the synthesis and characterization of  $\text{Zn}_{10}\text{S}_4$  cluster molecules. In fluid solution at room temperature, the  $\text{Zn}_{10}$  clusters are nonemissive, however, upon cooling to 77K, both the crystalline solid and glassy solutions emit blue light at  $\sim 450$  nm (Figures 2 and 3). The emission is broad and structureless, resembling charge-transfer emission commonly seen for inorganic molecules.

We have prepared new small  $\text{Zn}_4$  thiolate cluster compound  $(\text{NEt}_3\text{H})_2[\text{Zn}_4(\text{S-p-C}_6\text{H}_4\text{CH}_3)_{10}]$ , **1**, from  $\text{Zn}(\text{NO}_3)_2$  and thiocresol ( $\text{HS-p-C}_6\text{H}_4\text{CH}_3$ ) in triethylamine, Eq. (1).<sup>3</sup> Compound **1** was characterized in the solid state by single crystal x-ray diffraction analyses.



An ORTEP diagram of the molecular structure of the cluster anion is shown in Figure 4.

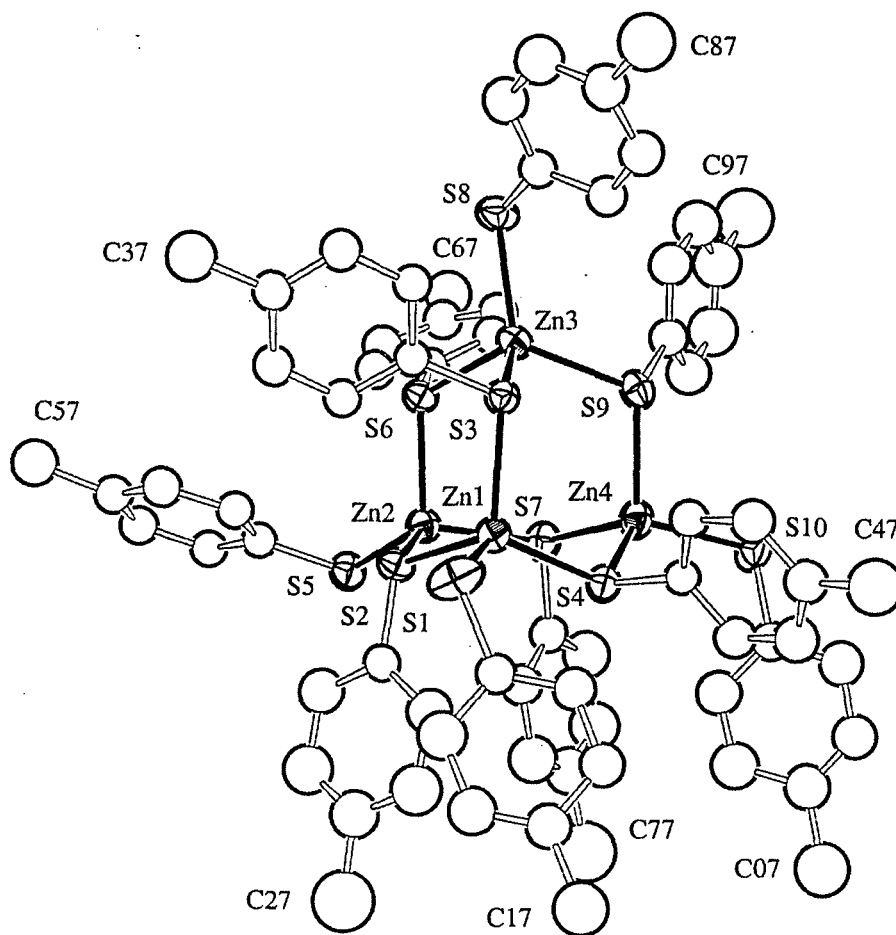


Figure 4

Figure 4. An ORTEP diagram of  $[\text{Zn}_4(\text{S-p-C}_6\text{H}_4\text{CH}_3)_{10}]^{2-}$  showing 40% probability thermal ellipsoids.

Each zinc ion is coordinated to four sulfur atoms from the thiolate ligands in a tetrahedral geometry. One of the four is a terminally coordinated thiolate ligand while the other three form bridges to neighboring zinc ions. These bonds are indicated by the solid lines. Surprisingly, even these small  $\text{Zn}_4$  clusters still photoemit (although at only 77 K) with a spectral distribution (Fig. 5) a similar to the  $\text{Zn}_{10}$  clusters. The corresponding  $\text{Cd}_4$  clusters are emissive only if the coordinating thiolate is extremely electron-withdrawing.<sup>4</sup> Because the emission and excitation are independent of size for the  $\text{Zn}_4$  and  $\text{Zn}_{10}$  clusters, it is likely that these spectra are due to localized charge-transfer states rather than size-dependent excitonic recombination. We are attempting to prepare halide derivatives of the Zn clusters in order to compare the optical effect the halide ligand has with that observed in our studies of the  $\text{Cd}_{10}$  case.

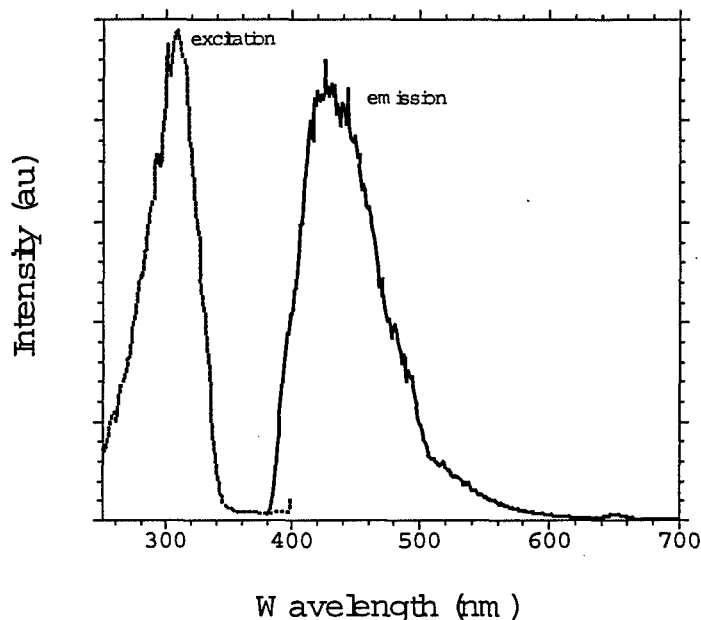


Figure 5. Excitation and emission spectra of  $[\text{Zn}_4(\text{S-p-C}_6\text{H}_4\text{CH}_3)_{10}]^{2-}$  in DMSO/methanol glass at 77 K.

### ***Publications and Technical Reports***

#### **Publication in print**

"Halide Enhancement of the Luminescence of  $\text{Cd}_{10}\text{S}_4$  Thiolate Clusters," R. D. Adams, B. Zhang, C. J. Murphy and L. K. Yeung, *Chem. Commun.* **1999**, 383.

#### **Publication submitted**

"A Comparison of the Photophysical Properties of Thiolate-Capped CdS Quantum Dots with Thiolate-Capped CdS Molecular Clusters," L. K. Yeung, K. Sooklal, R. Mahtab, B. Zhang, R. D. Adams and C. J. Murphy, submitted to *Mater. Res. Soc. Symp. Proc.*

#### **Presentations at national meetings**

1. *American Chemical Society National Meeting, August 23-27, 1998, Boston, MA:* "Well-Defined Semiconductor Nanoclusters with Tunable Photophysical Properties," Lee K. Yeung, Bin Zhang, Richard D. Adams, Catherine J. Murphy.



2. American Chemical Society National Meeting, March 21-25, 1999, Anaheim, CA: "Halide Enhancement of the Luminescence of Cd<sub>10</sub>S<sub>4</sub> Thiolate Clusters," Bin Zhang, Richard D. Adams, Catherine J. Murphy and Lee K Yeung.

3. Materials Research Society International Meeting, April 4-9, 1999, San Francisco, CA: "A Comparison of the Photophysical Properties of Thiolate-Capped CdS Quantum Dots with Thiolate-Capped CdS Molecular Clusters," Lee K. Yeung, Kelly Sooklal, Rahina Mahtab, Bin Zhang, Richard D. Adams and Catherine J. Murphy.

***Participating Personnel***

Richard D. Adams, PI  
Catherine J. Murphy, CoPI  
Lee Yeung  
Bin Zhang

**BIBLIOGRAPHY**

1. R. F. Service, *Science* 1996, 271, 920.
2. K. Sooklal, B. Cullum, S. M. Angel and C. J. Murphy, *J. Phys. Chem.* 1996, 100, 4551.
3. I. G. Dance, A. Choy, M. L. Scudder, *J. Am. Chem. Soc.* 1984, 106, 6285.
4. D. Y. Yoon, D. C. Selmarten, H. Lu, H.-J. Liu, C. Mottley, M. A. Ratner, J. T. Hupp, *Chem. Phys. Lett.* 1996, 251, 84.

University Research Initiative Program for Combat Readiness  
Annual Report 06/01/98-05/31/99

PART 53-FORMS

53.301-298

<b>REPORT DOCUMENTATION PAGE</b>		Form Approved OMB No. 0704-0188	
Public reporting burden for this collection of information is estimated to average 1 hour per response, including the time for reviewing instructions, searching existing data sources, gathering and maintaining the data needed, and completing and reviewing the collection of information. Send comments regarding this burden estimate or any other aspect of this collection of information, including suggestions for reducing this burden, to Washington Headquarters Services, Directorate for Information Operations and Reports, 1215 Jefferson Davis Highway, Suite 1204, Arlington, VA 22202-4302, and to the Office of Management and Budget, Paperwork Reduction Project (0704-0188), Washington, DC 20503.			
1. AGENCY USE ONLY (Leave blank)	2. REPORT DATE June 1, 1999	3. REPORT TYPE AND DATES COVERED Annual	
4. TITLE AND SUBTITLE The Design and Synthesis of Quantum Dot Based Lasers		5. FUNDING NUMBERS Grant No. N00014-97-1-0806 PR No. 97PR06312-00 PO Code 353, Disbursing Code N68892 AGO Code N66020, Cage Code 4B489	
6. AUTHOR(S) Richard D. Adams			
7. PERFORMING ORGANIZATION NAME(S) AND ADDRESS(ES) University of South Carolina		8. PERFORMING ORGANIZATION REPORT NUMBER N00014-97-1-0806	
9. SPONSORING / MONITORING AGENCY NAME(S) AND ADDRESS(ES) ONR		10. SPONSORING / MONITORING AGENCY REPORT NUMBER ONR	
11. SUPPLEMENTARY NOTES Prepared in coordination with University Research Initiative Program for Combat Readiness			
12a. DISTRIBUTION / AVAILABILITY STATEMENT APPROVED FOR PUBLIC RELEASE		12b. DISTRIBUTION CODE	
13. ABSTRACT (Maximum 200 words)  We have continued our investigations of the photoemission properties of thiolate containing cadmium sulfide Cd <sub>10</sub> S <sub>4</sub> cluster complexes. We have examined the photoemission of single crystals and performed measurements of the lifetimes of the excited states. In new directions we have turned our attention to investigation of the less toxic zinc homologs. We have prepared some new zinc thiolate cluster compounds (e.g. [NEt <sub>3</sub> H] <sub>2</sub> [Zn <sub>4</sub> (Stolyl) <sub>10</sub> ]) and have investigated their structural and photoluminescence properties. These compounds exhibit photoluminescence at 77K.			
14. SUBJECT TERMS Chemical and Biological Warfare, Target Acquisition, Anti-Submarine, Combat Medicine, Biodeterioration, And Command Control and Communication.		15. NUMBER OF PAGES 6	
		16. PRICE CODE	
17. SECURITY CLASSIFICATION OF REPORT  UNCLASSIFIED	18. SECURITY CLASSIFICATION OF THIS PAGE  UNCLASSIFIED	19. SECURITY CLASSIFICATION OF ABSTRACT  UNCLASSIFIED	20. LIMITATION OF ABSTRACT  UNCLASSIFIED

NSN 7540-01-280-5500

Standard Form 298 (Rev. 2-89)

Prescribed by ANSI Std. Z39-18  
298-102

## **Rapid Biodetection of Bacterial Cells By Laser Pyrolysis/Mass Spectrometry**

**Principal Investigator:**

Stephen L. Morgan

**Co-Investigators:**

Scott R. Goode, S. Michael Angel

Department of Chemistry & Biochemistry  
The University of South Carolina  
Columbia, SC 29208

Tel: (803) 777-2461

Fax: (803) 777-6104

Email: morgan@psc.sc.edu

## **Section 2-6: Rapid Biodetection of Bacterial Cells by Laser Pyrolysis/Mass Spectrometry**

Stephen L. Morgan

### **ABSTRACT**

This project involves an investigation of novel methods for biodetection of bacterial agents based on a combination of laser ablation/pyrolysis, fast gas chromatography (GC), and time-of-flight mass spectrometry. The new instrument to be developed combines a 266 nm Nd-Yag UV laser for micro sample ablation with time-of-flight mass spectrometry (TOF MS) for rapid bacterial characterization. Microlaser ablation will be employed to pyrolyze single cells or small populations of cells. TOF MS will be used to identify chemical markers in the mixture of cellular fragments. By rastering the surface of the sample with the laser, mass spectrometric "images" of the sample's chemical content can be produced. Goals include targeting specific cellular structures, reducing sample size requirements, and achieving high selectivity. A further focus of these studies is to couple extremely fast gas chromatographic separations to TOF MS for bacterial characterization. Chemometric data analysis using principal component analysis, multivariate discriminant analysis, and cluster analysis will permit statistical validation of the significance of differences observed between different samples.

### **FORWARD**

The total amount of the grant award is \$434,748.00 for the period from 6/1/97 to 5/31/00. Significant achievements during this second reporting period include:

- The new instrument has been designed. The microlaser ablation system is being coupled to a gas chromatograph using a cryofocusing trap for concentration of the ablation effluent prior to time-of-flight mass spectrometry.
- Preliminary investigations of rapid gas chromatographic techniques (specifically use of fast temperature programming, thin stationary phase films, and narrow diameter columns have been completed.
- Publications have been completed describing: (1) qualitative analysis of monomeric carbohydrate content in bacterial polysaccharides by Py-GC/MS, (2) comparisons of conventional and fast GC techniques for polymer analysis, and (3) quantitative analysis of polymer composition using pyrolysis GC/MS and principal component regression.

## REPORT

### *Statement of the problem*

Traditional microbial identification is performed after isolation and growth and taxonomic decisions are often based on morphology. The development of instrumental methods for direct chemical characterization of bacteria is of continuing relevance to rapid identification of bacteriological warfare agents. We have selected laser ablation coupled to time-of-flight mass spectrometry (TOF MS) as a candidate method. We are investigating existing commercial approaches, as well as some novel techniques, for sample introduction to TOF MS systems. A microlaser ablation/pyrolysis time-of-flight mass spectrometer system is under development for pyrolysis/desorption of material from single cells or small populations of cells. By focusing on single cells with a high resolution optical system, this approach also may be able to target specific cellular structures (cell wall, lipopolysaccharides, cytoplasm, intercellular content, *etc.*), reduce sample size requirements, and offer high selectivity.

### *Summary of the Most Important Results*

The laser microprobe subsystem has been acquired and tested. To satisfy the original design goal of using laser ablation to vaporize components of bacterial cells, we selected the Merchantek LUV266 laser ablation system (Carlsbad, CA). The system uses a computer controlled, frequency quadrupled, Q-switched Nd:YAG UV laser at 266 nm. A variable aperture enables control of the 5 mJ beam in 255 increments and the laser spot diameter is continuously adjustable from 5  $\mu\text{m}$  to 400  $\mu\text{m}$ . The flat beam profile allows reproducible analysis of thin layer sample surfaces with a 4 ns laser pulse length and repetition rate adjustable from 1-20 Hz.. The targeting of the laser beam can automatically raster in patterns evenly spaced around the crosshair focus with 0.25  $\mu\text{m}$  resolution. The laser ablation cell is a laminar flow cell constructed of Teflon and Viton with a replaceable laser grade window. Gas flow is computer controlled for on-line, bypass and purge operation. High-resolution color imaging from 100 $\times$  to >1000 $\times$  is provided on a computer monitor using a CCD camera and Parfocal video microscope. The laser microprobe is operated independently with full bi-directional exchange of numerical and visual data, status, and control information.

Initial tests conducted with the laser microprobe are shown in Figure 1. The first two images represent the statute of Abraham Lincoln in the Lincoln Memorial on the reverse side of a penny, before and after laser ablation with a 10 Hz repetition rate at 2.52 mJ power for 15 s. The resulting crater in the penny was 120  $\mu\text{m}$  in diameter. The third image (Figure 1C) is of a brass sample ablated at a low power setting with a 5  $\mu\text{m}$  laser spot size.



Figure 1. (A,B) Images of penny before and after ablation with resulting 120  $\mu$  spot size; (C) sample of brass after ablation with 5  $\mu$  spot size.

As described in our previous report, TOF MS offers high sensitivity because the entire collection of ions produced can be simultaneously analyzed. TOF MS is especially attractive for identification of components from macromolecular sources in microbial cells because of its high sensitivity and relatively high mass range and resolution. We are also exploring the use of fast GC methods to achieve extremely rapid GC analysis coupled to TOF MS.

Methods employing fast capillary gas chromatography have variously focused on narrow-bore columns, increased velocities, and rapid temperature programming to decrease separation times up to two orders of magnitude compared to conventional GC.<sup>1</sup> However, classic trade-offs exist: fast temperature programming decreases analysis time, but resolution may be compromised. The design of chromatographic instruments for fast GC must maintain narrow peak width throughout the system from injector to detector to produce good resolution<sup>2,3</sup>. Use of narrow diameter capillary columns produces both higher efficiency (sharper peaks) and a flatter van Deemter curve at higher flow rates. This means that high flow rates can be employed without degrading efficiency. The introduction of a smaller internal diameter column was among the first attempts at rapid GC. Hyvey and Phillips<sup>4</sup> and Ke *et al.*<sup>5</sup> demonstrated reduced analysis times using narrow capillary columns of 0.25 mm to 0.1 mm ID. Lee *et al.*<sup>6</sup> were apparently the first to suggest resistive heating of the column to increase temperature programming rates and to speed analyses. Hail and Yost<sup>7</sup> developed a GC inlet probe for mass spectrometry using direct resistive heating of aluminum clad columns. Jain and Phillips<sup>8</sup> coated capillary columns with a thin conductive film for resistive heating to achieve analysis times of seconds. Uneven heating, compromised mechanical stability, and limited column life for such coated columns prompted Ehrmann, *et al.*<sup>9</sup> to use a metal tube as the heating element combined with a sensor wire to measure the resistance and, thus, temperature of the column. Improved methods to achieve fast

temperature programming by resistive heating have resulted in applications such as high-speed air monitoring and screening for organic compounds<sup>10,11</sup>. We have investigated the use of a commercially available instrument, the Flash<sup>TM</sup>GC (Thermedics Corporation, Chelmsford, MA), which achieves rapid analyses by direct resistive heating of the chromatographic column at rates up to 30°C/s, without having to deal with the thermal mass of a column oven compartment.

The dependence of resolution and analysis time on experimental factors determining the column temperature programming conditions were investigated by varying two experimental factors ( $x_1$ , time;  $x_2$ , temperature) defining the intermediate point in a two-ramp temperature program in a 13-experiment central composite experimental design. A 19 component mixture was analyzed by the Flash<sup>TM</sup>GC under each set of conditions. Two performance measures were evaluated at each set of experimental conditions. The retention time of the last eluting peak was taken as a measure of chromatographic analysis time; the resolution of two closely eluting peaks was selected as a measure of resolution. These responses were fitted to full second-order models (Figure 2). Chromatograms produced under the conditions of fastest analysis time and best resolution with these constraints are shown in Figure 3. The response surfaces and chromatograms taken together illustrate the classic trade-off between analysis time and resolution. As might be expected, the two goals can not be simultaneously achieved at the same experimental conditions. Nevertheless, the performance for either set of conditions is excellent: resolution of a complex mixture of 19 components in less than 80-90 s.

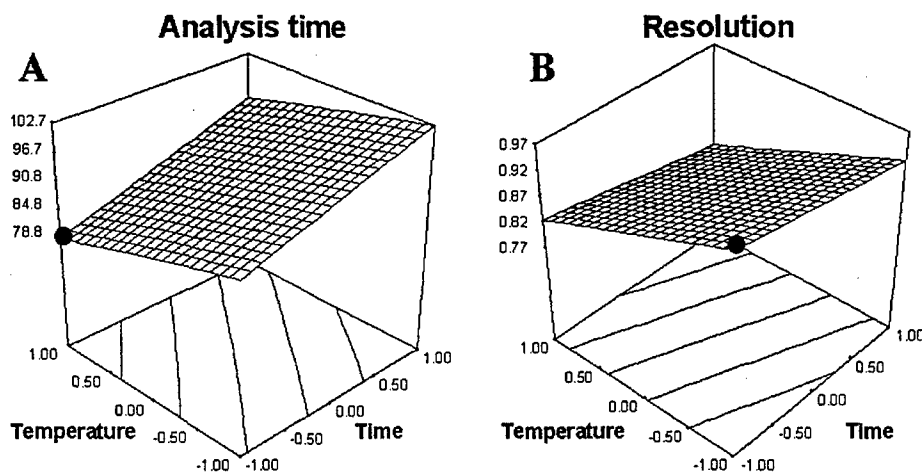


Figure 2. Fitted models for (A) analysis time, and (B) resolution responses. Dots mark conditions of fastest analysis time and best resolution within the factor ranges shown.

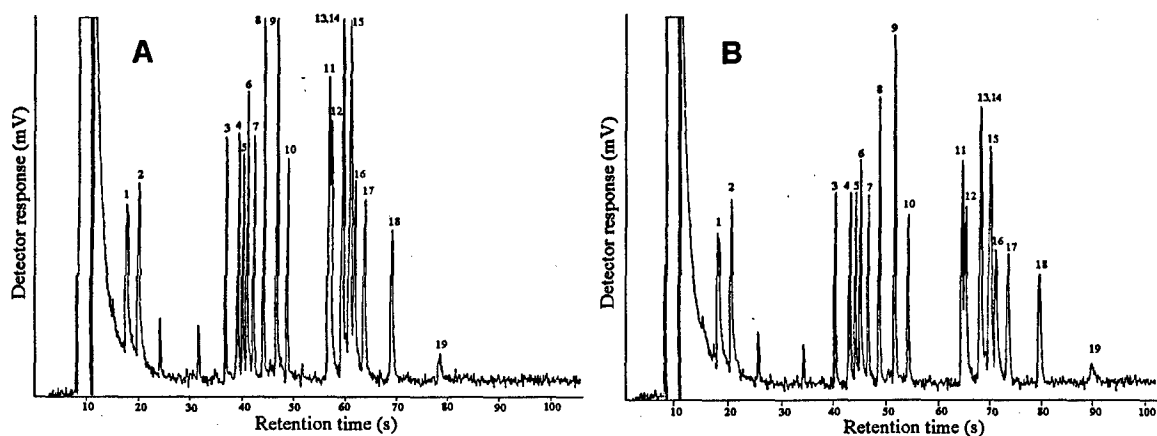


Figure 3. Flash<sup>TM</sup>GC chromatograms of the 19 component test mixture run under conditions of (A) fastest analysis time, and (B) best resolution of the worst separated pair of peaks.

To further evaluate resolution and analysis time trade-offs in the context of pyrolysis-fast GC techniques, a synthetic copolymer [poly(ethylene-co-methyl acrylate)] was pyrolyzed. Pyrolysis of the copolymer produces a chromatogram showing the typical repeating pattern of triplets from polyethylene. These triplets are a distribution of varying chain lengths of dienes, alkene, and alkanes. For analysis of the ethylene/methyl acrylate copolymer, adequate separation of the peaks forming the triplet groups of polyethylene is usually required. We analyzed this test sample by pyrolysis coupled to one of three different systems: (a) a Hewlett-Packard GCD instrument fitted with a conventional capillary column (30 m  $\times$  0.25 mm ID  $\times$  0.25  $\mu$ m df 5% phenyl-95% methyl polysiloxane coated column); (b) a Hewlett-Packard GCD instrument fitted with a short, small diameter, thin film capillary column (10 m  $\times$  0.1 mm ID  $\times$  0.10  $\mu$ m df 5% phenyl-95% methyl polysiloxane coated column (HP5, Hewlett-Packard)); and (c) a Flash GC instrument fitted with a 12 m  $\times$  0.25 mm ID  $\times$  0.25  $\mu$ m df 5% phenyl-95% methyl polysiloxane coated column (Rtx-5, Restek, Bellefonte, PA). Pyrograms from each GC system are presented in Figure 4. As expected, the triplet groups from polyethylene are well separated in the first half of each pyrogram and gradually merge into one peak coeluting all three components. As the analysis time decreases with the use of fast GC methods, however, some resolution is lost, as might be expected. There is one point of caution when using small ID columns for fast GC that is revealed by this comparison: the rate of data acquisition is critical. The typical scan rate for a quadrupole mass analyzer operating in a full scan mode (50-500 u) is approximately 1 Hz, compared to the set 100 Hz acquisition rate for the Flash GC FID. A slow scan rate combined with faster eluting peaks is responsible for insufficient sampling (only 3-5 points) of the chromatographic peak. This insufficient sampling can produce greater variation of peak areas among replicate samples; the number of ions collected and the quality of mass spectra taken for each peak is also reduced. We are presently working on a combined experimental/simulation paper showing the peak quality and mass spectral statistics under a variety of sampling conditions.



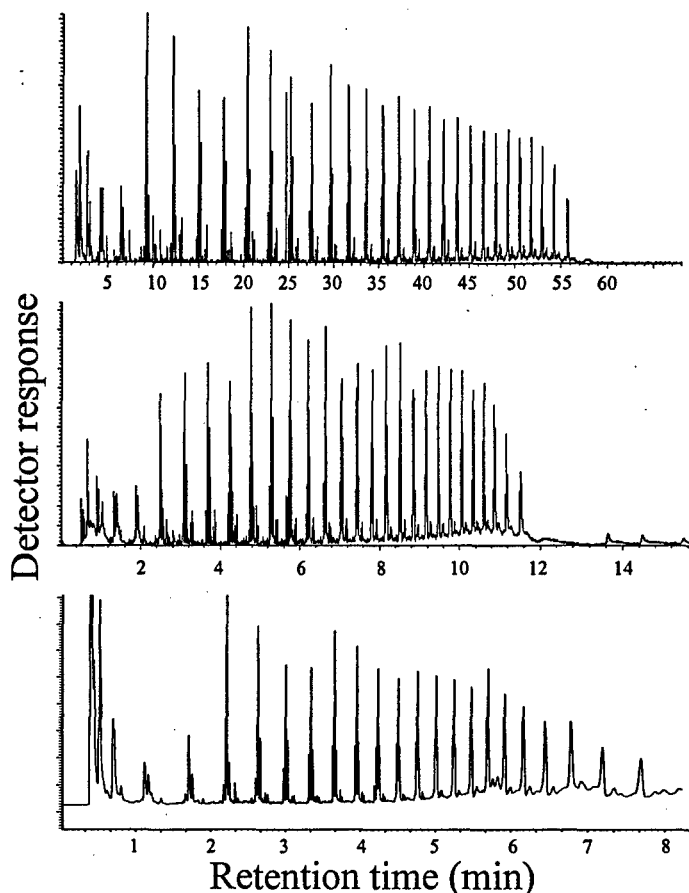


Figure 4. Pyrograms of a synthetic copolymer [poly(ethylene-co-methyl acrylate)] acquired using three different methods. (Top) Conventional GC method. (Center) Fast GC using small ID columns. (Bottom) Flash GC method.

Although we had originally considered a Comstock (Oak ridge, TN) Model LTOF-110 time-of-flight MS instrument, we have found an instrument that better matches the performance requirements of our project. The Leco Pegasus II GC/TOFMS we have selected is capable of fast mass spectral data acquisition. The system can detect and identify, narrow GC peaks from fast, high performance and conventional GC analysis using electron impact ionization. It is capable of dramatically expanding the data density of an analysis to encompass the requirements to perform mass spectral deconvolution of co-eluting compounds and compounds below the baseline while generating unskewed spectra and improving data quality. This reflectron-based instrument has a 1-meter flight tube and a mass range 5-1000 u. Most important is that the instrument has a acquisition frequency of up to 5KHz, with an integrated transient recorder to integrate and sum transient spectra into as many as *500 full mass range spectra per second*. This data acquisition speed meets our requirements for mass spectral quality under high speed GC conditions.

We are combining the laser ablation and TOF MS components as a direct laser ablation/TOF-MS system in which laser ablation/pyrolysis products are swept directly into the mass analyzer without prior chromatographic separation. The ability to separate the products of the laser

ablation/pyrolysis step by high speed gas chromatography is also desirable from a selectivity viewpoint. We are currently interfacing the laser ablation system to the gas chromatograph using a cryofocusing trap and a sub-system test to evaluate trapping efficiency is under way.

Investigations of fast GC methods for biologically relevant materials are also in progress. We have completed, but not yet submitted for publication, a manuscript on qualitative analysis of monomeric carbohydrate content in bacterial polysaccharides by Py-GC/MS. As our initial focus is on chemical markers generated from carbohydrate and amino acid/peptide cellular sources<sup>12-22</sup>, we are conducting studies using fast GC methods to investigate analysis of these thermally labile materials without degradation. After completion of testing of the separate system components, we are planning the evaluation of the laser ablation-GC-TOF MS system using a series of model compounds for bacterial cells and polysaccharides. Multivariate pattern recognition programs for analysis of MS or GC/MS data are under continual development. MatLab software has been written and tested for canonical variates analysis, and a manuscript describing neural network optimization, pruning, and interpretation in chemical terms has been submitted for publication.

#### ***Publications and Technical Reports***

W. J. Egan, S. M. Angel, and S. L. Morgan, "Rapid optimization and minimal complexity in neural network multivariate calibration," *Journal of Chemometrics*, **1999**, in press.

T. A. Williams, M. Riddle, S. L. Morgan, and W. E. Brewer, "Rapid gas chromatographic analysis of drugs of forensic interest," *J. Chromatogr. Sci.* **1999**, *40*, 61-64.

#### ***Participating Personnel***

1. Kristen Sellers, Ph. D. candidate, Department of Chemistry & Biochemistry, The University of South Carolina, Columbia, SC 29208.

2. Mary Peyton Davis, Ph. D. candidate, Department of Chemistry & Biochemistry, The University of South Carolina, Columbia, SC 29208.

#### **BIBLIOGRAPHY**

1. Sacks, R. D.; Smith, H.; Nowak, M. *Anal. Chem.* **1998**, *70*, 29A-37A.
2. Van Ysacker, P. G.; Janssen, H. G.; Snijders, H. M.; Cramers, C. A. *J. High. Resol. Chromatogr.* **1995**, *18*, 397-402.
3. Ewels, B. A.; Sacks, R. D. *Anal. Chem.* **1985**, *57*, 2774-2779.
4. Hyver, K. J.; Phillips, R. J. *J. Chromatogr. Sci.* **1987**, *399*, 33-46.
5. Ke, H.; Levine, S. P.; Mouradian, R. F.; Berkely, R. *Am. Ind. Hyg. Assoc. J.* **1992**, *53*, 130-137.
6. Lee, M. L.; Bartle, K. D.; Yang, S. J. *Open Tubular Gas Chromatography*, John Wiley & Sons, NY, **1984**.
7. Hail, M. E.; Yost, R. A. *Anal. Chem.* **1989**, *61*, 2410-2416.
8. Jain, V.; Phillips, J. B. *J. Chromatogr. Sci.* **1995**, *33*, 55-59.
9. Ehrmann, E. U.; Dharmasena, H. P.; Carney, K.; Overton, E. B. *J. Chromatogr. Sci.* **1996**, *34*, 533-539.

10. Akard, M. L.; Sacks, R. D. *J. Chromatogr. Sci.* **1994**, *32*, 499-505.
11. Sacks, R.; Klemp, M.; Akard, M. L. *Field Anal. Chem. Tech.* **1996**, *1*, 97-102.
12. S. L. Morgan, A. Fox and J. Gilbert, *J. Microbiol. Methods*, **9** (1989) 57.
13. M. D. Walla, P. Y. Lau, S. L. Morgan, and A. Fox, *J. Chromatogr.* **1984**, *288*, 399-413.
14. R. S. Whiton, S. L. Morgan, J. Gilbert, and A. Fox, *J. Chromatogr.* **1985**, *347*, 109-120.
15. J. Gilbert, A. Fox, R. S. Whiton, and S. L. Morgan, *J. Microbiol. Methods* **1986**, *5*, 271-282.
16. J. Gilbert, A. Fox, and S. L. Morgan, *European J. Clin. Microbiol.* **1987**, *6*(6), 715-723.
17. A. Fox, S. L. Morgan, and J. Gilbert, in *Analysis of carbohydrates by GLC and MS*, C. J. Bierman and G. McGinnis, eds., CRC Press, FL., 1989; Chapter 5.
18. C. S. Smith, S. L. Morgan, C. D. Parks, A. Fox and D. G. Pritchard, *Anal. Chem.*, **59**(1987) 1410.
19. C. S. Smith, S. L. Morgan and A. Fox, *J. Anal. Appl. Pyrol.*, **18** (1990) 97.
20. B. E. Watt, S. L. Morgan, and A. Fox, *J. Anal. Appl. Pyrol.*, **19** (1991) 237.
21. S. L. Morgan, B. E. Watt, and R. C. Galipo, "Characterization of microorganisms by pyrolysis GC, pyrolysis GC/MS, and pyrolysis MS", in: *Applied Pyrolysis Handbook*, T. Wampler, Ed., Plenum Press, NY, 1995.
22. J. W. Ezzell, Jr., T. G. Abshire, S. F. Little, B. G. Lidgerding, and C. Brown, *J. Clin. Microbiol.*, **28** (1990) 223.

University Research Initiative Program for Combat Readiness  
Annual Report 06/01/98-05/31/99

PART 53-FORMS

53.301-298

<b>REPORT DOCUMENTATION PAGE</b>		Form Approved OMB No. 0704-0188	
Public reporting burden for this collection of information is estimated to average 1 hour per response, including the time for reviewing instructions, searching existing data sources, gathering and maintaining the data needed, and completing and reviewing the collection of information. Send comments regarding this burden estimate or any other aspect of this collection of information, including suggestions for reducing this burden, to Washington Headquarters Services, Directorate for Information Operations and Reports, 1215 Jefferson Davis Highway, Suite 1204, Arlington, VA 22202-4302, and to the Office of Management and Budget, Paperwork Reduction Project (0704-0188), Washington, DC 20503.			
1. AGENCY USE ONLY (Leave blank)	2. REPORT DATE 1 June 1999	3. REPORT TYPE AND DATES COVERED Annual	
4. TITLE AND SUBTITLE  Rapid Biodetection of Bacterial Cells by Laser Pyrolysis/Mass Spectrometry		5. FUNDING NUMBERS Grant Number N00014-97-1-0806 PR Number 97PR06312-00 PO Code 353 Disbursing Code N68892 AGO Code N66020 Cage Code 4B489	
6. AUTHOR(S) Stephen L. Morgan (PI), Scott R. Goode, S. Michael Angel			
7. PERFORMING ORGANIZATION NAME(S) AND ADDRESS(ES) The University of South Carolina Columbia, SC 29208		8. PERFORMING ORGANIZATION REPORT NUMBER N00014-97-1-0806-1	
9. SPONSORING / MONITORING AGENCY NAME(S) AND ADDRESS(ES) ONR\		10. SPONSORING / MONITORING AGENCY REPORT NUMBER ONR	
11. SUPPLEMENTARY NOTES Prepared in coordination with University Research Initiative Program for Combat Readiness			
12a. DISTRIBUTION / AVAILABILITY STATEMENT APPROVED FOR PUBLIC RELEASE		12b. DISTRIBUTION CODE	
13. ABSTRACT (Maximum 200 words) This research project involves a systematic investigation of novel methods for biodetection of bacterial agents based on a combination of laser ablation/pyrolysis, fast gas chromatography (GC), and time-of-flight mass spectrometry. The new instrument to be developed combines a 266 nm Nd-Yag UV laser for micro sample ablation with time-of-flight mass spectrometry (TOF-MS) for rapid bacterial characterization. Microlaser ablation will be employed to pyrolyze single cells or small populations of cells. Time-of-flight mass spectrometry (TOF-MS) will then be used to identify chemical markers in the mixture of cellular fragments. By rastering the surface of the sample with the laser, mass spectrometric "images" of the sample's chemical content can be produced. Goals include targeting specific cellular structures (cell wall, lipopolysaccharides, cytoplasm, intercellular content, etc.), reducing sample size requirements, and achieving high selectivity. Another focus of these studies is to couple extremely fast (< min) gas chromatographic separations to TOF-MS for bacterial characterization. Chemometric data analysis using principal component analysis, multivariate discriminant analysis, and cluster analysis will permit statistical validation of the significance of differences observed between different samples.			
14. SUBJECT TERMS Chemical and Biological Warfare, Target Acquisition, Anti-Submarine, Combat Medicine, Biodeterioration, and Command Control and Communication		15. NUMBER OF PAGES	
		16. PRICE CODE	
17. SECURITY CLASSIFICATION OF REPORT UNCLASSIFIED	18. SECURITY CLASSIFICATION OF THIS PAGE UNCLASSIFIED	19. SECURITY CLASSIFICATION OF ABSTRACT UNCLASSIFIED	20. LIMITATION OF ABSTRACT  200 words

NSN 7540-01-280-5500

Standard Form 298 (Rev. 2-89)  
Prescribed by ANSI Std. Z39-18  
298-102

**SECTION III: COMMAND, CONTROL, AND COMMUNICATIONS**

**Dynamic Decision Support for Command, Control, and  
Communications in the Context of Tactical Defense**

John R. Rose

Department of Computer Science  
University of South Carolina  
Columbia, South Carolina 29208

Tel: (803)777-2405  
Fax: (803)777-3767  
Email: [rose@cs.sc.edu](mailto:rose@cs.sc.edu)

## **Section 3-1: Dynamic Decision Support for Command, Control, and Communications in the Context of Tactical Defense**

J. Rose

### **ABSTRACT**

Advances in communication and sensor technologies have brought about huge increases in the types and amounts of information available for battle management. Shortcomings in the ability to integrate and arbitrate missing and conflicting information and the current inability to correlate and reason about vast amounts of information in real-time are an impediment to providing a coherent overview of unfolding events. Integrating disparate information, such as voice, video images, and tactical displays, that has varying degrees of reliability is a first step towards battle management. Such integration can be accomplished through the application and further development of Bayesian network and intelligent agent methods. Bayesian networks provide a sound basis for a robust and potentially very efficient solution to the problems posed by incomplete and unreliable data and have proven suitable to the problem of integrating disparate types of data. Other aspects of managing different types of data can be addressed through intelligent agents.

Specific features of the decision support system that we are developing include:

- Dynamic Goal Reassessment
- Anytime Evaluation of Reliability and Value of Information
- Agent-Encapsulated Bayesian Models
- Local and Meta-level Agent Modeling
- Hierarchy of Collaborating Intelligent Agents
- Intelligent Routing to Reconfigure Interagent Information Flow

The overarching conceptual framework for the work in data fusion and battle management is Bayesian decision theory. The ability of commanders and warriors to perform risk assessment and make effective tactical decisions will be improved by a dynamic normative system that supports real-time integration and augmentation of disparate data.

### **FORWARD**

This project has been funded at the amount of \$410,399 with a starting date of 06/01/97 and an ending date of 06/29/00. Work did not begin on this project until 07/01/97 due to administration processing delays. The first year of development (07/01/97 – 06/30/98) resulted in a state-of-the-art survey of various sub-problems relevant to the problem domain. Furthermore the first year saw the completion of the initial design of an agent, an agent's model(s) and algorithms for

handling missing information and information reliability. In particular, the first year produced the following deliverables:

- General intelligent agent local model (Decision network)
- General intelligent agent meta-model (Decision network)
- Decision theoretic algorithm to evaluate information reliability
- Decision theoretic algorithm to assess the importance of missing information

In accord with the original proposal, a system is being developed using decision theoretic models (decision networks and Bayesian networks) for dealing with uncertainty and potentially unreliable data. Building on the analyses of sub-problems and the initial core design achieved during the first year of development, the second year (07/01/98 – 06/30/99) will round out the detailed design (and implementation) of an agent, its models and the mechanisms by which an agent interacts with its environment.

To that end, we are on track to have completed the development of the following deliverables by the end of the second year (06/30/99):

- Integrated agent including local and meta-models
- Algorithm for mapping agent hierarchy onto the existing network topology
- Evaluation of an agent in a stable environment
- Initial evaluation of an agent in a dynamic environment

## REPORT

### *Components Developed*

The overall design consists of a multiagent system capable of managing uncertainty and unreliability in a highly distributed and dynamic environment. The essential task of this system is data fusion for decision support. Therefore data fusion is the integration point of all other components. To support this task, each agent contains functionality for multiagent collaboration, dynamic goal reassessment, time-critical decision-making, handling of information reliability and probabilistic prediction. Each of these components is discussed in detail below. To evaluate these mechanisms, an evaluation will be conducted using a simulation.

### **Data Fusion**

Decision support requires timely information relevant to the task at hand.

By the end of the second year of work, the collaboration component will be fully integrated with the other components.

- Goal reassessor – more complete meta-model enabling better understanding of changes in goals and, therefore, in the desired effect on the organizational structure.
- Reliability handler – errors other than fail-stop faults can be detected and addressed with reorganizations to maximize expected utility.



- Value of information handler – domain-specific ranking of candidates for allocation into a role within the organization. Also adds domain-specific influence of message routing within the organization based on who values which pieces of information.
- Missing information handler – domain-specific initiated expansion of the organization's definition via dynamic addition of roles
- Temporal reasoner – input and output nodes relevant to any given time frame will be passed among agents via the collaboration component.

### **Multiagent Collaboration**

The mechanism to support multiagent collaboration is designed for a highly distributed, dynamic environment. The collaboration component must rationally respond to performance bottlenecks (unbalanced or improper assignment of resources given the task and the environment) and faults (fail-stop errors in agents, host systems and network connections). This is accomplished by introducing two mechanisms into the multiagent system designed according to design principles borrowed from human organizations and Organization Theory.

The first design principle is that of delegation (or decentralization) of decisions. The natural decomposition of the problem of situation assessment has led to a hierarchy of agents working to summarize relevant information to support users making decisions in response to the latest tactical military picture. When problems such as bottlenecks or faults occur, the handling of such problems should be as decentralized as possible without losing overall system consistency and coherency. The hierarchy provides a natural breakdown of the stages of data fusion. By embedding components that manage bottlenecks and faults at key points in the hierarchy, the hierarchy is both scalable and flexible. Decisions for reorganizations are decentralized just as decisions for data fusion. In particular, each non-leaf agent initiates and oversees reorganizations among that agent's subordinates in the hierarchy. The key to scalability is the flexibility of the distribution of work. If the workload and volatility of the environment are sufficiently low, many components of the overall system can be collapsed into relatively few agents. Conversely, components can be distributed and duplicated across multiple agents to decentralize processing or to add redundancy for fast recovery of faults.

The second design principle is that of coordination (or centralization) of the decision-makers. Again, the natural decomposition of the problem into a hierarchy provides a way to gather and distribute some context for localized decisions for reorganizations. Rational choices involve establishing the best organizational structure given the goals of the organization and the present situation. As the situation or goals change, the structure should change accordingly. It is this context for decisions (via the meta-model of an agent) together with decision-theoretic models that enable agents to quantify the benefits of possible reorganizations. The best structure is then chosen that maximizes the entire organization's expected utility. In particular, each agent considers the reorganization problem as a search in five-dimensional space that reduces the size of possible changes. This reduction is accomplished by casting each structural change in terms of increasing or decreasing the structure along one of five structural dimensions (stratification, diversification, duplication, preservation, and communication). Each decision-theoretic model

considers not only the local situation and goals, but also a summarization of the entire organization's situation and goals.

Scalability is demonstrated via a contest involving the embedded manager architecture and several existing approaches. In particular, there are four contestants:

1. completely centralized control
2. completely decentralized control
3. federation (hierarchy with fixed branching factor)
4. embedded manager architecture

A collection of various tasks and organization structures is considered. Each contestant is measured according to the time to task completion, overall resource usage and resource usage for reorganization control. The federations scale well within a particular range relevant to its branching factor. The embedded manager architecture must support a wider range due to the greater flexibility in its own structure as well as a lower overhead in the reorganization control.

Rationality is demonstrated by simulations that verify expected responses to induced loads and faults. The first battery of tests demonstrates the essential and obvious responses for a dynamic environment. A second battery of tests examines the accuracy of reorganizations by demanding a greater understanding of the overall organization's goals and situation.

### **Dynamic Goal Reassessment**

Goal reassessment involves plan generation and plan execution. This component will expand upon a myopic planning mechanism that carries out plans in uncertain environments using a greedy algorithm. There are two types of uncertainty with which to contend: informational and action-result. Informational uncertainty is caused by not knowing the exact state of the environment or not having complete confidence in the source of the information. Action-result uncertainty is from not knowing the exact results of an action to be taken. More complex plan generation includes conventional planning, for looking ahead more than one time slice and contingency planning which will involve planning to handle secondary possible results of actions.

To facilitate the use of Hugin decision networks in our agents, a Hugin-Java bridge was created. This is a translation of the Hugin API, written in C, to Java, the language we are using for our agents. Work has been completed in the areas of myopic planning, execution under certainty and execution under action-result uncertainty. Work is on schedule for completion in the areas of informational uncertainty, conventional planning and contingency planning.

### **Time Critical Decision Making and Reliability Handling**

An agent's optimal decisions depend not only on the given situation but also on delay caused by deliberation. Therefore, an intelligent agent making an optimal decision has to consider delay as well as the maximum utility principle. To support time critical decision making, we designed and implemented the following: (1) a time critical decision making engine; (2) a reliability checking module; (3) a value of information (VOI) computation module; (4) a missing information

module. Figure 1 gives an overview of how the time critical decision-making engine communicates with other modules to generate the optimal decisions. Each of these four parts are discussed in detail below:

- (1) Time critical decision-making: To support optimal time-critical decision, we use decision-networks that contain decision nodes and utility nodes as well as chance nodes. Since the cost of delay (utility loss by deferring optimal action) is dependent upon the amount of actual delay-time that the agent spends, we use time-functions to update the values of utility nodes. Delays for an agent normally take place when it is waiting for more information to improve its decision. Therefore it has to compute the net benefit for the information subtracted by the cost of delay before it asks and waits for information. The VOI (value of information) computation module for an agent has been implemented by using Maximal Expected Utility theory and a belief propagation method. An agent may select the proper input nodes according to the given time frame and VOI of the input nodes.
- (2) Time-functions (utility functions): Since these functions are domain dependent, there is no general method to build them. Two approaches to construct such functions are used. In the first approach, functions are extracted from the domain with an expert's help or a statistical approach is used to derive the function from raw data. The second approach requires a time frame based expanded model to simulate the function. The second method will be useful when we an expert's input is unavailable or there is not enough raw data available.

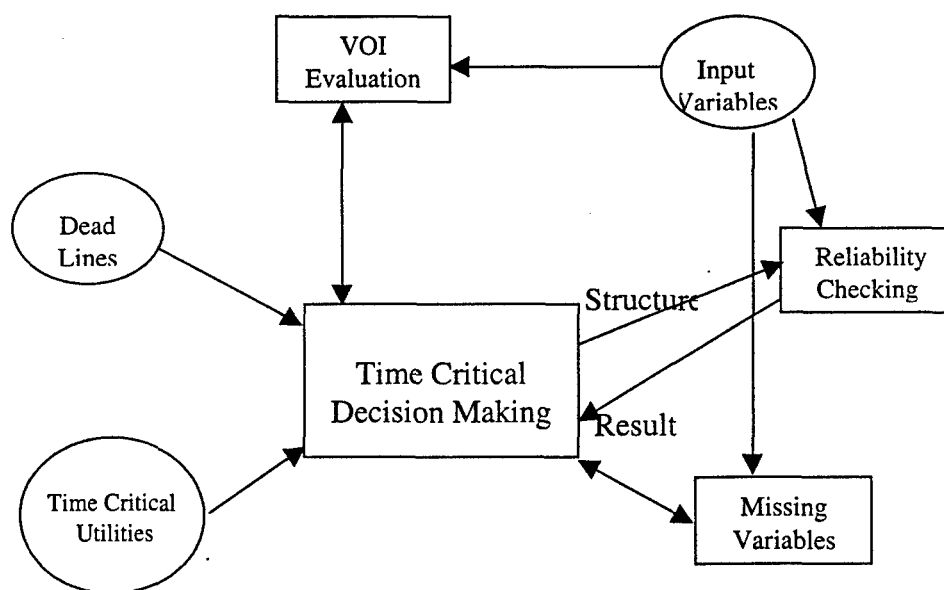


**Figure 1.**

- (3) Reliability Checking: Assurance of the data coming from other agents will be extremely important in a multiagent environment. Since sensor models normally generate output without an operator's supervision, the focus is on reliability checking in the sensor model. To check the reliability of a mode, the set of Markov blankets for each node is created and propagated. If the result values are different from what is expected, the sensor model has some problem. Since a probabilistic approach is used to determine the faulty nodes in the model, in the worst case, the checking algorithm will not be able to find the exact set of faulty nodes but instead will find a set of candidates.
- (4) Missing Information: When an agent waits for information from its neighbors, it must consider the delays that incur costs. Even though every input node (receiving information node) has its estimated delay, there are many possible causes of longer delay such as communication problems, death of agent or change of path. Therefore, when delay takes more time than what has been estimated, the agent must not query other agents for the information, but rather it should use prior probability values that are already in its local model. In a time critical decision making system, an agent asks for information and waits a certain amount of time. If this time elapses before a response is received, the agent considers the information to be missing and defaults to values from its own local model.

#### **A Probabilistic Approach to Prediction**

The Time-Frame Handler (TFH) provides a framework for predicting the evolution of different actions over time; combining temporal components, observations and decisions; and determining the changes in the internal state of the agent. Object-oriented techniques were used for designing TFH. The unified modeling language (UML) was used to describe the main steps of the design process. The main components of TFH are presented below with a brief description of how these components are interconnected with other components. The whole system is implemented using the Java language (JDK 1.7B). It makes use of Hugin 3.0 APIs for its Bayesian inference engine component and the Hugin-Java bridge.

The TFH provides a framework for defining temporal components and predicting the evolution of actions and observations. The main components of TFH are

- Defining temporal frames and sequence of temporal frames.
- Defining and accessing temporal schemes.
- Manipulating temporal components.
- Forecasting events based on temporal templates.

Object-oriented design (OOD) provides a strong modeling system process. It involves construction of models organized around software entities called objects by unifying data and the functions that operate on them. OOD was used to design the main components of TFH.

The TFH is described using three kinds of models:

- The component and class model, which describes the components, classes and the relationships among classes. This model captures *what* is changing or transforming in a system.
- The dynamic model, which describes the state of the objects, events and operations on the objects. This model shows *when* the changes occur.
- The functional model, which describes the processes in the system and the flow of data through those processes. This model describes *how* the changes occur.

### Component and Object Model

Component and object diagrams provide a graphical representation for modeling classes. The component diagram of TFH is presented in Figure 2. It exhibits the main packages related with TFH: Hugin/Java Bridge and the Hugin APIs.

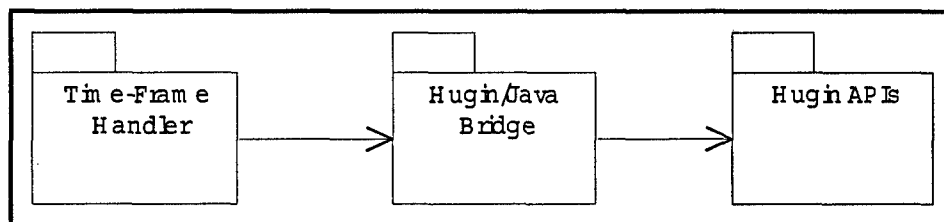


Figure 2. Package diagram of TFH.

### Dynamic Model

The dynamic model shows the states of each object in the class model and the operations that are performed as it receives events and changes state. It presents the sequence in which the processes are performed in the functional model. A dynamic model is depicted as a collection of *state diagrams*. A state diagram explains the behavior of a single class of objects.

### Functional Model

A functional or use case model shows the operations on the classes in the class model. It describes the functionality of the system. It includes the system's intended functions or use cases, its surroundings or actors, and relationships between uses cases and actors. In the particular case of TFH, use cases can be the following:

- Compute inter-frame connections.
- Propagate probabilities and move frames.
- Output temporal predictions.

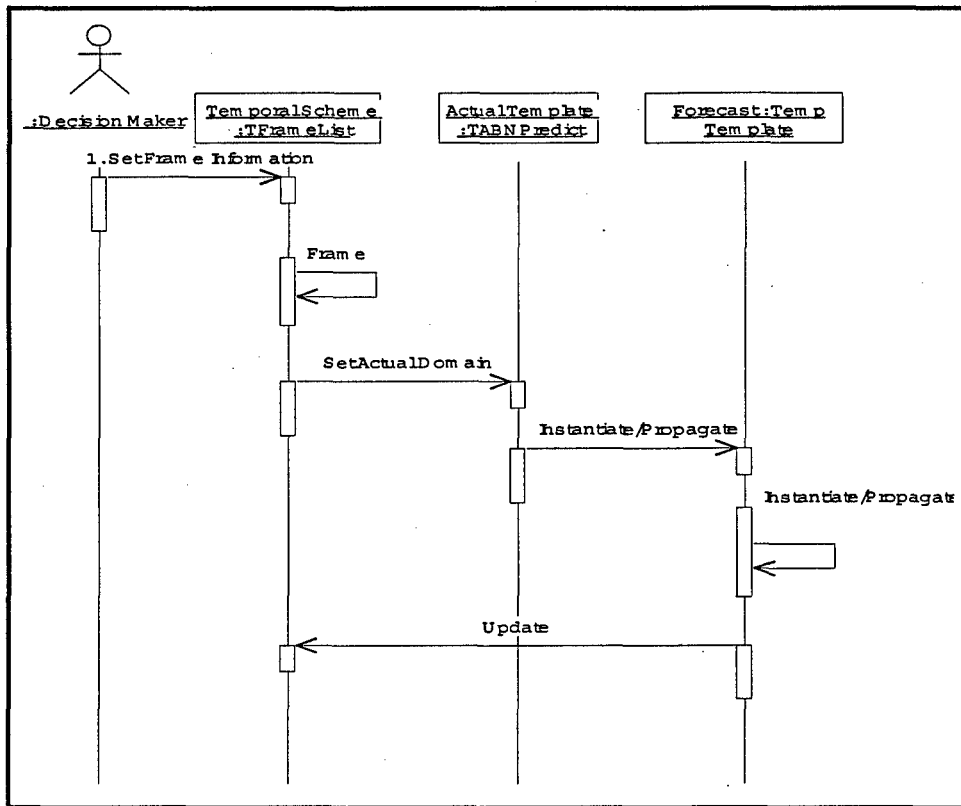


Figure 3. Sequence diagram for forecasting main events.

Sequence diagrams are graphical views of scenarios (instances of use cases) to show object interactions following a temporal sequence. It depicts the objects and classes involved in the scenario and the sequence of messages exchanged between the objects. Figure 3 shows a sequence diagram for forecasting main events. In this figure, a decision-maker is the actor that selects a temporal scheme by specifying the frame information and defining a sequence of temporal frames. A frame is selected as the actual Hugin domain for establishing the instantiation, probability propagation and prediction step. The next step corresponds to updating, propagating and being read for the following forecasting process.

### Testbed Simulation

A simulator has been designed using the high level architecture (HLA) design described by the DoD. This simulator will be used to run scenarios that our agent system will evaluate. The simulator will be able to distribute its load across multiple machines by decomposing the environment space into clusters. Sensors and emitters can then "communicate" using a radiosity model within cluster space.

### ***Summary of the Most Important Results***

The following deliverables have been designed and individually developed.

- Integrated agent including local and meta-models
- Algorithm for mapping agent hierarchy onto the existing network topology
- Evaluation of an agent in a stable environment
- Initial evaluation of an agent in a dynamic environment

We are on track to have completed the integration of these deliverables into a multiagent decision support system by the end of the second year (06/30/99).

### ***Publications and Technical Reports***

1. Barrientos, M.A., Juan E. Vargas. "A framework for the analysis of dynamic processes based on Bayesian networks and case-based reasoning". Expert systems with applications 15, pp. 287-294 (1998).
2. Presser, Clif, Dudley Girard, Wayne Smith, John Rose. "A Distributed Agent Environment System for Simulating a Naive Sensor/Emitter Model." Technical Report TR9901.
3. Presser, Clif, "Report on the use of HLA for DAG projects." Technical Report TR9902.
4. Presser, Clif, "Goal Management in Decision Networks." Technical Report TR9903.
5. Rose, John, Marco Valtorta, Miguel Barrientos, Young-Gyun Kim, Clif Presser, Wayne Smith, "Dynamic Decision Support for Command, Control, and Communication in the Context of Tactical Defense: An Architecture Specification." Technical Report TR9904.
6. Smith, Wayne A. "Rational Multiagent Organization and Reorganization." AAAI-98, p. 1182.
7. Smith, Wayne. "Intelligent Scalable Dynamic Distributed Systems: An Evaluation of an Architecture." Technical Report TR9905.
8. Smith, Wayne. "Using Organization Theory to Choose Rational Reorganizations in Multiagent Systems." Technical Report TR9906.
9. Smith, Wayne, Mark Bloemeke, Marco Valtorta. "Messages for Agent Encapsulated Bayesian Networks and How to Update Beliefs with Them." Technical Report TR9907.
10. Bloemeke, Mark, Wayne Smith. "Agent Encapsulated Bayesian Networks – A Solution to the Rumor Problem." Technical Report TR9908.

### ***Scientific Personnel***

Dr. John R. Rose  
Dr. Marco Valtorta  
Dr. Abhijit Sengupta  
Miguel Barrientos  
Young-Gyun Kim  
Clif Presser  
Wayne Smith

### ***List of Inventions***

#### **Distributed, Scalable Simulation Testbed**

A distributed environment that uses oct-tree decomposition of 3-space and radiosity models to simulate sensor-emitter behavior.

Reference: Presser, Clif, Dudley Girard, Wayne Smith, and John Rose. "A Distributed Agent Environment System for Simulating a Naive Sensor/Emitter Model." Accepted for presentation in the 31st Annual Summer Computer Simulation Conference (SCSC '99). Chicago, July 11-15, 1999.

#### **Scalable Multiagent Organizations**

The second innovation relevant to this component is an organization that is expected to be more scalable than existing approaches. The idea of a federation of services is commonly used in general distributed systems to achieve scalability. The architecture proposed for this grant uses the advantage of a federation, but minimizes the overhead of a separate hierarchy of service providers. Embedding the service providers within the basic organization of the system minimizes the overhead. Embedding has at least four advantages:

1. Message overhead reduced.
2. Branching factor constrained.
3. Processing overhead reduced.
4. Data recovery time reduced.

Reference: Wayne Smith. "Intelligent Scalable Dynamic Distributed Systems: An Evaluation of an Architecture." Submitted to SPECTS 1999 Conference.

#### **Rational Multiagent Reorganizations**

The second innovation is a rational reorganization handler that maps the organizational structure, the assigned task and the environment onto a five-dimensional search space. The problem of reorganization is reduced to choosing a direction to move within that space. The benefits of moving in any particular direction are quantified using decision theory. This enables an assessment manager component to choose the reorganization that maximizes its expected utility. Finally, the decision is made within a localized portion of the organization, but it takes into account a summarization of information across the entire organization. Thus, the value of certain changes is understood in context of what is valuable to the global optimum.

Reference: Wayne Smith. "Using Organization Theory to Choose Rational Reorganizations in Multiagent Systems." Submitted to Systems, Man Cybernetics 1999 Conference.

### **BIBLIOGRAPHY**

*See publications and technical reports.*



**University Research Initiative Program for Combat Readiness**  
**Annual Report 06/01/98-05/31/99**

PART 53-FORMS

53.301-298

<b>REPORT DOCUMENTATION PAGE</b>		Form Approved OMB No. 0704-0188	
Public reporting burden for this collection of information is estimated to average 1 hour per response, including the time for reviewing instructions, searching existing data sources, gathering and maintaining the data needed, and completing and reviewing the collection of information. Send comments regarding this burden estimate or any other aspect of this collection of information, including suggestions for reducing this burden, to Washington Headquarters Services, Directorate for Information Operations and Reports, 1215 Jefferson Davis Highway, Suite 1204, Arlington, VA 22202-4302, and to the Office of Management and Budget, Paperwork Reduction Project (0704-0188), Washington, DC 20503.			
1. AGENCY USE ONLY (Leave blank)	2. REPORT DATE  June 1, 1999	3. REPORT TYPE AND DATES COVERED  Annual	
4. TITLE AND SUBTITLE Dynamic Decision Support for Command, Control, and Communication in the Context of Tactical Defense		5. FUNDING NUMBERS Grant Number N00014-97-1-0806 PR Number 97PR06312-00 PO Code 353 Disbursing Code N68892 AGO Code N66020 Cage Code 4B489	
6. AUTHOR(S)  John R. Rose		8. PERFORMING ORGANIZATION REPORT NUMBER  N00014-97-1-0806-1	
7. PERFORMING ORGANIZATION NAME(S) AND ADDRESS(ES)  University of South Carolina		10. SPONSORING / MONITORING AGENCY REPORT NUMBER  ONR	
9. SPONSORING / MONITORING AGENCY NAME(S) AND ADDRESS(ES)  ONR		11. SUPPLEMENTARY NOTES  Prepared in coordination with University Research Initiative Program for Combat Readiness	
12a. DISTRIBUTION / AVAILABILITY STATEMENT  APPROVED FOR PUBLIC RELEASE		12b. DISTRIBUTION CODE	
13. ABSTRACT (Maximum 200 words) This second annual report describes progress made in the development of a system designed to provide dynamic decision support for command, control, and communication in the context of tactical defense. The document provides a synopsis of the key research areas that are being investigated to provide a robust solution to dynamic decision support in a failure-prone distributed environment. Current results and near-term results are summarized. Included are brief descriptions of the methods that have been developed. In addition, two publications and six technical reports that have come out of this research are listed.			
14. SUBJECT TERMS Command Control and Communication		15. NUMBER OF PAGES 11 pages including this page	
		16. PRICE CODE	
17. SECURITY CLASSIFICATION OF REPORT  UNCLASSIFIED	18. SECURITY CLASSIFICATION OF THIS PAGE  UNCLASSIFIED	19. SECURITY CLASSIFICATION OF ABSTRACT  UNCLASSIFIED	20. LIMITATION OF ABSTRACT  200 words

NSN 7540-01-280-5500

Standard Form 298 (Rev. 2-89)  
Prescribed by ANSI Std. Z39-18  
298-102

## **Survivable and Reconfigurable Optical/Wireless Tactical Networks**

Abhijit Sengupta

Department of Computer Science  
University of South Carolina  
Columbia, SC 29208

Tel: (803) 777-4635  
Fax: (803) 777-3767  
Email: gupta@cs.sc.edu

## **Section 3-2: Survivable and Reconfigurable Optical/Wireless Tactical Networks**

A. Sengupta

### **ABSTRACT**

High-speed real-time access and dissemination of intelligence and reconnaissance information are key components of combat readiness. To maximize the effectiveness and the timeliness of this information, it is necessary to have fast information flow through large bandwidth network infrastructure consisting of fixed and mobile networking elements. Optical networks by its capability of providing large bandwidth of the order of terabits are ideally suited for high-speed communication systems. In this project, solutions for networking problems are being developed to enhance the reliability and the capability of heterogeneous tactical networks for combat readiness. More specifically,

- Make wireless battlesite networks more reliable, adaptable, reconfigurable and secure
- Develop information processing and transmission systems for seamless integration of wireless battlesite network with large bandwidth command and control optical backbone network
- Enhance the reliability of on-board and on-shore optical networks through fault detection and fault management schemes
- Exploit multi-tiered network structures to filter local information for message overhead reduction
- Provide Quality of Service (QoS) guarantees for multimedia traffic in mobile networks that are subject to jamming.

### **FORWARD**

This project is funded for the amount of \$409,000 with a starting date of June 1, 1997 and an ending date of June 29, 2000. Due to administrative processing delays, research work on the project did not start until July 1, 1997.

In the original proposal, though modified versions of TCP and UDP protocols were suggested to be investigated for mobile component of the system, it was found that frequent mobility of users result in significant loss of TCP throughput causing poor network performance. Accordingly, a new protocol had been developed that allows an application to specify the expected reliability of packet delivery and provides feedback indicating if the desired goal was met, leaving any recovery, if needed, to the application.

In the original proposal, available simulation tools were proposed to be used to evaluate the invented protocols for routing in all-optical networks. It was found that these products are

significantly deficient in simulation of all-optical networks, particularly to capture the characteristics of WDM based all-optical networks. An attempt to modify one such product (COMNET III from CACI) to support the characteristics of all-optical networks resulted in unacceptably high cost. Accordingly, it was planned to build a suitable simulation package using an object-oriented model and using the language MODSIM III (a language specifically designed for writing simulation packages). The rationale for this software system was discussed with the project reviewers and received their approval. The software system will constitute a deliverable item in addition to the deliverables originally proposed in the proposal.

The research on the project is on track to have completed the following deliverables by the end of the second year (June 30, 1999):

- Automatic network configuration and management
- Extended mobile RTP for multihop wireless network
- Implementation of QoS guarantee for multimedia data
- Automatic network reconfiguration of all-optical networks
- Design of simulation system for evaluating all-optical networks (additional deliverable as mentioned above)

## REPORT

### *Statement of the problem*

During the second year of the project, the problems of design and analysis of efficient and reliable routing techniques in all-optical networks have been studied. Further, the quality of service (QoS) issue in a multihop wireless network was investigated needing efficient network management and data transfer protocol to support frequent change of network topology.

### **Logical Topology of All-optical Backbone**

The logical topology of an optical network is given by the routing protocol used by the nodes and determines the maximum achievable bandwidth in terms of the characteristics of network components. To exploit the high bandwidth capability of optical networks, an all-optical behavior of the backbone employing wavelength division multiplexing (WDM) technique is desirable. With a limited number of transmitters and receivers at a node, a multihop behavior is commonly employed resulting in a significant loss of maximum achievable throughput. Wavelength conversions in optical domain have been proposed to avoid a commonly used technique of opto-electronic conversion. With the non-availability of wavelength converters, such an approach is yet to meet practicality. Methodologies need to be developed to achieve the high network performance using available network components.

### **Distributed Routing Protocol**

Routing protocols for all-optical networks have commonly been defined as fixed lightpath allocation resulting in poor wavelength utilization. To improve performance, dynamic allocation has been considered as a centralized scheme where a central controller handles the allocation. Clearly the central controller might be a bottleneck in high traffic condition. A distributed

protocol needs to be designed to handle the network traffic and determine the routing lightpaths accordingly. Such an approach can also be readily adapted for handling fault situations.

#### Fault Management and Network Reconfiguration

Failures in network components can result in effects ranging from minor system performance degradation to catastrophic failures. Fault management in all-optical network has been little investigated. Most studies concentrated on single failure only. This was motivated by the fact that typical routing schemes are static by nature while the fault occurrences are inherently dynamic properties of the network. Moreover, with a static routing scheme, rerouting and reconfiguration need intervention of some central network controller, which might itself be a bottleneck in a high-speed network. Several problems need to be settled in this respect.

- In a network employing static routing scheme,
  - how the network controller gathers the information of faulty components?
  - how to use the existing setting of the routers to achieve a fault avoidance routing?
- In a network employing dynamic routing scheme,
  - what fault information are needed for a rerouting and reconfiguration scheme?
  - how to determine a fault avoiding routing plan?
- What is an acceptable performance degradation in a faulty situation?

Most of these questions are unanswered in the literature. A comprehensive investigation is needed to find answers and design efficient protocols for routing to achieve reliability.

#### QoS Issue for Multihop Wireless Traffic

It is expected that multihop wireless networks will be used handling multimedia data. With the node mobility, the network topology changes frequently and the multihop routing path needs to be determined in a dynamic manner. Moreover, for each of the intermediate hops, reservation of adequate bandwidth and allocation of enough buffers will be needed. Choice of intermediate nodes for data forwarding should consider issues like resource availability at intermediate nodes. Approaches designed for cellular networks can be adapted.

#### Network Configuration and Management

Most commonly used network management protocols performs poorly in a mobile wireless environment because of the frequent topology changes. Moreover, the security features contained in these protocols are inadequate for defense related mobile network activities. Widely used SNMP protocols for Internet might be appropriately modified to suit the need of wireless environment. Similar is the problem for data networks using TCP/IP protocols. Node mobility causes significant degradation in the performance of TCP throughput and UDP error rate. Efficient data transfer protocols need to be designed to handle node mobility and also to insure integration with TCP/IP protocols.

#### *Summary of the Most Important Results*

##### Logical Topology Design with wavelength translation

As mentioned earlier, wavelength translation improves network performance. Unfortunately, with wavelength translators not being available, the effect of wavelength translation has been achieved using available network components. This research group has investigated a new

scheme of virtual wavelength translation and it has been shown that such a scheme can achieve the network performance that would have been possible if every node had wavelength translation capability. Moreover, this scheme can attain the network performance without the need of wavelength translators in optical domain. The principle of the scheme can also be used to manage high link loading at hot-spots of the network, which limits the maximum load the network can handle. These results show that the need of wavelength translators in designing routing protocols can be avoided altogether. Results of this research have been presented in a paper presented at the 18<sup>th</sup> IEEE International Performance, Computing, and Communications Conference. A complete detail of the scheme is presented in the paper cited in [1]. Two other schemes of designing scalable logical topology were designed by this research group. The research papers detailing these techniques have been presented at international conferences and are cited in [4] and [5].

#### Distributed Routing Protocol

It is known that a static routing scheme has very low wavelength utilization. Moreover, a static routing scheme has the problem of scalability. When new nodes are added to the network, the static lightpath assignment problem has to be solved again and this makes the reconfiguration of the network for node addition a difficult chore. This research group presented distributed schemes of dynamic wavelength assignment for general networks. In this approach, the usable wavelength is determined in a distributed manner using each router with adequate memory and processing power. This approach improves the wavelength utilization by an order of magnitude. Moreover, by being a distributed scheme, there is no bottleneck controller as in some centralized scheme of dynamic routing. The principle of the distributed scheme can be extended simply to manage fault occurrence and corresponding reconfiguration of the network.

#### Fault Management and Network Reconfiguration

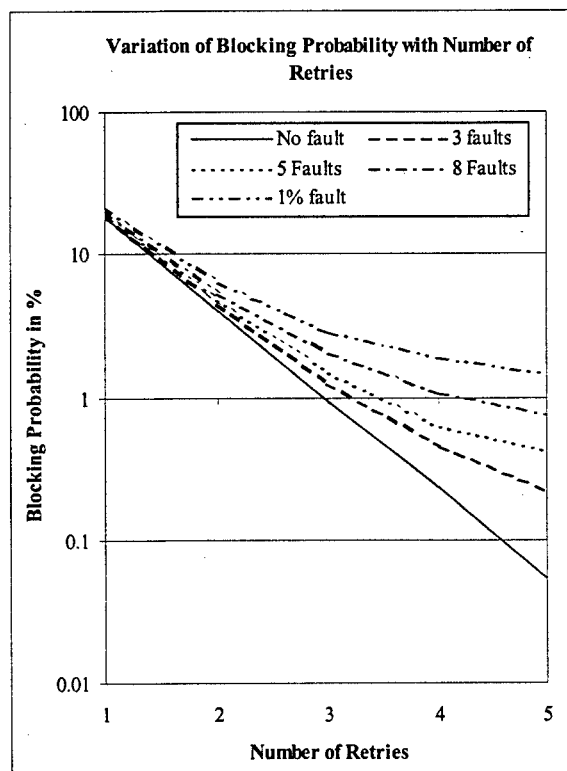
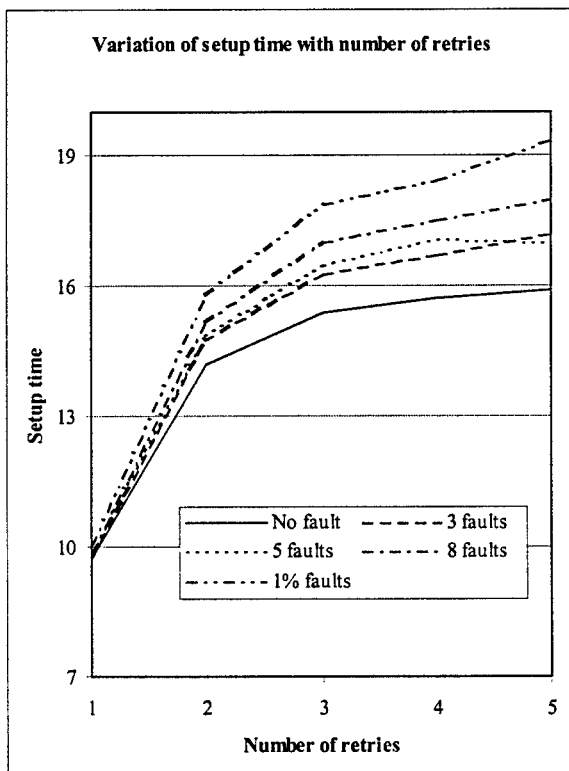
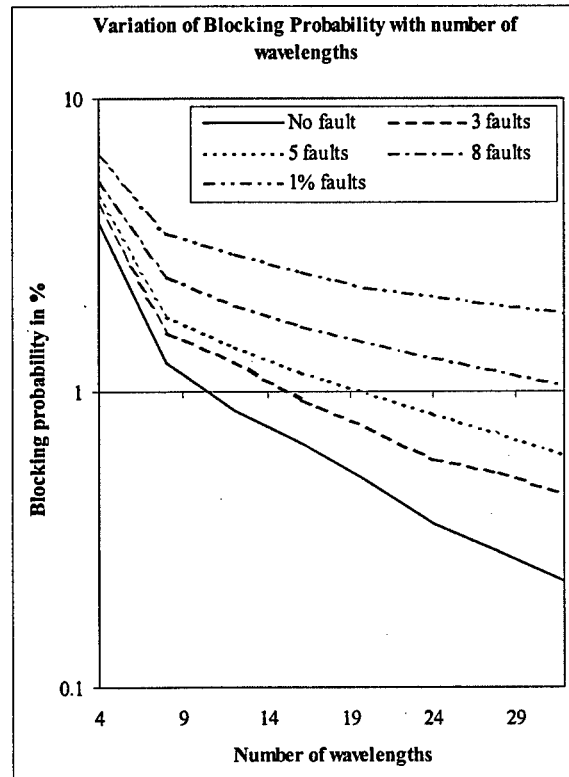
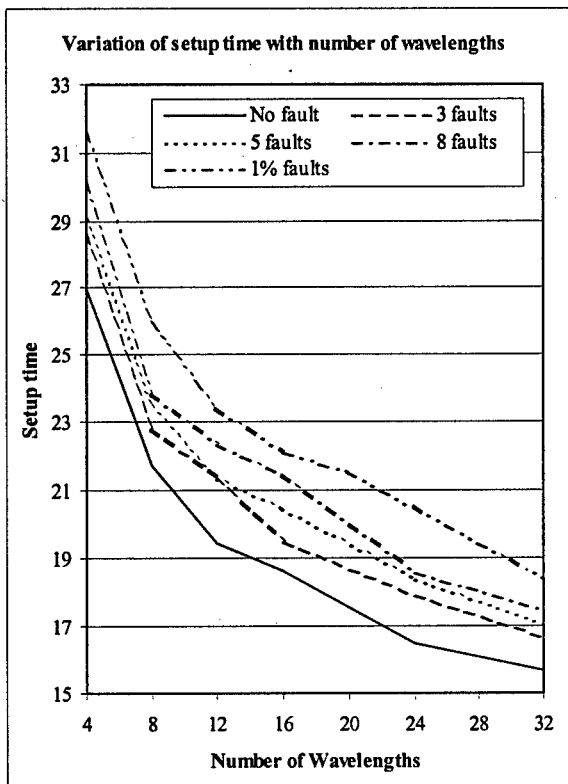
Fault management and network reconfigurations have been little addressed in the literature. Most of the works are based unrealistic assumption of single failure and can hardly be used for defense applications. The research results presented by this research group are the first known schemes to handle multiple failures and study the corresponding performance degradation. The papers cited in [2] and [6] consider the case when static routing is used in the network while the paper cited in [3] presents a distributed scheme of fault management and network reconfiguration when a dynamic routing scheme is used. It has been shown through simulation that the presented scheme can reconfigure the routing schemes to handle reasonably large number of failures with a very modest increase in setup time. In a large network with more than 1200 nodes, a blocking probability can be reduced to as low as .01% using only one tenth of the wavelengths needed for a static routing scheme. Some of the results of simulations are shown in the next page for illustrative purposes.

#### Simulation Tools for Evaluation of Optical Networks

As mentioned earlier, the performance of the proposed algorithms are being evaluated through discrete event simulation. As the existing simulation packages are found unsuitable to capture the characteristics of WDM based optical networks, a simulation package using an object oriented

model and using the language MODSIM III is being developed. The design of the system has been completed and about 50% of the implementation have been done. The system consists of several modules and these modules have been designed to implement known network components. For new network components, the simulation routine of these components can be plugged in the modules, which are kept open-ended.

- *Configuration Module*: module is used to define the physical topology of the network.
- *Routing Module*: module implements the routing algorithms.
- *Switching Modules*: module is used to define switching characteristics of switches.
- *Call Module*: module will be responsible for generation of traffic.
- *Fault Module*: module generates different classes of faults
- *Simulator Module*: module responsible for actual simulation and create resulting reports.





### **Network Configuration and Management**

A new network management protocol has been designed for multihop wireless networks. This protocol is based on a three level hierarchy and is based on SNMPv3. Each mobile node automatically configures itself into clusters, while each cluster is managed by a cluster-leader. An overall manager, on the other hand, manages all cluster-leaders. Moreover, a complete security model, based on the model used in the military (i.e., each node has a security clearance, each data type has a security level and data can be organized into compartments which nodes either have access to or not), have been implemented. Finally, an object-oriented interface is provided to manage the network.

### **Mobile Real-Time Protocol**

The conventional RTP (Real-Time Protocol) has been extended to support sessions where several nodes could be mobile and hence network topology is likely to change frequently. Such extension is completely integrated with conventional TCP/IP protocols by demonstration through actual networks. The extended RTP being implemented on top of our new data transfer protocol discussed above. The implementation is expected to be completed by the second year period.

### ***Publications and Technical Reports***

Publications from the research are listed in the bibliography.

### ***Participating Personnel***

Dr. Abhijit Sengupta

Dr. John R. Rose

Dr. Marco Valtorta

A. Ron Garber

B. P. Chandrasekhar

C. Jichen Qu.

### ***List of Inventions***

1. Distributed scheme of dynamic routing in WDM based all-optical network using wavelength translation through virtual translation scheme.
2. Algorithms for designing scalable logical topologies of optical networks.
3. Distributed scheme of fault management and network reconfiguration in all-optical networks employing dynamic routing scheme.
4. Fault management and network reconfiguration in all-optical networks employing static routing scheme.
5. A hierarchic design and implementation of network management protocol for wireless multihop network.
6. Design and implementation of extended RTP to support mobile nodes.

## BIBLIOGRAPHY

1. S. Bandyopadhyay, A. Jaekel and A. Sengupta, "On a virtual wavelength translation scheme for routing in all-optical networks", Proc. 18<sup>th</sup> IEEE International Performance, Computing, and Communications Conference (IPCCC'99), pp. 403-411, Phoenix/Scottsdale, Feb., 1999.
2. S. Bandyopadhyay and A. Sengupta, "On fault-tolerant routing in WDM based optical networks", Proc. PHOTONICS-98 International Conference on Fiber Optics and Photonics, pp. 931-935, New Delhi, December, 1998.
3. S. Bandyopadhyay, A. Sengupta and A. Jaekel, "Fault-tolerant routing scheme for all-optical networks", Proc. SPIE - All-Optical Networking: Architecture, Control and Management Issues, vol. 3231, pp. 420-431, Boston, November, 1998.
4. A. Jaekel, S. Bandyopadhyay and A. Sengupta, "A flexible architecture for multihop optical networks", IEEE International Conference on Computers, Communications and Networks (ICCCN98), pp. 472-478, Oct. 1998.
5. A. Jaekel, S. Bandyopadhyay and A. Sengupta, "A scalable logical topology for optical networks", Proc. 1998 International Conference on Parallel and Distributed Computing and Systems, pp. 83-88, Las Vegas, Oct., 1998.
6. A. Sengupta, "On fault-tolerant routing in iterated line digraph networks using optical interconnections", Proc. 36<sup>th</sup> Annual Allerton Conference, pp. 107-116, September, 1998.

**University Research Initiative Program for Combat Readiness**  
**Annual Report 06/01/98-05/31/99**

PART 53-FORMS

53.301-298

<b>REPORT DOCUMENTATION PAGE</b>		Form Approved OMB No. 0704-0188	
Public reporting burden for this collection of information is estimated to average 1 hour per response, including the time for reviewing instructions, searching existing data sources, gathering and maintaining the data needed, and completing and reviewing the collection of information. Send comments regarding this burden estimate or any other aspect of this collection of information, including suggestions for reducing this burden, to Washington Headquarters Services, Directorate for Information Operations and Reports, 1215 Jefferson Davis Highway, Suite 1204, Arlington, VA 22202-4302, and to the Office of Management and Budget, Paperwork Reduction Project (0704-0188), Washington, DC 20503.			
1. AGENCY USE ONLY (Leave blank)	2. REPORT DATE  June 1, 1999	3. REPORT TYPE AND DATES COVERED  Annual	
4. TITLE AND SUBTITLE  Survivable and Reconfigurable Optical/Wireless Tactical Networks		5. FUNDING NUMBERS  Grant Number N00014-97-1-0806 PR Number 97PR06312-00 PO Code 353 Disbursing Code N68892 AGO Code N66020 Cage Code 4B489	
6. AUTHOR(S)  PI: Abhijit Sengupta			
7. PERFORMING ORGANIZATION NAME(S) AND ADDRESS(ES) University of South Carolina		8. PERFORMING ORGANIZATION REPORT NUMBER  N00014-97-1-0806-2	
9. SPONSORING / MONITORING AGENCY NAME(S) AND ADDRESS(ES)  ONR		10. SPONSORING / MONITORING AGENCY REPORT NUMBER  ONR	
11. SUPPLEMENTARY NOTES  Prepared in coordination with University Research Initiative Program for Combat Readiness			
12a. DISTRIBUTION / AVAILABILITY STATEMENT  APPROVED FOR PUBLIC RELEASE		12b. DISTRIBUTION CODE	
13. ABSTRACT (Maximum 200 words)  This second annual report describes the progress made in the development of a reliable and reconfigurable large bandwidth networking system for command, control and communication in the context of combat readiness and tactical defense. The document presents an abridgment of the major research areas being investigated to achieve a reliable and large bandwidth network infrastructure in an environment subject to failures. Research results are summarized along with brief descriptions of corresponding invented techniques. These research results spanning six publications, presented in peer reviewed conferences, came out of this investigation and are listed as well			
14. SUBJECT TERMS  Chemical and Biological Defense, Target acquisition, Anti-Submarine, Combat Medicine, Biodeterioration and Command, Control and Communication		15. NUMBER OF PAGES	
		16. PRICE CODE	
17. SECURITY CLASSIFICATION OF REPORT  UNCLASSIFIED	18. SECURITY CLASSIFICATION OF THIS PAGE  UNCLASSIFIED	19. SECURITY CLASSIFICATION OF ABSTRACT  UNCLASSIFIED	20. LIMITATION OF ABSTRACT  200 Words

NSN 7540-01-280-5500

Standard Form 298 (Rev. 2-89)

Prescribed by ANSI Std. Z39-18  
298-102

## **Massively Parallel Optical Image Compression Using Optical Rank Annihilation**

M.L. Myrick

Department of Chemistry and Biochemistry  
University of South Carolina  
Columbia, SC 29208

Tel: (803) 777-6018  
Fax: (803) 777-9521  
Email: myrick@psc.sc.edu

## Section 3-3: Massively Parallel Optical Image Compression Using Optical Rank Annihilation

M.L. Myrick

### ABSTRACT

We have studied Lattice Boltzmann models for anisotropic diffusion of images, line processing systems, and Lattice Boltzmann simulation of flow by mean curvature. In addition we have modeled two distinct modes of operation for an optical data compression system using offset transmission masks. We are presently characterizing nonlinearities in transmission masks, modeling the behavior of mask fabrication errors and designing spectrum correction optics for non-uniformities of the optical transmission spectroscopy of the mask systems.

### FORWARD

This project was initially funded in June, 1997 at the level of \$400,000 over three years. In Y1 and early Y2, our project was severely hampered by the loss of three successive postdoctoral associates. We have recently been able to hire a postdoctoral associate (Dr. Lixia Zhang) who is committed to the project for the remainder of its term. Our recent milestones include:

- Using a computer simulation to successfully demonstrate how our data compression methodology will behave.
- Obtaining samples of microlens arrays for use in the project.
- modeling the optical transmission spectrum for film-based masks and designing corrective optics for them.

### REPORT

#### *Statement of the problem studied*

##### Background

As early as 1964, optical processing was proposed as a means of avoiding the costly/time-consuming task of computational transformations for real-time operations.<sup>1</sup> As a result of recent interest in optical transformations for the purpose of pattern recognition and image compression, a number of researchers have explored Fourier-optical approaches to achieving a usable transform.<sup>2-9</sup>

A host of problems plague Fourier-optical methods, not least of which are (a) complexity, (b) need for a laser, and (c) inflexibility. To date, no optical method for compressing images or interpreting them has found wide application, nor does it seem likely that any methods based on

current optical technologies will find real application in the next decade. In addition, Fourier decomposition of an image is not by any means the most compact representation of image data that is possible. Wavelet-based decompositions allow for a large number of different decompositions, allowing mathematical functions to be represented in a compact manner which yields quality approximations using very few free parameters. For example, wavelets are well suited for image compression and surface modeling, and for solving certain partial differential equations.

The Discrete Wavelet Transform (DWT) allows us to implement many multi-resolution schemes very efficiently with an  $O(N)$  transform. Still, there are many applications where this does not provide sufficient speed even when implemented on a state of the art computer. There are also many operations based on standard wavelets that lead to time-consuming operations. In addition, there are many wavelet type representations which cannot be implemented with an  $O(N)$  transform and there is a need to find more efficient methods for implementing these representations. Optical DWTs could potentially meet this need.

Funding for basic imaging spectroscopy work in our laboratory by the ARO has resulted in significant advances over the past three years in the conceptual processes underlying the recording of optical data. The fundamental new concept we have developed is that of optical rank annihilation (ORA). A succinct statement of ORA might be: *the number of channels used to record light should be no larger than the underlying degrees of freedom in the source*. For example, if an image can be adequately compressed by a factor of 10 with a DWT after a CCD has recorded it, then one way of thinking about this is to consider 90% of the original recording process by the CCD to be redundant, requiring a computational step to repair. The Third Law of Thermodynamics can be applied directly to this conventional process: if work is required to compress the data after it was recorded, then the recording step was non-optimized, or irreversible in the thermodynamic sense.

The question remains how to achieve the recording of optimized data. Fortunately, work already performed has provided the answer. Most of the work performed at USC has been in the area of spectroscopic compression, rather than spatial compression, but the concepts are the same. Conventional spectrometers function by converting a spectroscopic degree of freedom in wavelength space into a spatial degree of freedom. Consequently, the following discussion deals with our development of ORA for the prediction of physical and chemical properties of materials using optical spectroscopy.

The paradigm of today for predictive spectroscopy, just as for data compression, is computational: a complete spectrum is acquired and a computer performs the calculations of equation 1. ORA provides a more efficient alternative.

Mathematically, equation one is a recipe for a series of simple multiplication and addition steps. Such simple multiplications (e.g., multiplying an intensity measurement by 0.5) can be performed by a simple optical filtering method, as shown in Figure 4, whereby an optical filter with a transmission of 0.5 performs the "calculation" prior to the data being recorded. The

detector now records only half the original intensity of light, and its output, once digitized, reflects this value. Likewise, addition can be carried out all-optically: two beams of light both striking the same detector produce a detector output which sums the two individual beams (assuming incoherent light). ORA relies only on these simple forms of optical computing.

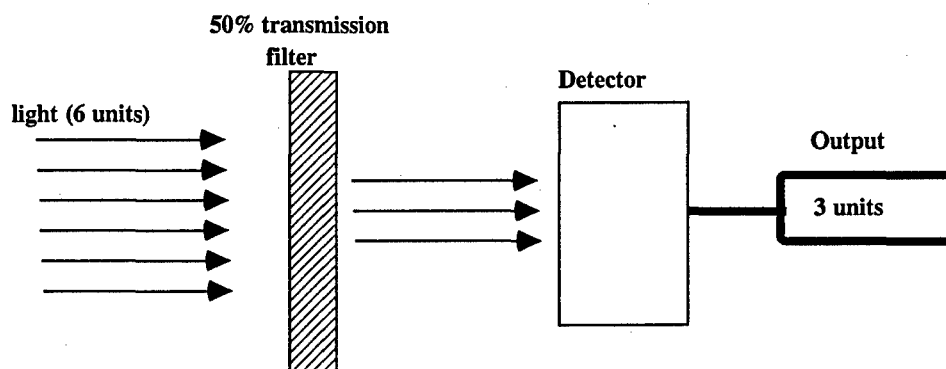


Figure 4. 6 units of light passes through a 50%-transmitting partially-transparent filter.

It is this reliance on simple forms of optical calculation that is the key to the successful implementation of ORA: no complex lasers or optics are necessary to produce a transformation. To achieve the full effect of equation 1 for the prediction of physical and chemical properties ORA, light passes through a partially-transparent filter whose transmission is dictated by the magnitude of the regression vector for each wavelength of light, designed by one of a number of methods (e.g., needle insertion method, modified inverse Fourier transform method, etc.). The analog output of a single detector is then proportional to the magnitude of the predicted quantity, and can be digitized or passed directly to a readout.

In the example above, the important information contained in an optical signal could be derived from the direct product of a single vector (the regression vector) with the main signal. For image compression, the number of basis vectors is much larger. A separate mask is required for each basis function. There are a handful of ways that this can be done, including fiber optic networks and networks of holograms. However, each of these methods suffers from the disadvantage of requiring a large technological step beyond current technology to be implemented.

On the other hand, graduated (as opposed to binary) spatial filtering provides a facile method for each calculation. Figure 2 shows the experimental setup for a single calculation via spatial filtering to obtain the magnitude of a particular 2-D basis function in an image using a graded mask. As this figure illustrates, a single transformation is not difficult.

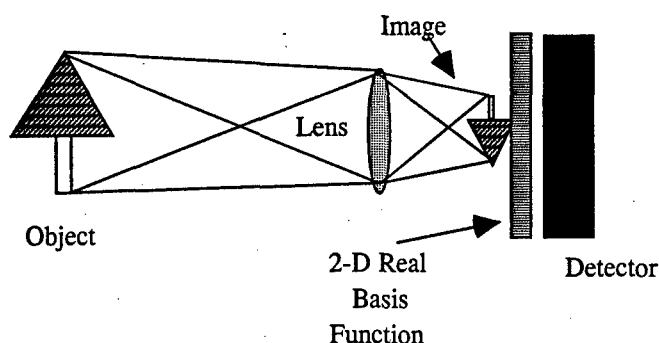


Figure 2 - Schematic of a simple transformation. The 2-D Real Basis Function is a graduated mask with a density proportional to the magnitude of the basis function at each location  $(x,y)$  in the image.

are then chemically removed. The remaining dots of resist are heated to melting, and surface tension causes the dots to form lens-like shapes. Reports indicate that lens arrays with lenses ranging from 5  $\mu\text{m}$  diameter to 5 mm diameter can be prepared, containing many thousands of lenses. The performance of these lenses is nearly diffraction limited, i.e., as good as a lens can be. Combining microlens arrays with photographically produced graded masks, and depositing the sandwich of these arrays and masks onto a CCD array can permit thousands of calculations simultaneously.

### ***Summary of the Most Important Results***

We have struggled with personnel problems through most of this program. A post-doc (Dr. Pramod Khulbe) was hired in the fall of 1997 primarily for this project, but he left in early 1998 after accepting a position elsewhere. Dr. Xuexin Fang was hired in the mid-spring of 1998 to replace Dr. Khulbe, but he invalidated his J-1 Visa, which terminated his employment in April, 1998. An additional scientist was brought into the project in the summer of 1998, but they could only work for 6 weeks. This series of losses was damaging, since the mathematics and concepts involved in the project require technical workers several weeks or even months to completely comprehend; none of the previous workers reached a level of complete competence before departing. Fortunately, after a nation-wide search, we have recently been able to hire Dr. Lixia Zhang (Ph.D. 1999, University of Texas at El Paso), whose husband is a graduate student in our Department of Chemistry and Biochemistry, which assures her continuation on the program. Dr. Zhang joined our group in late March, 1999.

Part of our project has involved understanding and correcting for the optical characteristics of mask materials. The linearity of camera films useful for this project is poor. Nevertheless, compared with color film, black-and-white film has the advantage of a relatively uniform film spectroscopy over a much wider spectral range. Our first few mask attempts were made using black-and-white negative films. However, the transmission characteristics of negative films are very poor – typically no better than 10-12% even for “unexposed” film. Reverse processing, done by the USC Instruction Services department, uses chemical agents that bleach silver halides out of the film and produce a more highly transmissive film base on which to work. As a result, we have decided to shift to film positives made by reversal processing from Kodak Tmax-100 negative film. Although this film is not one supported by our film printing system, its exposure

The problem arises when many thousands of transforms are necessary, as in image compression.

Microlens arrays offer the most versatile apparatus for actually achieving data compression via ORA. A microlens array can be made by a simple process known as resist melting. In resist melting, lithography is used to expose a resist in a particular pattern, the exposed portions of which



characteristics are similar enough to films that are support that it can be used almost equally well. Reversal processing is based around this film type, so it provides the best quality positive we can get.

We use MATLAB (the Mathworks, Natick, MA), augmented with image processing toolboxes, as the environment in which our masks are designed on computer. The exact relationship between the MATLAB image gray shade values and the optical transmittance of the resulting film mask positives measured with UV-vis spectroscopy is depicted in Figure 1. This experimental result is one that we have repeated many times in order to work out "bugs" in the processing by our instruction services department. These "bugs" consist of inconsistent processing that renders the quantitative relationship between gray scale value (GSV) and transmittance approximate at best, plus poor quality processing that renders the transmittance as a varying quantity across the face of a mask. In figure 1, GSV ranges over the 8 bits common to most imaging formats from 0 to 255, where 0 is assigned to black (nominally 0% transmittance) and 255 is assigned to white (nominally 100% transmittance). Figure 1 presents average transmittance over a wide spectral region, since film transmittance at different wavelengths is not exactly the same. A real UV-vis spectrum of a typical mask is displayed in figure 2.

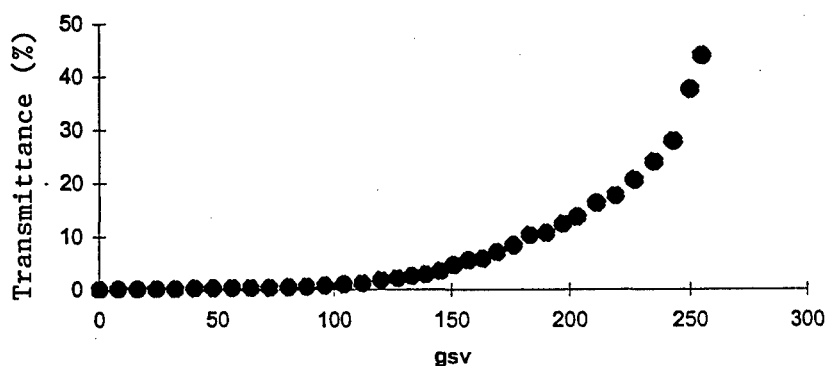


Figure 1: Relationship Between MATLAB GSV and Film Transmittance  
(Kodak TMAX 100)

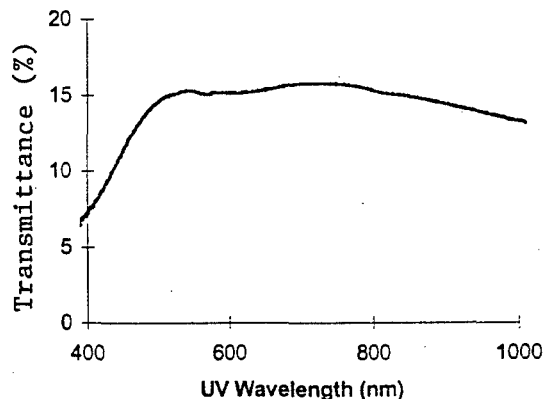


Figure 2: UV-vis Spectrum for a image mask

The Figure 1 result indicates a non-linear relation between GSV and transmittance. Since our project involves making precise transmittances, it is necessary to model the transformation of GSV into transmittance so that we can design masks with the "correct" values of GSV. We are presently using the following mathematical model to convert designed transmittance into GSV:

$$\text{GSV} = 260.78 - 155.24e^{(-0.07332t)} - 107.218e^{(-2.51147t)}$$

where  $t$  = transmittance

This model is very effective, as shown in Figure 3, where "o" represents the measured transmittances of the films and the "x" is from the model.

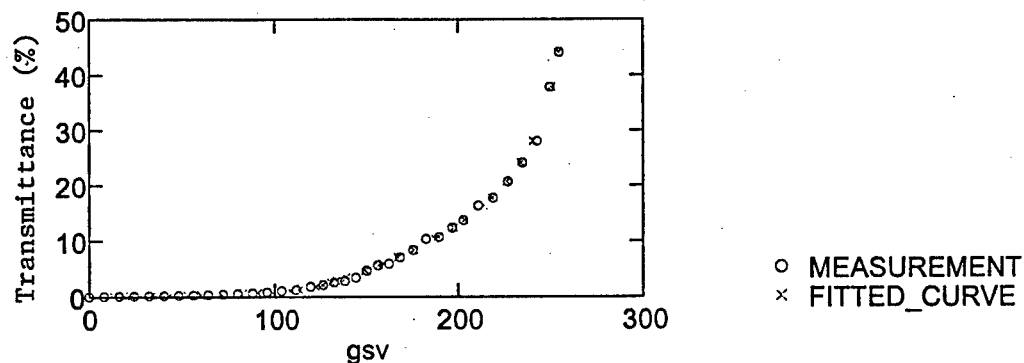


Figure 3: Curve Fitting Results

Figures 4 and 5 show how the model is used to design correct transmission masks. Figure 4 shows a cosine function to be used for a mask. It represents the actual transmission values desired. However, printed directly onto a film positive, the logarithmic response of the film latitude will distort the transmissions. In order to obtain the correct transmittances, the mask must be designed as shown in Figure 5. Printed directly onto a film positive, the Figure 5 GSVs will produce the desired cosine mask.



Figure 4: An Image of a 2x2 Cosine Pattern

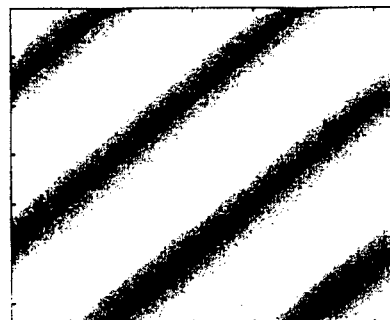


Figure 5: Image after Figure 3 is Calibrated  
Using the Mathematical Equation

We have found two main problems associated with film processing. The first is that the processing results for different brands of black-and-white films are very different. For example, Kodak Plus X Pan 125 films result in substantially lighter and more strongly non-linear models than Kodak TMAX 100 even they are processed at the same time and under the same conditions. The second problem is the reproducibility of the quality in the film processing. We are gradually improving the quality control of processing at USCIS using a new processing method that they have proposed and are now testing. With the quality control initially demonstrated in our first masks, transmission values varied by 5% or so from design.

Theoretically, if we make an image that is exactly the same as a mask cosine pattern, the summation of each point of the product of the image and the mask should be equal to the magnitude of the real part of the Fourier transform of the image. Other wise, the summation should be zero. We have demonstrated this in modeling. For example, in MATLAB, one cosine mask function can be designed to have two cycles in the x and y directions (Figure 4 is an example). This cosine function represents the real component of the 2X2 Fourier transform function. When an image is made using the same function, we can take a mathematical Fourier transform of the image, whose real component is illustrated in Figure 6.

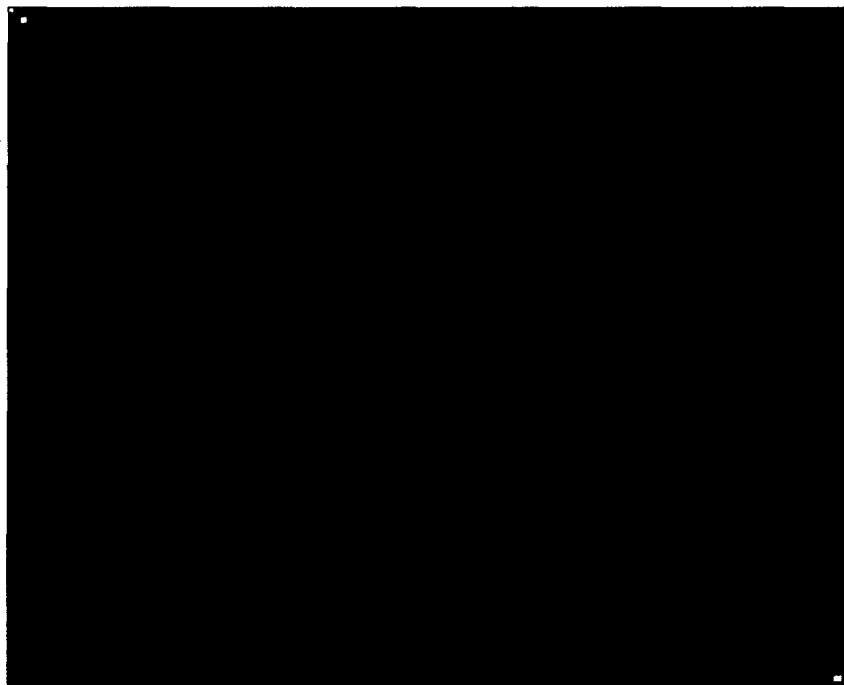


Figure 6: The Fourier Transform of the Cosine Pattern Image shown in figure 4.

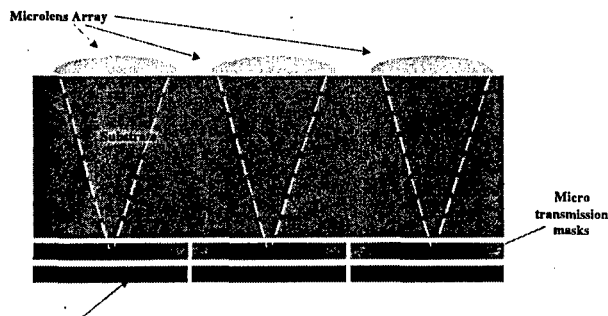


Figure 7 – design of compression elements

We find that this image should consist of only two Fourier components, the DC offset and the frequency  $(v_x, v_y) = (2, 2)$ . When we make masks that have this same set of components, we can exactly reproduce the effect of this transform. We are currently working on modeling the way mask production errors affect this result, while our Instructional Services department is effecting an improvement to their quality control for our experimental measurements.

The ultimate implementation of our project will work as shown in Figure 7. In this figure, the essential elements of an image compression system are shown. The uppermost elements are microlenses in a microlens array. A spacer substrate is then followed by the transmission masks, and then by CCD elements for detection.

Figure 8 below shows one of our sample microlens arrays. The left-hand image is of an array of 3600 lenses, each of which is  $250\text{ }\mu\text{m}$  in diameter, arranged in a  $60 \times 60$  square array. The individual lenses are not visible in this picture, but the right-hand image shows an atomic force microscope image of one of the lenses. This array was selected for testing because it is fabricated in a relatively inexpensive polyacrylic material, the lenses are approximately  $f/4$  and the substrate is 1 mm in thickness, which is the requisite thickness for a mask to be placed directly into the focal plane.

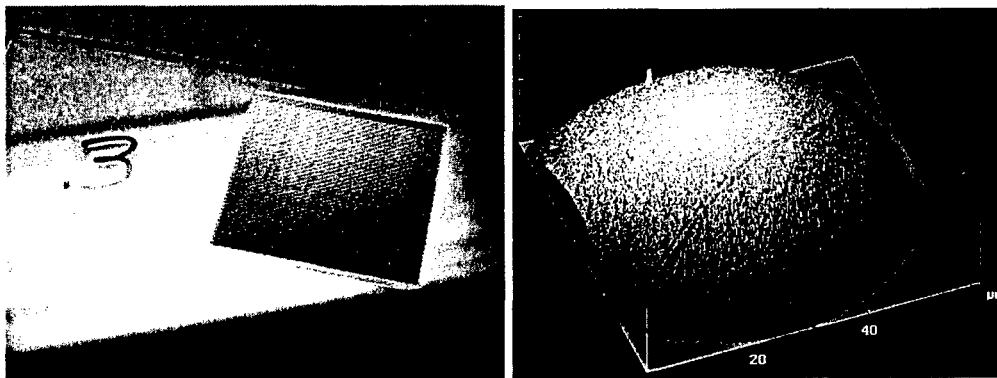


Figure 8 – microlens array for testing.

The Jawerth group has been continuing studies on lattice Boltzmann models for advanced image processing algorithms. The principal advantage of the lattice Boltzmann method over traditional

techniques for obtaining solutions of PDEs is that they are naturally well suited for fully parallel machines, resulting in very fast codes. Below we describe several different applications of the lattice Boltzmann model to sonar and image processing.

In recent years nonlinear diffusion has become a powerful tool for intra-region smoothing of images. The results of nonlinear diffusion can be used to obtain an enhanced image or as a precursor to higher-level processing such as image segmentation, shape description, and object detection and tracking. Based on our previously developed lattice Boltzmann models for anisotropic diffusion of images, we have developed a lattice Boltzmann model for image filtering by a reaction-diffusion equation. The advantage of using the reaction-diffusion equation is that it provides a nontrivial steady state, therefore eliminates the problem of choosing a stopping time in using the pure diffusion equation. We have tested our methods on various kinds of noisy images including infrared airborne radar images and sonar images. The results are promising.

Mean curvature motion appears in many natural and industrial problems in which sharp interfaces form and propagate. Notable examples include the growth of crystalline materials, the processing and enhancement of images, the propagation of flames, the evolution of ecological systems, and the waves of excitation that occur in heart and neural tissue. We have developed a lattice Boltzmann model for mean curvature motion. In our early approach we had focused on the level set formulation of mean curvature motion and had difficulty to obtain the proper collision operator in the lattice Boltzmann equation. We have overcome this difficulty by using the diffusion-generated motion by mean curvature approach.

#### ***Publications and Technical Reports***

There have been no reports of this work yet.

#### ***Participating Personnel***

In addition to the investigators, the following personnel have worked on this subproject.

Dr. Pramod Khulbe, post-doctoral associate with Dr. Myrick

Dr. Xuexin Fang, post-doctoral associate with Dr. Myrick

Jonathan Gibson, summer associate with Dr. Myrick

Dr. Lixia Zhang, post-doctoral associate with Dr. Myrick (beginning 20 March 1999).

Dr. Peng Lin, post-doctoral associate with Dr. Jawerth

#### **BIBLIOGRAPHY**

1. A. Vander Lugt "Signal Detection by Complex Spatial Filtering", *IEEE Trans. Informat. Theory* **10**(1964), 139-45.
2. F.T.S. Yu and Guowen Lu "Short-time Fourier transform and wavelet transform with Fourier-domain processing" *Appl. Opt.* **33**(1994), 5262-9.
3. H. John Caulfield and H.H. Szu "Parallel Discrete and Continuous Wavelet Transforms" *Opt. Eng.* **31**(1992), 1835-9.
4. H.H. Szu, B. Telfer and A. Lohmann "Causal Analytical Wavelet Transform" *Opt. Eng.* **31**(1992), 1825-9.

5. T.J. Burns, K.H. Fielding, S.K. Rogers, S.D. Pinski and D.W. Ruck "Optical Haar Wavelet Transform" *Opt. Eng.* **31**(1992), 1852-9.
6. Y. Sheng, D. Roberge and H.H. Szu "Optical Wavelet Transform" *Opt. Eng.* **31**(1992), 1840-5.
7. H. Szu, Y. Sheng and J. Chen "Wavelet Transform as a Bank of the Matched Filters" *Appl. Opt.* **31**(1992), 3267-77.
8. Y. Sheng, T. Lu, D. Roberge and H.J. Caulfield, "Optical  $N^4$  implementation of a two-dimensional wavelet transform", *Opt. Eng.* **31**(1992), 1859-1864.
9. B. Jawerth, Y. Liu, and W. Sweldens, "Signal Compression with Smooth Local Trigonometric Bases", *Opt. Eng.* **33**(1994), 2125-35.

**University Research Initiative Program for Combat Readiness**  
**Annual Report 06/01/98-05/31/99**

PART 53-FORMS

53.301-298

<b>REPORT DOCUMENTATION PAGE</b>		Form Approved OMB No. 0704-0188	
Public reporting burden for this collection of information is estimated to average 1 hour per response, including the time for reviewing instructions, searching existing data sources, gathering and maintaining the data needed, and completing and reviewing the collection of information. Send comments regarding this burden estimate or any other aspect of this collection of information, including suggestions for reducing this burden, to Washington Headquarters Services, Directorate for Information Operations and Reports, 1215 Jefferson Davis Highway, Suite 1204, Arlington, VA 22202-4302, and to the Office of Management and Budget, Paperwork Reduction Project (0704-0188), Washington, DC 20503.			
1. AGENCY USE ONLY (Leave blank)	2. REPORT DATE June 1, 1999	3. REPORT TYPE AND DATES COVERED Annual	
4. TITLE AND SUBTITLE Massively Parallel Optical Image Compression Using Optical Rank Annihilation		5. FUNDING NUMBERS Grant Number N00014-97-1-0806 PR Number 97PR06312-00	
6. AUTHOR(S) M.L. Myrick		PO Code 353 Disbursing Code N68892 AGO Code N66020 Cage Code 4B489	
7. PERFORMING ORGANIZATION NAME(S) AND ADDRESS(ES)  University of South Carolina		8. PERFORMING ORGANIZATION REPORT NUMBER  N00014-97-0806-1	
9. SPONSORING / MONITORING AGENCY NAME(S) AND ADDRESS(ES)  ONR		10. SPONSORING / MONITORING AGENCY REPORT NUMBER  ONR	
11. SUPPLEMENTARY NOTES Prepared in coordination with University Research Initiative Program for Combat Readiness			
12a. DISTRIBUTION / AVAILABILITY STATEMENT  APPROVED FOR PUBLIC RELEASE		12b. DISTRIBUTION CODE	
13. ABSTRACT (Maximum 200 words)  We have studied Lattice Boltzmann models for anisotropic diffusion of images, line processing systems, and Lattice Boltzmann simulation of flow by mean curvature. In addition we have modeled two distinct modes of operation for an optical data compression system using offset transmission masks. We are presently characterizing nonlinearities in transmission masks, modeling the behavior of mask fabrication errors and designing spectrum correction optics for non-uniformities of the optical transmission spectroscopy of the mask systems.			
14. SUBJECT TERMS Chemical and Biological Warfare, Target Acquisition, Snti-Submarine, Combat Medicine, Biodeterioration, Command Control and Communication		15. NUMBER OF PAGES 13	
		16. PRICE CODE	
17. SECURITY CLASSIFICATION OF REPORT  UNCLASSIFIED	18. SECURITY CLASSIFICATION OF THIS PAGE  UNCLASSIFIED	19. SECURITY CLASSIFICATION OF ABSTRACT  UNCLASSIFIED	20. LIMITATION OF ABSTRACT  200 WDS

NSN 7540-01-280-5500

Standard Form 298 (Rev. 2-89)

Prescribed by ANSI Std. Z39-18  
298-102

**Molecular Scale Electronic Arrays for the Design of Ultra-Dense and  
Ultra-Fast Computational Systems**

Jorge M. Seminario

Department of Chemistry and Biochemistry  
University of South Carolina  
Columbia, SC 29208

Tel: (803)777-9567  
Fax: (803)777-9521  
Email: [jorge@psc.sc.edu](mailto:jorge@psc.sc.edu)



## **Section 3-4: Molecular Scale Electronic Arrays for the Design of Ultra-Dense and Ultra-Fast Computational Systems**

Jorge M. Seminario

### **ABSTRACT**

In order to maintain technological superiority in command, control, and communications, new ultradense and ultrafast computation must continue to be developed. Conventional patterning techniques will not be suitable below the theoretical limit of 0.08  $\mu\text{m}$  resolution, a mere three-fold decrease in present commercial technology. We are therefore compelled to push the limits of densely-packed computational systems by striving for molecular-sized architectures. The study here describes (1) methods to model the electronic transport interactions in single molecules using density functional theory and quantum mechanics to provide a predictive tool for guiding the chemical syntheses of molecular wires and devices. This is the first computational approach of its kind to outline specific target molecules. And (2), outlined is a method to write arrays of single molecules on a surface and to address each one of those molecules. This will permit the addressing of molecular scale systems in the 10-50 Å regime. These studies will help to insure that the US maintains a technological edge in the race toward the ultimate technology in rapid computational systems for superiority of command and control issues. Excellent progress has already been achieved toward both of these proposed goals. The progress has been substantial in the development of molecular electronics that this work have triggered that the PI and one Co-PI get involved in a 2 million DARPA grant, involving researchers from top Universities, to develop a real molecular computer.

### **FORWARD**

Total award amount = \$293,000 for three years. No approach changes have been made from the original proposal. Three main achievements have been realized in the past two years:

- Method of computational analysis for molecular logic gates, alligator clips, and controllers.
- Writing of molecular patterns with an STM tip in a self-assembled monolayer.
- Ab initio design and analysis of molecule devices.

### **REPORT**

#### ***Statement of the problem***

A molecular CPU would be formed by small molecular units making the CPU itself a supramolecular unit. These units, which can be studied and designed exactly, will require parallel developments in synthetic efforts. New areas of technology would have to be created and developed like molecular control theory, molecular circuit theory, and molecular digital

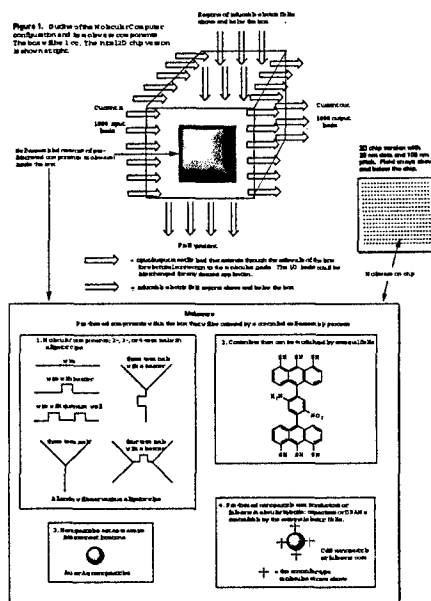
theory based on present ab initio theories of quantum chemistry. Given the tremendous computational power that can be obtained with molecular CPUs, a super high-level programming can be developed.

A molecular CPU would have to operate by electrostatic interactions rather than using electron currents as in present systems. Electron currents at the molecular level would generate energies per unit of area that are impossible to be dissipated before destroying the molecules. On the other hand, the use of the electrostatic potentials around the atoms of the molecules is a perfect choice because it can be controllable (as the current in a transistor) just by the rearrangement of a small amount of the charge density equivalent to a charge several orders of magnitude smaller than the charge of one electron, and also because these small changes in electrostatic potential are easily detected by the neighboring molecules.

Molecular-based systems can offer distinct advantages in uniformity and potential fabrication costs. If devices were to be based upon single molecules, using routine chemical syntheses, one could prepare  $6 \times 10^{23}$  (Avogadro's number) devices in a single reaction flask, hence, more devices than are presently in use by all the computational systems combined, world-wide [1,2]. However, the real problem facing synthetic chemists is how to arrange such a vast amount of molecular units. This process must be guided by precise laws of nature using quantum mechanics. Additionally, the properties of quantum systems can be used in a favorable manner at the molecular level. Thus molecular-based systems can offer distinct advantages in the density of structures that can be prepared and in their stability. Hence, molecular scale electronics would likely shift the software/hardware equilibrium in the direction of hardware, namely massively wired logic or CPU dominant. Molecular circuits offer the possibility of constructing large and fast CPUs with complicated functions. Using large molecular arrays, problems could be calculated within the CPU with minimal need for main or auxiliary memories. Wired-logic would supplant programmed-logic computing, thereby affording several additional orders of magnitude increase in performance [3-15].

### Configuration of the Molecular Computer

The Molecular Computer described here can not be justifiably compared with any known person-made system; the closest analogy is a truly biologically derived brain. Described is a top-down approach to the construction of a networked Molecular Computer (Figure 1): a  $1 \text{ cm}^3$  box that contains 1000 metallic inputs ( $m$ ), 1000 metallic outputs ( $n$ ), and 100 different  $l$  learning inputs. The box will contain an intelligently self-assembled array of  $\sim 10^{20}$  pre-designed active and passive components (moleware) which include molecular alligator clip-bearing 2-, 3-, and 4-terminal wires, resonant tunneling diodes, molecular switches, molecular controllers that can be modulated via the external peripheral fields, massive interconnect stations based on single



nanoparticles, DRAM components composed of molecular controller/nanoparticle or fullerene hybrids. Moreover, the Molecular Computer, once formed, can be further modified by new interconnect routes via electrochemically induced crosslinking of the nanoparticles or by "burning out" components through large induced fields, analogous to the operation of a field programmable gate array (FPGA). Arrays of Molecular Computers can be coupled using standard interconnect methods to form massive Molecular Computer Arrays or Mega-Molecular Computers. *The initial two-year target will be an "on-chip" 2D version possessing at least 100 inputs and 100 outputs.*

Figure 1 (above) outlines the configuration of the 3D Molecular Computer's box, I/O ports, and moleware components as well as the initial 2D "on-chip" version target for the two-year duration of this proposed study. The moleware (pre-assembled components made in beakers) will be added in a controlled successive manner to bridge the I/O connects within the box. The supporting matrix initially will be a 2D rectilinear grid fabricated on substrates (glass or silicon). A substrate-less approach is possible to attempt. Extension into a 3D scaffolding can be done by multilevel fabrication and MEMS-like release structures, but less fabrication-intensive and more "natural" approaches to creating a scaffolding will be explored.

The moleware would be added in a controlled sequence to:

- (5) Establish interconnection with the metallic leads and the organic systems.
- (6) Nanoparticle addition to provide the massive interconnection.
- (7) Three-terminal systems to provide the massive interconnection.
- (8) Controllers to provide the memory.

If high impedance is a problem, more nanoparticles will be added. The precise addition order and stoichiometry will be noted and recorded to insure reproducibility of the gross Computer features.

### **The Molecular Computer's Underpinning Capabilities**

16. Teachable. The system will be trainable, by forcing the correct  $n$  for a given  $F(X)$  (i.e.,  $F(X) = O(X, Y)$ ), by varying inputs  $Y$  until stability is achieved. One then sees if the system has "learned", by verifying  $F(X) = O(X, Y_0)$  in the absence of changes in  $Y_0$  and this can also be done during "growth".

17. Reconfigurable. The system could be reprogrammed by "burning out" specific functions as with a FPGA, or by successive re-training.

18. Possess logic. The truth table for the Molecular Computer would not be known *a priori*, however, it would be determinable once the Molecular Computer has been prepared, or "on the fly" as the self-assembly ensues.

19. Possess memory. Semiconductor nanoparticles such as CdS or CdSe coated with molecular controller elements, or  $C_{60}$  surrounded by controller elements, or even nanometer metallic particles sufficiently small to have sizeable Coulomb blockade, will be pre-formed and then permitted or induced to self-assemble as part of the neural network of the Molecular Computer. In an applied field, the controller will open thereby permitting semiconductive particle to store a charge, hence acting as a DRAM component.

20. Mega-Molecular Computers. The long-term goal of this study is to develop arrays of Molecular Computers that can be coupled using standard interconnect methods to form massive Molecular Computer Arrays, thereby rivaling any known synthetic system.

The molecular controllers are key element of the molecular computer since they serve as the switches and DRAMS the system. These are the systems that we have focused upon for our computational studies this year.

#### Controller molecules.

Top view of the molecular gate.

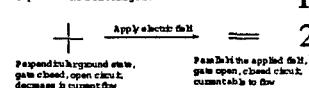


Fig. We are now proposing a system wherein the controller is modulated by an electric field component that is perpendicular to the current path (Figure 2). The molecular system will consist of

a molecule that has a three ring configuration (Figure 3). Simply a donor/acceptor component on adjacent rings in an applied field would stabilize the zwitterionic form making it more planar. In this manner, the starting orientation to the applied field is irrelevant, so no poling of the system during SAM formation would be needed. This would be specifically the molecular analog of a bipolar switch.

This uses a central molecular element that would reside in the "off" position, meaning negligible current would pass through the molecular chain, much like we demonstrated for a nanopore configuration previously [16]. Once the external field is applied, however, the central molecular element would switch to a more planar state with a smaller bandgap, and hence a more conductive configuration. One example of such a molecule is shown schematically (Figure 4).

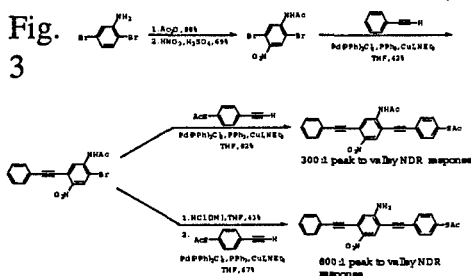
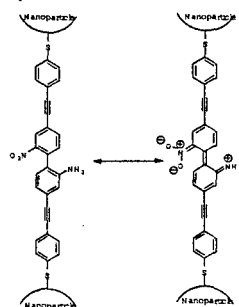


Fig. 4



The applied field makes the two a greater resonance contributor thus causing the dipole to orient in the applied field. Since the molecule is planar, there is a low bandgap and a low conductance. The other portion of the molecule is the non-polar and is shielded by the applied field, therefore, the molecule is shielded from the applied field. The entire structure is conductive and is shielded by the applied field.

The terms perpendicular and planar are not intended in the strict sense, only that the initial structure has a higher degree of twist than the latter structure. Hence, an electron transport will be more facile in the second structure. This is precisely what is needed for an electronic system. Note that DRAM systems generally are refreshed every  $10^{-3}$  seconds, therefore, even slight electronic retardations are sufficient. The initial biphenylnitroamine moiety would reside in a less planar state than the zwitterionic structure. However, a perpendicular electric field component should stabilize the zwitterionic state, thereby making that form a greater contributor to the resonance forms depicted. Once in that form, electronic passage should be

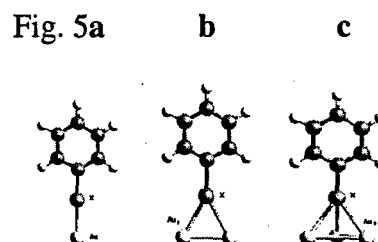
more facile. Even if there were multiple molecules attached to the nanoparticle, as long as one became more planar in the applied field, electrons could be trapped on the nanoparticle and the field then diminished for information storage.

Last year we described some molecular systems that could be turned from an on-state to an off-state based upon the temperature. Although a fine laboratory curiosity, switching based on temperature would never be a viable system. However, our newer generation molecules such as that shown in Figure 3 (with the syntheses) exhibit rapid switching based upon the applied field in a nanopore array.

### Summary of the Most Important Results

#### Alligator Clips

A density-functional-theory treatment has been carried out on chalcogenide- and isonitrile-containing molecular systems (alligator clips) involved at the interface of molecule/Au-electrode contacts. The B3PW91 functional was used with effective core potentials provided within the LANL2DZ potentials and basis set. An extended basis set,



HOMO, LUMO and gap energies for the three connections of the alligator clip with gold atoms using the B3PW91/LANL2DZ level of theory

X	HOMO (kcal/mol)			LUMO (kcal/mol)			$\Delta_{H-L}$ (kcal/mol)		
	a	b	c	a	b	c	ab	b	c
O	-122.8		nb <sup>a</sup>	-105.8			-17.0		
S	-124.4	-147.9	-142.7	-108.4	-97.1	-84.4	-16.0	-50.8	-58.3
	-121.3	-141.3	-143.7	-111.2	-94.4	-82.1	-10.2	-46.9	-60.9
Se									
	-117.4	-140.6	-139.2	-113.4	-99.0	-80.1	-4.0	-41.6	-59.1
Te									
	-97.8		nb <sup>a</sup>	-52.9			-44.8		
NC									

<sup>a</sup> No binding found.

LANL-E, was implemented by combining the valence, diffuse, and polarization basis from the 6-311++G\*\* for H, C, N, S, and Se and by adding polarization and diffuse functions for Te and Au atoms. Results, including bond lengths and angles, ionization potentials, electron affinities, and binding energies for small systems containing Au atoms, were obtained with acceptable precision for those systems with available experimental information. Predicted quantities are reported for other systems that, as yet, have no experimental information available. This study indicates that, of the alligator clips studied, S would provide the best embodiment followed closely by Se- and

Some of the optimized geometries of the lowest states and conformations of Pd<sub>4</sub> (distances in Å, and angles in degrees)

		Singlet	Triplet
		$d_1 =$	$d_1 =$
		2.907	2.761
		$d_2 =$	$d_2 =$
		2.920	2.613
		$d_1 =$	$d_1 =$
		2.871	2.579
		$d_2 =$	$d_2 =$
		2.871	2.582
		$d = 1.653$	$d =$
			2.449
		$d = 1.647$	$d =$
			2.705
		$d = 1.647$	$d =$
			2.705

Te-terminated molecules. This study also indicates that the precision obtained with calculations of first- and second-row atom-containing molecules can also be achieved with systems possessing heavier elements such as Au.

### Metallic Nanoprobes

Ab initio and density functional theory calculations were performed on small Pd clusters to assess their precise energy level characteristics. The ground states of Pd and Pd<sub>3</sub> are found to be singlets while Pd<sub>2</sub> and Pd<sub>4</sub> are triplets. Pd<sub>2</sub> is found to be a weak dimer with bond energy of 18 kcal/mol. The trimer is triangular and the tetramer of tetrahedral geometry. A non additive effect can be observed as the size of the cluster increases. Larger clusters are better bonded than smaller ones. The second lowest state of Pd<sub>4</sub> is a singlet of tetrahedral geometry. Modern DFT methods yield results of better quality than sophisticated standard ab initio methods, thereby providing an affordable avenue for the analysis of larger clusters and potential nanoelectronic probes.

### RTD

Recent experimental results obtained from a small group of molecules forming a nanopore show a behavior that can be considered as the one in a resonant tunneling diode (RTD). The curves shown in Figure 6 seem to indicate the existence of a peak at 3.5 V at about 4 K. The voltage of the peak seems to decrease monotonically as the temperature increases. An increase of temperature of about 150 K reduces the position of the peak from 2.3 to 1 V. The molecule in the

Fig. 6

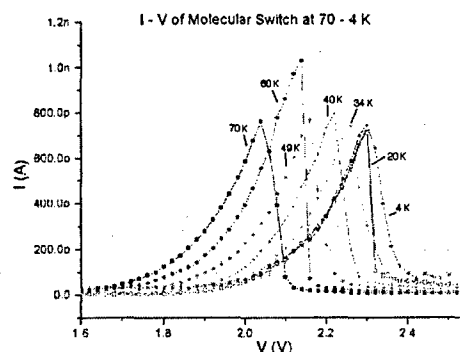


Fig. 7

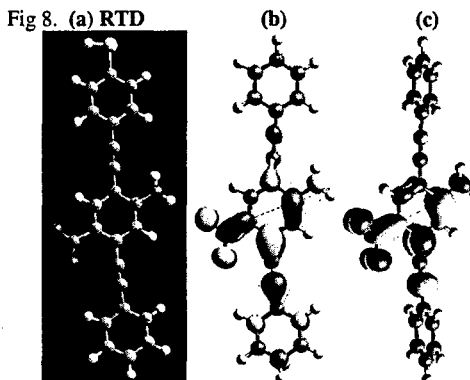


nanopore can be represented as indicated in Figure 7. In the nanopore, the molecules are self-assembled on the gold surface. Sulfur atoms served as alligator clips to the surface. The top terminal has been constructed by gold vapor deposition to the H terminated molecules. The exact nature of the bonding to the gold terminals is unknown, especially to the vapor deposited side. Our calculations clearly show that the sudden drop in current after a threshold voltage can not be explained by solely electronic arguments. Therefore this sudden drop may occur because the weakest bond in the chain is broken. The weakest bond is actually an Au-Au bond. If this very rapid on-to-off that occurs in the molecular RTDs within the nanopore were merely overlap of the LUMO with the Fermi of the gold, one would expect a far more gradual decline in the on-to-off rate. It may be that these very polar molecules, at a threshold voltage, actually pull away from the gold surface thereby breaking the connection. The bond strength of the gold thiolate (50 kcal/mol ~2 eV) is slightly more than the gold-gold energy on the surface (~40 kcal/mol). So likely a gold atom rips off with the sulfur atom. Reverse the bias and the molecules flip back down to make the connection with the surface. The energies of the bonds match perfectly with the field-induced energy as well as the recent energy seen by AFM studies in ripping a gold thiolate from a surface. This would make the ultimate switch by reversibly making and

breaking physical contact. The rate would be easily nano second since it would easily be on the order of bond vibrations, thus certainly within the time frame of the electrical ability to change the field. Although this is speculation at this point, the calculations are right on and it explains the non-gradual on-to-off process.

The value of the dipole moment is 5.54 D compared to water 2.08 D using B3PW91. And is almost perpendicular to the applied external field. The other alternative effect is the rotation of one of the rings with respect to the others. In this case decreasing further the transport of electrons through the molecule. It may happen that the rotation increases (decreasing the conductivity) due to an increase of the input voltage creating in this manner a region of negative differential resistance. This effect, the rotational, is certainly more important at elevated temperatures.

Figure 8.a, b, c (above) shows the molecule and the shape of the frontier orbital. As could be noticed the LUMO is less delocalized in the rotated configuration (Figure 8.c) corresponding to an increase in resistivity of the molecule. In general for the planar case the LUMO is somehow delocalized which is not the case of the tolane molecule where the conductance is much smaller. The RTD is one of the most important devices in electronics.



#### **Publications and Technical Reports**

- A. G. Zacarias, M. Castro, J. Tour, and J. M. Seminario, *Lowest Energy States of Pd Clusters Using Density Functional Theory and Standard ab Initio Methods. A Route to Understanding Metallic Nanoprobes*, J. Phys. Chem. (submitted).
- J. M. Seminario, A. G. Zacarias, and J. M. Tour, *Calculating Current/Voltage Characteristics in Molecular Junctions*, (submitted).
- J. M. Seminario and J. M. Tour, *Density Functional Theory for the Study of Single-Molecule Electronic Systems*, in *International Workshop on Electron Correlations and Material Properties, Proceedings*, edited by A. Gonis (Crete, Greece). In press.
- J. M. Seminario, *Ab Initio and DFT for the Strength of Classical Molecular Dynamics*, in *Molecular Dynamics: From Classical to Quantum Methods*, edited by P. B. Balbuena and J. M. Seminario (Elsevier, Amsterdam) In press.
- J. M. Seminario, A. G. Zacarias, and J. M. Tour, *Molecular Alligator Clips for Single Molecule Electronic. Studies of Group 16 and Isonitriles Interfaced with Au Contacts*, J. Am. Chem. Soc., **1999**, *121*, 411-416.
- J. M. Tour, M. Kosaki, and J. M. Seminario, *Molecular Scale Electronics: Approaches to Nanoscale Digital Computing*, J. Am. Chem. Soc., **1998**, *120*, 8486-8493.
- J. M. Seminario and J. M. Tour, *Ab Initio Methods for the Study of Molecular Systems for Nanometer Technology in Molecular Electronics: Science and Technology*, edited by A. Aviram and M. Ratner (Annals of the New York Academy of Sciences, New York 1998), pg. 68-94.

- J. M. Seminario, A. G. Zacarias, and J. M. Tour, *Theoretical Interpretation of Conductivity Measurements of a Thiotolane Sandwich. A Molecular Scale Electronic Controller*, *J. Am. Chem. Soc.*, **1998**, *120*, 3970-3974.
- D.-S. C. Kim, S. Huang, M. Huang, T. S. Barnard, R. D. Adams, J. M. Seminario, and J. M. Tour, *Revised Structures of N-Substituted Dibrominated Pyrrole Derivatives and their Polymeric Products. Termaleimide Models with Low Optical Bandgaps*, *J. Org. Chem.* **1998**, *63*, 2646-2655.

#### **Participating Scientific Personnel**

Jorge M. Seminario, Associate Professor for Research  
James M. Tour, Lipscomb Professor of Chemistry  
Angelica Garcia-Zacarias, Postdoctoral Research Associate  
Michael L. Myrick, Professor  
Michael Doescher, Graduate Student.

#### **List of Inventions**

- Use of electrostatic Potentials as Signals for atomistic and Molecular Scale Electronic Computation.
- Moleware and the Molecular Computer.

#### **BIBLIOGRAPHY**

1. M. S. Montemerlo, J. C. Love, G. J. Opiteck, D. Goldhaber-Gordon, and J. C. Ellenbogen, in *Technologies and Designs for Electronic Nanocomputers* (MITRE, McLean., Virginia, 1996).
2. J. M. Tour, *Conjugated Macromolecules of Precise length and Constitution: Organic Synthesis for the Construction of Nanoarchitectures*, *Chem. Rev.* **96**, 537-553 **1996**.
3. M. Bockrath, D. H. Cobden, P. L. McEuen, N. G. Chopra, A. Zettl, A. Thess, and R. E. Smalley, *Single-Electron Transport in Ropes of Carbon Nanotubes*, *Science* **275**, 1922-1925 **1997**.
4. A. Credi, V. Balzani, S. J. Langford, and J. F. Stoddart, *Logic Operations at the Molecular Level. An XOR Gate Based on a Molecular Machine*, *J. Am. Chem. Soc.* **119**, 2679-2681 **1997**.
5. M. Dorogi, J. Gomez, R. Osifchin, R. P. Andres, and R. Reifengerger, *Room-temperature Coulomb blockade from a Self-assembled Molecular Nanostructure*, *Phys. Rev. B* **52**, 9071-9077 **1995**.
6. R. P. Andres, T. Bein, M. Dorogi, S. Feng, J. I. Henderson, C. P. Kubiak, W. Mahoney, R. G. Osifchin, and R. Reifengerger, *"Coulomb Staircase" at Room Temperature in a Self-Assembled Molecular Nanostructure*, *Science* **272**, 1323-1325 **1996**.
7. A. J. Aviram, *Molecules for Memory, Logic, and Amplification*, *J. Am. Chem. Soc.* **110**, 5687-5692 **1988**.
8. C. Joachim, J. K. Gimzewski, R. R. Schlittler, and C. Chavy, *Electronic Transparency of a Single C<sub>60</sub> Molecule*, *Phys. Rev. Lett.* **74**, 2102-2105 **1995**.



9. A. Yazdani, D. M. Eigler, and N. D. Lang, *Off-Resonance Conduction Through Atomic Wires*, Science 272, 1921-1924 **1996**.
10. C. M. Fischer, M. Burghard, S. Roth, and K. v. Klitzing, *Microstructured Gold/Langmuir-Blodgett Film/Gold Tunneling Junctions*, Appl. Phys. Lett. 66, 3331-3333 **1995**.
11. H. Grabert, *Single Charge Tunneling: A Brief Introduction*, Z. Phys. B 85, 319-325 **1991**.
12. C. Joachim and J. K. Gimzewski, *Electromechanic amplifier single molecule*, Chem. Phys. Lett. 256, 353-357 **1997**.
13. V. Mujica, M. Kemp, and M. A. Ratner, *Electron Conduction in Molecular Wires. II. Application to Scanning Tunneling Microscopy*, J. Chem. Phys. 101, 6856-6864 **1994**.
14. S. J. Tans, M. H. Devoret, H. Dai, A. Thess, S. Richard E, L. J. Geerligs, and C. Dekker, *Individual Single-wall Carbon Nanotubes*, Nature 386, 474-477 **1997**.
15. R. M. Metzger, B. Chen, U. Höpfner, M. V. Lakshmikantham, D. Vuillaume, T. Kawai, X. Wu, H. Tachibana, T. V. Hughes, H. Sakurai, J. W. Baldwin, C. Hosch, M. P. Cava, L. Brehmer, and G. J. Ashwell, *Unimolecular Electrical Rectification in Hexadecylquinolinium Tricyanoquinodimethanide*, J. Am. Chem. Soc. 119, 10455-10466 **1997**.
16. J. M. Seminario, A. G. Zacarias, and J. M. Tour, *Theoretical Interpretation of Conductivity Measurements of Thiotolane Sandwich. A Molecular Scale Electronic Controller*, J. Am. Chem. Soc. In press **1998**.

University Research Initiative Program for Combat Readiness  
Annual Report 06/01/98-05/31/99

PART 53-FORMS

53.301-298

<b>REPORT DOCUMENTATION PAGE</b>			Form Approved OMB No. 0704-0188	
Public reporting burden for this collection of information is estimated to average 1 hour per response, including the time for reviewing instructions, searching existing data sources, gathering and maintaining the data needed, and completing and reviewing the collection of information. Send comments regarding this burden estimate or any other aspect of this collection of information, including suggestions for reducing this burden, to Washington Headquarters Services, Directorate for Information Operations and Reports, 1215 Jefferson Davis Highway, Suite 1204, Arlington, VA 22202-4302, and to the Office of Management and Budget, Paperwork Reduction Project (0704-0188), Washington, DC 20503.				
1. AGENCY USE ONLY (Leave blank)	2. REPORT DATE  June 1, 1999	3. REPORT TYPE AND DATES COVERED  "Annual"		
4. TITLE AND SUBTITLE  Molecular Scale Electronic Arrays for the Design of Ultra-Dense and Ultra- Fast Computational Systems		5. FUNDING NUMBERS Grant Number N00014-97-1-0806 PR Number 97PR06312-00 PO Code 353 Disbursing Code N68892 AGO Code N66020 Cage Code 4B489		
6. AUTHOR(S) Jorge M. Seminario				
7. PERFORMING ORGANIZATION NAME(S) AND ADDRESS(ES)  University of South Carolina		8. PERFORMING ORGANIZATION REPORT NUMBER  N00014-97-1-0806-2		
9. SPONSORING / MONITORING AGENCY NAME(S) AND ADDRESS(ES)  ONR		10. SPONSORING / MONITORING AGENCY REPORT NUMBER  ONR		
11. SUPPLEMENTARY NOTES  Prepared in coordination with University Research Initiative Program for Combat Readiness				
12a. DISTRIBUTION / AVAILABILITY STATEMENT APPROVED FOR PUBLIC RELEASE			12b. DISTRIBUTION CODE	
13. ABSTRACT (Maximum 200 words)  In order to maintain technological superiority in command, control, and communications, new ultradense and ultrafast computation must continue to be developed. Conventional patterning techniques will not be suitable below the theoretical limit of 0.08 $\mu$ m resolution, a mere three-fold decrease in present commercial technology. We are therefore compelled to push the limits of densely-packed computational systems by striving for molecular-sized architectures. The study here describes (1) methods to model the electronic transport interactions in single molecules using density functional theory and quantum mechanics to provide a predictive tool for guiding the chemical syntheses of molecular wires and devices. This is the first computational approach of its kind to outline specific target molecules. And (2), outlined is a method to write arrays of single molecules on a surface and to address each one of those molecules. This will permit the addressing of molecular scale systems in the 10-50 $\text{\AA}$ regime. These studies will help to insure that the US maintains a technological edge in the race toward the ultimate in rapid computational systems for superiority of command and control issues. Excellent progress has already been achieved toward both of these proposed goals.  The progress has been substantial in the development of molecular electronics that this work have triggered that the PI and one Co-PI get involved in a 2 million DARPA grant, involving researchers from top Universities, to develop a real molecular computer.				
14. SUBJECT TERMS Command Control and Communication, Molecular Scale Electronics		15. NUMBER OF PAGES		
		16. PRICE CODE		
17. SECURITY CLASSIFICATION OF REPORT  UNCLASSIFIED	18. SECURITY CLASSIFICATION OF THIS PAGE  UNCLASSIFIED	19. SECURITY CLASSIFICATION OF ABSTRACT  UNCLASSIFIED	20. LIMITATION OF ABSTRACT  200 words	

NSN 7540-01-280-5500

Standard Form 298 (Rev. 2-89)

Prescribed by ANSI Std. Z39-18  
298-102

**SECTION IV: COMBAT MEDICINE**

## **Laboratory for Genetic Diagnosis and Control of Mosquitoes**

Richard G. Vogt

Department of Biological Sciences  
University of South Carolina  
Columbia, SC 29208

Tel: (803) 777-8101  
Fax: (803) 777-4002  
Email: vogt@biol.sc.edu

## Section 4-1: Laboratory for Genetic Diagnosis and Control of Mosquitoes

Richard G. Vogt

### ABSTRACT

Mosquitoes are annoying and potentially dangerous pests for U.S. military personnel. Mosquito bites can be irritating, become infected, or be the source of debilitating diseases including malaria, yellow fever, dengue fever, and encephalitis. Although most of these pathogens can be controlled with medication and/or vaccination, the cost, side-effects, and development of insecticide-resistant strains diminishes the long-term viability of these treatments. Current chemical control methods of mosquitoes are of questionable compatibility with human health. A biorational integrated approach to control mosquitoes is desired. This project focuses on two specific aspects: (1) developing molecular genetic approaches for the rapid and efficient identification of species with high risk as pathogenic vectors; and (2) developing biorational control strategies for the repulsion of mosquitoes in areas of risk. Aim I is being met by identifying specific DNA sequences that discriminate South American *Anopheles* species. A virtual field kit will be designed employing these sequences for the rapid identification of potential disease vectors. Aim II is being met by identifying olfactory specific proteins (receptors) responsible for host odor recognition. These proteins will be used as probes to elucidate behaviorally specific olfactory pathways and as molecular tools for designing olfactory repellents and attractants.

### FORWARD

This project is funded at \$500,000 for the period 6-1-97 to 5-31-2000.

The project aim is two fold: (1) development of a genetically based diagnostic approach to distinguish and identify specific mosquito species in the field, and (2) identification of odor recognition molecules in mosquito responsible for host odor discrimination.

During the first 9 months of this project, we have successfully...

- ◆ developed a protocol for collecting approximately 40 South American *Anopheles* species, and initiated that collection process,
- ◆ developed a protocol and initial focus on four closely related *Anopheles* species, determining genetic criteria discriminating between these four species and two out group species,
- ◆ developed a protocol for identifying the full range of initial odor recognition proteins in one model species of mosquito.

## **REPORT**

### **Background**

Mosquitoes and the pathogens that they transmit are a worldwide problem for human health. Mosquitoes spread malaria, yellow fever, dengue fever, and several forms of encephalitis. Malaria alone infects nearly 500 million people worldwide and causes more than 2 million deaths annually (Goddard 1993). Malaria is endemic to much of the world, particularly developing nations where the U.S. military may be called on for regional conflict resolution and relief missions. Almost 99% of the malaria cases in the U.S. are due to infections acquired in other countries (Goddard 1993). Thus, the prevention and control of mosquito borne diseases is of particular concern to the U.S. military because significant numbers of U.S. military personnel may spend time where they will be exposed to mosquito species that transmit dangerous pathogens.

### **Vector Identification**

There are more than 3,000 species of mosquito. Nearly 10% of these species are dangerous vectors of human parasites; many vector species include differentiated populations (subspecies) with varying parasitic risks. Rapid identification of specific mosquito species and populations at a given location is critical for determining what parasites and diseases military personnel will be exposed to, and what control strategies should be employed.

Although almost all female mosquitoes must feed on blood to acquire adequate nutrition to lay eggs, relatively few mosquito species carry the most dangerous pathogens. The relative abundance of these mosquitoes varies over geographic regions and time, as does the frequency of pathogens within individuals of the species. Unnecessary vaccination and/or medication of personnel is expensive and not without potentially harmful side-effects. Thus, two questions must be addressed before deploying personnel: 1) are particular pathogens present (e.g., Armstrong et al. 1995), and 2) are species present which are known to transmit particular pathogens (e.g., Wilkerson et al. 1995). Answers to the first question are directly relevant for human health concerns. However, it is very difficult to be certain that pathogens are absent even when they are not detected. Answering the second question concentrates on the disease vectors. Disease vectors are generally much easier to detect. Additionally, detection of potential disease vectors is more likely to suggest precautions - even against pathogens that are not detected directly. Concentrating on disease vectors emphasizes planning for and solving a broader range of potential health problems than may be suggested by direct sampling for pathogens.

Mosquito species are traditionally identified by anatomical differences (i.e. by looking at physical characters such as wing shape or bar patterns on the abdomen); this can be extremely difficult. Some species can be anatomically identified only through laboratory rearing and examination of multiple life stages (e.g. larval, pupal, and adult). Some anatomical groups actually include several "cryptic" species that are not discernible by morphology.

Mosquito species and differentiated populations can be readily distinguished by using DNA analysis (Wilkerson et al., 1993). We will, therefore, characterize DNA differences within and among anatomical groups (taxa) to identify mosquito species. We will focus on mosquito species that are known malaria vectors. We will collect and use DNA sequence data from these species to develop easy to use assays for mosquito identification. Using these assays will allow military personnel to assess the presence of malaria vectors at previously uncharacterized sites without calling in mosquito experts or waiting for analysis of specimens shipped to experts.

### **Vector disruption.**

Mosquitoes are actively attracted to humans through a number of sensory modalities, including body odors, heat and CO<sub>2</sub> (Bowen 1991). While this is generalizable to all problematic mosquito species and varieties, detailed study has primarily focused on one species, *Aedes aegypti*, and work has been superficial at best. Sensory neurobiology has developed dramatically in the last 15 years, elucidating fundamental mechanisms at the molecular genetic level that allow insects to detect specific signals. Applying these developments to mosquito species will identify the specific molecular/neural pathways employed in host attraction, and thus define molecular targets against which to design biorational control strategies for the disruption of host attraction behavior.

While many species of mosquito act as vectors of pathogens dangerous to human health, only a subset of these species are attracted to humans (anthophilic); the remaining species are attracted to non-human hosts (zoophilic) for blood meals. The basis of these differential attractions is not understood, but likely involves host specific sensory cues. Of the sensory cues available, host specific body odors are the most likely discriminating signal.

The initial biomolecular step in odor recognition in insects, including mosquitoes, is the interaction between the odor molecule and an Odorant Binding Protein (OBP) (Vogt et al., 1991a,b; Vogt, 1995). Odorant Binding Proteins (OBPs) are small (15 kd), abundant water soluble proteins uniquely expressed in the olfactory sensilla of insect antenna. OBPs solubilize and transport volatile odorants in a specific manner, transporting odorants to neuronal receptor proteins. Each insect species has multiple OBP types which are differentially expressed among the functional classes of olfactory neurons/sensilla; the specific complement of OBPs have been proposed to reflect the odor types of interest to the insect (Vogt, 1995).

OBPs will be identified and sequenced from mosquito antennae. These proteins will provide molecular templates that can be used to design host odor attractants and repellents specifically tailored to the species of interest. Comparisons of OBP sequences among an assemblage of mosquito species will elucidate the olfactory genetic differences controlling anthophilic vs. zoophilic attractions and establishing genetic markers which can predict these attractions for untested mosquito species.

## **Outcome.**

An integrated approach to the control of mosquitoes will emerge from these studies. Rapid and efficient identification of problematic species or varieties will specify a need of action. The employment of targeted control strategies will maximize the impact on the mosquito vector while minimizing the impact on human health. Molecular systematic and molecular physiological approaches integrate to yield new and biorational approaches to mosquito management in areas of need.

## **EXPERIMENTAL APPROACH**

Mosquito species vector a multitude of pathogens of significant human health risk; however, only a subset of these species are actually attracted to human hosts. The purpose of this project is to develop new strategies for the prevention of mosquito vector borne disease in humans. To that end, two approaches are being taken.

- ◆ **Approach I.** A virtual diagnostic kit is being developed, based on genetic markers, for the rapid in-field identification of mosquito host species, to discriminate species which pose human health risks from species which do not.
- ◆ **Approach II.** The initial molecular step in host odor recognition by mosquitoes is being characterized by the identification and sequencing of mosquito Odorant Binding Proteins (OBP); it is expected that OBP phylogenies will discriminate anthophilic (human seeking) from zoophilic (non-human seeking) species of mosquito independent of mosquito-pathogen associations. Both approaches are being developed in model species, and will subsequently be expanded and tested on a larger set of South American *Anopheles* species.

## **SUMMARY OF RESULTS TO DATE**

This project has three components indicated below as (1) Species Collection (Dr. Richard Wilkerson), (2) Genetic Analysis (Drs. Joseph Quattro, Travis Glenn) and (3) Olfactory Analysis (Dr. Richard Vogt).

### **I. Species Collection.**

Dr. Richard Wilkerson (Department of Entomology, Walter Reed Army Institute of Research) is responsible for collecting and supplying complete assemblages of two South American *Anopheles* groups belong to two subgenera (*Nyssorhynchus* and *Kerteszia*). The complete species list is shown below (Table 1).

The rationale for these assemblages is that they represent complete genera of *Anopheles* species including members that are human relevant vectors of the malaria parasite. Not all of the species



seek out human hosts, and therefore they offer an opportunity to test the resolving power of Odorant Binding Proteins in the discrimination between anthophilic and zoophilic species.

Dr. Wilkerson's collection schedule is indicated below (Table 2). We stress that the bulk of our progress to date (and expenditures) has been associated with specimen acquisition. We have only recently begun steps II and III.

**TABLE 1.**

	<b>Subgenus <i>Nyssorhynchus</i></b>	40	<i>darlingi</i>
21	<i>albimanus</i>	41	<i>albitarsis</i> (4 cryptic sp.)
22	<i>oswaldoi</i>	42	<i>braziliensis</i>
23	<i>konderi</i>	43	<i>parvus</i>
24	<i>galvaei</i>	44	<i>nigritarsis</i>
25	<i>evansae</i>	45	<i>antunesi</i>
26	<i>aquasalis</i>	46	<i>lutzii</i>
27	<i>ininii</i>		<b>Subgenus <i>Kerteszia</i></b>
28	<i>anomolophylus</i>	1	<i>rollai</i>
29	<i>rangeli</i>	2	<i>gonzalezrinconesi</i>
30	<i>trinkae</i>	3	<i>auyantepuiensis</i>
31	<i>nuneztovari</i>	4	<i>neivai</i>
32	<i>strodei</i>	5	<i>pholidotus</i>
33	<i>rondoni</i>	6	<i>lepidotus</i>
34	<i>benarrochi</i>	7	<i>bambusicolus</i>
35	<i>triannulatus</i>	8	<i>homunculus</i>
36	<i>argyritaris</i>	9	<i>cruzii</i>
37	<i>sawyeri</i>	10	<i>bellator</i>
38	<i>lanei</i>	11	<i>laneanus</i>
39	<i>pictipennis</i>	12	<i>boliviensis</i>

**TABLE 2.**

	date	site	species	species
1	1/98	Sao Paulo	<i>cruzei</i> , <i>homunculus</i> , <i>bellator</i> , <i>laneanus</i> , <i>galvaoi</i>	9, 8, 10, 11, 24
2	4/98	Nicaragua.	<i>anomolophyllus</i> , <i>albimanus</i> , <i>strodei</i>	28, 21, 32
3	9/98	Venezuela	First 3 <i>Kerteszia</i> species	1, 2, 3
4	1998	Cochabamba , Bolivia	<i>boliviensis</i> , <i>lepidotus</i> -- Collection by Army collaborator in Rio de Janeiro	12, 6
5	1998	Meta, Colombia	<i>boliviensis</i> , <i>bambusicolus</i> -- Collection and rearing by Colombian collaborator	12, 7
6	1/99	Trinidad, Guyana	<i>neivai</i> , <i>homunculus</i> , <i>bellator</i> (return to US for rearings)	4, 8, 10
7	4/99	Para and Ceara, Brazil	<i>inini</i> , <i>sawyeri</i> (rearings by collaborators in Belem)	27, 37
8	9/99	Ecuador or Colombia	sp. nr. <i>triannulatus</i>	35
9	1/00	Peru, Iquitos and vic.	<i>benarrochi</i> .	34
10	7/00	Panama	<i>pholidotus</i> . I still need a Panamanian collaborator	5
11	12/00	Chile	<i>pictipennis</i> .	39

## II. Genetic Analysis

Dr. Joseph Quattro (Department of Biological Sciences, University of South Carolina) is responsible for developing the methodology of genetic identification of *Anopheles* species. We began the development of DNA-based diagnostic assays by focusing on a small, closely-related group of Brazilian malaria vectors. The group comprises four cryptic taxa within the *Anopheles albitarsis* species complex: *A. albitarsis*, *A. marajoara*, *A. deaneorum*, and *A. albitarsis* "sp. B". Two closely related congeners (*A. darlingi* and *A. braziliensis*) are included as outgroup taxa. RAPD DNA and to some degree morphological analyses are the only suitable techniques for discriminating species within the *albitarsis* complex, and these methods are cumbersome and not entirely suitable for a rapid, field-based assay.

Our initial work involved methods for the preservation of field samples for subsequent DNA isolation. Ethyl-alcohol (70%) has proven to be an inexpensive, yet effective means for transporting field material. Nucleic acid isolation from alcohol preserved samples has yielded DNA samples of sufficient quantity for Polymerase Chain Reaction (PCR) amplification. However, we have had considerable difficulties in PCR amplification from ethanol preserved mosquitoes. Several alternative DNA isolation protocols have been employed, and a commercially available extraction kit (QIAGEN tissue prep) has been most useful particularly for mitochondrial DNA loci. Unfortunately, nuclear gene amplifications are somewhat capricious, and we are working to circumvent these problems using column purification techniques.

We designed PCR amplification oligonucleotides that target sufficiently variable regions of the mitochondrial DNA (mtDNA) genome for phylogenetic/diagnostic assays. To date, several assays have been designed and employed including the mitochondrial 16S rRNA (*16S*), cytochrome-b (*Cytb*), and cytochrome-oxidase-II subunit (*COII*) loci.

Our initial amplifications with the *16S* and *Cytb* primer sets were promising in trials with members of the *albitarsis* species complex including outgroups. However, reactions within the group were often weak and in quantities insufficient for subsequent characterization. Attempts to optimize reaction performance including designing alternative, more specific primers, were not successful. We have subsequently adopted the *COII* locus for further assays for several reasons:

- ◆ The *COII* locus is suitable for studies at or below the species level in a variety of invertebrate taxa including Dipterans.
- ◆ A large number of Dipteran sequences are available in GenBank.
- ◆ Amplifications with this primer set have been very promising in trials with all members of the *albitarsis* species complex including outgroups.

We are continuing these assays by sequencing products from many individuals representing each species within the *albitarsis* species complex throughout their range. Phylogenetic analyses on these sequences suggest that species do not form monophyletic groups; the idea of discrete species within the *albitarsis* species group is not substantiated. This result was rather unexpected, and forced us to evaluate several hypotheses that explain sequence relatedness within the *albitarsis* species group:

- ◆ The four members of the *albitarsis* species group are 'good' species, but diverged a short time ago; lineage sorting has hindered our ability to define monophyletic groups.
- ◆ Hybridization has been a factor in the evolutionary history of the *albitarsis* species group.

To differentiate among these hypotheses, we have developed analyses that target a nuclear locus that is obviously unlinked to the mitochondrial *COII*. Specifically, we have developed PCR amplification primers that target an intron within the white locus (*wl*) of mosquitoes. Amplifications of *wl* from many individuals within the *albitarsis* species group have suggested that the intron has actually been lost in three of the cryptic species, while one species, *marajoara*, maintains the intron. Thus simple amplification and gel electrophoresis can distinguish *marajoara* from the other three species on the basis of product size. Our studies are still preliminary, but several *marajoara* individuals appear to harbor *COII* haplotypes similar to the other three species, but *wl* alleles that contain an intron and are obviously 'marajorara-like'. We are pursuing this system further, and are expanding to other species outside of the *albitarsis*

species group. However, it appears that hybridization within the *albitarsis* species group is the most likely scenario explaining the present molecular results.

### III. Olfactory Analysis

Dr. Richard Vogt (Department of Biological Sciences, University of South Carolina) is responsible for developing the olfactory analysis of mosquitoes. One common feature of the insect OBPs is their high abundance within antennal tissue. This suggests, and has been affirmed in several species, that large percentage of antennal mRNA is comprised of mRNAs encoding OBPs. For example, in the moth *Manduca sexta*, Robertson and colleagues sequenced about 400 randomly selected cDNAs, and found that 50 encoded the OBP Pheromone Binding Protein; among the residual cDNAs, 6 additional OBPs were identified, most multiple times. This suggested that such a brute force effort might be economical in identifying OBP sequences from mosquito antenna.

During the first year of this project, we established the parameters of mosquito rearing, tissue collection, and the successful isolation of mRNA from mosquito antennae. This initial effort enabled us to estimate the amount of mRNA was available from a single antenna, and thus the number of animals necessary to perform a representative characterization of antennal mRNAs through the construction and sequencing of an antennal cDNA library.

During the second year of this project, we constructed cDNA libraries from male and female antennae of the mosquito *Ae. aegypti*, sequenced 100 clones from each library, identified numerous mRNAs, and successfully identified one OBP from the male library. We refer to this protein as OBPRP*Ae.ae.* (Odorant binding protein related protein, *Aedes aegypti*).

To construct cDNA libraries from such small amounts of tissue as the antennae of mosquito, we isolated mRNA from 200 antennae removed from 100 individual animals, both for males and females. Previously, animals had been raised from eggs and flash frozen within 24 hours following adult emergence. To avoid mRNA degradation by ribonuclease activity, frozen animals were lyophilized to dryness directly from the frozen state, and antennae were subsequently removed at room temperature. Collected antennae were homogenized in a porcelain mortar and pestle under liquid nitrogen and in the presence of guanidinium isothiocyanate, and mRNA isolated following acid:phenol extraction, after Vogt et al., (1991b). mRNA was then converted to cDNA using oligo-dT and MMLV reverse transcriptase, and the cDNA was A-tailed using terminal transferase. The resulting cDNA was amplified by PCR using anchored oligo-dT primers, and the resulting PCR product ligated into pCRscript plasmid DNA (Stratagene), and transfected into bacteria. Colonies were preserved for sequencing in a matrix array on master agar plates. DNAs were purified for sequencing using QiaGen columns. One hundred randomly selected clones (colonies) from each of a male antennal library and female antennal library were sequenced in both directions using an ABI 370 automated DNA

sequencer. Sequences were analyzed by NCBI BLAST analysis, and aligned using either Sequencher contig program or ClustalX alignment program.

We have analyzed the sequences of 44 full length OBPs characterized from 17 insect species representing 5 insect orders (Lepidoptera, Diptera, Coleoptera, Hemiptera, Hymenoptera). This analysis revealed considerable divergence among the OBPs, but that the OBPs could be viewed as belong to several distinct groups. OBPRP*Ae.ae.* clearly associates with sequences previously identified from *Drosophila*; this is as would be expected for OBP related proteins from two diptera, as *Ae. aegypti* and *Drosophila* are. The surprising finding is from a comparison of the OBPRP*Ae.ae.* sequence with two reputed homologues of this family isolated from the African malaria mosquito *An. gambiae* (unpublished but kindly provided by Dr. Laurence Zwiebel, Vanderbilt University). BLAST analysis of the *An. gambiae* OBP related proteins indicates they are closely related to a family of OBPs to date only identified within Lepidoptera (moths); such a relationship between a dipteran OBP related protein and the moth "specific" group of OBPs is entirely inconsistent with relationships of the entire family of published OBP sequences.

The previously identified *An. gambiae* OBP related proteins may represent evidence of an interesting evolution of the insect OBPs. However, the inconsistency of phylogenetic relationship, and our identification of a dipteran-like OBP related protein (OBPRP*Ae.ae.*) raises the question of the validity of the identification of the *An. gambiae* proteins. At the very least, these differences point to a very interesting divergence of olfactory related genes among different genera of mosquitoes for whom humans represent very attractive hosts.

Our current work is focusing on the characterization of the OBPRP*Ae.ae.* protein, specifically confirming its tissue specific expression, the cellular location of its expression within the antenna, and its presence or absence within female antennae. We are further evaluating the sequence of the OBPRP*Ae.ae.* protein against its apparent near relatives, to determine the possibility of designing PCR primers that would be useful for identifying additional homologues within *Ae. aegypti* and its near relative *Ae. albopictus*. Armed with several sequences from related species, it will be more likely possible to elaborate this family among the mosquitoes.

#### **In summary:**

- ◆ We constructed male and female antennae of the yellow fever mosquito *Aedes aegypti*, and sequenced 100 clones from each library, establishing a small EST library for *Ae. aegypti* antennae;
- ◆ We successfully identified an Odorant Binding Protein related protein, OBPRP*Ae.ae.*, from male antennae;
- ◆ Sequence analysis of the OBPRP*Ae.ae.* protein indicates its relationship to other previously identified OBP related proteins is consistent with the dipteran subgroup, but NOT consistent with two putative OBP related proteins previously identified by another group from the

African malaria mosquito *An. gambiae*, either raising serious doubt about the validity of the *An. gambiae* OBP identifications, or indicating a very unusual evolution in the olfactory systems of these two genera of human host seeking mosquitoes;

- ◆ We are currently characterizing the OBPRP*Ae. ae.* protein, specifically with respect to its tissue location and sex specific patterns of expression, and its relationship to other OBP related proteins towards the identification of additional mosquito homologues.

### ***Participating Personnel***

<b>Name</b>	<b>Degree</b>	<b>Years on Project</b>
Richard G. Vogt	Ph.D. (1984)	1997-present
Joseph M. Quattro	Ph.D. (1991)	1997-present
Travis Glenn	Ph.D. (1997)	1997-present
Richard Wilkerson	Ph.D. (1995)	1997-present
Ge Xin	Ph.D. (1990)	1997-1998
Zhaoyuan Hou	M.S. (1996)	1997-1998
Matthew Rogers	Ph.D. Student	1998-present
Jonathan Bohbot	Ph.D. Student	1998-present
Robbie Young	BS (1998)	1998-present
Katherine Coykendall	BS (1998)	1998-present

### **BIBLIOGRAPHY**

1. Armstrong, P., D. Borovsky, R. E. Shope, C. D. Morris, C. J. Mitchell, N. Karabatsos, N. Komar, and A. Spielman. 1995. Sensitive and specific colorimetric dot assay to detect Eastern Equine Encephalomyelitis viral RNA in mosquitoes (Diptera: Culicidae) after polymerase chain reaction amplification. *J. Med. Entomol.* 32(1): 42-52.
2. Audtho M, Tassanakajon A, Boonsaeng V, Tpiankijagum S., and Panyim S (1995) Simple nonradioactive DNA hybridization method for identification of sibling species of *Anopheles dirus* (Diptera: Culicidae) complex. *Journal of Medical Entomology* 32(2): 107-111.
3. Bowen MF (1991) The sensory physiology of host-seeking behavior in mosquitoes. *Annual Review of Entomology* 36, 139-158.
4. Bruce-Chwatt LJ (1985) Mosquitoes, malaria, and war: Then and now. *J. R. Army Medical Corps* 131: 85-99.
5. Gershon D. (1995) DNA diagnostic tools for the 21st century: Technologies in DNA diagnostics on the horizon. *Nature Medicine* 1(2): 102-103.
6. Goddard J (1993) *Physian's guide to arthropods of medical importance*. CRC Press, Inc., Boca Raton, FL.

7. Pelosi P (1996) Perireceptor events in olfaction. *Journal of Neurobiology* 30, 3-19.
8. Robertson HM, Martos R, Sears C and Nardi JB (1998) Expressed sequence tags from the antennae of male *Manduca sexta* reveal diversity of odorant binding proteins. Unpublished sequences, Genbank Accession numbers AI172627, AI172639, AI187633, AI172726, AI172668, AI172734, AI187476.
9. Steinbrecht RA (1996) Are odorant-binding proteins involved in odorant discrimination? *Chemical Senses* 21, 719-727.
10. Vogt RG (1995) Molecular genetics of moth olfaction: a model for cellular identity and temporal assembly of the nervous system. In *Molecular Model Systems in the Lepidoptera*. MR Goldsmith, AS Wilkins Eds. Cambridge University Press, Cambridge, pp. 341-367.
11. Vogt RG, Riddiford LM (1981) Pheromone binding and inactivation by moth antennae. *Nature* 293, 161-163.
12. Vogt RG, Koehne AC, Dubnau JT, Prestwich GD. (1989) Expression of pheromone binding proteins during antennal development in the gypsy moth *Lymantria dispar*. *Journal of Neuroscience* 9, 3332-3346.
13. Vogt RG, Prestwich GD, Lerner MR (1991a) Odorant-Binding-Protein subfamilies associate with distinct classes of olfactory receptor neurons in insects. *Journal of Neurobiology* 22, 74-84.
14. Vogt RG, Rybczynski R, Cruz M, Lerner MR (1993) Ecdysteroid regulation of olfactory protein expression in the developing antenna of the tobacco hawk moth, *Manduca sexta*. *Journal of Neurobiology* 24, 581-597.
15. Vogt RG, Rybczynski R, Lerner MR. (1991b) Molecular cloning and sequencing of General-Odorant Binding Proteins GOBP1 and GOBP2 from the Tobacco Hawk Moth *Manduca sexta*: Comparisons with other insect OBPs and their signal peptides. *Journal of Neuroscience*. 11, 2972-2984.
16. Wilkerson RC, Parsons TJ, Albright DG, Klein TA, Braun MJ. (1993) Random amplified polymorphic DNA (RAPD) markers readily distinguish cryptic mosquito species (Diptera: Culicidae: *Anopheles*). *Insect Molecular Biology* 1, 205-211.
17. Wilkerson RC, Parsons TJ, Klein TA, Gaffigan TV, Bergo E, Consolim J. (1995) Diagnosis by random amplified polymorphic DNA polymerase chain reaction of four cryptic species related to *Anopheles (Nyssorhynchus) albitarsis* (Diptera: Culicidae) from Paraguay, Argentina, and Brazil. *Journal of Medical Entomology* 32, 697-704.

**University Research Initiative Program for Combat Readiness**  
**Annual Report 06/01/98-05/31/99**

PART 53-FORMS

53.301-298

<b>REPORT DOCUMENTATION PAGE</b>		Form Approved OMB No. 0704-0188	
Public reporting burden for this collection of information is estimated to average 1 hour per response, including the time for reviewing instructions, searching existing data sources, gathering and maintaining the data needed, and completing and reviewing the collection of information. Send comments regarding this burden estimate or any other aspect of this collection of information, including suggestions for reducing this burden, to Washington Headquarters Services, Directorate for Information Operations and Reports, 1215 Jefferson Davis Highway, Suite 1204, Arlington, VA 22202-4302, and to the Office of Management and Budget, Paperwork Reduction Project (0704-0188), Washington, DC 20503.			
1. AGENCY USE ONLY (Leave blank)	2. REPORT DATE June 1, 1998	3. REPORT TYPE AND DATES COVERED ANNUAL	
4. TITLE AND SUBTITLE  Laboratory for Genetic Diagnosis and Control of Mosquitoes		5. FUNDING NUMBERS Grant Number N00014-97-1-0806 PR Number 97PR06312-00 PO Code 353 Disbursing Code N68892 AGO Code N66020 Cage Code 4B489	
6. AUTHOR(S) Richard G. Vogt			
7. PERFORMING ORGANIZATION NAME(S) AND ADDRESS(ES) University of South Carolina, Columbia, SC 29208		8. PERFORMING ORGANIZATION REPORT NUMBER N00014-97-1-0806-1	
9. SPONSORING / MONITORING AGENCY NAME(S) AND ADDRESS(ES) ONR		10. SPONSORING / MONITORING AGENCY REPORT NUMBER ONR	
11. SUPPLEMENTARY NOTES Prepared in coordination with University Research Initiative Program for Combat Readiness			
12a. DISTRIBUTION / AVAILABILITY STATEMENT APPROVED FOR PUBLIC RELEASE		12b. DISTRIBUTION CODE	
13. ABSTRACT (Maximum 200 words) Mosquitoes are annoying and potentially dangerous pests for US military personnel. Mosquito bites can be irritating, become infected, or be the source of debilitating diseases including malaria, yellow fever, dengue fever, and encephalitis. Although most of these pathogens can be controlled with medication and/or vaccination, the cost, side-effects, and development of insecticide-resistant strains diminishes the long-term viability of these treatments. Current chemical control methods of mosquitoes are of questionable compatibility with human health. A biorational integrated approach to control mosquitoes is desired. This project focuses on two specific aspects: (1) developing molecular genetic approaches for the rapid and efficient identification of species with high risk as pathogenic vectors; and (2) developing biorational control strategies for the repulsion of mosquitoes in areas of risk. Aim I is being met by identifying specific DNA sequences that discriminate South American <i>Anopheles</i> species. A virtual field kit will be designed employing these sequences for the rapid identification of potential disease vectors. Aim II is being met by identifying olfactory specific proteins (receptors) responsible for host odor recognition. These proteins will be used as probes to elucidate behaviorally specific olfactory pathways and as molecular tools for designing olfactory repellents and attractants.			
14. SUBJECT TERMS Chemical and Biological Warfare, Target Acquisition, Anti-Submarine, Combat Medicine, Biodeterioration, and Command Control and Communication		15. NUMBER OF PAGES	
		16. PRICE CODE	
17. SECURITY CLASSIFICATION OF REPORT  UNCLASSIFIED	18. SECURITY CLASSIFICATION OF THIS PAGE  UNCLASSIFIED	19. SECURITY CLASSIFICATION OF ABSTRACT  UNCLASSIFIED	20. LIMITATION OF ABSTRACT  200 WORDS

NSN 7540-01-280-5500

Standard Form 298 (Rev. 2-89)

Prescribed by ANSI Std. Z39-18  
298-102



**Insure Access to Allogeneic Bone Marrow Transplantation  
for Correction of Marrow Failure and Hematologic Malignancies**

P. Jean Henslee-Downey, M.D.  
and  
Ivan N. Rich, Ph.D.

Center for Cancer Treatment and Research  
7 Richland Medical Park  
Columbia, SC 29036

Tel: (803) 434-3550  
Fax: (803) 434-3949  
Email: [jhd.sccc@rmh.edu](mailto:jhd.sccc@rmh.edu)

## **Section 4-2: Insure Access to Allogenic Bone Marrow Transplantation for Correction of Marrow Failure and Hematologic Malignancies**

P. Jean Henslee-Downey, M.D. and Ivan N. Rich, Ph.D.

### **ABSTRACT**

Although an identical sibling is the ideal donor for a recipient requiring a transplant of hematopoietic cells after being exposed to radioactive, chemical or biological weapons resulting in hematological aplasia or cancer, only 25% of the patients would have the opportunity of receiving a transplant from their HLA-identical sibling. On the other hand, more than 95% of the patients could receive a transplant if a partially mismatched related donor (PMRD) was used. However, this type of transplant must be accompanied not only by pre-transplant high dose chemotherapy and consolidation, but also by post-transplant immunosuppression geared to finding a balance between suppressing graft versus host disease and allowing for a graft versus leukemia effect to occur.

In the on-going work of this project, we have continued to focus efforts toward improving outcome following haploidentical transplantation. These areas include:

1. the identity of primitive hematopoietic stem cells that will provide the greatest long-term repopulating potential to ensure an established stable chimera.
2. the removal of lymphocyte subsets from the stem cell graft, which are responsible for the development of acute and chronic graft versus host disease.
3. the identity and production of lymphocyte subsets that could provide effective immune function against potentially fatal opportunistic infection during the extended lag in post-transplant immune reconstitution.
4. the identity and preparation of lymphocyte subsets that can provide an anti-leukemic effect when required.

Each of these areas has been further developed during the second year of funding and additional areas of work have been initiated.

### **FORWARD**

During the second year of a three year grant award work has progressed in all areas described in the original proposal and is highlighted by exploration of new methodology for understanding the cellular components and process of hematopoiesis and post-transplant immune function. In the arena of stem cell biology, two principal aspects have determined our research pathway during the second year of this grant-funding period. The first is the realization that although primitive hematopoietic stem cells for transplantation can be detected, their "stemness" and numbers cannot be maintained without an efficient and reproducible technique. The second aspect is the

recent discovery in our laboratory of a new method of killing leukemic cells that could provide a new adjunct anti-leukemic therapy.

In the translational and clinical arena, we have continued to provide access to transplant for the majority of patients who do not have a matched sibling donor nor can identify unrelated donors from either the National Marrow Donor Program (NMDP) or through cord blood banks. In the on-going clinical trial using haploidentical related donors, we have secured consistent engraftment across major-HLA barriers to allogeneic transplant. While the development of acute graft versus host disease remains satisfactorily controlled, limited to less than one-fourth of patients, the difficulty in achieving prompt and adequate immune reconstitution to avoid fatal infections remains a primary goal of newly developing viral specific immunotherapy. In addition, we have continued a focus on the development of immunotherapy that is targeted against the patients underlying disease in an effort to decrease treatment failure from relapse.

## **REPORT**

A description of work performed, in progress and planned is summarized below.

### **1. Primitive hematopoietic stem cells: their source, capability and expansion.**

In our report for the first year of this grant, we described the detection, using flow cytometry, of primitive hematopoietic stem cells present in the umbilical cord blood CD34<sup>+</sup> population. We used two new phenotypic markers to identify a minute population of CD34<sup>+</sup> cells in addition to the CD90 marker. These were AC133 and CD15. The use of the latter marker, which is primarily present on human monocytes and granulocytes, was chosen because it is the human homologue of the murine stage-specific embryonic antigen-1 (SSEA-1) present on the most primitive of stem cell populations detectable, namely the primordial germ cell (PGC). Although CD34<sup>+</sup>/AC133<sup>+</sup>/CD15<sup>+</sup> could also be detected in human bone marrow, the volumes required from both this and umbilical cord blood to perform reproducible and statistically significant experiments were impossible to obtain. In addition, in vitro expansion experiments using stationary cultures performed in tissue culture flasks, could not provide a reproducible and efficient expansion of virtually any CD34<sup>+</sup> subpopulation. It should also be mentioned that although we have taken possession, in late 1998, of a new high-speed cell sorter (MoFlo) from Cytomation Inc. (Ft. Collins, Colorado), we have not yet been able to perform multiparameter cell sorting. As a result, we are now in the process of taking a new direction, which we hope will enable us to insure usefulness and availability of primitive stem cell populations for future transplantation purposes.

This new direction uses perfusion culture techniques to better simulate the physio-chemical and cellular microenvironment necessary to maintain and expand hematopoietic stem cell subpopulations. Extensive preliminary studies by one of us (INR) using simple perfusion culture chambers could demonstrate the maintenance and expansion of primitive murine stem cell populations. This was performed as follows. Cells were inoculated into 60 mm diameter perfusion chambers fitted with a single inlet and outlet. The cells were cultured on hydrophobic

(non-adherent) or hydrophilic (adherent) Teflon foils. Since Teflon foils are gas-permeable, the gas mixture used for incubation, which contained 5% CO<sub>2</sub> and 5% N<sub>2</sub>, i.e. low oxygen tension, could come into direct contact with the cells on the growth surface. Low oxygen tension facilitates decreased free radical formation and therefore higher plating efficiencies. Sufficient medium containing serum and growth factors was prepared in a reservoir, which was kept in a refrigerator adjacent to the incubator. A Teflon tube connected the reservoir to the chamber and another tube allowed the medium efflux to be collected into another reservoir. The medium was pumped into the perfusion chamber at a rate of 10ml/day for a total of 7-10 days. In this way, the cells always received a supply of fresh nutrients. During the incubation period, the cells built a microenvironment which allowed hematopoiesis to be sustained. This principal of stem cell culture will be used in both an experimental and preparative manner. For experimental studies, we will not only be using this technique for hematopoietic, but also non-hematopoietic stem cell populations. For preparative studies, we are now in the process of formulating a new DOD grant proposal which will utilize all the advantages of a perfusion culture system, but at a manufacturing level. Almost all of the methodological aspects described above are incorporated into a fully automated cell expansion system devised, developed and produced by Asstrom Inc. (Ann Arbor, Michigan). Although not yet approved in the U.S., the Aatsrom RepliCell Cell Production System has been approved in Europe for hematopoietic stem cell expansion and use of the cells for transplantation purposes. The system not only allows expansion of primitive hematopoietic stem cells, but also other cell types, such as dendritic cells and lymphocyte subpopulations, which can then also be expanded (under different culture conditions) and used for immunotherapy.

Finally, this system will also be used to investigate whether granulocyte colony-stimulating factor (G-CSF) mobilized peripheral blood and/or bone marrow stem cells can be further expanded to increase the total number of CD34<sup>+</sup> cells in an effort to overcome HLA boundaries, thereby decreasing graft versus host disease and increase immunoreconstitution. In our report for year one of this grant, we showed that mobilized bone marrow was probably a better source of stem cells than peripheral blood. From a research viewpoint, total CD3<sup>+</sup> cells remained stable in the peripheral blood CD34<sup>+</sup> fraction, while in bone marrow the total CD3<sup>+</sup> cells reached the lowest point on day 6. CD19<sup>+</sup> or CD20<sup>+</sup> cells did not show any significant differences between peripheral blood and bone marrow during the G-CSF mobilization. Intracytoplasmic cytokine measurement also demonstrated higher IL-2-producing cells in the bone marrow than peripheral blood during G-CSF mobilization. These data indicate that mobilized bone marrow may produce a lower instance of graft versus host disease than mobilized peripheral blood, although clinical correlation is required to test this hypothesis. To this end, a clinical protocol has been submitted to the IRB to study the effect of G-CSF - mobilized bone marrow on matched sibling donor bone marrow transplantation.

## **2. Identify and remove lymphocyte subsets that result in the development of acute and chronic graft versus host disease (GvHD).**

In our previous report, we demonstrated that partial T-cell depletion, rather than extensive T-cell depletion, permits successful engraftment of a haploidentical graft. Thus, it appears that some

donor T-cells in the graft are necessary to overcome recipient barriers to engraftment. We showed preliminary results in evaluation of two anti-CD3 monoclonal antibodies (T10B9 and OKT3), activated by complement, to produce subset T-cell depletion of a more moderate degree. Expansion of these clinical studies has led to interesting observations regarding the influence of T-cell content and major cellular subsets within the marrow graft.

We have been able to analyze 210 recipients of haploidentical transplantation to compare the graft composition in the clinical preparation using either T10B9 or OKT3 monoclonal antibodies activated with rabbit complement. There were significant differences in the degree of T-cell depletion achieved and the resulting cellular subsets as shown below:

**Graft Results T10B9 OKT3 p value**

Nucleated cells / kg	$1.51 \times 10^8$	$0.89 \times 10^8$	$p < 0.001$
T-cell by LDA / kg	$7.9 \times 10^4$	$4.3 \times 10^4$	$p < 0.001$
T-cell Log Depletion	1.8	2.58	$p < 0.001$
CFU-GM / kg	$6.93 \times 10^4$	$4.52 \times 10^4$	$p < 0.001$

This retrospective analysis of graft composition clearly indicated that the use of OKT3 was more effective in removing mature T-cells however, there was greater effects on bystander cells with a significant reduction in growth potential as indicated by the CFU-GM assay and reduction in the total nucleated cell dose. Based on published data regarding the effect of cell dose on subsequent engraftment and post-transplant outcome, we could expect that these differences might have resulted in inferior clinical results.

A change was made in the conditioning therapy for patients who received OKT-3 prepared marrow grafts. Due to concern that an increase in the dose of total body irradiation (TBI) to 1500 cGy, in the patients who received T10B9 depleted grafts, the OKT-3 group received a lower TBI dose of 1400 cGy and additional immunoablation using a short course of anti-thymocyte globulin given during high-dose chemotherapy.

An analysis of the clinical outcome of these patients showed that there was no significant difference in the degree of mismatch in the two treatment groups. There was a greater proportion of patients in the OKT3 group who were at high-risk status by virtue of advanced disease status. There was a significant difference in achieving successful engraftment, which occurred at a median of 16 days in 99% of patients in the OKT-3 group compared to a median of 19 days in 88% of the T10B9 group ( $p < 0.001$ ). Furthermore, there was no difference in time to engraftment based on a nucleated cell dose above or below the median ( $p = 0.983$ ). The only other factor that appeared to effect engraftment was the length of time between diagnosis and

transplant. Patients transplanted > 1 year from diagnosis experienced poorer engraftment. The OKT3 group was analyzed separately for factors that influenced engraftment and no differences were detected based on degree of HLA mismatch in the donor (rejection direction), CD34+ cell dose, nor nucleated cell dose. Our conclusion was that the graft composition, within the ranges observed, had minimal influence on engraftment. Moreover, the host conditioning that was apparently enhanced by the addition of anti-thymocyte globulin had a significant and favorable effect on successful engraftment. Other post-transplant outcomes of interest, including the incidence of acute GvHD, survival and DFS were not different in the two groups. There appeared to be a trend toward more chronic GvHD in the OKT3 group, which might be partly related to retarded immune reconstitution as a consequence of a lower graft T cell dose. Future studies will examine T cell add back as a method to enhance both immune reconstitution and development of tolerance.

In the previous year we planned to initiate pre-clinical studies to evaluate a more refined and controlled method of graft engineering. The progress was delayed in part by the partnership that dissolved with CellPro due to an unfavorable outcome of a patent ruling. Subsequently we have developed plans with a subsidiary division of Baxter to use their FDA-approved monoclonal antibody columns to compare a positive-selection enrichment method versus a negative-selection depletion method.

In addition, we are planning to examine a new method of graft preparation using a monoclonal antibody blockade of the B7:CD28 co-stimulation pathway as a way to create energy between the T cell and the presentation of foreign HLA. Preliminary results from a clinical pilot study using haploidentical donors indicated that patients could engraft without serious GvHD and there was preservation of donor response to other antigenic stimulation resulting in accelerated immune reconstitution. In the next year, we hope to initiate a clinical trial in our Center to explore this promising approach to T cell modulation without depletion.

**3. Identify and produce lymphocyte subsets that could provide effective immune function against potentially fatal opportunistic infection during an extended lag in post-transplant immune reconstitution.**

During this year, we have successfully recruited a new faculty member to serve as director of a newly established cellular immunotherapy laboratory. We are initiating projects in this laboratory to develop cloned cytotoxic lymphocytes against cytomegalovirus (CMV) and the Epstein Barr virus (EBV), both potentially invasive and fatal infections in immunocompromised patients.

Human herpes viruses including CMV and EBV are ubiquitous in the population and by early adult life most individuals carry these viruses latent in the peripheral blood (PB). In the normal, immunocompetent host reactivation of CMV and EBV are suppressed by virus specific cytotoxic T-cells (CTL's). Reactivation of latent CMV and EBV occurs in immunocompromised individuals in the first 6 months after allogeneic BMT. EBV oncogenically transforms B-lymphocytes leading to a fulminant proliferation of malignant B-lymphocytes of donor origin.

This disease, EBV-lymphoproliferative disease (EBV-LPD), is poorly responsive to drug therapy and is rapidly fatal. EBV-LPD occurs predominantly after BMT from unrelated or mismatched family donors. Reactivation of CMV on the other hand gives rise to an interstitial pneumonia, which is the leading, infectious cause of death in BMT recipients. Hence, both CMV and EBV are significant causes of mortality after allogeneic BMT and require better management strategies. We plan to develop culture systems for the expansion of EBV and CMV specific CTL's from the PB of bone marrow donors, and adoptively transfer these virus specific CTL's to the recipient in the early post BMT period. We will monitor 1) reconstitution of the immune response, 2) measure viral load in the PB by semiquantitative PCR and 3) determine clinical efficacy.

### ***3a. Generation of EBV specific T cell lines.***

B-lymphocytes in vitro transformed by EBV (LCL's) express a similar range of viral latent cycle antigens to those observed in the cells of EBV-LPD. In addition, LCL's are highly immunogenic by expressing both HLA-class II antigens and co-stimulatory molecules. LCL's are therefore ideally suited for the generation of EBV specific CTL's. Furthermore normal donors have a high frequency of EBV specific CTL's circulating in the PB which should further facilitate EBV specific CTL expansion. We propose to transform PB cells from the donor with EBV in vitro and use these donor derived LCL's for the stimulation of donor T-cells in order to generate EBV specific CTL's.

### ***3b. Generation of CMV specific T cell lines.***

The dominant cellular immune response to CMV is directed at the matrix protein pp65. Vaccination of BMT donors with pp65 protein may be possible, but is not of help in the setting of mismatched transplantation since removal of T-cells from the transplant inoculum is required to prevent GvHD. Instead, we plan to use donor derived professional antigen presenting cells, dendritic cells (DC's), to present pp65 to donor T-cells for the raising of CMV CTL's. We will culture DC's in vitro from PB monocytes from the donor and pulse these DC's with recombinant pp65 protein prior to adding donor T-cells. Restimulation of the donor T-cells will be carried out with pp65 loaded donor monocytes. We hope that this system for raising CMV specific CTL's can be extended to the raising of other antigen specific lymphocytes including leukemia specific CTL's.

## **4. Identify and manipulate lymphocyte subsets that can provide an anti-leukemic effect when required.**

During this year, we have continued to examine the anti-leukemic effects of a subpopulation of lymphocytes, the  $\gamma\delta$  T cells, which we previously demonstrated to be associated with a decreased rate of relapse and improved disease-free survival in patients with leukemia. In on-going studies we are exploring methods to stimulate and expand  $\gamma\delta$  T cells with the aim to develop highly specific post-transplant immunotherapy.

#### **4a. The mechanism of $\gamma\delta$ T cell mediated anti-leukemia cytotoxicity**

In previous studies,  $\gamma\delta$ + T cells have been shown to have cytolytic activity against tumor cell lines. Clinical data from our laboratory and others show a statistically significant association between an increase in  $\gamma\delta$ + T cells post-BMT and improved disease-free survival following BMT. We have also shown that a graft engineering technique which spares  $\gamma\delta$ + T cells significantly increases the incidence of patients with high numbers of  $\gamma\delta$ + T cells. This in turn reduces the rate of post-BMT relapse, although all patients with increased  $\gamma\delta$ + T cells in this study showed a trend toward decreased relapse regardless of TCD protocol. Finally, preliminary data from our laboratory show that +CD4-CD8- donor T cells that bind and lyse recipient primary leukemia can be generated and expanded *in vitro*.

It has recently become apparent that  $\gamma\delta$ + T cells may be preferentially cytotoxic to acute lymphocytic leukemias, possibly due to recognition of a leukemia-associated antigen or a nonclassical MHC antigen. To date, B-ALL blasts + pan- $\delta$  mAb have consistently supported outgrowth of V $\delta$ 1+ cells which are cytotoxic to the primary B-ALL, lymphoid cell lines, and K562 cells but are not cytotoxic to myeloid cell lines. In contrast, the cultures that grew out CD4+ cells and V $\delta$ 2+ cells were derived from AML or biphenotypic ALL expressing myeloid antigens. These data are of particular interest since the few relapses that we have seen in our clinical observations of patients with increased  $\gamma\delta$ + T cells have all been from patients with myeloid or biphenotypic leukemias. The patients with increased  $\gamma\delta$ + T cells and ALL remain in remission, some for up to five years. Although these data hold promise, they are insufficient to definitively state that an ALL-associated antigen is the target.

#### **4b. Use of dendritic cells to expand $\gamma\delta$ T cells**

In contrast, expansion of  $\gamma\delta$ + T cells on dendritic cells both from autologous and allogeneic donors have resulted in nonspecific activation of the  $\gamma\delta$ + T cells. Cell-cell contact and CD4+ T cell help is required for this expansion and activation. Activation is enhanced by anti- $\delta$  and anti-CD3 antibodies. Since these initial data were collected from experiments performed in culture with fetal bovine serum (FBS) the possibility of activation via a processed bovine peptide cannot be ruled out. Further experiments are underway which evaluate dendritic cell/ $\gamma\delta$ + T cell interactions in autologous human serum based cultures.

To date, the most promising data has come from  $\gamma\delta$ + T cell/ALL co-cultures described above. In the next year, we therefore propose to determine if donor-derived  $\gamma\delta$ + T cells are cytotoxic to primary acute leukemias from BMT recipients by testing this cytotoxicity in several donor-recipient pairs and by detailed functional, phenotypic, and molecular analysis of cytotoxic  $\gamma\delta$ + T cells expanded *in vitro*. We plan to apply these observations to test activated/expanded donor-derived  $\gamma\delta$ + T lymphocytes against leukemic blasts obtained from BMT patients *in vitro* to begin the process of developing a clinical protocol for their use as immunotherapy for relapse or prevention of relapse.



Based on our findings, we hypothesize that  $\gamma\delta$ + T cells possess cytolytic activity against primary acute lymphoblastic leukemia and may constitute an effective form of cellular immunotherapy against relapse or residual ALL in the allogeneic BMT setting. Specific aims for the next phase of this study will be to determine the phenotype, clonality, activation state, and cytotoxicity to the recipient leukemia of donor-derived  $\gamma\delta$ + T cells from patients who receive BMT for acute leukemia. These data will also be used to determine the response of engrafted and reconstituting  $\gamma\delta$ + T cells to primary ALL or AML, or various subsets thereof.

In addition, we will attempt to determine if a  $\gamma\delta$ + T cell specific graft-versus-leukemia effect can be replicated and enhanced in vitro by expanding donor-derived cytotoxic  $\gamma\delta$ + T cells with cytotoxic activity against BMT recipient acute leukemia. These data will also be used to determine if freshly obtained donor-derived  $\gamma\delta$ + T cells can be engineered to bind and lyse primary ALL or AML, or various subsets thereof.

#### **5. A potentially new adjunct anti-leukemic therapy.**

A rapidly emerging and translational aspect of our basic research program, fueled by the Human Genome Project has been the use of "genomics". This is the identification of specific genes involved in the tumor process. The products of these genes can then be targeted with specific drugs to induce an anti-tumor therapy.

Ongoing research in our laboratory has demonstrated that nearly all primary leukemic cell populations exhibit a statistically significant greater  $pH_i$  than normal peripheral blood or bone marrow. We have also shown that this increase in  $pH_i$  is directly correlated with the cell cycle status of a population. It has been known for some time that increased  $pH_i$  is associated with a proliferative response. However, this is the first time that such correlations have been made on primary tumor cells. Since  $pH_i$  regulation is of utmost importance in the normal functioning of the cell, the principal gene that regulates  $pH_i$  is also a household gene, known as the sodium/hydrogen exchanger isoform 1 (NHE-1). The gene is present at chromosome location 1p35-36.1 and therefore relatively close to the putative tumor suppressor p73, located at position 1p36 and shown to be capable of inducing apoptosis. The protein p73 shows remarkable sequence similarity to p53 and has been implicated in the development of neuroblastoma and several other tumors. The product of the NHE-1 gene (designated APNH) is a ubiquitous, growth factor activatable, amiloride-sensitive membrane protein transporter which extrudes hydrogen ions out of the cell, thereby maintaining the normal  $pH_i$ . However, when the exchanger is activated, not only is there an increase in the efflux  $H^+$  ions, but an increase in the influx of  $Na^+$  ions leading to a transient alkaline state, which in turn can stimulate cell proliferation. All of these facts led us to postulate that if the NHE-1 could be inhibited in leukemic cells, then the  $pH_i$  of the cells would decrease and induce apoptosis. Indeed, this was the prediction of the correlations mentioned above. Using both flow cytometry and fluorescence ratio imaging microscopy to measure  $pH_i$  and annexin-V and TUNEL methodologies to detect apoptosis, we can now demonstrate that primary patient leukemic cells can be induced into apoptotic cell death by in vitro incubation with pharmacological doses of NHE-1 inhibitors. These inhibitors are specific and potent analogues of the potassium-sparing diuretic, amiloride. However, our results

also indicate that there is a differential effect between normal and leukemic cells to these inhibitors. Thus, although these agents will kill a proportion of normal cells, it would appear that a far greater percentage of leukemic cells are induced into apoptosis. In fact, after a 5-hr incubation of primary acute lymphoblastic leukemic (ALL) cells, more than 90% were either undergoing apoptosis or had been killed. The results from these in vitro experiments are now being transferred to a pre-clinical model using leukemia-infected NOD-SCID mice.

This new and exciting aspect of  $pH_i$  regulation has at least three important significant aspects. The first is that  $pH_i$  can be used as a biomarker for leukemic cells and other tumor cell types. The second is the novel approach to using NHE-1 inhibitors as potential anti-leukemic adjunct therapeutic agents. The third aspect is to further characterize the molecular signature of normal and leukemic cells in order to define the pathway of apoptosis resulting from the use of the inhibitors. In this way, other potential gene target products can be identified allowing the alternative or combined use of drugs for anti-leukemic therapies. By reducing the overall tumor burden, the patient would be in a better situation to receive a transplant and hopefully be less likely to relapse.

## BIBLIOGRAPHY

Abhyankar SH, Chiang KY, McGuirk JR, Pati AR, Godder KT, Welsh JA, Waldron RL, McElveen JL, Henslee-Downey PJ. Late onset Epstein-Barr virus-associated lymphoproliferative disease after allogeneic bone marrow transplant presenting as breast masses. *Bone Marrow Transplant* 1998; 21:295-297.

Christiansen NP, Bridges K, Hazlett L, Abhyankar S, Chiang KY, Godder K, Lee C, Neglia W, Parrish R, Henslee-Downey PJ. Partially mismatched related donor transplant is highly effective for patients with early leukemia. Submitted and accepted for presentation at the American Society of Clinical Oncology, Atlanta, GA, 1999.

Fleming DR, Henslee-Downey PJ, Ciocchi G, Romond EH, Marciniak E, Munn R, Thompson JS. The use of partially HLA-mismatched donors for allogeneic transplantation in patients with mucopolysaccharidosis-1. *Ped Transplant* 1998; 2:299-304.

Garden O, Musk P, Worthington-White, D, Rich IN. Sequence analysis of the human hematopoietic sodium/hydrogen exchanger: Implications for leukemogenesis. In preparation.

Godder KT, Abhyankar SH, Lamb LS, Best RG, Geier SS, Pati AR, Gee AP, Henslee-Downey PJ. Donor leukocyte infusion for treatment of graft rejection post partially mismatched related donor bone marrow transplant. *Bone Marrow Transplant* 1998; 22:111-113.

Henslee-Downey PJ: Extending the donor pool using mismatched transplants. In Baxter Monograph: Cellular Support for the Oncology Patient. Barrett (ed), Baxter Healthcare Corporation, Deerfield, IL, 1999, p 57-74.

Henslee-Downey PJ: Haploidentical transplantation. In Advances in Allogeneic Stem Cell Transplantation. Burt (ed). *In press*.

Henslee-Downey PJ and Gluckman E: Allogeneic Transplantation from donors other than HLA-identical siblings. In Hematology/Oncology Clinics of North America, Schiller GD (Ed), W. B. Saunders Company, Philadelphia, PA, *In press*.

Lamb LS, Gee AP, Henslee-Downey PJ, Geier SS, Hazlett L, Pati AR, Godder K, Abhyankar SA, Turner MW, Harris WG, Parrish RS. Phenotypic and functional reconstitution of peripheral blood lymphocytes following T-cell depleted bone marrow transplantation from partially mismatched related donors. *Bone Marrow Transplant* 1998, 21:461-471.

Lamb LS, Hazlett LJ, Musk P, O'Hanlon TP, Geier SS, Folk RS, Harris WG, McPherson K, Parrish RS, Lee C, Gee AP, Henslee-Downey PJ. Influence of T cell depletion method on circulating  $\gamma\delta^+$  T cell reconstitution and potential role in the graft versus leukemia effect. *Cytotherapy*, *In press*.

Lamb LS, Abhyankar SA, Hazlett L, O'Neal W, Folk FS, Vogt S, Parrish RS, Bridges K, Henslee-Downey PJ, Gee AP. Expression of CD 134 (OX-40) on T cells during the first 100 days following allogeneic bone marrow transplantation as a marker for lymphocyte activation and therapy-resistant graft versus host disease. Submitted to *Cytotherapy*.

Lamb LS, Musk P, Ye Z, Rich I, Henslee-Downey PJ: Generation of  $\gamma\delta^+$  T cells with antileukemic activity. 1998 Basic Research Conference, San Diego, CA.

Lamb LS, Gee AP, Musk P, O'Hanlon TP, Hazlett LJ, Geier SS, Folk RS, Harris WG, McPherson K, Parrish RS, Lee C, Henslee-Downey PJ. Influence of T cell depletion method on circulating  $\gamma\delta^+$  T cell reconstitution and potential role in the graft versus leukemia effect. *Blood* 1998; 92(Suppl 1):493a. Presented at 1998 American Society of Hematology,

Lamb LS, Musk P, Ye Z, Rich IN, Harris WG, Henslee-Downey PJ. Anti-leukemic effect of in vitro activated  $\gamma\delta^+$  T lymphocytes. *Blood* 1998; 92(Suppl 1):655a. Presented at 1998 American Society of Hematology,

Noé G, Riedel W, Kubanek B, Rich IN. An ELISA specific for murine erythropoietin. *Brit J Hematol* 104:838-840 (1999).

Rich IN, Brackmann I, Dewey MJ, Worthington-White D. Activation of the sodium/hydrogen exchanger via the fibronectin-integrin pathway results in hematopoiesis stimulation. *J Cell Physiol*. 177:109-122 (1998).

Rich IN. Homeobox genes and hematopoiesis: An emerging picture for genomic therapy. *J Hematotherapy* 7:515-520 (1998).

Rich IN, Worthington-White D, Musk P, Harris G, Lamb L, Henslee-Downey PJ. Relationship between intracellular pH and cell cycle allows induction of apoptosis of leukemic cells by inhibition of ion transporters. *Blood* 1998; 92(Suppl 1):505a. Presented at the American Society of Hematology, 1998.

Rich IN, Worthington-White D, Garden O, Musk P. Apoptosis of leukemic cells by inhibition of the  $\text{Na}^+/\text{H}^+$  exchanger. *In preparation*.

Ye Z, Gee AP, Lamb LS, van Rhee F, Haley S, Harris G, Lee C, Geier SS, Rich IN, Henslee-Downey PJ: Using dendritic cells and CD4<sup>+</sup> helper T-cells to expand human  $\gamma\delta^+$  T-cells for Immunotherapy. *In preparation*.

University Research Initiative Program for Combat Readiness  
Annual Report 06/01/98-05/31/99

PART 53-FORMS

53.301-298

<b>REPORT DOCUMENTATION PAGE</b>		Form Approved OMB No. 0704-0188	
Public reporting burden for this collection of information is estimated to average 1 hour per response, including the time for reviewing instructions, searching existing data sources, gathering and maintaining the data needed, and completing and reviewing the collection of information. Send comments regarding this burden estimate or any other aspect of this collection of information, including suggestions for reducing this burden, to Washington Headquarters Services, Directorate for Information Operations and Reports, 1215 Jefferson Davis Highway, Suite 1204, Arlington, VA 22202-4302, and to the Office of Management and Budget, Paperwork Reduction Project (0704-0188), Washington, DC 20503.			
1. AGENCY USE ONLY (Leave blank)	2. REPORT DATE June 1, 1999	3. REPORT TYPE AND DATES COVERED Annual	
4. TITLE AND SUBTITLE Insure Access to Allogeneic Bone Marrow Transplantation for Correction of Marrow Failure and Hematologic Malignancies		5. FUNDING NUMBERS Grant Number N00014-97-1-0806; PR Number 97PR06312-00; PO Code 353; Disbursing Code N68892; AGO Code N66020; Cage Code 4B489	
6. AUTHOR(S) P. Jean Henslee-Downey, M.D. Ivan N. Rich, Ph.D.			
7. PERFORMING ORGANIZATION NAME(S) AND ADDRESS(ES)  University of South Carolina Columbia, South Carolina 29208		8. PERFORMING ORGANIZATION REPORT NUMBER  N00014-97-1-0806-2	
9. SPONSORING / MONITORING AGENCY NAME(S) AND ADDRESS(ES)  ONR		10. SPONSORING / MONITORING AGENCY REPORT NUMBER  ONR	
11. SUPPLEMENTARY NOTES Prepared in coordination with University Research Initiative Program for Combat Readiness			
12a. DISTRIBUTION / AVAILABILITY STATEMENT  APPROVED FOR PUBLIC RELEASE		12b. DISTRIBUTION CODE	
13. ABSTRACT (Maximum 200 words) Although an identical sibling is the ideal donor for a recipient requiring a transplant of hematopoietic cells after being exposed to radioactive, chemical or biological weapons resulting in hematological aplasia or cancer, only 25% of the patients would have the opportunity of receiving a transplant from their HLA-identical sibling. On the other hand, more than 95% of the patients could receive a transplant if a partially mismatched related donor (PMRD) was used. However, this type of transplant must be accompanied not only by pre-transplant high dose chemotherapy and consolidation, but also by post-transplant immunosuppression geared to finding a balance between suppressing graft versus host disease and allowing for a graft versus leukemia effect to occur.			
14. SUBJECT TERMS  Chemical and Biological Defense, Target Acquisition, Anti-Submarine, Combat Medicine, Biodeterioration, and Command Control and Communication		15. NUMBER OF PAGES 11	
		16. PRICE CODE	
17. SECURITY CLASSIFICATION OF REPORT  UNCLASSIFIED	18. SECURITY CLASSIFICATION OF THIS PAGE  UNCLASSIFIED	19. SECURITY CLASSIFICATION OF ABSTRACT  UNCLASSIFIED	20. LIMITATION OF ABSTRACT  200

NSN 7540-01-280-5500

Standard Form 298 (Rev. 2-89)  
Prescribed by ANSI Std. Z39-18  
298-102

**Tissue-Engineered Cartilage and Advanced Bioadhesives for the Rapid  
Healing of Combat and Training Injuries to Bone**

Brian Genge

Department of Chemistry and Biochemistry  
University of South Carolina  
Columbia, SC 29208

Tel: (803) 777-6470  
Fax: (803) 777-9521  
Email: [genge@psc.sc.edu](mailto:genge@psc.sc.edu)

### **Section 4-3: Tissue-Engineered Cartilage and Advanced Bioadhesives for the Accelerated Healing of Combat and Training Injuries to Bone**

Brian Genge, Licia Wu, Glenn Sauer, and Roy Wuthier

#### **ABSTRACT**

Chondrocytes in fracture callous play a critical role in the process of repairing broken bones. Acceleration of growth, differentiation and mineralization of chondrocytes is key to developing effective therapies for more rapid healing and fracture repair of battlefield injuries to bone. It is known that expression of local growth factors plays a pivotal role in normal development and calcification of fracture-callous cartilage. Our ability to grow mineralizing chondrocyte cultures provides an outstanding opportunity to create a biomaterial that enables the expedited healing and repair of bone injuries. Using formulations of specific cytokines and growth factors, our chondrocyte cultures can be tissue-engineered to produce a matrix-mineral composite that may be implanted into the injury sites. We also propose to develop an advanced synthetic bioadhesive for immediate, in the field repair of fractured bone. We have discovered several distinct biochemical components crucial to bone mineral formation and have developed a proprietary process enabling a unique recombination of the purified components. This material can be formulated to harden with 2 hours and may be used to provide a bone-like weld in fractured bone to stabilize the injury. We anticipate that these novel biomaterials could tremendously speed the bone healing process.

#### **FORWARD**

The total amount of this award is \$900,000 for the period 6-1-97 to 5-31-00.

The long-term design goals of this grant is to provide rapid stabilization of bone fractures, even to weight bearing bones, and to aid and accelerate the normal cell-mediated healing process of injured bones. During the first grant period, we succeeded in developing formulations of self-hardening bone pastes that may be useful for first aid to bone injuries. Compression testing of those formulations showed superior strength when compared to other calcium phosphate-based materials reported in the scientific and patent literature. During this past grant period, we have improved upon the properties of our bone cement and demonstrate that the cement paste can cure *in vivo* after being surgically injected. Accomplishments for this second year include the following:

- Continued refinement and improvement in the synthesis of our calcium phosphate bone cement formulation, yielding a much faster hardening rate and a further increase in compressive strength.
- Discovery of biological and organic macromolecules that act as cohesion promoters that can be used in conjunction with our bone cement.
- Initiated pilot studies demonstrating the feasibility of direct, *in situ* injection of our bone cement paste as a potential delivery system for skeletal repair.

- Tissue section preparation, preliminary histological analysis and implant evaluation of our bone cement by Dr. David Van Sickle (Purdue University, Department. of Basic Medical Sciences) after being injected into an avian metatarsal defect model.
- Collaborated with Dr. Hari Reddi (University of California Davis Medical Center, Department of Orthopedics Research) on a preliminary short-term experiment in living mice and demonstrated that subcutaneous injections of our bone cement paste harden *in situ* and is non-toxic to the host.
- Completed a material transfer agreement and received from Dr. Constance Cepko (Harvard Medical School, Department of Genetics) avian retroviral vectors to be used for the genetic engineering of our growth plate chondrocyte cultures.

## REPORT

To date, a wide variety of implant materials have been used to repair and augment bone. These include bone, synthetic polymers, and most commonly, inert metals. Often times, hip or tibial plateau fractures require major surgery to insert metal screws, pins and plates to stabilize the break, a lengthy hospital stay, and then a second surgery to remove the hardware. The drawbacks of such a protocol include patient pain, risk of infection during each operation, cost, and the inserted hardware can further damage the bone. Therefore, a major goal of biomaterial scientists and plastic and reconstructive orthopedic surgeons is to develop novel bone substitutes that can be used for skeletal repair. Hydroxyapatite [ $\text{Ca}_{10}(\text{PO}_4)_6(\text{OH})_2$ ] biomaterials have attracted much interest as a substitute for injured bone over the past two decades due to their chemical and crystallographic similarities to the principal inorganic constituent of these hard tissues. However, sintered, preformed hydroxyapatite prosthetic devices are difficult for the surgeon to work with, they cannot support heavy loads, and they are not resorbed by the host. More recently, calcium and phosphate-based bone cements and pastes have garnered much attention and generated a lot of excitement in the scientific and medical community as potentially superior bone substitutes because they show excellent biocompatibility and appear to be resorbed. However, calcium phosphate-based bone cements developed by other researchers lack sufficient compressive strength and are therefore only suitable for use in treating injuries to **nonweight-bearing** bones such as wrist fractures [1] and craniofacial augmentation [10].

We are developing an injectable calcium phosphate based biomaterial that may be used in the field to repair injuries and fractures to **weight-bearing** bones. The compressive strength of the hardened product that forms from our paste developed this past year can exceed 90 megaPascals.

Our goal is to produce a biocomposite with the following desirable characteristics [1, 9, 10]: 1.) Ability to be surgically implanted into the injury site by injection. 2.) Our bone paste will resist disintegrative washout upon contact with blood and injection into the wound. 3.) The bone paste will be able to bond to living bone. 4.) Once implanted, it will be able to harden and stabilize the fracture within a short period of time. 5.) The composite material will cure to form a mineral phase compatible with living bone. 6.) The biomaterial will have excellent tissue compatibility. 7.) After the biomaterial has stabilized the fracture, it will be soluble enough to be resorbed and replaced by the normal activity of osteoclasts in living bone. 8.) The biomaterial may be formulated to contain agents and genetically modified cells that promote and accelerate the normal cell mediated healing process.



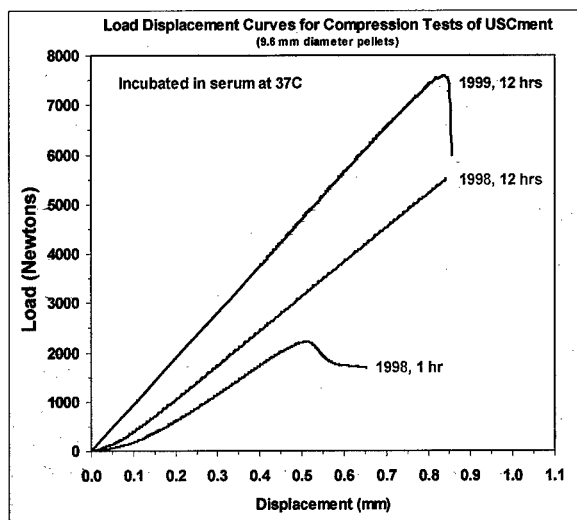


Fig. 1. Load displacement curves for compression tests of USCment hardened in serum at 37°C.

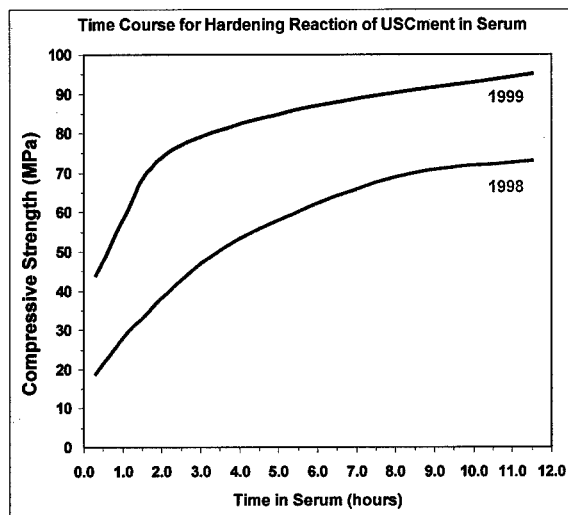


Fig. 2. Time course study shows compressive strength of USCment increases when incubated in serum.

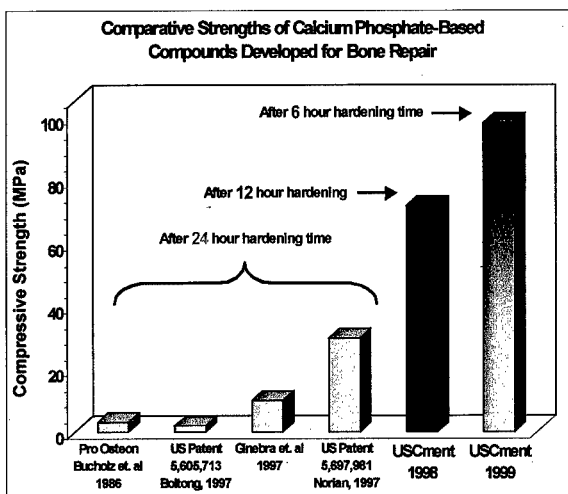


Fig. 3. Compressive strength comparison of USCment to other calcium phosphate biomaterials used in bone repair.

## FURTHER IMPROVEMENT OF THE REACTIVITY AND PHYSICAL PROPERTIES OF OUR BONE CEMENT

As stated previously, to date, calcium and phosphate based biomaterials have been used only to aid in the repair of non-weight bearing fractures and boney defects. This is primarily because of their relatively low compressive strength compared to cortical bone. Our study of the reaction responsible for the setting of our bone cement using X-ray diffraction, FTIR, and SEM have lead to improved biochemical and physical properties previously developed cement formulations. For example, this past grant period, we have developed an improved manufacturing process for the synthesis of our bone cement. We are now able to prepare formulations that can attain a compressive strength of over 90 megapascals (MPa) in just 12 hours, even when it is immersed in serum. (Figs.1-3). Continued efforts towards the refinement and improvement in the synthesis of our calcium phosphate bone cement formulation has yielded a product with a much faster hardening rate and a further increase in compressive strength compared to last year (Figs. 2, 3). In fact, after only 15 minutes, our new preparations attain a compressive strength equal to or superior to other researcher's calcium phosphate cements after 24 hours (Figs. 2, 3). These other calcium phosphate biomaterials (1-10) have been shown to have only about ~5-50% of this strength, even after 24 hours (Fig. 3).

## PRELIMINARY SHORT-TERM STUDIES USING USCMET

Sintered hydroxyapatite (HAP) blocks and ceramic granules are well known to have good biocompatibility. This is because HAP tends to bond with the bone over time, it causes little inflammation and it can be osteoconductive. A possible complication associated with the clinical use of hydroxyapatite is that it is not easy to contour the blocks to the shape of the defect or bone surface while the granules, on the other

hand, are difficult to deliver and tend to wash out of the site. Furthermore, the surrounding bone does not resorb the HAP ceramics. Therefore, in addition to having excellent tissue compatibility, biomaterials developed for skeletal repair should also be easily contoured and resorbable. Calcium phosphate bone cement pastes offer an appealing alternative to presintered HAP blocks because they can be shaped and molded to fit the boney defect, however, most formulations do not set *in vivo* due to the marked inhibitory effect of  $Mg^{2+}$  ions from the serum on the hardening reaction. Furthermore, many calcium phosphate cement pastes tend to disintegrate upon early contact with blood or other bodily fluids, which has limited widespread clinical use of these materials for bone repair, reconstruction and skeletal augmentation (12).

Our goals therefore has been to produce a calcium phosphate formulation that can be surgically implanted as a paste into the injury site, with the preferred method of delivery being injection. After injection, our bone paste will resist disintegrative washout from the wound upon contact with the surrounding blood. Once implanted, it will be able to harden and stabilize the fracture within a short period of time.

We have conducted several pilot studies this past grant period toward achieving these goals. For example, in December 1998, we collaborated with Dr. Hari Reddi (University of California Davis Medical Center, Department of Orthopedics Research) on a preliminary short-term experiment in living Long-Evans rats. Dr. Hari Reddi is a world-renowned pioneer in osteoconduction research and is also the discoverer of osteogenic protein-1. Osteogenic protein-1 is a potent morphogen that induces *de novo* bone formation. At UC Davis Medical Center, using Dr. Reddi's rodent model and protocol, we subcutaneously implanted ~ 1.0 gram of USCment paste, with and without the addition of his osteogenic protein-1, bilaterally to the thorax of the rats. These studies were conducted to determine the setting capability of USCment *in vivo*. The samples were harvested 11 days after implantation. Unfortunately, but not unexpectedly, while the samples were being prepared and sectioned for histological analysis, they shattered as a result of the microtome movement through the hardened cement and were unable to be processed further. We did discover however, that our calcium phosphate cement paste was able to set and harden *in vivo*, even when the paste was *immediately* submersed in the internal body fluids that were present at the implantation site. Furthermore, all four rats survived the duration of the experiment without incident, suggesting that the cement pastes were well tolerated.

Since our cement pastes, when implanted in the rats, became very hard and could not be cut by a microtome and processed using conventional histological techniques, alternative protocols were explored. Since Purdue University and Indiana University School of Medicine have strong ties to several of the largest orthopedic device companies in the world, we contacted Dr. David Van Sickle (Purdue University, Department. of Basic Medical Sciences). Dr. Van Sickle has the specialized resources and instrumentation (an Exakt-cutting-grinding System) capable of processing our samples and the expertise to critically evaluate the properties of bone around a wide variety of implant materials. Accordingly, we tested the feasibility of using the Exakt System for histological preparation of our specimens. Using an avian metatarsus as a convenient model, USCment was percutaneously injected into the intramedullary cavity of a fractured bone. A 16-gauge needle of a syringe containing USCment was used to create a unicortical hole superior to the fracture (Fig. 4). After 12 hours incubation at 37°C in growth media, cross-sections of the bone were made with a band saw (Fig. 5). Note that our hardened bone cement paste forms excellent contact with the endosteal layer of the bone. To more closely examine the bone-cement interface by microscopy, a 3-mm unicortical defect was created in the diaphyseal shaft of an avian metatarsus. The hole was injected with USCment then incubated in serum (Fig. 6). After 12 hours, the sample was fixed in

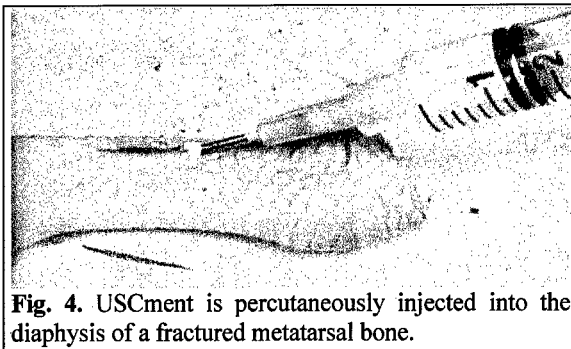


**Fig. 4.** USCment is percutaneously injected into the diaphysis of a fractured metatarsal bone.

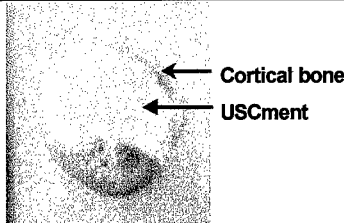


**Fig. 5.** Cross-section of the fractured bone shown in Fig. 4, 12 h after injection. USCment (white, center) is shown having excellent contact with the cortical bone.

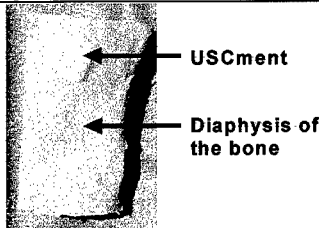


**Fig. 6.** Longitudinal, frontal view of a metatarsal bone shaft section. Shown is a 3 mm defect that has been filled with USCment and hardened *in situ*. Note the bond between the cement and the bone.

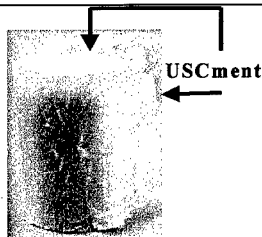


**Fig. 7.** Lateral view of the bone shown in Fig. 6. Note that the defect has been completely filled with USCment.

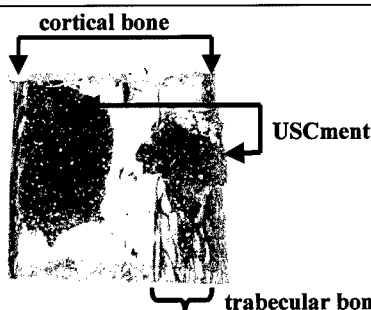


**Fig. 8.** Toluidine blue stain of an undecalcified cross-section of the region of the bone containing the defect shown in Figs. 6 & 7. Note USCment (purple) is in direct contact with the bone (blue).

10% phosphate-buffered formalin for 7 days then sent to Dr. Van Sickle's laboratory where it was dehydrated using a graded series of ethanol then embedded in polyester resin. Sections, (2 mm thick) were made using a specialized cutting machine designed for hard tissue, then ground to 75-150- $\mu$ m using a 200- $\mu$ m thick diamond tip. The cutting-grinding technique is a method used to obtain thin sections for histological examination of specimens that cannot be cut by conventional techniques.

Our preliminary tests demonstrated that USCment hardens even when it is injected into a fresh bone fracture (Fig. 5) or bone defect site (Fig. 6). Furthermore, Dr. Van Sickle was able to successfully process our samples, using the Exakt System. Detailed histomorphological analyses are forthcoming. In brief, toluidine blue staining of an *undecalcification* longitudinal section of the region of the bone containing the defect shown in Figs. 6 & 7 reveals that USCment (purple) is in direct contact with the bone (blue) (Fig. 8). There was also strong evidence that USCment was in intimate contact with the cortical bone (Fig. 9A) and was able to infiltrate the trabecular bone (Fig. 9B). The hardened cement showed a macroporous structure conducive to the infiltration of osteoblasts and blood vessels. USCment did not appear to induce an immediate-early inflammatory reaction (Figs. 9A & 9B).

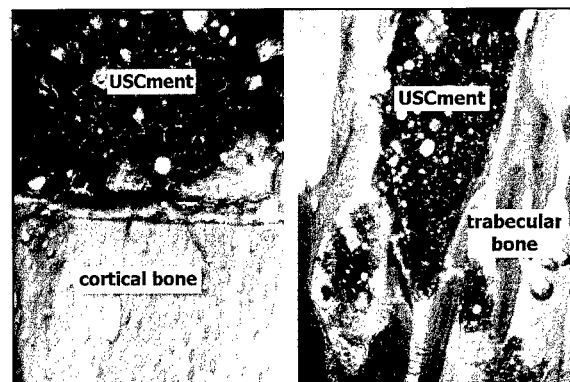


**Fig. 9A & 9B.** Light micrograph of a Toluidine blue stained, 75  $\mu$ m longitudinal-section of the region of the bone containing the defect shown in Figs. 6 & 7. Note the excellent interface that is formed between USCment and the living bone and the macroporous structure of the cement.



**Fig. 10.** An avian metatarsus, obtained as a by-product from a poultry-processing plant, was manually fractured and the cornified epithelium is peeled back to expose the break.

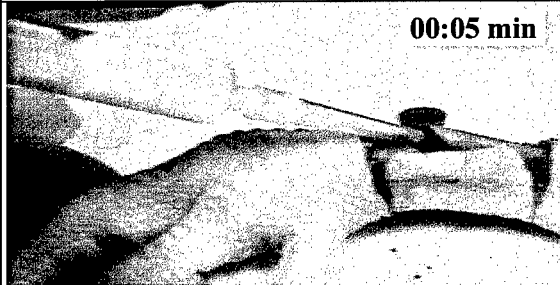


**Fig. 11.** Next, a small volume of USCment paste was injected with a syringe into the fracture site.

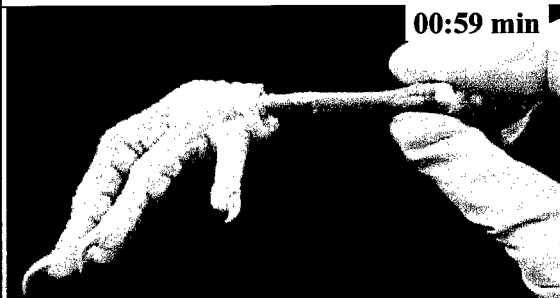


**Fig. 12.** After 1 hour at 37°C the cement hardened and sufficiently stabilized the fractured bone so that it could be suspended by supporting it only at one end.

## **EXPERIMENTAL BONE FRACTURE REPAIR USING USCMENT:**

### **A PRELIMINARY SHORT-TERM STUDY USING AVIAN METATARSAL BONES**

Pilot studies using avian metatarsal bones were conducted to determine the potential clinical usefulness of USCment. Since these “chicken feet” are obtained as a by-product from a local poultry-processing plant, and since the cells remain viable for over 24 hours, they make an excellent alternative to live animal testing for performing pre-clinical evaluations of the USCment. Accordingly, metatarsal bones were obtained and manually fractured in the diaphyseal region of the bone (Fig. 10). A small volume of USCment powder was mixed with an aqueous buffer in a chilled, sterilized mortar and pestle. The resulting paste was placed into a syringe, then injected into the fracture site (Fig. 11). The bone was then submersed in cell culture media containing 20% serum at 37°C. After 1 hour, the cement hardened and stabilized the fractured bone sufficiently so that it was able to support its own weight by suspending it from only one end of the bone (Fig. 12).

## **TISSUE ENGINEERING OF GROWTH PLATE CHONDROCYTES**

Tissue engineering is an emerging technology for the application of scientific and engineering knowledge to understanding the processes of normal and pathological tissue formation. It can be used for the development of biological substitutes to repair, restore, maintain, or improve tissue functions. Tissue engineering involves the use of living cells, genetically modified cells, or living cells plus natural or inert synthetic extracellular materials in the development of biological substitutes for tissue replacements. Our goal is to develop an implantable biomaterial that accelerates the normal rate of the fracture healing processes known to occur *in vivo*. To date, we have shown this can be accomplished by the addition of growth factors and mineralization promoters to isolated chondrocytes. We now show it is possible to genetically engineer our chondrocytes to overexpress key proteins such as Annexin-5 that are involved in the mineralization pathway. Together with our bone cement as a substratum, it should now be possible to tissue engineer our chondrocyte cultures to make a biomaterial that enables the rapid healing and repair of bone injuries.

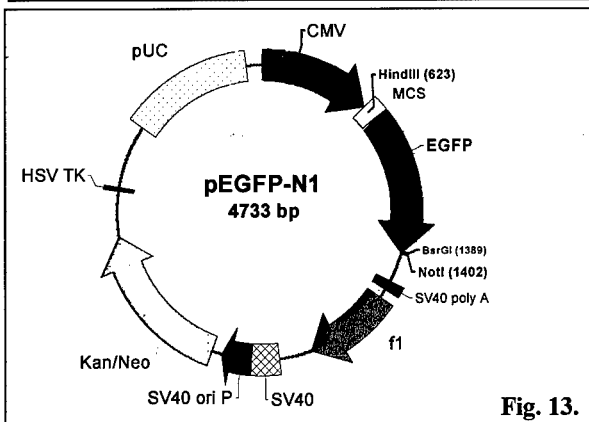


Fig. 13.

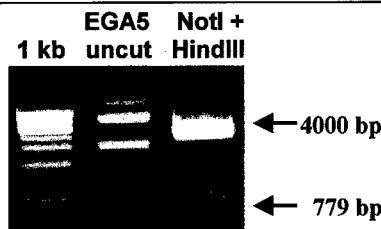


Fig. 14. Restriction enzyme digest of pEGFP mammalian expression vector (4733 bp), showing the excision of GFP gene (779 bp).

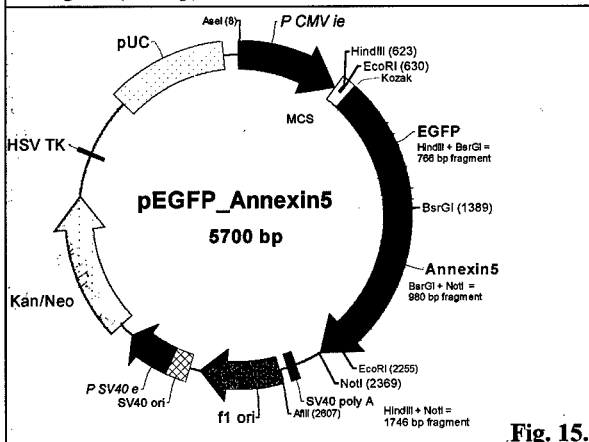


Fig. 15.

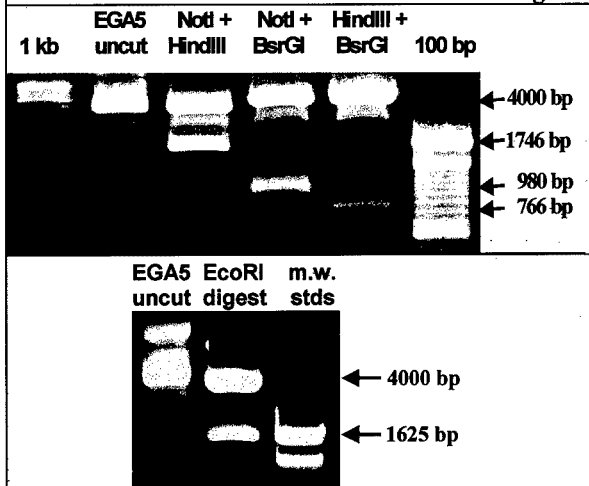
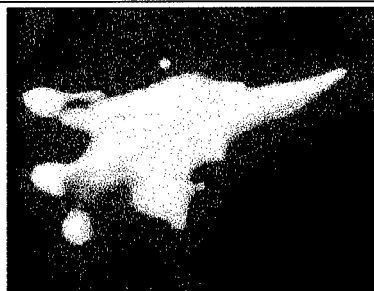


Fig. 16. EcoR I restriction enzyme digest of our pEGFP\_Annexin5 mammalian expression construct excises the GFP-Annexin fusion gene (1625 bp) from the vector.

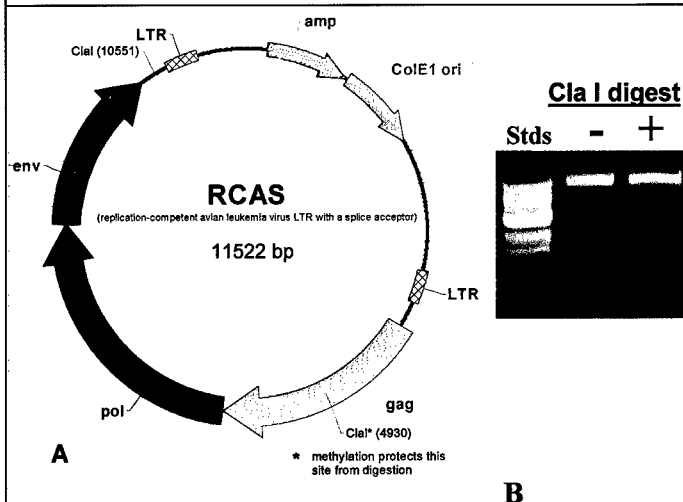
## MANIPULATING GENE EXPRESSION OF CHONDROCYTES USING EUKARYOTIC AND REPLICATION-COMPETENT RETROVIRAL VECTORS

In order to develop useful gene therapy systems, several major obstacles must be overcome. These include efficient transfer of the desired gene to target cells, the gene must remain in those cells for an extended period of time and the gene expression should be able to be regulated. Mammalian expression vectors have been used successfully to express proteins in a variety of cell types. One example is a plasmid that expresses an enhanced green fluorescent protein (EGFP) (Fig. 13).

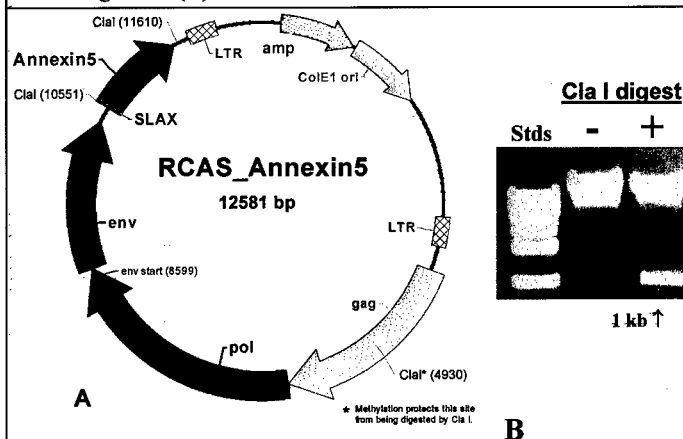
Green fluorescent protein (GFP) from the jellyfish *Aequorea victoria* is a revolutionary reporter molecule for monitoring gene expression and protein localization *in vivo*, *in situ* and in real time [11]. GFP fluoresces bright green upon mere exposure to ultraviolet light. GFP fluorescence can be monitored non-invasively in living cells. Eukaryotic expression vectors for fusing heterologous proteins to either the C- or N-terminus of EGFP are available commercially. We have recently succeeded in excising the GFP gene (Fig. 14) and fusing it with Annexin-5 to create an EGFP-Annexin5 expression vector (Fig. 15). The fusion protein is expressed under control of the immediate early promoter of human cytomegalovirus (CMV). We cloned Annexin-5 into pEGFP so that it was in-frame with the EGFP coding sequences with no intervening stop codons. Restriction digest mapping of the plasmid strongly indicates we have made the desired vector (Fig. 16). At the time of this report, we are currently verifying the construct by DNA sequence analysis, however. The recombinant EGFP-Annexin5 vector was transfected into our primary chondrocyte cultures using a liposomal-based transfection agent. After 48 hours, cells were visualized by fluorescent microscopy. We made the exciting discovery that EGFP retained its fluorescent properties when fused to



**Fig. 17.** Fluorescent microscopic imaging of a cultured chondrocyte 2 days after it was transfected with our pEGFP-Annexin5 expression vector. Note the intense fluorescence in both the cell and the cell-derived microstructures (matrix vesicles).



**Figs. 18A & B.** Gene map of the replication-competent retroviral (RCAS) vector (A). Restriction enzyme digestion of RCAS with Cla I specifically cuts the vector at one site, without removing any DNA fragments (B).



**Figs. 19A & B.** Gene map of RCAS-Annexin5 expression vector (A). Restriction enzyme digestion of RCAS-Annexin5 with Cla I cuts the vector at two sites, creating a 11.5-kilobase parent fragment and a 1-kilobase insert containing the Annexin-5 gene (B).

Annexin-5, thus allowing real-time, *in situ* localization of the GFP-Annexin-5 fusion protein (Fig. 17). Since Annexin-5 may be one of the mineralization promoters of healing fractures, it is important to understand its role in the calcification process. Using this EGFP-Annexin5 chimeric construct, tremendous strides in the knowledge of the function of this key protein can now be gained. This information will be used to rapidly advance our tissue engineering studies of growth plate chondrocytes.

Two main problems associated with the use of eukaryotic expression vectors are that stable transfection is not possible and the transfection frequency is too low. Retroviral-mediated gene delivery has several advantages over the transient transfection that is achieved using conventional expression vectors. This is primarily because the gene expression is stable and the percentage of infected cells will increase over time if the virus is replication-competent. For this reason, replication-competent retroviral vectors based on the avian Rous sarcoma virus (RCAS) (Fig. 18) are becoming increasingly popular for expressing genes in both primary cell cultures and embryonic chick tissues (13). We used RCAS (14) (gift from Constance Cepko, Harvard Medical School, Department of Genetics) to design and construct an RCAS-Annexin5 expression vector (Fig. 19). The high efficiency of the viral promoter in RCAS-based vectors should allow us to achieve sufficiently high levels of expression of Annexin-5 in the chondrocytes. We are currently testing the hypothesis that overexpression of Annexin-5 by RCAS-based self-replicating vectors will dramatically affect the chondrocyte's mineralization.

### ***Participating Personnel***

<b>Name</b>	<b>Degree</b>	<b>Year</b>
Genge, Brian	Ph.D.	1989
Wu, Licia N.Y.	Ph.D.	1977
Sauer, Glenn	Ph.D.	1986
Wuthier, Roy	Ph.D.	1960
Lu., Min	M.S.	1997

### **BIBLIOGRAPHY**

1. Constanz, B., Ison, I., Fulmer, M., Poser, R., Smith, S., VanWagoner, M., Ross, J., Goldstein, S., Jupiter, J., Rosenthal, D. Skeletal repair by in situ formation of the mineral phase of bone. *Science* **264**:1796-1799, 1995.
2. American Dental Association Health Foundation, Chow, L. and Takagi, S. Self-setting calcium phosphate cements and methods for preparing and using them. *United States Patent* # **5525148**, Issued 1996.
3. Monma, H., Kanazawa, T. The hydration of  $\alpha$ -tricalcium phosphate. *Yogyo-Kyokai-Shi* **84**: 209-213, 1976.
4. Bohner, M., Lemaître, J., Legrand, A., d'Espinose, J., Caillerie, d., Belgrand, P. Synthesis, X-ray diffraction and solid-state  $^{31}\text{P}$  magic angle spinning NMR study of  $\alpha$ -tricalcium othophosphate. *J. Materials Science: Materials in Medicine* **7**: 457-463, 1996
5. Einhorn, T. Current concepts review: Enhancement of fracture-healing. *J. Bone and Joint Surgery* **77**: 940-956, 1995.
6. Bucholz, R., Carlton, R., Holmes, R. Interporous hydroxyapatite as a bone graft substituted in tibial plateau fractures. *Clinical Orthopedics* **240**: 53-62, 1989.
7. Boltong, M. Process for the preparation of calcium phosphate cements and its application as bio-materials. *United States Patent* # **5605713**, Issued 1997.
8. Ginebra MP, Fernandez E, Maeyer EP, Verbeeck, RH, Boltong MG, Ginebra FM, Driessens FC, Planell JA: Setting Reaction and Hardening of an Apatitic Calcium Phosphate Cement. *J. Dental Research* **76**: 905-912, 1997.
9. Norian Corporation, Constanz et al. Method for repairing bone. *United States Patent* # **5697981**, Issued 1997.
10. Shindo ML, Costantino PD, Friedman CD, Chow LC. (1993) Facial skeletal augmentation using hydroxyapatite cement. *Arch Otolaryngol Head Neck Surg*, **119**: 185-90.
11. Chalfie M, Tu Y, Euskirchen G, Ward WW, Prasher DC. (1994) Green fluorescent protein as a marker for gene expression. *Science*, **263**: 802-5.
12. Cherng A., Takagi S., Chow L. Effects of hydroxypropyl methylcellulose and other gelling agents on the handling properties of calcium phosphate cement. *J. Biomedical Material Research* **35**(3):273-277, 1997.
13. Morgan BA, Fekete DM. (1996) Manipulating gene expression with replication-competent retroviruses. *Methods Cell Biol*, **51**: 185-218.
14. Cepko CL, Fields-Berry S, Ryder E, Austin C, Golden J. (1998) Lineage analysis using retroviral vectors. *Curr Top Dev Biol*, **36**: 51-74

University Research Initiative Program for Combat Readiness  
Annual Report 06/01/98-05/31/99

PART 53-FORMS

53.301-298

<b>REPORT DOCUMENTATION PAGE</b>		Form Approved OMB No. 0704-0188	
Public reporting burden for this collection of information is estimated to average 1 hour per response, including the time for reviewing instructions, searching existing data sources, gathering and maintaining the data needed, and completing and reviewing the collection of information. Send comments regarding this burden estimate or any other aspect of this collection of information, including suggestions for reducing this burden, to Washington Headquarters Services, Directorate for Information Operations and Reports, 1215 Jefferson Davis Highway, Suite 1204, Arlington, VA 22202-4302, and to the Office of Management and Budget, Paperwork Reduction Project (0704-0188), Washington, DC 20503.			
1. AGENCY USE ONLY (Leave blank)	2. REPORT DATE  June 1, 1999	3. REPORT TYPE AND DATES COVERED  ANNUAL	
4. TITLE AND SUBTITLE Tissue-Engineered Cartilage and Advanced Bioadhesives for the Rapid Healing of Combat and Training Injuries to Bone		5. FUNDING NUMBERS Grant Number N00014-97-1-0806 PR Number 97PR06312-00 PO Code 353 Disbursing Code N68892 AGO Code N66020 Cage Code 4B489	
6. AUTHOR(S) Genge, Brian			
7. PERFORMING ORGANIZATION NAME(S) AND ADDRESS(ES) University of South Carolina		8. PERFORMING ORGANIZATION REPORT NUMBER N00014-97-1-0806-1	
9. SPONSORING / MONITORING AGENCY NAME(S) AND ADDRESS(ES) ONR		10. SPONSORING / MONITORING AGENCY REPORT NUMBER ONR	
11. SUPPLEMENTARY NOTES Prepared in coordination with University Research Initiative Program for Combat Readiness			
12a. DISTRIBUTION / AVAILABILITY STATEMENT APPROVED FOR PUBLIC RELEASE		12b. DISTRIBUTION CODE	
13. ABSTRACT (Maximum 200 words) Chondrocytes in fracture callous play a critical role in the process of repairing broken bones. Acceleration of growth, differentiation and mineralization of chondrocytes is key to developing effective therapies for more rapid healing and fracture repair of battlefield injuries to bone. It is known that expression of local growth factors plays a pivotal role in normal development and calcification of fracture-callous cartilage. Our ability to grow mineralizing chondrocyte cultures provides an outstanding opportunity to create a biomaterial that enables the expedited healing and repair of bone injuries. Using formulations of specific cytokines and growth factors, our chondrocyte cultures can be tissue-engineered to produce a matrix-mineral composite that may be implanted into the injury sites. We also propose to develop an advanced synthetic bioadhesive for immediate, in the field repair of fractured bone. We have discovered several distinct biochemical components crucial to bone mineral formation and have developed a proprietary process enabling a unique recombination of the purified components. This material can be formulated to harden with 2 hours and may be used to provide a bone-like weld in fractured bone to stabilize the injury. We anticipate that these novel biomaterials could tremendously speed the bone healing process.			
14. SUBJECT TERMS Chemical and Biological Warfare, Target Acquisition, Anti-Submarine, Combat Medicine, Biodeterioration, and Command Control and Communication.		15. NUMBER OF PAGES	
		16. PRICE CODE	
17. SECURITY CLASSIFICATION OF REPORT UNCLASSIFIED	18. SECURITY CLASSIFICATION OF THIS PAGE UNCLASSIFIED	19. SECURITY CLASSIFICATION OF ABSTRACT UNCLASSIFIED	20. LIMITATION OF ABSTRACT 200 words

NSN 7540-01-280-5500

Standard Form 298 (Rev. 2-89)

Prescribed by ANSI Std. Z39-18  
298-102



**SECTION V: ANTI-SUBMARINE WARFARE**

**Wavelet-Based Algorithms for Acoustic and Non-Acoustic  
Antisubmarine Warfare**

Terry Huntsberger

Intelligent Systems Laboratory  
Department of Computer Science  
University of South Carolina  
Columbia, SC 29208

Tel: (803)777-2404  
Fax: (803)777-3767  
Email: [terry@cs.sc.edu](mailto:terry@cs.sc.edu)

Björn Jawerth

Industrial Mathematics Initiative  
Department of Mathematics  
University of South Carolina  
Columbia, SC 29208

Tel: (803)777-6218  
Fax: (803)777-3783  
Email: [bj@math.sc.edu](mailto:bj@math.sc.edu)

## **Section 5-1: Wavelet-Based Algorithms for Acoustic/Non-Acoustic Antisubmarine Warfare**

Terry Huntsberger and Björn Jawerth

### **ABSTRACT**

The two main detection methods used in tactical antisubmarine warfare (ASW) are acoustic (sound) and nonacoustic. For the acoustic studies we are exploiting the similarity between the Helmholtz equation and Laplace's equation for the development of fast solver techniques for multi-line towed sonar array systems currently fielded by the Navy. Our work in non-acoustic ASW methods has concentrated on the study of boundary value problems for Maxwell's equations on arbitrary nonsmooth domains, in arbitrary dimensions and on the detection and analysis of submarine wakes from low grazing angle (LOGAN) radar data.

### **FORWARD**

This project was funded for \$525, 000 for the period June 1, 1997 to May 30, 2000. We have decided to use the SKY Computer system with 4 PowerPCs/36 SHARC DSP chips for the implementation of the algorithms. This decision was made after consideration of Navy needs and examination of the algorithms. The system has been ordered and is to be shipped May 1, 1998. The original Year 1 Milestone was the port of our algorithms to the Intel Paragon system, which was postponed due to system downtime.

### **REPORT**

#### ***Statement of the problem***

The Navy has recently developed a new lightweight directional hydrophone suitable for deployment in large numbers from aircraft. This is coupled with the multi-line towed sonar array system which has long-range capabilities and much wider field coverage. The images that are assembled from the towed sonar arrays can be efficiently processed and analyzed in the wavelet domain. In addition, operations such as image enhancement can be performed very efficiently in the wavelet coefficient space.

The results of preliminary studies demonstrate that appropriate layer potential singular integral operators can be used to obtain solutions to the time independent, or reduced, Maxwell's equations in three dimensions. Techniques centered around the second generation wavelets seem to be flexible enough to adapt to the efficient numerical treatment of full time dependent scattering problems even on nonsmooth domains. During the first phase of the project we have concentrated on the characterization of acoustic and electromagnetic scattering from surfaces and objects.

### ***Summary of the Most Important Results***

#### **Lattice Boltzmann Models for Advanced Sonar and Image Processing**

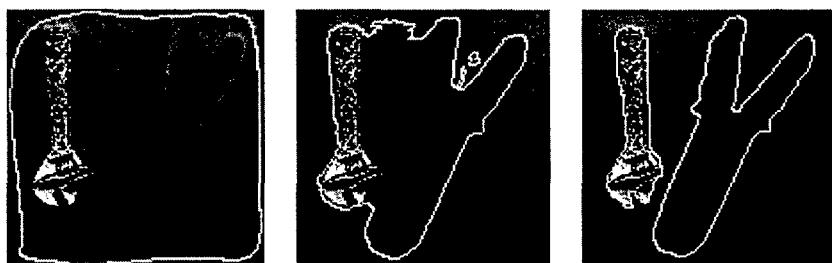
We have been continuing our studies on lattice Boltzmann models for advanced image processing algorithms. The principal advantage of the lattice Boltzmann method over traditional techniques for obtaining solutions of PDEs is that they are naturally well suited for fully parallel machines, resulting in very fast codes. Below we describe several different applications of the lattice Boltzmann model to sonar and image processing.

In recent years *nonlinear diffusion* has become a powerful tool for intra-region smoothing of images. The results of nonlinear diffusion can be used to obtain an enhanced image or as a precursor to higher-level processing such as image segmentation, shape description, and object detection and tracking. Based on our previously developed lattice Boltzmann models for anisotropic diffusion of images, we have developed a lattice Boltzmann model for image filtering by a reaction-diffusion equation. The advantage of using the reaction-diffusion equation is that it provides a nontrivial steady state, therefore eliminates the problem of choosing a stopping time in using the pure diffusion equation. We have tested our methods on various kinds of noisy images including infrared airborne radar images and sonar images. The results are promising.

*Mean curvature motion* appears in many natural and industrial problems in which sharp interfaces form and propagate. Notable examples include the growth of crystalline materials, the processing and enhancement of images, the propagation of flames, the evolution of ecological systems, and the waves of excitation that occur in heart and neural tissue. We have developed a lattice Boltzmann model for mean curvature motion. In our early approach we had focused on the level set formulation of mean curvature motion and had difficulty to obtain the proper collision operator in the lattice Boltzmann equation. We have overcome this difficulty by using the diffusion generated motion by mean curvature approach.

An important goal of computer vision is to recover the shapes of objects from various type of visual data. *Shape recovery* aids the tasks of object representation and recognition. Based on *diffusion generated motion*, we have developed a shape recovery system. We use the diffusion equation where the diffusion coefficient function depends on the image gradient. We initialize our system by using a simple image consisting of a black and a white area, where the black area covers the part of the image in which the objects need to be detected. Our system works by tracking the sharp interface between the black and the white region during the diffusion process. The diffusion coefficient function is constructed so that it forces the sharp interface to stop at the object boundary. Our system is capable of recovering shapes of multiple objects, and it automatically changes topology as it searches for the object boundary.

Recently, a new class of image coding methods, referred to as *second-generation image coding techniques*, has been developed. These methods attempt to describe the image in terms of physical entities such as sketch data or regions, to obtain a compact representation of the image. These second-generation image coding techniques have shown significant improvement over the traditional waveform representation based schemes, at low bit rates. However, one of the drawbacks of these methods is the large amount of computation time spent in the image reconstruction step. Recently we have developed a multi-scale lattice Boltzmann image reconstruction method for sketch based image compression. This method allows us to reduce the processing time for a 512x512 image from half an hour to 30 seconds, on a single 150MHz processor.



### Feature Driven Compression for Curves by Curvature

The purpose of this project is to develop a feature driven compression of curves represented as polygons. There are lots of applications (for example in computer vision) where objects can be represented as curves. An object may be represented by its contour or an image may be represented by its edges, for example.

Our goal is to construct a method for the compression of a curve, which maintains the shape of the curve. The meaning of the shape of a curve is not obvious, and should reflect properties perceived important by a human observer. Experimental studies on people shows that points on the curve with maximum curvature are considered to be the most significant parts of a curve. Since our curves are discrete, i.e., polygons, we therefore use a discrete measure of the curvature. We have used the definition of discrete curvature developed by B. Dahlberg, and also developed a discrete curvature measure more suited to our compression scheme.

We have investigated two types of compression methods. The first uses the lifting scheme as described Schroeder and Sweldens. The second is based on curve flows, and we have developed a discrete curvature based curve flow for polygons.

## **Electromagnetic Scattering from Non-Smooth Domains**

The boundary value problem for the time-harmonic Maxwell equations for a domain in 3D or 2D, can be reduced to solving a layer potential integral equation on the boundary (a surface in 3D or a curve in 2D) of the domain. Our goal is to develop fast wavelet-based solvers for layer potentials for the Laplace and Helmholtz equation.

To start with we have developed a new general class of piecewise polynomial wavelet bases. These are needed when discretizing the equations using the Galerkin method. The wavelet bases can also be constructed on triangulations. Our main goal has been to design bases for the numerical solution of integral and differential equations, but we also believe these bases could be used in CAGD.

The advantage of reducing a differential equation to a boundary integral equation is the reduction in dimension. A drawback, however, is that the discretization matrix becomes dense (for a differential equation the discretization matrix is sparse). Representing the matrix in a wavelet basis it becomes almost diagonal, though. The solution of linear systems arising from the discretizations of PDEs is today usually solved with multigrid methods. We have developed a wavelet-multilevel method similar to multigrid in structure and performance. Our method is applicable also to hierarchical bases, for example.

Currently, we are developing adaptive methods for the layer potentials as well as C++ class libraries for the numerical routines based on SparseLib++.

## **Hidden Markov Models and Automatic Target Detection**

We are currently investigating the use of HMM for detection and recognition of sonar signals. We are also trying to apply 3D gesture analysis methods from computer vision for object tracking in sonar image sequences.

### ***Publications and Technical Reports***

1. E.D. Sinzinger and B.D. Jawerth, "Surface representation from photometric stereo with wavelets", in *Proc. SPIE Conf. on Wavelet Applications*, Vol. 3169, San Diego, CA, 1997.
2. E.D. Sinzinger, "Numerical Methods for Ill-Posed Problems in Image Processing and Computer Vision", M.S. Thesis, Department of Computer Science, University of South Carolina, Columbia, SC, 1998.
3. T. Kubota and T. L. Huntsberger, "Edge dipole and edge field for boundary detection," in *Proc. SPIE Conf. Hybrid Image and Signal Processing VI*, Vol. 3389, Orlando, FL, Apr 1998.
4. F. Espinal and R. Chandran, "Wavelet-based fractal signature for texture classification," in *Proc. SPIE Conf. on Wavelet Applications V*, Vol. 3391, Orlando, FL, Apr 1998.

5. T. Kubota and T. L. Huntsberger, "Adaptive pattern recognition system for scene segmentation," *Optical Engineering, Special Section on Advances in Pattern Recognition*, Vol. 37, No. 3, pp. 829-835, 1998.
6. F. Espinal, T. L. Huntsberger, B. Jawerth, and T. Kubota, "Wavelet-based fractal signature analysis for automatic target recognition," *Optical Engineering, Special Section on Advances in Pattern Recognition*, Vol. 37, No. 1, pp. 166-174, 1998.
7. G. Fernandez and T. L. Huntsberger, "Wavelet-based system for recognition and labeling of polyhedral junctions," *Optical Engineering, Special Section on Advances in Pattern Recognition*, Vol. 37, No. 1, pp. 158-165, 1998.
8. T. Kubota, T. L. Huntsberger and C. O. Alford, "A vision system with real-time feature extractor and relaxation network," to appear in *Int. Journal Pattern Recognition and Artificial Intelligence*, May 1998.
9. B.D. Jawerth, P. Lin, and E.D. Sinzinger, "Lattice Boltzmann methods for anisotropic diffusion of images", *Mathematical Imaging*, in review.
10. H. Karlsson and L. Svensson, "Feature Driven Compression for Curves by Curvature", Master's Thesis, Chalmers University of Technology, Sweden.

#### ***Participating Personnel***

Dr. Terry Huntsberger, PI  
Dr. Björn Jawerth, co-PI  
Dr. Toshiro Kubota  
Dr. Weimin Zheng  
Dr. Peng Lin  
Dr. Jimmy Lu  
Dr. Chong Li  
Eric Sinzinger, M.S., Computer Science  
Martin Lindberg  
Henrik Storm  
Goran Kronquist  
Marcus Kozica, M.S., Mathematics  
Michael Cox

#### **BIBLIOGRAPHY**

- [HORN77] B. K. P. Horn, "Understanding image intensities", *Artificial Intelligence*, Vol. 8, pp. 201-231, 1977.
- [MARR79] D. Marr and T. Poggio, "A computational theory of human stereo vision", *Proceedings of the Royal Society of London*, Vol. 204, pp. 301-308, 1979.
- [ULLM79] S. Ullman, *The Interpretation of Visual Motion*, MIT Press, Cambridge, MA, 1979.
- [WOOD80] R. J. Woodham, "Photometric method for determining surface orientation from multiple images", *Optical Engineering*, Vol. 19, pp. 139-144, 1980.

University Research Initiative Program for Combat Readiness  
Annual Report 06/01/98-05/31/99

PART 53-FORMS

53.301-298

<b>REPORT DOCUMENTATION PAGE</b>		Form Approved OMB No. 0704-0188	
Public reporting burden for this collection of information is estimated to average 1 hour per response, including the time for reviewing instructions, searching existing data sources, gathering and maintaining the data needed, and completing and reviewing the collection of information. Send comments regarding this burden estimate or any other aspect of this collection of information, including suggestions for reducing this burden, to Washington Headquarters Services, Directorate for Information Operations and Reports, 1215 Jefferson Davis Highway, Suite 1204, Arlington, VA 22202-4302, and to the Office of Management and Budget, Paperwork Reduction Project (0704-0188), Washington, DC 20503.			
1. AGENCY USE ONLY (Leave blank)	2. REPORT DATE June 1, 1999	3. REPORT TYPE AND DATES COVERED Annual	
4. TITLE AND SUBTITLE Wavelet-Based Acoustic/Non-Acoustic AntiSubmarine Warfare		5. FUNDING NUMBERS Grant Number N00014-97-1-0806 PR Number 97PR06312-00 PO Code 353 Disbursing Code N68892 AGO Code N66020 Cage Code 4B489	
6. AUTHOR(S) PI: Björn Jawerth			
7. PERFORMING ORGANIZATION NAME(S) AND ADDRESS(ES) University of South Carolina		8. PERFORMING ORGANIZATION REPORT NUMBER N00014-97-1-0806-1	
9. SPONSORING / MONITORING AGENCY NAME(S) AND ADDRESS(ES) ONR		10. SPONSORING / MONITORING AGENCY REPORT NUMBER ONR	
11. SUPPLEMENTARY NOTES Prepared in coordination with University Research Initiative Program for Combat Readiness			
12a. DISTRIBUTION / AVAILABILITY STATEMENT  APPROVED FOR PUBLIC RELEASE		12b. DISTRIBUTION CODE	
13. ABSTRACT (Maximum 200 words)  The two main detection methods used in tactical antisubmarine warfare (ASW) are acoustic (sound) and nonacoustic. For the acoustic studies we are exploiting the similarity between the Helmholtz equation and Laplace's equation for the development of fast solver techniques for multi-line towed sonar array systems currently fielded by the Navy. Our work in non-acoustic ASW methods has concentrated on the study of boundary value problems for Maxwell's equations on arbitrary nonsmooth domains, in arbitrary dimensions and on the detection and analysis of submarine wakes from low grazing angle (LOGAN) radar data.			
14. SUBJECT TERMS Antisubmarine Warfare, Wavelets		15. NUMBER OF PAGES 6 pages	
		16. PRICE CODE	
17. SECURITY CLASSIFICATION OF REPORT  UNCLASSIFIED	18. SECURITY CLASSIFICATION OF THIS PAGE  UNCLASSIFIED	19. SECURITY CLASSIFICATION OF ABSTRACT  UNCLASSIFIED	20. LIMITATION OF ABSTRACT  200 words

NSN 7540-01-280-5500

Standard Form 298 (Rev. 2-89)  
Prescribed by ANSI Std. Z39-18  
298-102



## **Real-Time UV Fluorescence for Dissolved Hydrocarbon Tracking**

M.L. Myrick

Department of Chemistry and Biochemistry  
University of South Carolina  
Columbia, SC 29208

Tel: (803) 777-6018  
Fax: (803) 777-9521  
Email: [myrick@psc.sc.edu](mailto:myrick@psc.sc.edu)

## Section 5-2: Real-Time UV Fluorescence for Dissolved Hydrocarbon Tracking M.L. Myrick

### ABSTRACT

We have begun and nearly completed construction of our underwater fluorimeter system following the Y1 design process. Initial testing has yielded detection limits for fluorescein of 2 *parts per trillion* in clean water, with integration times of a few seconds, about 1000 times better than with our first generation instrument before this project. The result will be a very sensitive, unique underwater fluorimeter capable of analyzing complex organic mixtures in water. We have also done studies of water from local rivers, and have shown that we can use 2-D fluorimetry to distinguish water from two nearby watersheds with great ease, and can follow the mixing of these natural water sources for two miles below the confluence of the rivers. In addition, we are participating in a joint proposal with Oregon State University for oceanographic applications of our 2-D fluorimetry system, and commercial development to follow this project by WETLabs, Inc. of Philomath, OR.

### FORWARD

This project was initially funded in June, 1997 at the level of \$293,000 over three years. Our important milestones this year have been:

- construction of hardware
- measurement of the first 2-D fluorescence spectra with our instrument under development
- Demonstration of the use of 2-D fluorimetry in identifying water sources.
- Detection limits of 2 ppt for fluorescein in water.

### REPORT

#### *Statement of the problem*

Our project is to design and construct a 2nd-generation two-dimensional fluorimeter for rapid detection and speciation of organic compounds in seawater. The purpose of this detection is to recognize the presence of anthropogenic hydrocarbons associated with submarine activity, and to use this hydrocarbon signature for tracking purposes.

#### *Background*

Aromatic hydrocarbons are pervasive environmental contaminants of waters, originating from both natural and man-made sources. Examples are humic and fulvic acids, which are naturally-occurring mixtures of aromatic organic acids leached from decaying plant matter, and petroleum refinates containing heavier polyaromatic compounds such as naphthalene (C<sub>10</sub>H<sub>8</sub>) and

anthracene (C<sub>14</sub>H<sub>10</sub>), and pesticides. Complex residues of many compounds are found as contaminants in water that originate from fuels and dissolution of plasticizers from polymers. Examples of these residues might include marine greases leaching into seawater or the dissolution of diesel fuel from the leaking seals of an engine into water.

Conventional methods for detecting aromatic hydrocarbons (e.g., GC-MS) in water rely on sampling the water and transporting the sample to a laboratory for analysis, often requiring a week or more. While extremely sensitive and accurate, such cumbersome and expensive procedures prevent extensive study of transport phenomena for aromatic compounds in aqueous media and frustrate the continuous monitoring that would be necessary to control discharges and/or provide real-time location of sources.

Fluorescence is an extremely sensitive method for detecting compounds which fluoresce, typically yielding detection limits approaching or exceeding 1 ppb. Using appropriate instrumentation, fluorescence spectra can be acquired on the 1-second to 10-second time scale, enabling measurements in near-real-time. Conventional fluorescence measurements are performed by selecting a particular wavelength for sample excitation (typically in the UV spectral region for small organic compounds), and then monitoring the emission intensity of the sample as a function of wavelength. The primary limitation in the use of these conventional measurements is that spectra of mixtures tend to be highly overlapped, so that clear distinction of the contributions made by individual components is difficult. As a result of this spectroscopic overlap, fluorescence is rarely used in cases where the concentrations of a single or few components are desired from a complex or unknown matrix.

One way around this problem is to record emission spectra using a series of different excitation wavelengths - the resulting excitation-emission-matrix (EEM) spectrum has the format of an "image" rather than a "spectrum", and contains sufficient information to differentiate contributions from distinct species in the mixture. The statistical basis for "higher-order" data analysis is currently being refined. The Investigator (M.L. Myrick) and his laboratory have been involved in the development of optical methods for the detection of organic residues in water for 3+ years, and have recently published reports of extremely rapid (e.g., <10 second total analysis) 2-D detection of contaminants.[1,2]

### ***Summary of the Most Important Results***

The project can be divided into the following tasks:

Year 1 tasks: (a) hire a post-doctoral associate with experience in two-dimensional spectroscopic analysis, (b) train the post-doc in higher-order data analysis, programming and instrument design/construction as needed, (c) review available light sources, spectrometers and detectors, (d) determine whether commercial components are compatible with the design goals of the instrumentation we are to construct and evaluate, (e) in cases where commercial components are inadequate to meet the goals of the system, design adequate components, (f) evaluate computational and communication needs and review available technology, resolving any problems that will be unique to the new instrumentation.

Year 2 tasks: (g) acquire components and begin construction and assembly, (h) write dedicated software to implement the selected three-mode data analytical methodology selected above and to control all aspects of the instrument operation and data interpretation, (i) complete instrument construction in pressure vessel, (j) integrate software and hardware and test on prepared standard samples, and

Year 3 tasks: (k) deploy instrument in Lake Murray, S.C. and at the USC Marine Field Station.

All of the Y1 tasks were completed. In the Y2 task list, tasks g and i are essentially complete, and tasks h and j are partially complete. We added a task to the Y2 list as well: the demonstration of 2-D fluorimetry in determining the sources of water in rivers below their confluence.

We will first deal with the hardware aspects of our construction over the past year.

**Components for the 2-Dimensional Fluorimeter.** Necessary optical components such as a 75W Xenon lamp (Oriel), EB-CCD camera including interface to computer (Hamamatsu), optical lenses (Newport), etc were purchased. Some mechanical components such as the lamp housing, mechanical frames and attachments to hold optical components were designed and built to fit into a 6-inch diameter metal pressure case made of aluminum. The pressure case has also been manufactured. Power supplies for the low-wattage lamp and CCD camera were purchased.

**Instrument Development.** The design for the instrument is shown in Figure 1. The instrument is designed to fit into two 6-inch diameter, 25 inch long cylinders which serve as pressure cases. The cylinders, on completion, will be oriented at 90 degrees to one another and sealed together with o-rings. Thus far, everything is complete about the instruments except the underwater sampling system, installation of leakproof power and data connectors and the sealing ring to connect the two cases together.

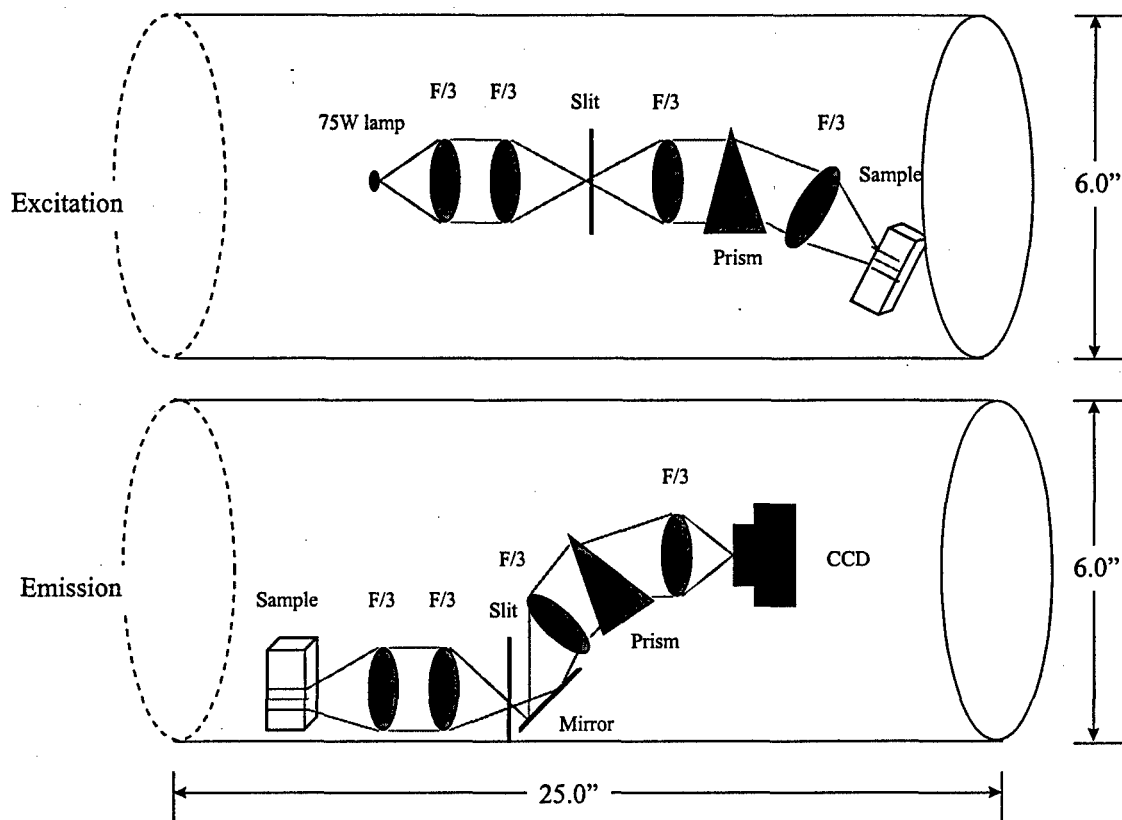


**Figure 1** Side view schematic of the 2-dimensional fluorometer.

Figure 2 below shows the instrument in its current state of construction. The instrument is currently being assembled on a laboratory bench, and therefore the pressure cases are not encasing the rest of the optics in the photographs. The final assembly into the pressure cases should be completed by approximately June, 1999.

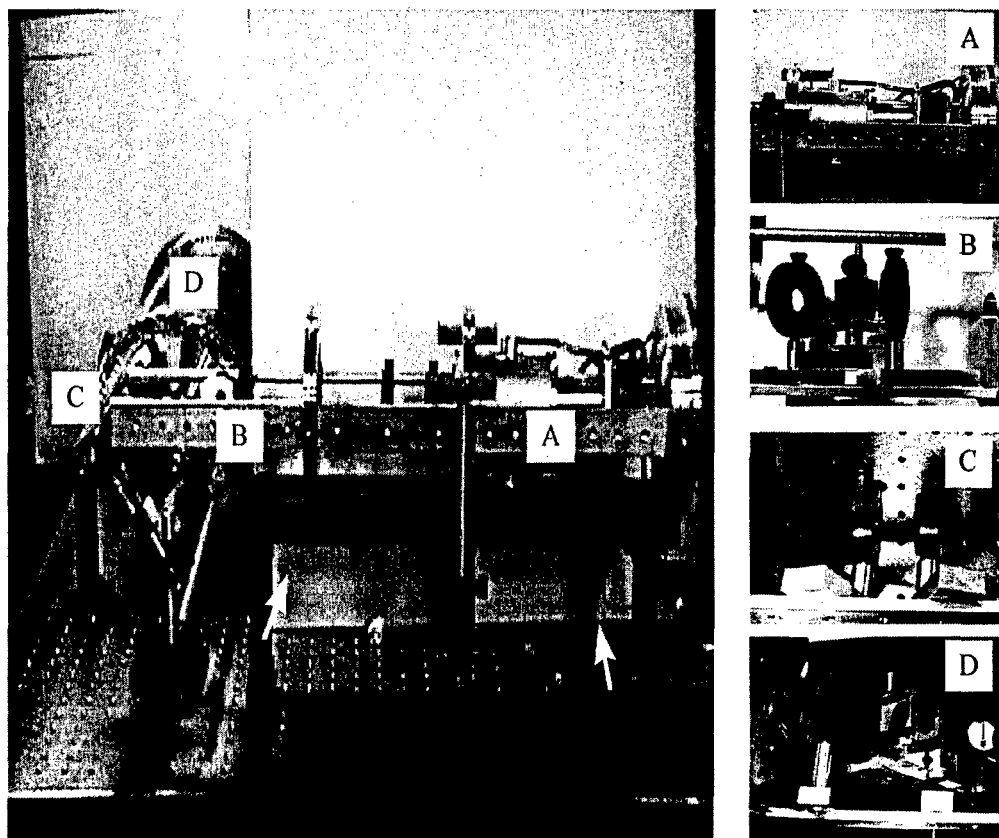


**Figure 2** Photographs of the 2-dimensional fluorometer at present.

**Experimental Data.** The system, although not complete, is sufficiently complete for experimental work on the laboratory bench where it is being assembled. Two-dimensional fluorescence spectra of Fluorescein, Rhodamine 6G, and Nile Red are shown in Figure 3. We note that these samples are poor for demonstrating the system because they all absorb and emit in the visible portion of the spectrum, where the prism spectrometers perform poorly. Nevertheless, we can easily see the differences in and the structures of the 2-D fluorescence spectra of these samples: the  $\lambda_{ex}/\lambda_{em}$  of Fluorescein, Rhodamine 6G, and Nile red are at 490/526, 520/554, and 560/630 nm. We measured the detection limits for Fluorescein and Rhodamine 6G as 0.01 nM and 0.1 nM, respectively, with our new instrument with only a few seconds of measurement. These values correspond to approximately 2 and 20 parts per trillion, about  $10^3$  better than were

obtained with our first generation instrument using a much higher-power lamp system for excitation. The differences in sensitivity can be attributed to increased quantum efficiency of the detector (about a factor of 20) and to the increased optical throughput of the spectrometers (approximately a factor of 20 in this wavelength range), plus the somewhat higher power density of the lamp. All these factors were designed into the instrument during Y1.

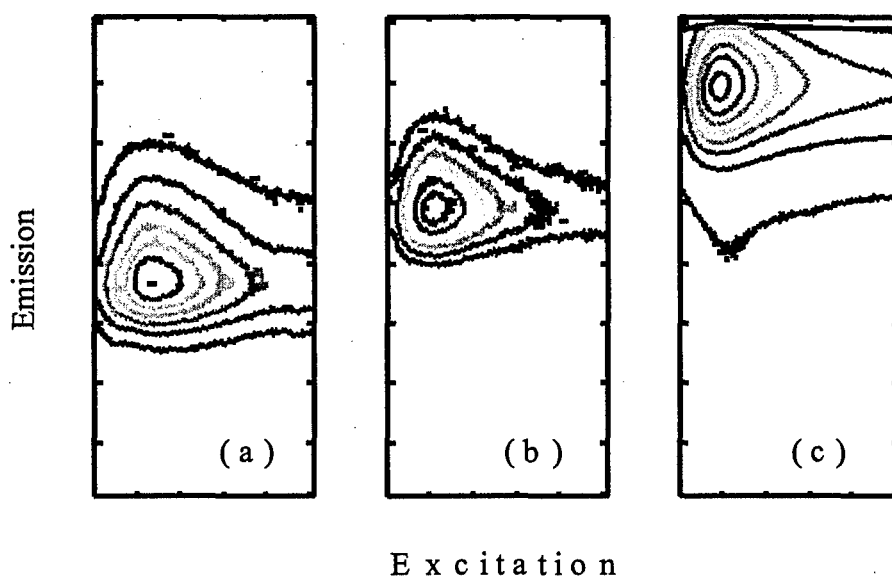


**Figure 3** 2-Dimensional fluorescence spectra of 20 nM Fluorescein (a), 20nM Rhodamine 6G (b), and 50 nM Nile Red (c) got by our 2-dimensional fluorometer.

#### **Determination of Water Sources in the Congaree River.**

During the passage of water through a river drainage basin, a variety of natural and anthropogenic organic compounds can enter the water and be transported great distances. Examples of the type of compounds that can be found in rivers include natural humic and fulvic acids, plant pigments, agricultural chemicals, petroleum distillates, and the residues from upriver industrial processes. A real-time knowledge of the types of compounds occurring in river waters can be used for a variety of purposes. As examples, minor leaks from submerged pipelines could be detected and repaired before major spillage occurs, upstream agricultural practices could be deduced, chemical releases could be tracked and some knowledge of upstream covert chemical processing could be gleaned.

In this study, we explored two-dimensional (2-D) fluorescence spectroscopy as a tool for elucidating the complex chemical composition and diverse sources of DOM in natural water. Two types of DOM fluorescence signals have often been observed in natural water, (a) a humic-like, or gelbstoff fluorescence, which occurs at 420-450 nm from excitation at 230-260 and 320-350 nm, and (b) a protein- or amino acid-like fluorescence with maxima between 300-305 nm and 340-350 nm with excitation at 220 and 275 nm, respectively<sup>1-8</sup>. In the present report, we have applied 2-D fluorescence to water samples from the Congaree River, the Broad River and the Saluda River in SC. These last two rivers converge at Columbia, SC to form the Congaree, and we use 2-D fluorescence to identify the constituent waters and how they mix at the confluence of the rivers.

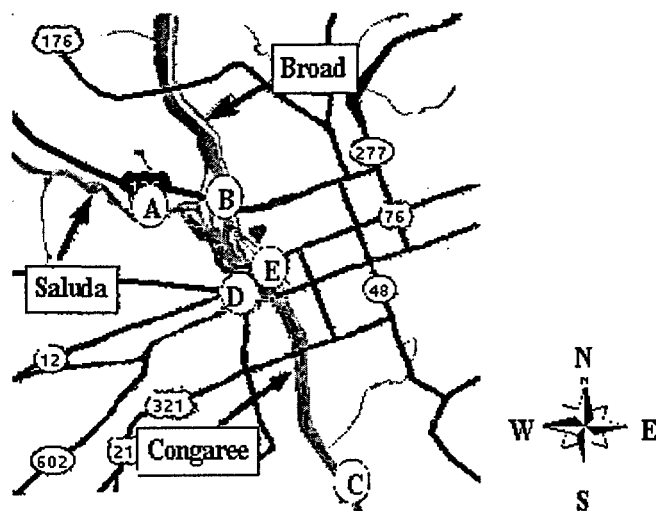


Figure 4 – Sampling Sites

Figure 4 shows a map of the Columbia area and the sites, A-E, at which river samples were taken on six separate occasions. Two of the sites (A and B) were on the convergent rivers, the Saluda and Broad. Two of the remaining three were at the point of confluence but opposite sides of the Congaree River, with site D being on the Saluda side, and site E being on the Broad side. The last site, site C, was two miles below the confluence.

Figure 5 below shows 2-D fluorescence for the first three sampling times

(covering three weeks) at sites A and B. As the figures show, there are distinct differences between the two rivers.



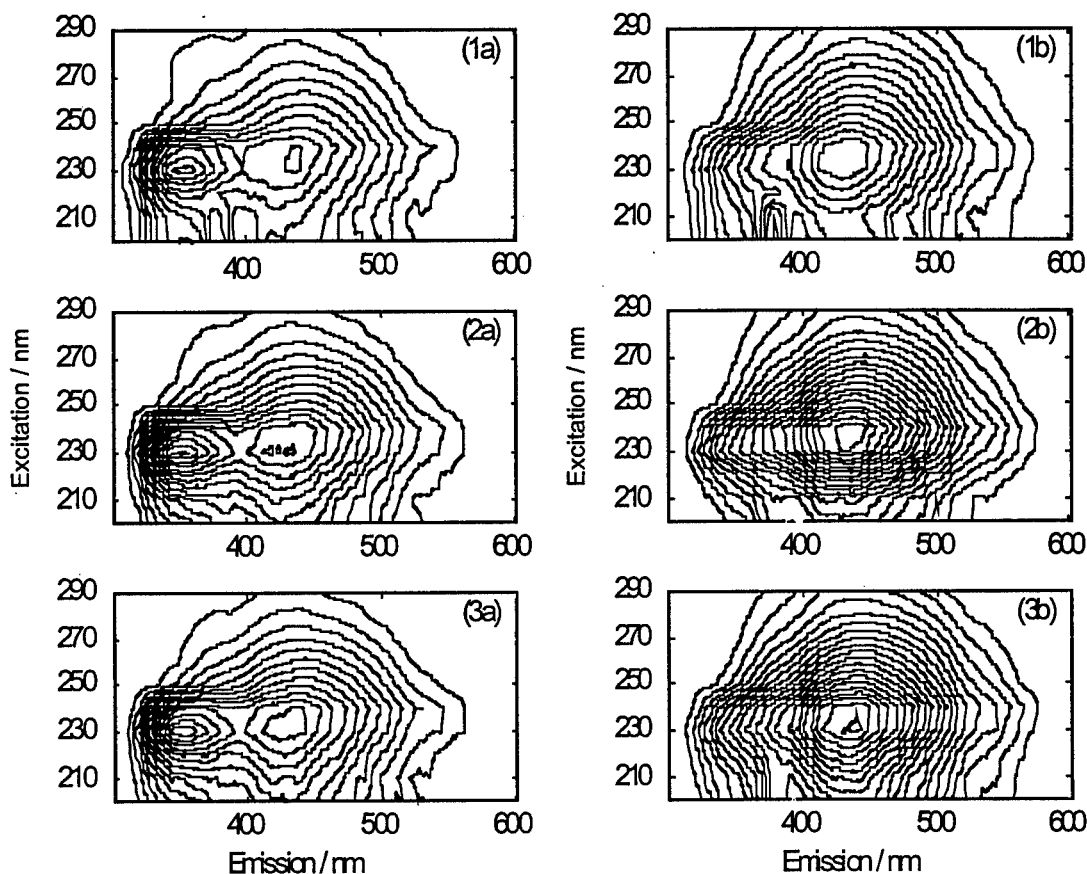


Figure 5 – Saluda (a) and Broad (b) river samples on the first three sampling occasions.

We were able to show that these waters form additive mixtures, which means that linear modeling is sufficient to make predictions of the relative concentrations of the two source waters in the Congaree at any point, with an error of less than 5% v/v. When we made such a model, we found that Site D in the Congaree was nearly pure Saluda river water, while Site E was nearly pure Broad river water. Site C showed nearly complete mixing of the two rivers.

We were also able to use PARAFAC modeling to show that there were two main contributors to the fluorescence of the water samples, and to extract their excitation and emission spectra. Figure 6 below shows the excitation and emission profiles were determined for the two water species (called Factors in the modeling).

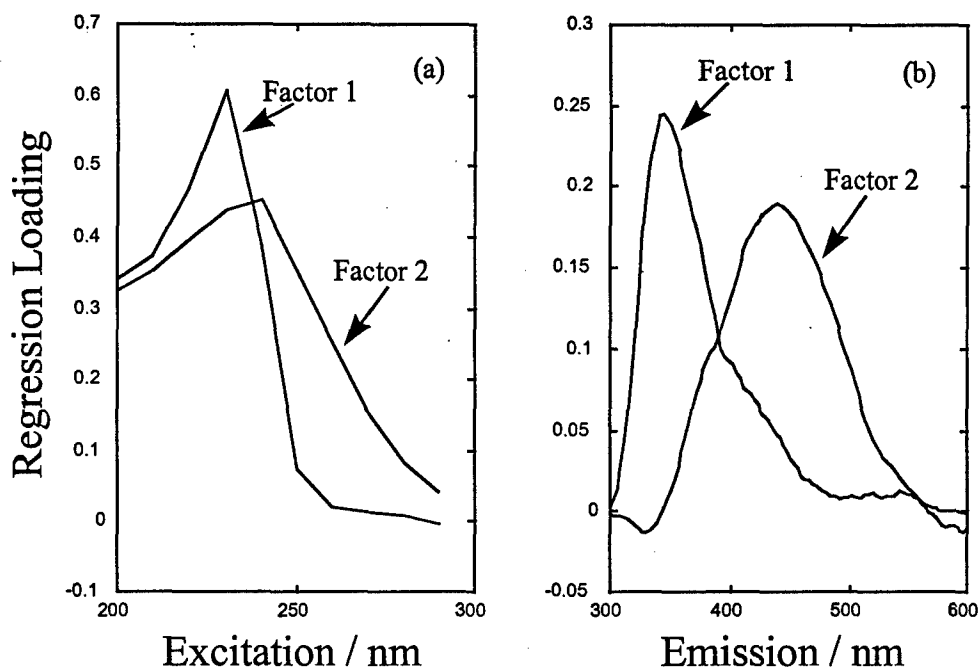


Figure 6 – Excitation and Emission spectra for humic and fulvic acids in Columbia Rivers

### Collaborations

A collaboration has developed with Dr. Nathan Brandstater, an assistant professor in the Department of Chemistry at East Carolina University, in Greenville, NC. Dr. Brandstater is currently using one of our 2-D fluorimeters in his laboratory for environmental studies, and works with Dr. Paul Gemperline of the same institution on multivariate mathematical modeling for application to 2-D fluorescence spectroscopy.

In addition, a collaboration may develop between the Drs. Timothy J. Cowles and Dr. Russell Desiderio of the Oceanography department at Oregon State University. We plan to submit a collaborative separate grant for follow-up work on 2-D fluorescence using the instrument constructed under the present project; NSF is the likely funding source for this grant.

### Publications and Technical Reports

- 1) "Detection of Water-Soluble Petrochemicals by UV-induced Fluorescence" A. Muroski, M. Groner, E.L. Raleigh and M.L. Myrick Marine Pollution Bulletin (submitted, 1999).
- 2) "Determination of Water Sources for the Congaree River in Columbia, SC Using Two Dimensional Fluorescence Spectroscopy" Yuan Yan, Hong Li and M.L. Myrick Marine Chemistry (submitted, 1999).
- 3) "Construction and Characterization of an Underwater High-Performance Two-Dimensional

Fluorescence Spectrometer System" Yuan Yan and M.L. Myrick (manuscript in preparation, 1999).

- 4) "Using Two-Dimensional Fluorescence Spectra to Determine the Origin of Water in the Congaree River in Columbia" Yuan Yan, Hong Li and M.L. Myrick presented at the Pittsburgh Conference on Analytical Chemistry, March 7-12, 1999, Orlando Florida.

#### ***Participating Personnel***

A post-doctoral associate, Dr. Yuan Yan, was hired in January, 1998. Dr. Matthew P. Nelson has also been supported partially by this subgrant. Dr. Nelson received his Ph.D. in December, 1998.

#### **BIBLIOGRAPHY**

1. "Single-Measurement Excitation/Emission Matrix Spectrofluorometer for Determination of Hydrocarbons in Ocean Water 1. Instrumentation and Background Correction" A.R. Muroski, K.S. Booksh and M.L. Myrick Anal. Chem. 68(1996), 2524.
2. "Single-Measurement Excitation/Emission Matrix Spectrofluorometer for Determination of Hydrocarbons in Ocean Water 2. Calibration and Quantitation of Naphthalene and Styrene" K.S. Booksh, A.R. Muroski and M.L. Myrick Anal. Chem. 68(1996), 3539.
3. O.V. Mazurin, M.V. Streltsina and T.P. Shvaiko-Shvaikovskaya "Handbook of Glass Data: Part A", Elsevier (New York), 1983.
4. "Multiple Excitation Fluorometer for In Situ Oceanographic Applications" R.A. Desiderio, C. Moore, C. Lantz and T.J. Cowles Appl. Optics 36(1997), 1289.
5. "Microstructure Profiles of Laser Induced Chlorophyll Fluorescence Spectra: Evaluation of Backscatter and Forward Scatter Fiber Optic Sensors" R.A. Desiderio, T.J. Cowles, James N. Moum, Michael Myrick J.Atmos.Oceanic Tech. 10(1993),209.
6. "Fluorescence Microstructure using a laser/fiber optic profiler" T.J. Cowles, R.A. Desiderio, J.N. Moum, M.L. Myrick, D.G. Garvis, S.M. Angel Ocean Optics 10 R.W. Spinrad, Ed., SPIE Vol. 1302, p. 336 (1990).

University Research Initiative Program for Combat Readiness  
Annual Report 06/01/98-05/31/99

PART 53-FORMS

53.301-298

REPORT DOCUMENTATION PAGE		Form Approved OMB No. 0704-0188	
Public reporting burden for this collection of information is estimated to average 1 hour per response, including the time for reviewing instructions, searching existing data sources, gathering and maintaining the data needed, and completing and reviewing the collection of information. Send comments regarding this burden estimate or any other aspect of this collection of information, including suggestions for reducing this burden, to Washington Headquarters Services, Directorate for Information Operations and Reports, 1215 Jefferson Davis Highway, Suite 1204, Arlington, VA 22202-4302, and to the Office of Management and Budget, Paperwork Reduction Project (0704-0188), Washington, DC 20503.			
1. AGENCY USE ONLY (Leave blank)	2. REPORT DATE June 1, 1999	3. REPORT TYPE AND DATES COVERED Annual	
4. TITLE AND SUBTITLE Real-Time UV Fluorescence for Dissolved Hydrocarbon Tracking		5. FUNDING NUMBERS Grant Number N00014-97-1-0806 PR Number 97PR06312-00	
6. AUTHOR(S) M.L. Myrick		PO Code 353 Disbursing Code N68892 AGO Code N66020 Cage Code 4B489	
7. PERFORMING ORGANIZATION NAME(S) AND ADDRESS(ES)  University of South Carolina		8. PERFORMING ORGANIZATION REPORT NUMBER  N00014-97-0806-1	
9. SPONSORING / MONITORING AGENCY NAME(S) AND ADDRESS(ES)  ONR		10. SPONSORING / MONITORING AGENCY REPORT NUMBER  ONR	
11. SUPPLEMENTARY NOTES Prepared in coordination with University Research Initiative Program for Combat Readiness			
12a. DISTRIBUTION / AVAILABILITY STATEMENT  APPROVED FOR PUBLIC RELEASE		12b. DISTRIBUTION CODE	
13. ABSTRACT (Maximum 200 words) We have begun and nearly completed construction of our underwater fluorimeter system following the Y1 design process. Initial testing has yielded detection limits for fluorescein of 2 parts per trillion in clean water, with integration times of a few seconds, about 1000 times better than with our first generation instrument before this project. The result will be a very sensitive, unique underwater fluorimeter capable of analyzing complex organic mixtures in water. We have also done studies of water from local rivers, and have shown that we can use 2-D fluorimetry to distinguish water from two nearby watersheds with great ease, and can follow the mixing of these natural water sources for two miles below the confluence of the rivers. In addition, we are participating in a joint proposal with Oregon State University for oceanographic applications of our 2-D fluorimetry system, and commercial development to follow this project by WETLabs, Inc. of Philomath, OR.			
14. SUBJECT TERMS Chemical and Biological Warfare, Target Acquisition, Snti-Submarine, Combat Medicine, Biodeterioration, Command Control and Communication		15. NUMBER OF PAGES 13	
		16. PRICE CODE	
17. SECURITY CLASSIFICATION OF REPORT  UNCLASSIFIED	18. SECURITY CLASSIFICATION OF THIS PAGE  UNCLASSIFIED	19. SECURITY CLASSIFICATION OF ABSTRACT  UNCLASSIFIED	20. LIMITATION OF ABSTRACT  200 WDS

NSN 7540-01-280-5500

Standard Form 298 (Rev. 2-89)

Prescribed by ANSI Std. Z39-18  
298-102

**SECTION VI: BIODETERIORATION**

## **Accelerated Research in Biofouling Control**

Madilyn Fletcher

Belle W. Baruch Institute for Marine Biology and Coastal Research  
University of South Carolina  
Columbia, SC 29208

Tel: (803)777-5288  
Fax: (803)777-3935  
Email: [fletcher@biol.sc.edu](mailto:fletcher@biol.sc.edu)

## **Section 6-1: Accelerated Research in Biofouling Control**

M.Fletcher

### **ABSTRACT**

The formation of biofouling communities on deployment devices, sensors, and on ship and submarine hulls represents a significant limitation to the efficient operation of instrumentation and vessels. We have proposed novel approaches for control of microbial biofouling by (1) developing fouling-resistant surfaces based on information gained through experiments with alkanethiol self-assembled monolayers (SAMs), and (2) determining the microbial community structures that comprise the biofouling process, particularly those that form on surface chemistries with reduced fouling potential. Initial experiments focused on disordered layers of polar organic structures, whereas we have now turned to alkanethiol SAMs and are developing a combinatorial approach for assessment of a wide range of surface chemistries. Methods have been developed to prepare and assay multiple SAMs (20-30 per assay) for bacterial attachment, to quantify the extent of bacterial colonization over time, and to identify bacterial colonizers using molecular techniques (16S rRNA cloning and sequencing). We have yet to identify a surface chemistry that resists bacterial attachment and colonization. However, molecular biology approaches have demonstrated that different species attach to different surfaces within the first few days of exposure to seawater, and that these differences diminish with time as colonization proceeds. Future research will focus on (1) an extensive screening of the antifouling potential of functionally diverse SAMs, and (2) molecular identification of pioneer bacterial species, as well as differences in colonizing communities on different surfaces, particularly those which ultimately demonstrate the greatest antifouling potential.

### **FORWARD**

The total award for this project is \$383,251 for the budget period of 6/01/97-6/29/2000. In the initial stage of the project period, work has focused on (1) generation of a range of organic polymer surfaces with potential antifouling properties, (2) measurement of bacterial attachment to these test surfaces, and (3) characterization of microbial communities attached to a subset of the test surfaces. Early in this project, we shifted from our originally proposed test surfaces (self-assembled monolayers (SAMs) to organic oligomer and polymer coatings, in order to address robust material with the potential for application in situ. However, to date, the oligomers tested have not reduced bacterial attachment and progress has been relatively slow because of the time required to produce and analyze these coatings. Thus, we have returned to our original concept of utilizing SAMs to determine specific chemistries that prevent attachment of fouling organisms.

We have developed a rapid and efficient method for constructing and testing the antifouling potential SAMs on glass slides and microtiter plates. The SAM-coated glass-slides and microtiter plates are easily manipulated for immersion in marine environments for defined periods. The abundance of microorganisms colonizing a test surface can be approximated by staining with acridine orange (AO) and using a specially-equipped microtiter plate reader which can detect fluorescence at specific emission/excitation wavelengths. The advantage of this method over previous methods developed by us is that we are now able to rapidly screen multiple SAMs in a single microtiter plate without the need of performing laborious and time-consuming microscopic analysis. We are now focusing on upscaling the production and testing of SAM-coated microtiter plates in order to approach the problem of biofouling and cell adhesion from a new, combinatorial direction. Identification of test surfaces having high or low bacterial abundances will be further characterized by using multiphoton microscopy. To determine if the distribution of cells and polymers on SAMs with surface chemistries of interest. Characterization of the whole community by stable low-molecular weight 5S rRNA (SLMW-RNA) analysis has revealed that there was no apparent difference in the community compositions on different surface chemistries after 7 days incubation in marine mesocosms and in the environment. Analysis of constituent species in microbial biofilms by 16S RNA sequencing and of biofilm polymers has been initiated. Results from 16S RNA sequencing revealed that specific groups of bacteria colonize different surfaces on days 1 to 3. This finding supports the concept that some groups of bacteria seek certain kinds of surfaces to attach to, and that those that attach become the "first colonizers". It is important to recognize that the "first colonizers" may only be a transitory phase of biofilm development since SLMW-RNA research indicate that the "first colonizers" are probably not a significant component of the biofilm on day 7. Future experiments are needed to support or refute this hypothesis.

Major achievements for this report period are:

- Methods have been developed to use combinatorial chemistry for depositing novel SAMs on glass slides and microtiter plates.
- Methods have been developed for quantifying microbial abundances by using microscopic image analysis and by using a specially-equipped microtiter reader.
- Molecular biology approaches have indicated that different species colonize different surfaces in the first stages of colonization (1-3 days), but communities develop into similar compositions on all surfaces tested to date by day 7.

## REPORT

### *Statement of the problem*

The future of combat-readiness in ocean systems will involve the use of "tactical oceanography" to promote successful accomplishment of military missions. This will include sensor deployments, the use of sophisticated undersea coastal surveillance systems to detect, recognize, and track potential "unfriendly" objects (Incze, 1996). Such



systems will reduce risks to U.S. forces while maximizing the probability of success on a mission (Parrish et al., 1996). The formation of biofouling communities on deployment devices, sensors, and on ship and submarine hulls represents a significant limitation to the efficient operation of vessels and sensors.

The formation of a biofouling community occurs through a sequence of specific, poorly understood chemical and biological processes. Biofouling begins with formation of a conditioning layer of solutes which forms spontaneously on any submerged surface (Marshall, 1985). Once the conditioning film is in place, bacterial attachment to the surface and the formation of a biofilm microbial community begins. The climax biofilm microbial community then develops through a series of successional events (Lappin-Scott and Costerton, 1989; Wolfaardt et al., 1994), which are particularly poorly understood for surfaces in the marine environment. During and after the development of the biofilm microbial community, planktonic juveniles of sessile invertebrate species recruit onto the surface, ultimately resulting in a mature biofouling community with all its attendant problems.

The proposed research focuses on two aspects of the biofouling process: (1) initial attachment of bacteria to newly immersed surfaces and the development of attachment-resistant surfaces, and (2) colonization of surfaces by assemblages of microorganisms and microbial interactions that stabilize fouling communities. Preliminary studies (Wienczek and Fletcher, 1995; Ista et al., 1996) indicate the self-assembled monolayers (SAMs) offer a new approach for developing highly effective, fouling resistant surfaces. Researchers of the University of South Carolina (USC) are at the forefront in the construction of SAMs of various types and evaluating bacterial adhesion on such substrata. Our ultimate objective is to create a specific organic polymer surface that is virtually fouling-resistant.

### ***Summary of the Most Important Results***

**Production of functionalized surfaces.** In initial studies, sample preparation of the test surfaces was a lengthy process requiring at least 48-h for the front and reverse sides of the plastic plates to be cured. Small plastic coupons (7.6 x 2.5 cm) were needed for the microscopic analysis and large coupons (30 x 30 cm) were needed for molecular analysis. The large plates were necessary because preliminary studies revealed that too few microorganisms were attached to the small plastic coupons to perform molecular analysis. Test surfaces were prepared as follows (Fig. 1): (1) the protecting sheet of the plastic coupon was removed, (2) the coupon was placed in a fume hood and spray-coated with a clear epoxy paint, (3) the cured epoxy layer was sprayed with an overlayer of polyurethane paint, and (4) the functionalized polymers were applied (the top-coat) (Fig. 1). The polyurethane consisted of a polyester polyol (Desmophen R-221-75) and the isocyanurate of hexamethylenediisocyanate (Desmodur N-3300), which react to form the polyurethane. Cobalt 2-ethylhexanoate was used as catalyst for the crosslinking of the polyurethane components. Desmodur was used in a 10 % molar excess on one side to leave some available isocyanate groups with which the top-coat can react. The top-coat

was cured at room temperature in a glove bag with a constant flow of nitrogen to prevent atmospheric moisture from reacting with the isocyanate moiety, weakening the surface coating.

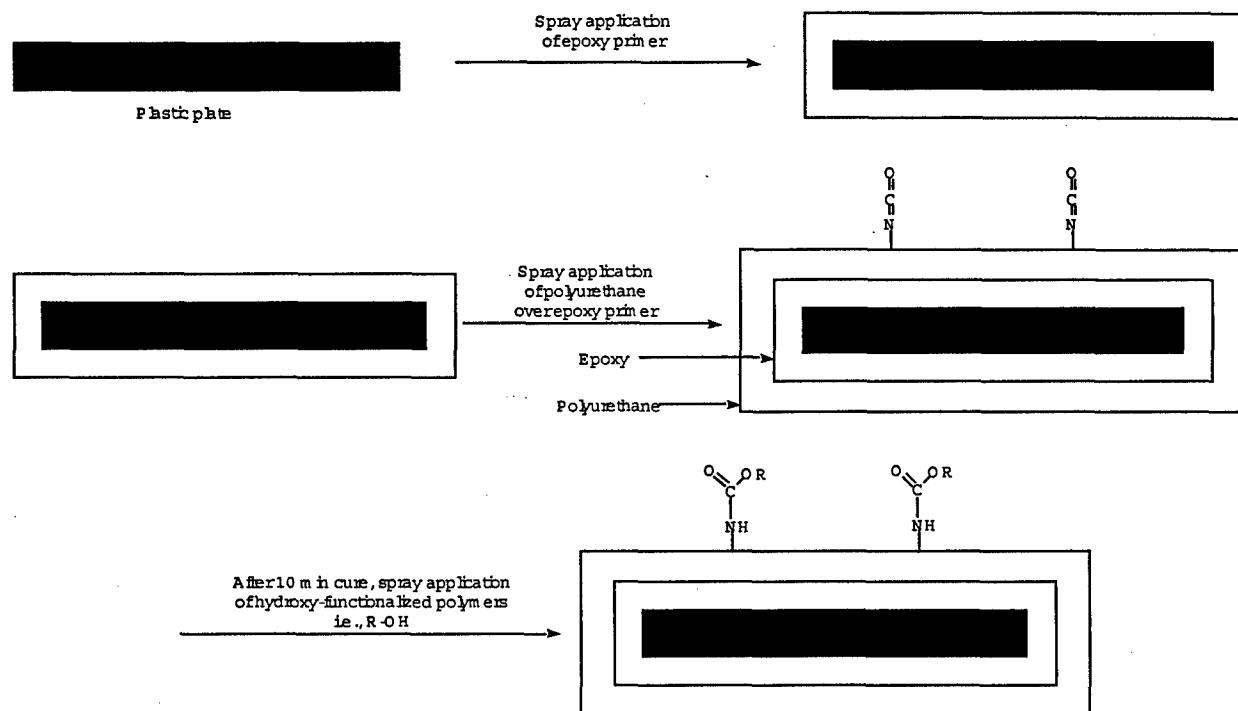


**Fig. 1.** Schematic diagram of protocol to coat plastic coupons with monomers and polymers.

The surfaces which have been generated are: (1) PEG-OH (hydroxy-terminated PEG) with 200, 300, 400, 600, 1,000 and 35,000 MWs; (2) PEG-OMe (methoxy-terminated PEG) of 350, 550, 750 MWs; (3) polyvinyl alcohol (PVA) of 13,000 - 23,000 MWs; (4) poly(2,6-dibromophenylene oxide; 6000 (Br(p)); and (5) bis (2-hydroxyethyl ether) of tetrabromo bisphenol-A (Br(m)). The Br(m) and Br(p) are bromophenyl compounds have similar structures to those found in sponge-associated bacteria *Micrococcus luteus* (Bultel-Ponce et al., 1998). Such compounds have antimicrobial activity. Water contact angles calculated for each batch of surfaces indicated that PVA changed significantly with time ( $P < 0.05$ ) while the other surfaces were relatively stable (Table 1).

**Development of organic-based biocides.** One of the goals of this project was to develop surfaces that possess biocidal activity towards adherent microorganisms. We compared our 'new' surfaces to those of commercially-available biocides. Two phenolic-based and two quarternary -ammonium-based biocides (Albemarle Corp.) (Table 2) were mixed with a solution of PU and applied via spray gun to the surface of plastic coupons. The resulting surfaces were smooth and lacked the sticky characteristics of the PEG-based surfaces. Microscopic analysis of biocide-containing plastic coupons

placed in the marine mesocosms for 7 days revealed that these surfaces did not prevent the attachment of bacteria.

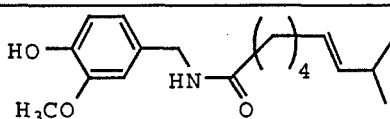
**Table 1.** Changes in contact angle of surfaces as a function of incubation time. Each measurement is based on five samples.

Surface:	Contact angle by incubation time (days):						Significance
	1		8		15		
PEG 300	44.5 ± 2.3		40.4 ± 1.8		43.6 ± 4.1		$P < 0.10$
PEG-Ome 350	59.9 ± 4.2		58.3 ± 3.6		59.3 ± 2.5		ns
PVA	76.8 ± 1.0		71.6 ± 5.6		66.4 ± 7.6		$P < 0.04$
PU	73.6 ± 1.9		75.2 ± 0.9		76.0 ± 2.7		ns
Br(m)	71.0 ± 4.2		73.0 ± 2.8		75.0 ± 2.1		ns
Br(p)	76.1 ± 3.0		77.4 ± 1.2		77.3 ± 1.6		ns

In addition to the biocides, we investigated whether or not capsaicin (Table 2), and a variety of antioxidants (Table 3) would prevent microbial adherence. Microscopic analysis of biocide-containing plastic coupons and antioxidants placed in the marine mesocosms and in the field for 7 days revealed that these surfaces did not prevent the attachment of microorganisms.

**Screening of test surfaces for resistance to bacterial attachment.** To screen the various test surfaces for their ability to resist bacterial colonization, considerable work was focused on establishing protocols to enumerate individual bacteria and colonies (>5 aggregates), and to determine the surface area of both bacteria and colonies. Protocols were also developed to determine if the collected data were statistically significant. The following protocol was developed for use in laboratory seawater systems containing fish: (1) slides used as test surfaces were placed vertically in housing devices that minimized particle settling, (2) after 72 or 168 h of incubation, the slides were removed, fixed with 5% formalin (5 min), and stained with Sytox Green (20  $\mu$ M) a nucleic acid stain (excitation/emission 504/523 nm), (3) 20 fields per slide (2 slides) were analyzed using an image analysis system (IPLab Spectrum 3.1, Signal Analytics Corp., Fairfax, VA), and (4) the results were transferred to a spreadsheet (MS Excel) and analyzed by using Statistical Analysis System (SAS, Cary, NC).

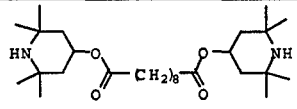
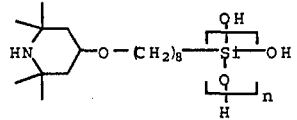
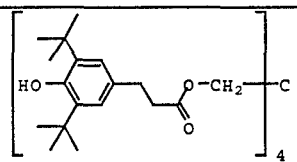
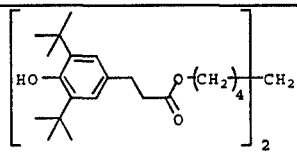
**Table 2.** Potential biocides tested.

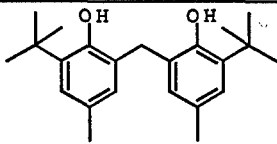
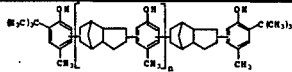
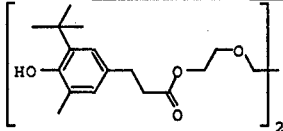
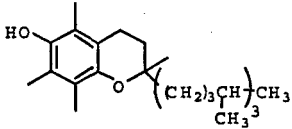
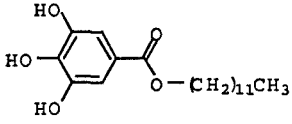
Substance	Structure
Capsaicin (trans-8-methyl-N-vanillyl-6-nonenamide)	
Stepan - Path-o-cide (Biocide)	Phenolic
BQ-451 (Biocide)	Quaternary Amine
DDAC-1010(Biocide)	Quaternary Amine
Huntington Matar Phenolics (Biocide)	Phenolic

Analysis of variance of counts and surface area data indicated a complex interaction between microbial colonization and the test surfaces (Fig. 2). Individual cell counts at 72 hours were significantly lower on surfaces coated with Br(m) and PU than the other substrata tested ( $p=0.05$ ). Similar results were obtained for colony counts and surface area of cells and colonies (Fig. 2) indicating that, at least initially, fewer microorganisms attach to Br(m) and PU surfaces than the other surfaces tested. The number of attached microorganisms significantly increased with incubation time (Fig. 2). In general, there was no difference in the number of attached microorganisms on different surfaces suggesting that given an adequate incubation time all surfaces will eventually become fouled (Fig. 2).

**Development of SAMs and a rapid method for screening SAM surfaces.** One of our goals was to develop a rapid and automated screening method for screening hundreds (and eventually thousands) of surfaces for resistance to microbial attachment. Previous approaches using a combination of microscopy and image analysis were costly or labor intensive. Our new approach was to first identify surfaces that either promoted or prevented microbial attachment and second, to further characterize selected surfaces by using multiphoton microscopy. Such an approach could be used to investigate the attachment of pioneering species (see below) as well as characterize the final community structuring which leads to the formation of a mature biofilm.

**Table 3.** Antioxidants tested.

Antioxidant	Common Name	Structure
bis(2,2,6,6-tetramethyl-4-piperidiny)-sebacate	LOWLITE 77	
poly-methylpropyl-3-oxy-[4(2,2,6,6-tetramethyl)piperidiny] siloxane	UVASIL 299LM	
tetrakis(methylene (3,5-di-tert-butyl-4-hydroxyhydrocinnamate) methane	ANOX 20	
2,2'-thiodiethyl bis-(3,5-di-tert-butyl-4-hydroxyphenyl) propionate	ANOX 70	

Antioxidant	Common Name	Structure
2,2'-methylene-bis-(4-methyl-6-tert-butyl-phenol)	LOWINOX 22M46	
polymeric sterically hindered phenol	LOWINOX CPL	
triethyleneglycol-bis-(3-tert-butyl-4-hydroxy-5-methylphenyl) propionate	LOWINOX GP-45	
Vitamin E		
Lauryl gallate		

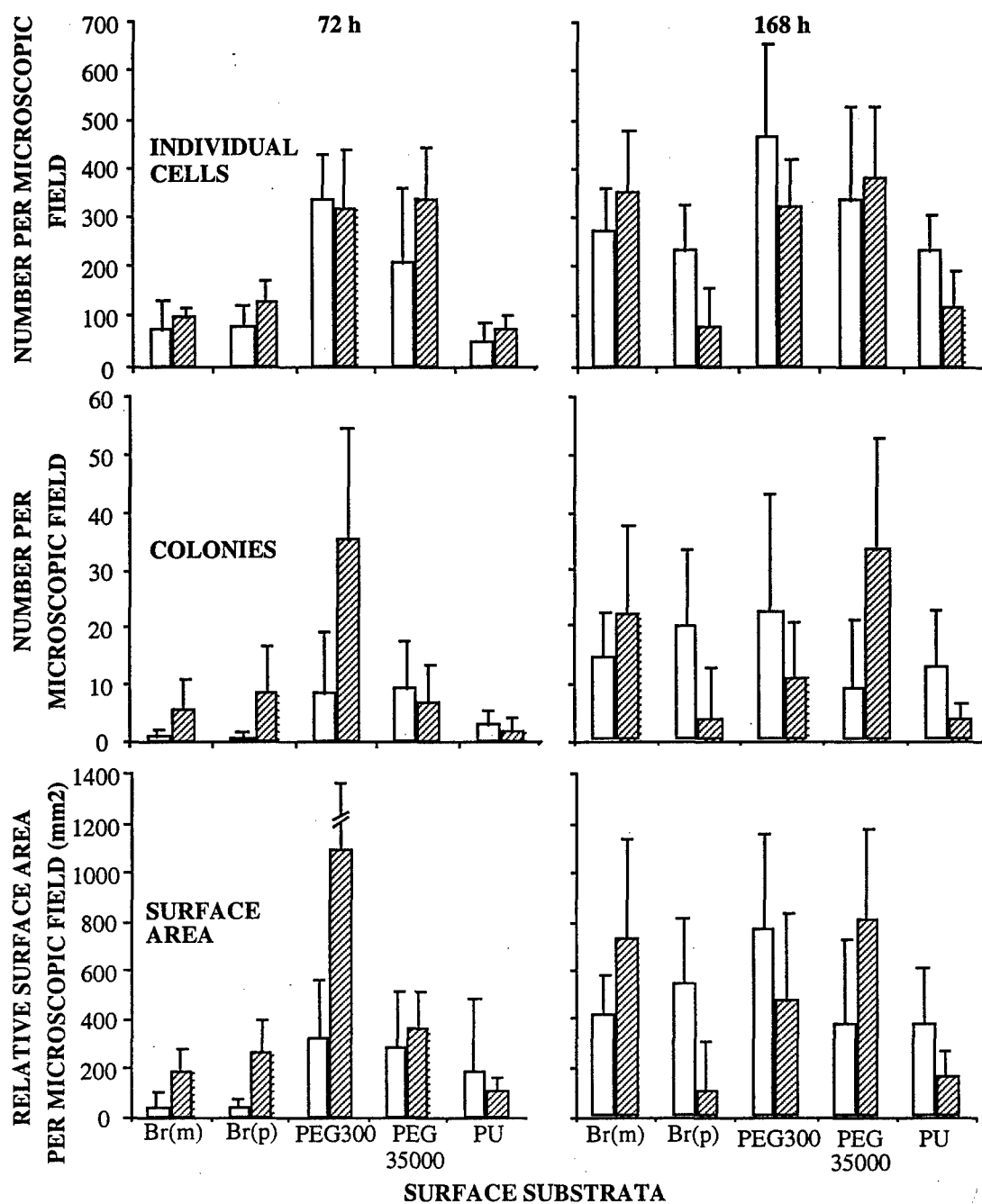


Fig. 2. Relationship between attached individual cells, colonies (>5 aggregates) and surface area of cells and colonies as a function of surface substrata and incubation time. Clear and striped bar represent the results of trials 1 and 2, respectively. Each trial is based on image analysis results obtained from 2 slides and at least 20 microscopic fields. Error bars indicate standard deviation of the mean.

Aldrich Chemical currently has 550 commercially available thiols that can be used to make SAMs. Only a fraction of these compounds have been screened for biofouling

inhibition. We have recently developed techniques for coating gold onto 24- and 96-well polystyrene microtiter culture plates and attaching selected alkanethiols to each of the wells (Fig. 3). Commercially available microtiter plates were mounted in a high-vacuum evaporative plater and coated with 200 nm of gold at  $5.0 \times 10^{-6}$  Torr. The gold adhered well to the untreated plates, producing a physically robust metallic coating. The gold-coated plates were then treated with ethanolic solutions of thiols, thereby putting different SAMs in each of the wells. The microtiter plates were then rinsed with ethanol and argon dried (Fig. 3). The plates were then immersed in a tank which simulates an ocean environment so that a variety of microorganisms come in contact with the plate and have an opportunity to adhere to and grow on the plate.

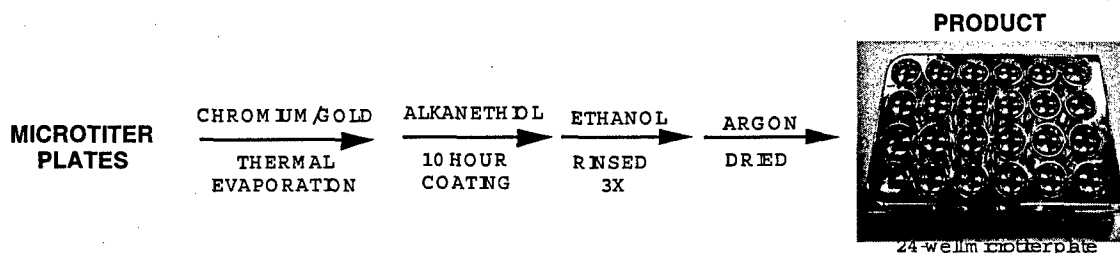


Fig. 3. SAM construction.

Our new approach uses a specially-equipped fluorescent microtiter reader which is able read fluorescent at a variety of emission wavelengths. For the initial experiments, we used 24-well microtiter plates. In these experiments, 8 wells served as controls (gold only), 8 wells were treated with a methyl-terminated SAM (dodecane thiol; hydrophobic), and the remaining 8 wells were treated with an hydroxy-terminated SAM (11-mercapto-1-undecanol; hydrophilic). The finished product was incubated in a laboratory seawater system for 7 days, stained with 0.1% acridine orange (AO; excitation/emission of 500/526 and 460/650), rinsed with distilled water, and read on the fluorescent reader. Initial studies focused on quality-control issues such as: (i) what was the best dye for staining adherent microorganisms given the restricted emission and excitation capabilities of the microtiter reader? (ii) what was the optimal concentration of the best dye? (iii) what is the optimal reading time for each well (e.g., 0.1 s to 1 s)?, (iv) what are the effects of multiple rinsings on the fluorescence readings, and (v) does the selected fluorescent dye interact with the SAMs?

The initial experiments yielded the following results: (i) the optimal dye for the microtiter reader was AO, (ii) testing concentrations ranging from 0.1 to 0.005% revealed that the optimal AO concentration was 0.1%, (iii) the optimal reading time was 0.5 s, (iv) rinsing the stained surface 3 to 6 times had no statistically significant effect on the microtiter readings, and (v) there was no interaction between AO and the SAMs.

After 7 days of incubation in the mesocosm, there was no statistical difference in the number of attached microorganisms on the hydrophilic and hydrophobic SAM surfaces. However, there was a significant difference in the number of microorganisms attached to

the gold surface and both SAMs ( $P < 0.0001$ ). Examination of the two SAM surfaces and the gold (control) slides by multiphoton microscopy also demonstrate that more microbes were attached to the SAMs than the gold surface (data not shown). However, we have only just begun to test the alkanethiol functionalities available to us.

Future studies will focus on screening surfaces with specific functional groups (~100) to identify chemical properties that promote and deter microbial attachment. The real advantage of this system would come into play if one took the chemistry a step further and did multi-step reactions in the gold-coated wells of the cell culture plates. We would like to ultimately develop a system in which thiols containing a reactive functionality on them were first coated on the gold surfaces, making a reactive SAM. This reactive SAM could then be treated with a variety of other compounds to extend the SAM further or cap off the reactive surface. By combining different reactive SAMs and different capping compounds, one would be doing true combinatorial chemistry and one could screen thousands of different systems for antibiofouling effects. For example, one could do a three-step synthesis in the wells using a reactive thiol first to create a reactive SAM. This reactive SAM could then be treated with a spacer compound that also had a reactive end group producing a new reactive SAM. Finally, the SAM could be treated with a capping compound, affording the final three-part SAM. If one used a combination of 20 different reactive thiols, 20 different spacers, and 20 different capping materials, 8000 different SAM could be made.

#### **Characterization of attached microorganisms by multiphoton microscopy**

To examine the morphology and structure of microorganisms attached to different surfaces, we used multiphoton microscopy and image analysis. This is a new multiphoton system (BioRad 1024) purchased as part of the cost share for this grant, similar to laser scanning confocal microscopy in that living biological systems can be examined at high resolution in real time, but with the advantages of higher resolution and penetration of living systems. Since the system has been in place only a few months, we are currently optimizing protocols for examining cells and associated polymers.

After 7 days of incubation, the microorganisms on the slide were fixed in 5% formalin for 5 min, dried and stained with Sytox Green (15  $\mu$ M) and Concanavalin A-Texas Red conjugate (20  $\mu$ M). Sytox Green is a nucleic acid stain with an excitation/emission of 504/523 nm. Concanavalin A is a lectin-specific stain for the sugar monomers mannopyranosyl and glucopyranosyl, and has an excitation/emission of 595/608 nm. Texas Red is a fluorochrome which is attached to unbound Concanavalin A and has quenched fluorescence. Upon binding of the Concanavalin A to the sugar molecule, the quenching is minimized, and one is able to "see" the fluorescent stain. Using the multiphoton microscope, we are able to see both dyes on two separate screens as well as the combined image. To confirm the presence of the polysaccharides of the attached microbes, we used a lectin from *Vicia faba* (Sigma) which was linked to fluorescein



isothiocyanate (FITC; 20  $\mu$ M). This lectin binds to glucose and mannose and has an excitation/emission of 494/518 nm.

Initial observations of colonized SAMs have demonstrated that there were significantly more microorganisms attached to the SAMs than the gold-coated surface (control), with no differences in the morphology or structure of the microbial communities attached to the surfaces.

Future studies will focus on characterizing the initial attachment of microbes on different surfaces on days 1, 3 and 7. We will examine "interesting" surfaces which have been selected by the rapid SAMs screening method described above.

### **Characterization of microbial biofilms by molecular analysis**

#### **(1) SLMW-RNA analysis**

A significant component of this study has been to use molecular approaches to "fingerprint" microbial communities on surfaces, in order to determine whether surfaces of different chemistries were selectively colonized by different organisms. Molecular analysis of microbial communities was carried out on test surfaces exposed to running seawater in the Baruch Institute running seawater facility or in field conditions in the North Inlet estuary. Communities were "fingerprinted" by extraction and polyacrylamide gel electrophoresis of their stable low molecular weight (SLMW) RNA (5S ribosomal RNA and tRNA). In the first phase of this project, we established protocols for extracting SLMW RNA from organic polymer-coated surfaces. In the second phase of this project, we used these protocols to determine if microbial community compositions differed between surfaces. Initially, we reported that microbial community compositions from brominated surfaces (i.e., Br(m) and Br(p)) differed in one major band in the 116 nt region from communities obtained from organic polymer test surfaces (i.e. PEGs). However, after repeated sampling, we could not replicate this finding (Table 4).

**Table 4.** Number of SLMW RNA samples examined.

	Number of SLMW RNA samples processed by collection site:		
Surface:	Mesocosm		Field
Br(m)	3		6
Br(p)	8		3
PEG-OH (200 MW)	- <sup>a</sup>		1
PEG-OH (300 MW)	5		9
PEG-OH (400 MW)	9		-
PEG-OH (400 MW)	-		-
PEG-OH (35000 MW)	-		3
PEG-Ome (350 MW)	-		8
PEG-Ome (550 MW)	16		-
PVA	-		4
PU	5		6
Total samples	46		40

<sup>a</sup>, not determined.

Subsequent experiments ( $n > 70$ ) of microbial community compositions from surfaces incubated in either a mesocosm or in the field revealed only one 119 nt band, suggesting that the microbial communities attached to the different surfaces may be quite similar after 7 or more days of incubation. It is important to recognize that the 119 nt band may represent several phylogenetically different bacteria which happen to have the same size 5S rRNA. PCR amplification, cloning and sequencing of these microorganisms (see below) will provide information necessary to determine if these organisms are, in fact, similar. Nonetheless, the predominance of one band indicates that the developing biofilms are quite similar after 7 days of incubation irrespective of the surface.

Comparisons of the attached microbial communities to those in the free-living phase revealed that they were significantly different irrespective of whether the samples were incubated in the mesocosms or in the field. This demonstrates that microorganisms that attach and colonize surfaces are a subset of the total microbial community.

It was necessary to limit our analysis to samples collected 7 days of incubation because we could not obtain enough RNA from attached microbes on days 1 and 3 to perform SLMW RNA analysis. Extracting high quality and quantity of RNA was further hampered by some surface coatings (e.g. PU) interfering with the radiolabelling of RNA. Another problem with incubating the sample for greater than 7 days was the presence of settling invertebrates (juvenile sea urchins; 10-30 $\mu$ m dia.) observed by multiphoton microscopy. These organisms were seen to be grazing attached bacteria and therefore altering the biofilm development.

Because of the lack of any marked differences between communities on different surfaces and the difficulty in obtaining sufficient SLMW RNA, we have discontinued SLMW RNA analysis of attached communities. Rather, we are now focusing on the initial attachment of microorganism by (i) performing PCR amplification of 16S rRNA, cloning of amplified products and sequencing, (ii) developing a rapid method for screening SAM surfaces, and (iii) characterizing attached microorganisms by multiphoton microscopy. Our current strategy is to focus on the initial attachment of pioneering microbes on day 1 and to follow the subsequent growth of attached microbes on days 3 and 7.

## **(2) PCR amplification of 16S rRNA, cloning of amplified products and sequencing**

The goals of this research were to determine the existence, identify, and quantify pioneer species of bacteria that are able to colonize surfaces having a broad range of chemistries, to identify the pioneer organisms, and to track their dynamics and determine their modes of growth during surface colonization. The abilities of these organisms to facilitate subsequent colonization by additional bacterial species is also of interest since these interactions may strongly influence the development of biofilms and more extensive surface fouling.

Plexiglass test plates were coated with several different monomeric and polymeric test surfaces as described previously. The plates were deployed at Oyster Landing in the North Inlet salt marsh, completely submerged, and allowed to incubate. Replicate surfaces were sampled at timed intervals (1-day, 3-days, 14-days, and 30-days) and surface growth recovered by swabbing. The swabs were stored at -70°C pending DNA extraction and purification. Due to extensive macrofouling on all surfaces after 14 and 30 days of incubation, only the 1- and 3-day incubation surfaces were analyzed. Surfaces analyzed included PU (control), PVA, PEG-OH-300, PEG-OMe-350, and PEG-OH-35,000, and Br(p).

DNA was purified from the swabs using established methods (Lovell and Piceno, 1994). Near full-length 16S rRNA genes (16S rDNA) were recovered from these DNA samples by PCR amplification and cloned into the plasmid vector pGEM-T. A clonal library was constructed from each DNA sample and screened via RFLP analysis using the restriction endonucleases *Hha*I and *Msp*I. These libraries had percent coverage values ranging from

45-85% and encompassed substantial diversity. A total of 127 unique clones were recovered from the six surfaces (Table 5).

**Table 5.** Numbers of unique clones recovered from the different test surfaces after 1 and 3 days of incubation.

Surface	Incubation time (day):	
	1	3
Br(p)	27	22
PEG-OH-300	21	16
PEG-OMe-350	17	16
PEG-OH-35000	18	21
PVA	15	25
PU	36	29

A number of clones were able obtained from organisms to colonize all test surfaces within 24 h. Some of these persisted through day 3 of the incubation while others were lost from the assemblages by day 3. Each test surface also carried a number of types of organisms recovered only from that surface. The PU control was especially specious.

We have selected 25 clones from the total collection of 127 for our first round of sequence analysis. We sequenced a 515 bp region within each 16S rDNA sequence for use in phylogenetic analysis. This region represents a relatively short length flanked by universal primer sequences. The short length and primers allow us to obtain sequences in a single run without the need for additional internal primers. Numerous studies have shown this region to be suitable for phylogenetic analysis and it contains many diagnostic variable sequence regions. We have begun sequence analysis of the initial set of clones and will supplement that set with additional clones as deemed necessary.

In the next phase, we will use the sequences obtained from our clones to perform phylogenetic analysis. This will allow us to determine what major phylogenetic lineages our clones represent and to identify species-specific sequences that can be used as probes for surface colonization. The probes will be used in *in situ* hybridization experiments, using multiphoton microscopy, to quantitatively track the colonization of the surfaces by specific non-surface selective (i.e., able to colonize multiple different surfaces) and surface selective (i.e., restricted to particular surfaces) organisms. This analysis will also allow us to determine the degree of cell-cell interactions with other species, and thus the potential of the pioneer colonists to facilitate subsequent colonization by other species. We will also attempt to isolate into pure culture pioneer species that do facilitate further colonization for subsequent studies of biofilm and biofouling development and dynamics.

Our goal in this set of studies is to identify pioneer species that colonize numerous surfaces and facilitate subsequent colonization by other organisms. On the basis of the clonal library results, we have found pioneer organisms. Quantitative assessment of their dynamics and identification of the organisms involved will require *in situ* hybridization, DNA sequence analysis, and pure culture isolation studies. These will be conducted in the third year of the project.

#### ***Publications and Technical Reports***

Poster presentation at the annual meeting of the American Society for Microbiology, Chicago, IL, June 2nd, 1999. "Attachment of marine microbial communities to synthetic oligomeric and polymeric substrata".

#### ***Participating Scientific Personnel***

Madilyn Fletcher, Professor

James M. Tour, Professor

Charles R. Lovell, Associate Professor

Alan W. Decho, Assistant Professor

Peter A. Noble, Research Assistant Professor

Wally Scrivens, Research Assistant Professor

Graduate students: Hongyue Dang, Monica Hoffman, Wesley Johnson, Steven T. Lindsay,

D. Brian Shortell

M. Caroline Roper, Research Technician

Undergraduate students: Joshua A. Barber, Elizabeth Strojny

#### **BIBLIOGRAPHY**

1. Bidle, K.D., Fletcher, M. Appl. Environ. Microbiol. 1995, 61, 944-952
2. Bultel-Ponce, V., Debitus, C., Berge, J.-P., Cerceau, C. and Guyot, M. 1998. Metabolites from the sponge-associated bacterium *Micrococcus luteus*. J. Mar. Biotechnol. 6:233-236.
3. Incze, B.I., Sea Technol. 1996, 37, 43-49.
4. Ista, L.K.; Fan, H.; Baca, O.; Lopez, G.P. FEMS Microbiol. Lett. 1996, 142, 59.
5. Lappin-Scott, H.M.; Costerton, J.W. Biofouling 1, 323-342.
6. Marshall, K.C. Mechanisms of bacterial adhesion at solid-water interfaces, pp. 133-161. In D.C. Savage and M. Fletcher (eds.) Bacterial Adhesion, Plenum Press, New York, 1985.
7. Noble, P.A., Bidle, K.; Fletcher, M. Appl. Environ. Microbiol. 1997, 63, 1762-1770.
8. Parrish, J.; Jensen, S; Hollis, W.C. Sea Technol. 1996, 37, 51-60.
9. Wiencek, K.M.; Fletcher, M. J. Bacteriol. 1995, 177, 1959-1966.
10. Wolfaardt, G.M.; Lawrence, J.R.; Robarts, R.D.; Caldwell, S.J.; Caldwell, D.E. Appl. Environ. Microbiol. 1994, 60, 434-446

**University Research Initiative Program for Combat Readiness**  
**Annual Report 06/01/98-05/31/99**

PART 53-FORMS

53.301-298

<b>REPORT DOCUMENTATION PAGE</b>		Form Approved OMB No. 0704-0188	
Public reporting burden for this collection of information is estimated to average 1 hour per response, including the time for reviewing instructions, searching existing data sources, gathering and maintaining the data needed, and completing and reviewing the collection of information. Send comments regarding this burden estimate or any other aspect of this collection of information, including suggestions for reducing this burden, to Washington Headquarters Services, Directorate for Information Operations and Reports, 1215 Jefferson Davis Highway, Suite 1204, Arlington, VA 22202-4302, and to the Office of Management and Budget, Paperwork Reduction Project (0704-0188), Washington, DC 20503.			
1. AGENCY USE ONLY (Leave blank)	2. REPORT DATE  June 1, 1999	3. REPORT TYPE AND DATES COVERED  Annual	
4. TITLE AND SUBTITLE Accelerated Research in Biofouling Control		5. FUNDING NUMBERS Grant Number N00014-97-1-0806 PR Number 97PR06312-00 PO Code 353 Disbursing Code N68892 AGO Code N66020 Cage Code 4B489	
6. AUTHOR(S) Madilyn Fletcher			
7. PERFORMING ORGANIZATION NAME(S) AND ADDRESS(ES) University of South Carolina		8. PERFORMING ORGANIZATION REPORT NUMBER N00014-97-1-0806	
9. SPONSORING / MONITORING AGENCY NAME(S) AND ADDRESS(ES) ONR		10. SPONSORING / MONITORING AGENCY REPORT NUMBER ONR	
11. SUPPLEMENTARY NOTES Prepared in coordination with University Research Initiative Program for Combat Readiness			
12a. DISTRIBUTION / AVAILABILITY STATEMENT APPROVED FOR PUBLIC RELEASE		12b. DISTRIBUTION CODE	
13. ABSTRACT (Maximum 200 words) The formation of biofouling communities on deployment devices, sensors, and on ship and submarine hulls inhibits efficient operation of instrumentation and vessels. We have proposed novel approaches for control of microbial biofouling by (1) developing fouling-resistant surfaces based on information gained through experiments with alkanethiol self-assembled monolayers (SAMs), and (2) determining the microbial community structures that comprise the biofouling process, particularly those that form on surfaces with reduced fouling potential. We are developing a combinatorial approach for production of SAMs and assessment of a wide range of surface chemistries. Methods have been developed to prepare and assay multiple SAMs for bacterial attachment, to quantify the extent of bacterial colonization over time, and to identify bacterial colonizers using molecular techniques. We have yet to identify a surface chemistry that resists bacterial attachment. However, molecular biology approaches have demonstrated that different species attach to different surfaces within the first few days of exposure to seawater, and that these differences diminish with time as colonization proceeds. Future research will focus on (1) extensive screening of the antifouling potential of functionally diverse SAMs, and (2) molecular identification of pioneer bacterial species and differences in communities on different surfaces, particularly those which ultimately demonstrate the greatest antifouling potential.			
14. SUBJECT TERMS Chemical and Biological Defense, Target Acquisition, Anti-Submarine, Combat Medicine, Biodeterioration, and Command Control and Communication		15. NUMBER OF PAGES	
		16. PRICE CODE	
17. SECURITY CLASSIFICATION OF REPORT UNCLASSIFIED	18. SECURITY CLASSIFICATION OF THIS PAGE UNCLASSIFIED	19. SECURITY CLASSIFICATION OF ABSTRACT UNCLASSIFIED	20. LIMITATION OF ABSTRACT 200 words

NSN 7540-01-280-5500

Standard Form 298 (Rev. 2-89)

Prescribed by ANSI Std. Z39-18  
298-102

**SECTION VII: SUPPORTING RESEARCH**

## **Development of a Field-Portable LIBS System for Elemental Analysis**

Scott R. Goode

Department of Chemistry and Biochemistry  
University of South Carolina  
Columbia, SC 29208

Tel: (803)777-2601  
Fax: (803)777-9521  
Email: goode@sc.edu



## **Section 7-1: Development of a Field-Portable LIBS System for Elemental Analysis**

Scott R. Goode

### **ABSTRACT**

The fabrication and testing of a laser induced breakdown spectroscopy (LIBS) system is complete. The LIBS spectrometer utilizes a high-resolution dispersion device (an echelle grating) in concert with a charge-induced device (CID) array detector and Nd-YAG laser. The LIBS system uses the laser to form a plasma, and then uses fiber optics to bring the emission from the plasma to the spectrometer. The device provides quantitative chemical analysis of solid samples without any dissolution or pretreatment step. LIBS spectra of alloys including samples of brass, steel, and aluminum have been obtained with the instrument and parametric studies have begun. Studies of multi-pulse LIBS have started with the use of dual-pulse LIBS for alloy identification.

### **FORWARD**

The award is for the period 6/1/97 - 6/29/00 and in the amount of \$434,700.

During the first year the following objectives have been addressed:

- Instrument fabrication completed
- Instrument certified by Laser Safety
- Interface to utilize fiber optic collection completed
- LIBS data have been collected
- Data interpretation has begun

During the second year the following objectives have been addressed:

- An additional spectrometer has been specified
- LIBS data have been obtained
- Studies of the effect of the matrix on the generation of the LIBS signals have begun
- Dual-pulse experiments have been initiated

### **REPORT**

#### ***Statement of the problem***

Laser-Induced Breakdown Spectroscopy (LIBS) shows great potential as a method for determining the composition of solid samples without preparation. The method can be adapted to field use, and is applicable to nearly all types of samples. The LIBS signal is proportional to

analyte concentration, but the matrix influences this proportionality. If the technique is to be applied to a wide variety of samples, the factors that influence the signal must be studied, and methods that use LIBS must be validated. The proposed research examines two important samples, the determination of the lead content of dried paint, and the determination of the composition of metallic alloys.

### ***Summary of the Most Important Results***

#### **Instrumentation**

The research is progressing well, and the first phase, fabricating the instrument, is essentially complete. Since the ultimate goal of the project is to supply a system capable of remote analysis fiber optics are employed to deliver the light to form the plasma and to gather the light from the LIBS plasma. We chose to perform this important research task before obtaining any spectra because it would allow us to obtain artifact-free information, and it provided an exceptionally flexible optical entrance that we could exploit in several future stages of the research. The LIBS produces images of the high spectral resolution by using an echelle spectrometer.

The results obtained with the first generation instrument have allowed us to design a second spectrometer system that should provide the time resolution needed for several analyses as well as the rapid data acquisition that will be needed to characterize alloys in the field.

#### **Measurements of alloy composition**

Initial studies have revolved around the signals from binary alloys. We have chosen to use brass samples for our initial work because their composition is relatively simple; steel samples will be investigated at the next phase. Certified reference samples of brasses of different composition have been purchased. These brasses are primarily copper, with added zinc. The first experiments measure the emission ratio of zinc (relatively volatile) to copper (relatively nonvolatile) as a function of laser spot size. Changing the sample-to-lens distance changes the spot size in this study. Two typical experiments are show below.

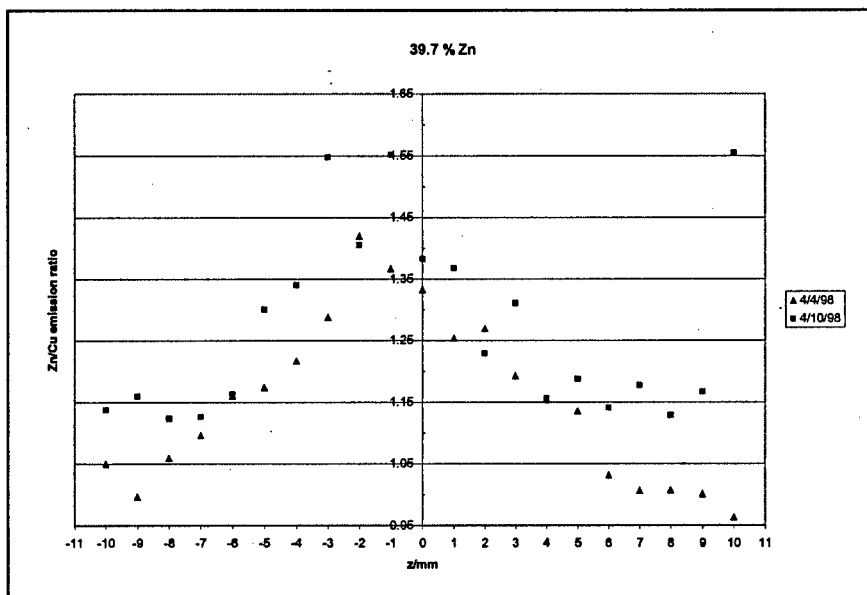


Figure 1. Zinc-to-copper emission ratios for a sample containing 39.7% Zn. Zero represents focus at the surface, negative numbers indicate a focal point below the surface and positive above.

The figure shows data replicated approximately one week apart. The important point to note is that the graph shows bilateral symmetry; the maximum emission is seen when the focus is at the surface, and the emission ratio decreases as the focal point changes.

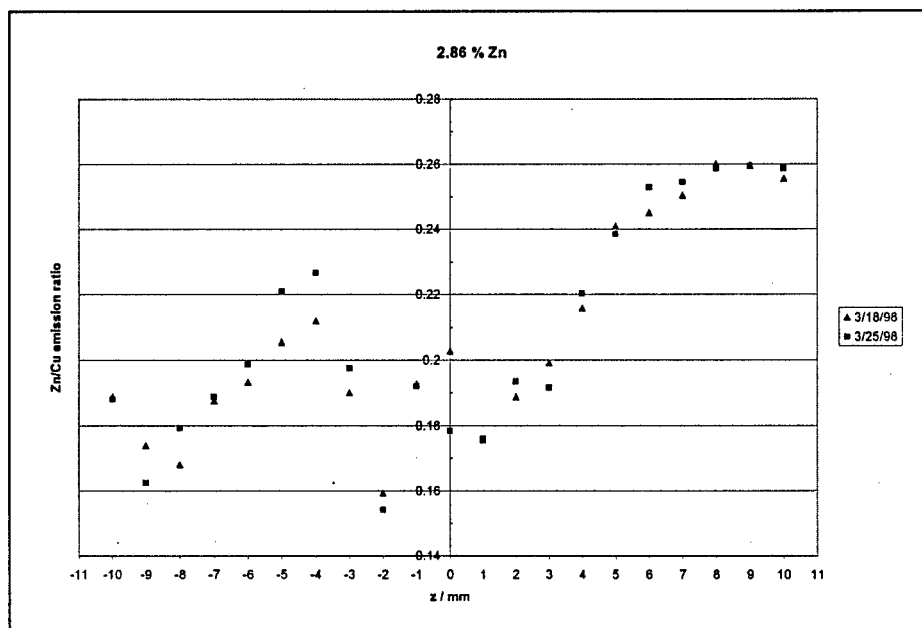


Figure 2. Zinc-to-copper emission ratios for a sample containing 2.86% Zn.

The effect of the matrix is clear. When the brass contains a substantial concentration of zinc, (Figure 1) defocusing the laser produces predictable results that can be explained by a simple theory --the emission increases with power density.

Figure 2 indicates that this model fails for samples with low zinc, since the results shown are asymmetric. These results are consistent with prior experience using LIBS with glass samples and with literature reports of similar behavior.

The results are reproducible, both with the same samples and with different samples. The identical asymmetric relationship is seen in all samples in which the zinc concentration is less than approximately 15%. As the concentration of zinc goes from high to low, the behavior smoothly changes from that shown in Figure 1 to that shown in Figure 2.

Although these results indicate that the matrix influences the signal, additional experiments show that under appropriate conditions, the signal can be made independent of the matrix, an important accomplishment that is necessary if LIBS is to find wide use in the analysis and identification of metallic alloys. Figures 3 and 4 show electron micrographs of craters formed by low power (Figure 3) and high power (Figure 4) pulses on a brass sample that contains 24.8% zinc.

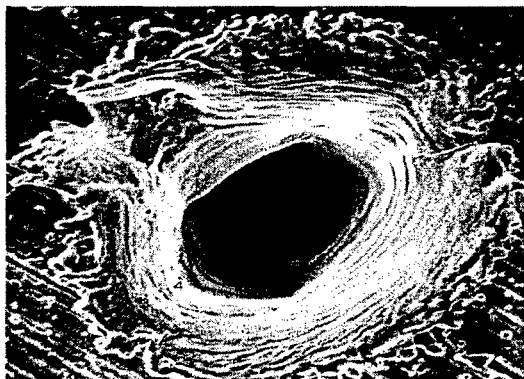


Figure 3 Low Power



Figure 4 High Power

Relative zinc concentration at location	Relative zinc concentration at location
1. 130.0	1. 101.3
2. 7.8	2. 89.1
3. 62.0	3. 57.9
4. 75.4	4. 93.3
5. 88.0	5. 100.0
	6. 106.7
	7. 100.8

The crater formed under low powers is smaller in diameter, but deeper than the one formed at high powers. The zinc concentration at different locations was measured by x-ray fluorescence, and expressed as a percentage of the nominal concentration. The low powers used in Figure 3 areas of high zinc concentration near areas of low zinc concentration. The variation is quite large. Figure 4, in which higher laser powers were used, shows a much more homogeneous concentration distribution.

These results are consistent with sampling that occurs by volatilization at low powers and by a percussive dielectric breakdown at high powers. Although the high powers may not be as effective in terms of vaporizing large amounts of material, the material that is vaporized is representative of the bulk of the sample, so matrix effects are minimized by operating in a region of percussive vaporization.

#### Determination of the lead content of paint

Factors affecting the LIBS signal from lead are being investigated using a time-resolved imaging apparatus that consists of an acousto-optic tunable filter (AOTF) along with a gated intensified charge-coupled device (ICCD). This instrument allows us to obtain time-resolved images of the emission from a single atomic transition. Time-resolved plasma images obtained have shown lead emission intensity to increase as well as the overall shape of the plasma with increasing number of laser shots.

This effect is summarized in Figure 4 for two different delay times. The same general trend of increasing plasma emission height is observed at the 1.0  $\mu\text{s}$  as well as the 2.5  $\mu\text{s}$  delay times. In addition, the 2.5  $\mu\text{s}$  delay time plasma images are overall higher than the 1.0  $\mu\text{s}$  delay time since the plasma has expanded and grown up over time.

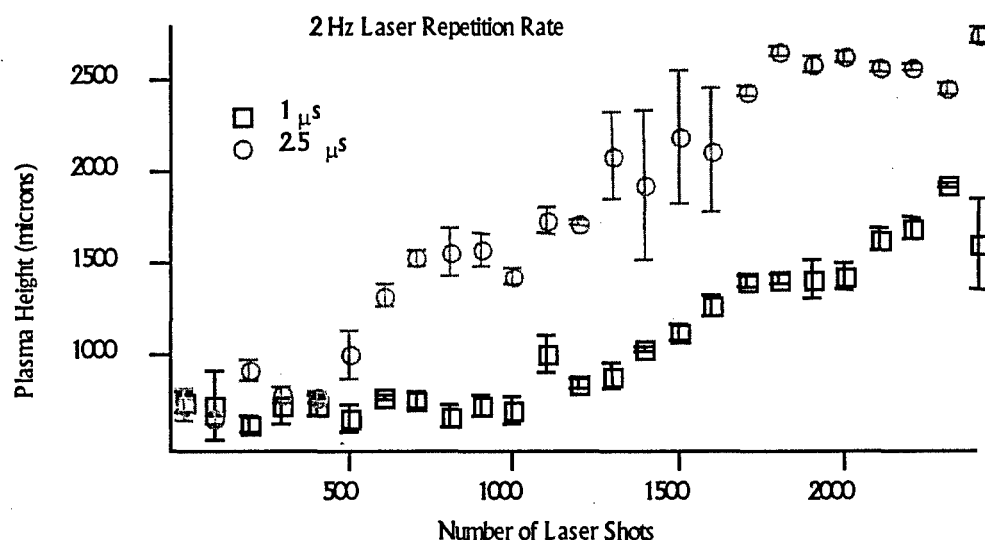


Figure 4. Height of plasma as a function of the number of laser pulses, measured at two different delay times.

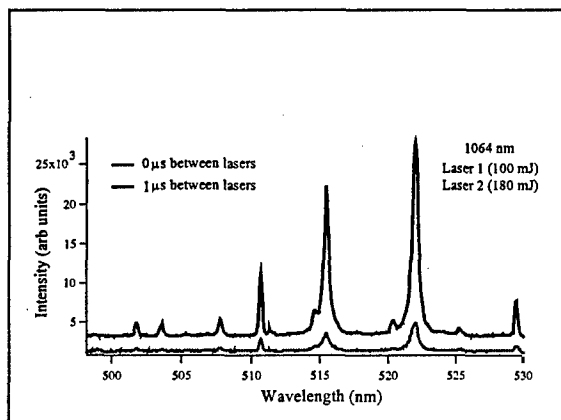
The change of the plasma emission intensities seems to be related to the size and shape of the crater that is formed in the lead sample. One explanation for the signal enhancement is that increasing laser shots causes deeper craters with a defined shape that may act to funnel the ablated material preferentially in the direction of the incoming laser beam. This effect would increase the laser/particle interactions and thereby increase the excitation and emission observed.

### DUAL PULSE LIBS

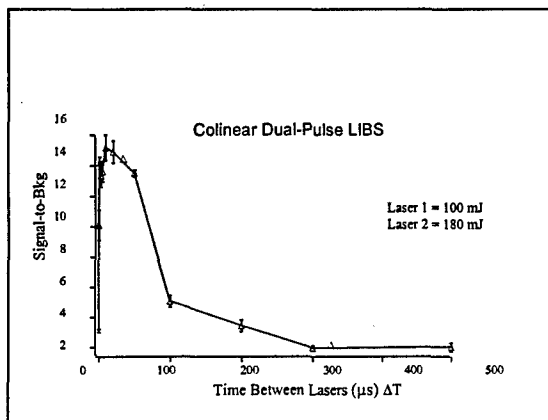
The use of two separate laser pulses, separated by a microsecond, results in dramatically improved LIBS signals. Figure 6 shows the improvement obtained when a second laser pulse is delayed by 1  $\mu$ s, compared to an experiment in which the two laser pulses are coincident in time. Although each experiment has the same laser power, in the same two pulses, the time-delayed dual pulse experiment shows almost 5 times as much emission as does the time coincident experiment. The increase in emission, as measured by the signal-to-background ratio, is seen to be a strong function of the delay time.

Figure 6. Dual pulse LIBS

A. Effect on spectra



B. Influence of time delay on SBR



### Publications and Technical Reports

Brian J. Marquardt, S.M. Angel, Scott R. Goode, and David A. Cremers, "Fiber-Optic Imaging LIBS Probe For Remote Elemental Microanalysis," Winter Conference on Plasma Spectrochemistry, Phoenix, AZ, 1998. ()

Scott R. Goode, Paul Harhay, Allison Oxsher, and Mary Peyton Davis "Factors Influencing Selective Volatilization in Laser Induced Breakdown Spectroscopy," Pittcon, March, 1999, Orlando FL

Scott R. Goode "Matrix Effects in Laser Induced Breakdown Spectroscopy," CMST, March 1999, Gaithersburg MD.

B.J. Marquardt, D.N. Stratis, D.A. Cremers and S.M. Angel, "Novel Probe for Laser-Induced Breakdown Spectroscopy and Raman Measurements Using an Imaging Optical Fiber," *Appl. Spectrosc.* **52**, 1148 (1998).

Dimitra N. Stratis, Kristine L. Eland and S. Michael Angel "Optimization of Laser Parameters for Dual-Pulse LIBS," presented at 25th Annual Conference of the Federation of Analytical Chemistry and Spectroscopy Societies (FACSS), Paper **583**, Austin, TX, October 11-15, 1998.

Dimitra N. Stratis, Kristine L. Eland and S. Michael Angel "Wavelength Optimization for Fiber-optic LIBS," presented at 25th Annual Conference of the Federation of Analytical Chemistry and Spectroscopy Societies (FACSS), Paper **707**, Austin, TX, October 11-15, 1998.

Brian J. Marquardt, Dimitra N. Stratis, David A. Cremers and S. Michael Angel, "Fiber-optic LIBS/Raman Imaging Probe for In-Situ Elemental Microanalysis," The Pittsburgh Conference on Analytical Chemistry and Applied Spectroscopy, New Orleans, Louisiana, March 1-5, Abstract **942** (1998).

Dimitra N. Stratis, Brian J. Marquardt and S. Michael Angel, "Temporal and Spatial Characterization of Laser-Induced Plasmas," The Pittsburgh Conference on Analytical Chemistry and Applied Spectroscopy, New Orleans, Louisiana, March 1-5, Abstract **268** (1998).

Dimitra N. Stratis, Kristine L. Eland and S. Michael Angel, "Characterization of laser-induced plasmas for fiber-optic probes," SPIE Proceedings, Vol. **3534-88**, November 1-5, Boston, MA (1998).

S. Michael Angel, H. Trey Skinner, and Brian J. Marquardt "Imaging Spectroscopy using Optical Fibers," presented at ANACHEM Award Symposium at 24th Annual Conference of the Federation of Analytical Chemistry and Spectroscopy Societies (FACSS), Providence, RI, invited paper October 27-31, 1997.

S. Michael Angel, H. Trey Skinner, and Brian J. Marquardt "Imaging Spectroscopy using Fiber Optics," presented at Microscopy and MicroAnalysis '97, Cleveland, Ohio, invited paper August 13, 1997.

Brian J. Marquardt, Scott R. Goode and S. Michael Angel, "Spatial Profiling of Laser-Induced Plasmas for the Purpose of Optimizing Fiber-Optic LIBS Probe Designs," The Pittsburgh Conference on Analytical Chemistry and Applied Spectroscopy, Atlanta, Georgia, March 16-21, Abstract **816** (1997).

D. Stratis, K. Eland, and S. M. Angel, "Characterization and Optimization of Parameters for Dual-Pulse LIBS," Pittcon, 1999

D. Stratis, J. Chance Carter, and S. M. Angel, "A Comparison of Acousto-Optic and Liquid Crystal Tunable Filters for Time Resolved Plasma Imaging," Pittcon, 1999.

K. Eland, D. Stratis, and S. M. Angel, "Optimization of Wavelength for Remote Fiber Optic LIBS Measurements," Pittcon, 1999

### ***Participating Personnel***

Andrea Thomas, third year Ph.D.

Allison Oxsher, second year Ph.D. student

Dimitra Stratis, third year Ph.D. candidate

Kristine Eland, second year Ph.D. student

Scott Goode (summer) Principal Investigator

S. Michael Angel (summer) Co-Principal Investigator

University Research Initiative Program for Combat Readiness  
Annual Report 06/01/98-05/31/99

PART 53-FORMS

53.301-298

<b>REPORT DOCUMENTATION PAGE</b>		Form Approved OMB No. 0704-0188	
Public reporting burden for this collection of information is estimated to average 1 hour per response, including the time for reviewing instructions, searching existing data sources, gathering and maintaining the data needed, and completing and reviewing the collection of information. Send comments regarding this burden estimate or any other aspect of this collection of information, including suggestions for reducing this burden, to Washington Headquarters Services, Directorate for Information Operations and Reports, 1215 Jefferson Davis Highway, Suite 1204, Arlington, VA 22202-4302, and to the Office of Management and Budget, Paperwork Reduction Project (0704-0188), Washington, DC 20503.			
1. AGENCY USE ONLY (Leave blank)	2. REPORT DATE June 1, 1999	3. REPORT TYPE AND DATES COVERED Annual	
4. TITLE AND SUBTITLE Development of a Field-Portable LIBS system for the Identification of Alloys		5. FUNDING NUMBERS Grant No. N00014-97-1-0806 PR No. 97PR06312-00 PO Code 353 Disbursing Code N68892 AGO Code N66020 Cage Code 4B489	
6. AUTHOR(S) Scott R. Goode			
7. PERFORMING ORGANIZATION NAME(S) AND ADDRESS(ES) University of South Carolina		8. PERFORMING ORGANIZATION REPORT NUMBER N00014-97-1-0806-2	
9. SPONSORING / MONITORING AGENCY NAME(S) AND ADDRESS(ES) ONR		10. SPONSORING / MONITORING AGENCY REPORT NUMBER ONR	
11. SUPPLEMENTARY NOTES Prepared in coordination with the University Research Initiative Program for Combat Readiness			
12a. DISTRIBUTION / AVAILABILITY STATEMENT APPROVED FOR PUBLIC RELEASE		12b. DISTRIBUTION CODE	
13. ABSTRACT (Maximum 200 words)  The fabrication and testing of a laser induced breakdown spectroscopy (LIBS) system is complete. The LIBS spectrometer utilizes a high-resolution dispersion device (an echelle grating) in concert with a charge-induced device (CID) array detector and Nd-YAG laser. The LIBS system uses the laser to form a plasma, and then uses fiber optics to bring the emission from the plasma to the spectrometer. The device provides quantitative chemical analysis of solid samples without any dissolution or pretreatment step. LIBS spectra of alloys including samples of brass, steel, and aluminum have been obtained with the instrument and parametric studies have begun. Studies of multipulse LIBS have started with the use of dual pulse LIBS for alloy identification.			
14. SUBJECT TERMS Chemical and Biological Defense, Target Acquisition, Anti-Submarine, Combat Medicine, Biodeterioration, and Command Control and Communication		15. NUMBER OF PAGES	
		16. PRICE CODE	
17. SECURITY CLASSIFICATION OF REPORT  UNCLASSIFIED	18. SECURITY CLASSIFICATION OF THIS PAGE  UNCLASSIFIED	19. SECURITY CLASSIFICATION OF ABSTRACT  UNCLASSIFIED	20. LIMITATION OF ABSTRACT  200 words

NSN 7540-01-280-5500

Standard Form 298 (Rev. 2-89)

Prescribed by ANSI Std. Z39-18  
298-102





*Enotee*

UNIVERSITY RESEARCH INITIATIVE PROGRAM  
FOR COMBAT READINESS

MAY 31 1999

Dr. Donald E. Polk  
Office of Naval Research  
Program Officer  
Ballston Center Tower One  
800 N. Quincy Street  
Arlington, VA 22217-5660

RE: Annual Report N00014-97-1-0806

Dear Dr. Polk:

Enclosed is an organizational chart which we neglected to include as part of our recently submitted YR2 Annual Technical Progress Report for the above referenced grant, *University Research Initiative Program for Combat Readiness*. This sheet should be inserted immediately following Page 2 of the Executive Summary in that document.

We apologize for any inconvenience this may cause you. Should you have any questions, please do not hesitate to contact me.

Sincerely,

*T. S. Little*

T. Scott Little, Program Manager  
University Research Initiative for Combat Readiness

Cc Director of Naval Research  
ATTN: Code 5227  
4555 Overlook Drive  
Washington, DC 20375-5326

Defense Technical Information Center  
8725 John J. Kingman Road  
STE 0944  
Ft. Belvoir, VA 22060-6218

800926011 1990526008  
A363445